MOLECULAR MOTION IN CONDENSED PHASES. NUCLEAR MAGNETIC RELAXATION AND RAMAN LINESHAPE STUDIES OF SEVERAL SMALL MOLECULES

Dissertation for the Degree of Ph. D.

MICHIGAN STATE UNIVERSITY
DAVID ALLEN WRIGHT

1974

This is to certify that the

thesis entitled

MOLECULAR MOTION IN CONDENSED PHASES.
NUCLEAR MAGNETIC RELAXATION AND RAMAN LINESHAPE
STUDIES OF SEVERAL SMALL MOLECULES

presented by

David Allen Wright

has been accepted towards fulfillment
of the requirements for

Ph.D. degree in Chemistry

Max T Rogers
Major professor

Date Nov 12, 1974

O-7639

Near threshold

In order to

near experim

Measurements

carried out

A general m

may be lac

Noise spect

called by the

necessary for

Values

the colle

least-squares

the data p

immediate

the simple

particularly

ABSTRACT

MOLECULAR MOTION IN CONDENSED PHASES. NUCLEAR MAGNETIC RELAXATION AND RAMAN LINESHAPE STUDIES OF SEVERAL SMALL MOLECULES

By

David Allen Wright

Raman lineshape measurements were used to augment NMR relaxation data in order to investigate molecular motion in liquids and solids. The Raman experiments were done only at room temperature while pulsed NMR measurements of T_1, T_2 and the self-diffusion coefficient D_S were carried out over as wide a range of temperature as possible.

A general method has been developed by which two-pulse experiments may be largely automated by interfacing a minicomputer to an NMR pulse spectrometer. The necessary pulses and time delays are supplied by the computer and the interface converts these to the levels necessary for the rf oscillator and power amplifier of the spectrometer. Values of the relaxation times (T_1, T_2, T_{1p}) are extracted from the collected data by data analysis subroutines which perform a least-squares fit of the data to an exponential decay. Deviations of the data points from the least-squares slope are displayed to permit an immediate visual check for experimental errors. The advantages of the simple pulse sequences are retained while their disadvantages, particularly inefficient data collection for very long or very short

relaxation times, are greatly reduced. The lower limit of relaxation times which may be measured by this method is about 100 μsec.

A simpler interface was constructed which allowed Raman spectra to be digitized and punched onto IBM cards for analysis on the CDC 6500 computer. A FORTRAN computer program was written which calculated the reorientational broadening of Raman A_1 lines, from which the rotational correlation time was calculated.

Deuterium quadrupole coupling constants have been obtained for two symmetric-top molecules in the liquid phase by combining NMR relaxation data with Raman line-shape analysis of bands of $\underline{A}_1$ symmetry. The Raman lines have been corrected for vibrational and instrumental broadening by comparing the polarized and depolarized components of a single line. More than one $\underline{A}_1$ line has been studied for each molecule. The previously uncertain deuterium quadrupole coupling constant for $CDBr_3$ has been determined in this work to be 170±5 kHz and deuterium coupling constants in CDX_3 molecules are discussed. The procedure described here provides a different method for obtaining nuclear quadrupole coupling constants in the liquid phase. The temperature dependence of the ^2D spin-lattice relaxation rate was used to analyze published ^{13}C relaxation data for $CHBr_3$, and limits were placed on the anisotropy of rotational motion, which at 20° C were $1.5<D_{||}/D_{\perp}<1.0$. Motion in liquid $CDBr_3$ was compared to motion in the much more intensively studied liquid $CDCl_3$ system.

Spin-lattice and spin-spin relaxation rates at 56 MHz were measured in CF_3CCl_3 from 141° K to 432° K. More limited measurements were made of T_1 at 15.87 MHz and the self-diffusion coefficient in the liquid phase. A phase transition was observed in the solid at

[illegible] a [illegible]

by means of [illegible]

[illegible] relative [illegible]

[illegible] contribution [illegible]

[illegible] and [illegible]

[illegible] these processes [illegible]

[illegible] 1.0 [illegible]

[illegible] 1.5, [illegible]

[illegible] the trans[illegible]

[illegible] coefficient [illegible]

[illegible] or 1.3×10[illegible]

[illegible]

The separat[illegible]

made on the [illegible]

temperature-dependent [illegible]

[illegible] the rotational [illegible]

[illegible]. The rotat[illegible]

[illegible] model, [illegible]

[illegible] interaction pr[illegible]

[illegible] nearest a[illegible]

[illegible] hexagonal ele[illegible]

Spin-lattice [illegible]

[illegible] the critical [illegible]

[illegible] coefficient was [illegible]

[illegible] point.

[illegible] various me[illegible]

[illegible] due to [illegible]

147° K from a discontinuity in the T_1 data.

By means of linewidth, T_2, and variable-field T_1 measurements, spin-lattice relaxation in plastic crystalline CF_3CCl_3 was found to have contributions from intramolecular dipole-dipole interactions, translational diffusion, and spin-rotation. The activation energies for these processes were determined to be 1.8 kcal/mole, 12.9 kcal/mole, and ∿-1.8 kcal/mole, respectively.

At 56 MHz, spin-rotation was found to be more important in the solid than translational diffusion. The value of the translational diffusion coefficient at the melting point was determined to be 2.1 x 10^{-8} or $1.3 \cdot 10^{-8}$, depending on whether the crystal structure is fcc or bcc.

The separation of the liquid phase ^{19}F relaxation in CF_3CCl_3 was made on the basis of self-diffusion measurements and a single room temperatureRaman measurement coupled with the temperature dependence of the rotational correlation time determined from the solid phase data. The rotational motion was discussed in terms of Gordon's extended diffusion model, and it was found that the Hubbard relation for isotropic reorientation predicted angular momentum correlation times which were in approximate agreement with the diffusion models, indicating that off-diagonal elements of the spin-rotation tensor are small in CF_3CCl_3.

Spin-lattice relaxation rates were measured from the melting point to the critical point for CF_3Br and CF_2Br_2; also the self-diffusion coefficient was measured in liquid CF_3Br from room temperature to the melting point. The separation of $R_{1,total}$ into the contributions from various mechanisms was discussed but was not quantitatively successful due to difficulties in obtaining satisfactory values for the

[illegible]

[illegible] The use of [illegible] were [illegible] generally, [illegible] densities were [illegible] correlation coefficient [illegible] in the [illegible] in R_1 in [illegible] relaxation [illegible] "effective" [illegible] the relaxation [illegible] shielding [illegible] good, indicating [illegible] were small [illegible].

intermolecular dipole-dipole relaxation rate.

Spin-lattice and spin-spin relaxation rates were measured over a limited temperature range for CF_2ClCCl_3, $CFCl_2CFCl_2$, CF_3CF_3, and CF_3I. The use of the difference R_2-R_1 to obtain the scalar coupling constant J_{FX}, where X is the other halogen, was discussed, but it was not, in general, possible to obtain reliable values. These substituted ethanes were found to behave very similarly to CF_3CCl_3 in that spin-rotation dominated the liquid range, with translational diffusion only a minor contribution to the total spin-lattice relaxation rate (R_1) both in the liquid and solid, at 56 MHz. Also the presence of a minimum in R_1 in the solid indicated the probable presence of a spin-rotational relaxation mechanism.

"Effective" spin-rotation interaction constants were calculated from the relaxation rate at the critical point, and were compared with chemical shielding derived values. The agreement was found generally to be good, indicating that off-diagonal elements of the spin-rotation tensor were small for these compounds and that the motion was roughly isotropic.

in p

MOLECULAR MOTION IN CONDENSED PHASES. NUCLEAR MAGNETIC RELAXATION AND RAMAN LINESHAPE STUDIES OF SEVERAL SMALL MOLECULES

By

David Allen Wright

A DISSERTATION

Submitted to

Michigan State University

in partial fulfillment of the requirement

for the degree of

DOCTOR OF PHILOSOPHY

Department of Chemistry

1974

To my Parents

ACKNOWLEDGMENTS

The author would like to express his appreciation to Professor Rogers for allowing him the freedom to pursue a research problem which at times strayed from the area of magnetic resonance.

In addition, thanks are due to Dr. Scott Blackwell and Professor G. E. Leroi for their theoretical and experimental assistance in Raman spectroscopy, to Professor R. I. Cukier for helpful discussions on a number of topics in this Dissertation, and to the Departmental staff, particularly Mr. Martin Rabb and Mr. Wayne Burkhart, without whose skills much of the experimental equipment would have been much more difficult to construct.

Finally, the author wishes to acknowledge the financial support of the Department of Chemistry throughout his years as a Graduate student.

[illegible]

[illegible]

[illegible]

[illegible]

I. Corre[illegible]

A. [illegible]

B. [illegible]

II. The [illegible]

A. S[illegible]

B. [illegible]

III. The [illegible]

Rehar[illegible]

[illegible]

I. Wh[illegible]

A.

B.

C.

D.

II. Rea[illegible]

A.

B.

C.

D.

E.

F.

TABLE OF CONTENTS

Page

LIST OF TABLES. . . . . .

LIST OF FIGURES . . . . . .

INTRODUCTION. 1

THEORETICAL 4

I. Correlation Functions in Spectroscopy 4

A. Calculation of Correlation Functions from Molecular Models. 9

B. The Correlation Function for Anisotropic Rotational Diffusion 13

II. The Theory of NMR Relaxation. 18

A. Spin-Lattice Relaxation. 18

B. Density Matrix Theory of NMR Relaxation. . . . 21

III. The Theory of Reorientational Broadening of Raman Bands 24

HISTORICAL. 38

I. NMR Relaxation Mechanisms 38

A. Dipole-Dipole Relaxation 38

B. Scalar-Coupled Relaxation. 41

C. Quadrupolar Relaxation.. 42

D. Spin-Rotational Relaxation 43

II. Rotational Motion in Liquids. 47

A. Modifications to the Bloembergen, Purcell and Pound-Debye Treatment. 47

B. Anisotropic Rotational Diffusion 49

C. Non-Diffusional Models 53

D. The Extended Diffusion Model 54

E. Experimental Tests of Extended Diffusion . . . 59

F. Investigations of Extended Diffusion by Visible and Infrared Spectroscopy. 62

Page

III. Plast

A.

B.

C.

METHODS

I. The W

A.

B.

C.

D.

E.

F.

II. Meas

A.

B.

C.

III. The E

IV. The R

V. Sample

A.

B.

C.

RESULTS . . .

I. Meas

II. Meas

III. Self

DISCUSSION. . .

Chapter Page

III. Plastic Crystals. 64

A. Phase Transitions in the Solid 64

B. Spectroscopic Studies of Phase Transitions . . 65

C. The Pople-Karasz Theory of Melting..... .68

EXPERIMENTAL

I. The NMR Spectrometer. 73

A. Introduction 73

B. The Pulse Spectrometer 78

C. The Computer Interface 81

D. The Probe. 90

E. Field Gradients for Diffusion Measurements . . 94

F. Temperature Control and Measurement. 97

II. Measurement of Relaxation Times 100

A. The Computer Program 100

B. Performance of the Computer-Controlled NMR System 107

C. Adjustments for Various Pulse Sequences. . . . 108

III. The External Lock 111

IV. The Raman Spectrometer. 118

V. Sample Preparation. 123

A. NMR Samples. 123

B. Raman Samples. 123

C. Preparation of Materials 126

RESULTS 127

I. Measurements of Spin-Lattice Relaxation Rates . . . 128

II. Measurements of Spin-Spin Relaxation Rates. 139

III. Self-Diffusion Coefficients 145

DISCUSSION. 155

PAGE

I. Gener

A.

B.

C.

D.

E.

II. NMR a

A.

B.

C.

D.

E.

III. Relax

IV. Coher

V. Spin-

A.

VI. Spin-

Summary . . . .

REFERENCES. . .

APPENDIX

A. RELAX

1.

2.

3.

Chapter Page

I. Raman and NMR Relaxation Studies of $CDCl_3$ and $CDBr_3$ 155

A. Introduction 155

B. Analysis of Raman Spectra of $CDBr_3$ and $CDCl_3$. 159

C. Effect of ^2D on Diffusional Motion 165

D. Deuteron Quadrupole Coupling Constants 166

E. The Rotational Diffusion Tensor in $CDBr_3$ . . . 168

II. NMR and Raman Studies of CF_3CCl_3. 179

A. Determination of the Second Moment 181

B. Translational Diffusion in the Solid 182

C. Translational Diffusion in the Liquid. 190

D. Rotational Motion. 195

E. Demonstration of Isotropic Motion From Raman Data 200

III. Relaxation of ^{19}F in CF_3Br and CF_2Br_2 201

IV. Other Systems 212

V. Spin-Spin Relaxation. 218

A. Anamalous T_2 Behavior. 218

VI. Spin-Rotation Tensors 220

SUMMARY 229

REFERENCES. 233

APPENDIX A. 247

A. RELAX2. 247

1. Commands and Constants 247

2. Acquiring Data 248

Multiple Pulse Experiments 248

Two Pulse Experiments. 248

3. Display Routines 249

Extracting Data from Pulse Trains. 250

4.

5.

6.

3. Other

1.

2.

3.

4.

C. PMA-

1.

2.

3.

Chapter Page

4. The Discrete Data Set. 252
Fitting to an Exponential Decay. 252
5. Other Features 254
6. Listing. 259

B. Other Nicolet Programs. 300

1. Pulsed Field Gradient Timing and Data Collection 300
2. Triplet T_1 Timing and Data Collection. 301
3. Calculation of the Second Moment of an Absorption Line. 308
4. Raman Correlation Function Division. 311

C. RMANFIT 313

1. Operation. 313
2. Suggestions for Improvements 315
3. Listing. 317

The relat

spectral

Experiment

action in

Experiment

Activation

processes

The outcu

determine

A comparis

temperatu

Measured

the sampl

300° K.

Spin-latt

Spin-lat

15.07 MH

Spin-lat

Spin-lat

Spin-lat

Spin-la

LIST OF TABLES

TABLE		Page
1	The relationships between the Cartesian and spherical components of a 3x3 tensor.	31
2	Experimental measurements of anisotropic motion in liquids	52
3	Experimental tests of extended diffusion.	60
4	Activation energies for nuclear relaxation processes in plastic crystalline solids.....	69
5	The output from the "pulse booster" unit as determined by the input from the computer	89
6	A comparison of experimentally determined temperatures with accepted literature values.	101
7	Measured values of temperature gradients across the sample area of the probe for temperatures below 300° K.	102
8	Spin-lattice relaxation rates in CF_3CCl_3.	128
9	Spin-lattice relaxation rates in CF_3CCl_3 at 15.87 MHz	130
10	Spin-lattice relaxation rates of ^2D in $CDBr_3$.	131
11	Spin-lattice relaxation rates of ^{19}F in CF_3Br	132
12	Spin-lattice relaxation rates of ^{19}F in CF_2Br_2. . . .	134
13	Spin-lattice relaxation rates of ^{19}F in CF_2ClCCl_3 . .	135

Spin-latt

Spin-latt

Spin-latt

Spin-spin

Spin-spin

Spin-spin

Spin-spin

Spin-spin

Determina

of the se

Determina

of the se

Mean lif

Mean co

$CCBr_3$ -

NMR and

coupling

The rela

constant

The temp

relaxat

Physical

Table | Page

14 Spin-lattice relaxation rates of ^{19}F in $CFCl_2CFCl_2$. . 136

15 Spin-lattice relaxation rates of ^{19}F in CF_3I. 137

16 Spin-lattice relaxation rates of ^{19}F in CF_3CF_3. . . . 138

17 Spin-spin relaxation rates of ^{19}F in solid CF_3CCl_3. . 139

18 Spin-spin relaxation rates of ^{19}F in liquid CF_3CCl_3 . 140

19 Spin-spin relaxation rates of ^{19}F in CF_2Br_2 141

20 Spin-spin relaxation rates of ^{19}F in CF_3CF_3 142

21 Spin-spin relaxation rates of ^{19}F in CF_2ClCCl_3. . . . 143

22 Determination of the field gradient and measurement of the self-diffusion coefficient in CF_3CCl_3. 145

23 Determination of the field gradient and measurement of the self-diffusion coefficient in CF_3Br. 146

24 Raman linewidth measurements. 148

25 Raman correlation times reported for $CDCl_3$ and $CDBr_3$ 163

26 NMR and Raman results and deuteron quadrupole coupling constants in $CDCl_3$ and $CDBr_3$ 164

27 The relations between coupling constants, force constants, and structure for sp^3 hybridized carbon. . 167

28 The temperature dependence of ^{13}C spin-lattice relaxation in $CDBr_3$ 169

29 Physical properties of $CDCl_3$ and $CDBr_3$. 178

[illegible]

[illegible] The contr[illegible]
spin-latt[illegible]
carried o[illegible]

[illegible] The contr[illegible]
spin-latt[illegible]
from the [illegible]
viscosity [illegible]

[illegible] Physical [illegible]

[illegible] Scribed [illegible]

[illegible] The contr[illegible]
the total [illegible]
from the [illegible]

[illegible] The contr[illegible]
the total [illegible]
from the [illegible]

[illegible] Spin-rota[illegible]
molecules [illegible]
chemical [illegible]
data. [illegible]

[illegible] Effectiv[illegible]
from the [illegible]
critical [illegible]

[illegible] Legal co[illegible]

[illegible] Useful a[illegible]

Table Page

30 The contribution of translational diffusion to spin-lattice relaxation in solid CF_3CCl_3 and the derived values of the mean jump time, τ_d. 189

31 The contribution of translational diffusion to spin-lattice relaxation in liquid of CF_3CCl_3 calculated from the self-diffusion coefficient or the macroscopic viscosity 192

32 Physical properties of CF_3CCl_3. 193

33 Smoothed relaxation rates in CF_3CCl_3. 194

34 The contribution of translational diffusion to the total relaxation rate in CF_3Br, calculated from the reported density and viscosity 205

35 The contribution of translational diffusion to the total relaxation rate in CF_2Br_2, calculated from the reported density and viscosity 206

36 Spin-rotation constants for ^{19}F in various molecules as determined from molecular beam (MB), chemical shielding (σ),or NMR relaxation (NMR) data. 224

37 Effective ^{19}F spin-rotation constants obtained from the spin-lattice relaxation rate at the critical point with the assumption of $\tau_J^* = 1.0$. 227

A1 Legal commands for RELAX2. 256

A2 Useful addresses 258

The

1 The rel
perturb
model.

2 Beam S

3 The eff
Equipr
tive co
cule ad
oblate
derived
the mol

4 The te
of the
crystal
are th
types

5 Plot of
reduce
molecu
open c

6 Block
VWR sa

7 Timing
of rf

LIST OF FIGURES

Figure		Page
1	The relationship between τ_θ and τ_J for the perturbed free rotor model and the Debye model	14
2	Raman 90° scattering geometry	27
3	The effect of axial ratio n and the angle θ_0 upon the ratio τ_{eff}/τ_c: τ_{eff} is the effective correlation time obtained by assuming the molecule as (a) a small prolate spheroid, (b) a small oblate spheroid, and τ_c is the correlation time derived by the Debye-Bloembergen theory, assuming the molecule as a small sphere	51
4	The temperature dependence of the second moment of the resonance line for a typical plastic crystalline solid, hexamethylethane. Also shown are the second moments calculated for different types of motions	67
5	Plot of reduced transition temperature (T_t^*) and reduced melting temperature (T_m^*) versus Γ for molecular crystals. Solid points are T_m^* data, open circles T_t^* data	72
6	Block diagram of computer-interfaced pulsed NMR spectrometer	76
7	Timing diagram (x axis to scale). (a) Timing of rf pulses. (b) internal timing in the	

Interfa

The

voltage

The arr

tured

the tra

Warning

allow

range

by Σ

Δ .

Interfa

are Th

are 1,

capaci

where

Detail

contro

The c

ferrin

Pulse

Wiring

those

The p

for ge

are 1,

Figure | Page

7 interface. The levels are 0 V and +5 V. (c) Timing of the interface output. Positive voltages are ∿2 V, negative voltages -15 V 77

8 The arrangement of crossed diodes and tuned cables for the purpose of isolating the transmitter from the receiver 80

9 Modification of the tuned spectrometer to allow nuclei to be observed in the frequency range 4-30 MHz. Crossed diodes are denoted by ⧅, low-noise amplifiers are denoted by ▷ 82

10 Interface circuit diagram. All npm transistors are T1S98; all pnp are 2N3645. All resistors are 1/4 w 7.5 kΩ except where noted; all capacitors are 10,000 pfd 500 VDC mica except where noted 83

11 Details of the switching circuit for $T_1/T_{1\rho}$ control 85

12 The circuit diagram of the switch for transferring control of the spectrometer from the pulse programmer to the computer. The other wiring details of all IC's are identical with those shown on the top IC 87

13 The pulse booster circuit and the circuit for generating a third pulse. All resistors are 1 kΩ, 1/4 W, except as noted 88

Figs

1 The log
grid c
2 Circuit
3 Photogr
ment of
and the
4 The cir
field-g
the cur
5 Detail
general
6 General
for th
7 Basic
than t
gradie
Pulse
8 Correc
train
9 The pr
10 The ar
trans-
lock.
11 The c
and re

Figure Page

14 The logical circuit for generating the third pulse 89

15 Circuit diagram of the probe. 91

16 Photograph of the probe showing the placement of the Dewar, the field gradient coils and the external lock 92

17 The circuit for providing a variable-length field-gradient pulse by means of altering the current to the z-shim coils 96

18 Details of the coils and coil form for generating a pulsed field gradient. 98

19 Generalized flow diagram of the software for timing and measurement control. 104

20 Basic timing for sequences involving more than two pulses. (a) the pulsed field-gradient sequence, and (b) generalized multiple-pulse sequence. 106

21 Correctly adjusted phasing as shown by a train of 90° pulses 110

22 The probe circuit for the external lock 113

23 The arrangement of modulation coils and transmitter/receiver coil in the external lock. 114

24 The circuit for coupling the transmitter and receiver in the external lock 116

Figs

[illegible] A block
circuit
[illegible] The co
experi
[illegible] A block
record
[illegible] The de
relaxa
tangen
[illegible] A semi
versus
secuen
degree
[illegible] A typi
degree
time
from w
calcul
[illegible] Polari
spectr
tion c
Loren
(
[illegible] Polari
(
Polari

Figure Page

25 A block diagram of the external lock circuit 117

26 The optical train for the Raman scattering experiment. 119

27 A block diagram of the apparatus for digitally recording Raman lineshapes. 121

28 The design of 5 mm NMR sample tubes for relaxation time measurements up to the critical temperature 124

29 A semi-logarithmic plot of magnetization versus time in the 180°-τ-90° T_1 measuring sequence, showing the typical linearity and degree of scatter observed 144

30 A typical KINFIT plot of experimental and theoretical values of magnetization versus time in the two-pulse spin echo experiment, from which the diffusion coefficient is calculated. 147

31 Polarized spectrum (——), depolarized spectrum(· · ·), and calculated convolution of the polarized component with a Lorentzian reorientational spectrum (- - -), for the 222 cm^{-1} line of $CDBr_3$ 149

32 Polarized spectrum (——), depolarized spectrum (· · ·), and calculated convolution of the polarized component with a Lorentzian

Fig.

2 recrie
SCL cm
2 Polari
spectr
of the
recrie
2250 cm
34 Polari
(...
polari
orienta
cm^{-1} ;
35 Polari
(...
polari
orient
cm^{-1} ;
36 Polari
(...
polari
orient
cm^{-1} ;
37 Corre
Raman
of the

Figure Page

32 reorientational spectrum (- - -), for the 521 cm^{-1} line of $CDBr_3$. 150

33 Polarized spectrum (——), depolarized spectrum (· · ·), and calculated convolution of the polarized component with a Lorentzian reorientational spectrum (- - -), for the 2250 cm^{-1} line of $CDBr_3$ 151

34 Polarized spectrum (——), depolarized spectrum (· · ·), and calculated convolution of the polarized component with a Lorentzian reorientational spectrum (- - -), for the 650 cm^{-1} line of $CDCl_3$. 152

35 Polarized spectrum (——), depolarized spectrum (· · ·), and calculated convolution of the polarized component with a Lorentzian reorientational spectrum (- - -), for the 2256 cm^{-1} line of $CDCl_3$. 153

36 Polarized spectrum (——), depolarized spectrum (· · ·), and calculated convolution of the polarized component with a Lorentzian reorientational spectrum (- - -), for the 714 cm^{-1} line of CF_3CCl_3. 154

37 Correlation functions calculated from $CDBr_3$ Raman lines; (a) uncorrected low frequency side of the 521 cm^{-1} line, (b) low frequency side

of the

preser

cuency

Spin-l

temper

^{13}C-br

cycle-

tion ra

(^{13}C)

The te

to the

scalar

reorier

The te

to the

couplin

orierta

tropic

J_{C3r} =

Spin-l

solid

The te

tion a

depend

in so

Figure Page

of the 521 cm^{-1} line corrected for the presence of a hot band, and (c) low frequency side of the 222 cm^{-1} line. 160

38 Spin-lattice relaxation rates as a function of temperature for ^{2}D in $CDBr_3$ (O), and ^{13}C in $^{13}CHBr_3$ (|_|). Also shown are the calculated dipole-dipole contribution to the ^{13}C relaxation rate (- - -), and [$R_{1,total}(^{13}C) - R_{1,dd}(^{13}C)$](●). 172

39 The temperature dependence of the contribution to the ^{13}C relaxation rate in $^{13}CHBr_3$ from scalar coupling to ^{79}Br, assuming isotropic reorientation 175

40 The temperature dependence of the contribution to the ^{13}C relaxation rate in $^{13}CHBr_3$ from scalar coupling to bromine predicted by (a) isotropic reorientation with J_{CBr} = 91 Hz (——), and (b) anisotropic reorientation with $E_{a,sc}$ = 1.59 kcal/mole, J_{CBr} = 55 Hz and $D_{||}/D_{\perp}$ = 1.49 at 20° C (- - -) . . .177

41 Spin-lattice relaxation of ^{19}F in liquid and solid CF_3CCl_3 180

42 The temperature dependence of spin-spin relaxation and the temperature and frequency dependence of spin-lattice relaxation in solid CF_3CCl_3. 183

Figure

43 The te
the
44 The te
loss c
solid
45 A comp
between
extend
46 The te
relaxa
contr
47 The te
arc s
a sepa
or the
diffus
depend
dipole
relaxa
48 Choice
49 The te
diffus
two-p
compar
as de
for c

Figure Page

43 The temperature dependence of the width of the ^{19}F resonance line in solid CF_3CCl_3 187

44 The temperature dependence of the mean jump time for translational diffusion in solid CF_3CCl_3 188

45 A comparison of the experimental relations between τ_θ^* and τ_J^* with the predictions of the extended diffusion model. 199

46 The temperature dependence of spin-lattice relaxation in CF_3Br, and the calculated contribution from translational diffusion 202

47 The temperature dependence of spin-lattice and spin-spin relaxation in CF_2Br_2, showing a separation into different contributions based on the calculated contribution from translational diffusion and equal but opposite temperature dependence of $R_{1,dd}$ and $R_{1,sr}$. The dipole-dipole relaxation rate predicted from dielectric relaxation data is given by (●). 203

48 Choice of axes for the CF_2Br_2 molecule. 208

49 The temperature dependence of the self-diffusion coefficient (D_S) measured by the two-pulse, steady gradient, spin-echo method, compared with the temperature dependence of D_S as derived from the macroscopic viscosity and density for CF_3Br 211

Figure Page

50 The temperature dependence of the spin-lattice spin-relaxation rate of ^{19}F in liquid and solid CF_2ClCCl_3 and the spin-spin relaxation rate in the liquid 213

51 The temperature dependence of the spin-lattice relaxation rate of ^{19}F in solid and liquid $CFCl_2CFCl_2$ 214

52 The temperature dependence of the spin-lattice and spin-spin relaxation rate of ^{19}F in CF_3CF_3 215

53 The temperature dependence of the spin-lattice relaxation rate of ^{19}F in liquid CF_3I. 216

54 The temperature dependence of the spin-spin relaxation rate of ^{19}F in solid CF_2ClCCl_3 217

55 The temperature dependence of the difference R_2-R_1 for various fluorohalocarbons, (O) CF_3CCl_3, (|_|) CF_2Br_2, and (●) CF_2ClCCl_3 219

A1 Core map of RELAX2. 255

A2 Flow chart for the operation of RELAX2. 257

INTRODUCTION

Nuclear magnetic relaxation studies have been extremely useful in understanding the details of molecular motion in fluids. This is especially true for nuclei which have large spin-rotational contributions to the relaxation rate, as information about the correlation of angular momentum is important in terms of testing a molecular model but difficult to obtain by other methods. To date, studies which rigorously test a model of molecular reorientation have been performed solely on molecules of rather special nature. Since the predictions of the extended diffusion model have been borne out very well for those molecules, it would be of interest to attempt such a rigorous study on molecules of a more common nature. To this end, ^{19}F spin-lattice relaxation measurements have been performed on molecules of C_{3v} symmetry containing $-CF_3$ groups (CF_3CCl_3, CF_3CF_3, CF_3Cl, CF_3Br, and CF_3I) to varying degrees of thoroughness. In addition, less symmetric molecules containing other $-CF_2$ and -CF- groups were investigated to aid in understanding the results in the $-CF_3$ containing molecules.

A major problem in NMR relaxation studies is that there are often too many unknowns for precise values of the correlation times to be determined. To alleviate this difficulty, the NMR data may be augmented with Raman line-shape data, which can reduce by one the number of NMR unknowns by supplying the rotational correlation time. Although variable-temperature Raman data would be most useful, even a single room-temperature measurement would be helpful. In this investigation,

-ly large de
ture data, a
-to be relate
ly, and also
ne of cosmo
mmensible in
ture of the
-ly experime
tricular acti
ne microscopi
ruse from t
ction, and t
ms of a spe
he theoret
ticular part o
tory function
to now now a
ll of molecula
ller now this
tical effects
ements which
tory function
introducing of
he Historic
tracting the
ternal measu

a single Raman measurement in conjunction with NMR temperature-dependent relaxation data, has been used to separate the spin-rotational contribution to the relaxation rate from the dipole-dipole contribution in CF_3CCl_3, and also to determine the coupling constants (J_{FCl} in CF_3CCl_3 and the ^2D quadrupole coupling constant in $CDCl_3$ and $CDBr_3$) which are not observable in the high-resolution spectrum due to the rapid relaxation of the quadrupolar nucleus.

Any experimental measurement which is sensitive to the details of molecular motion may be divided into two parts; the determination of the microscopic parameter(s) of interest (correlation times, in this case) from the measured macroscopic property (namely, the relaxation time), and the interpretation of the microscopic parameter(s) in terms of a specific model for molecular motion.

The Theoretical section of this dissertation will consider only the latter part of this problem by discussing the role of time correlation functions in spectroscopy. The result of this section will be to show how a correlation function is calculated from a given model of molecular motion. This approach is taken in order that it be clear how this correlation function may then be applied to explain motional effects in many seemingly diverse experiments. The two experiments which will be discussed explicitly in terms of this correlation function are NMR relaxation through molecular motion and the broadening of Raman lines.

The Historical section will address itself to current methods of extracting the microscopic parameters of interest from the experimental measurements. The experiments most pertinent to the

present work will be those which transcend the boundaries of the NMR experiment for a better understanding of the motions responsible for spin-lattice relaxation.

Accurate and rapid measurements of relaxation times are generally more conveniently performed when a computer handles a major portion of the experimental details. A considerable section of this work is devoted to describing a computer-controlled two-pulse NMR spectrometer which, within its design specifications, is extremely versatile and was used to acquire nearly all of the NMR data discussed herein.

THEORETICAL

I. Correlation Functions in Spectroscopy

Although the early development of NMR relaxation theory was in terms of time correlation functions, in learning this theory one rather rapidly discards correlation functions for correlation times and consequently misses much of the significance of the correlation function approach. Recently many diverse non-equilibrium phenomena have been discussed in terms of time correlation functions. There exist a large number of excellent reviews on the use of time correlation functions[1-5]; the best introductory articles in this field are those of Zwanzig[1] and Gordon[2]. Of particular concern to this investigation is the time correlation function describing the rotational motion of molecules in fluids, which must be governed by the anisotropic part of the intermolecular potential. While classical methods of investigating fluids, such as measurements of viscosity or heat capacity, are insensitive to angle-dependent intermolecular forces, spectroscopic methods such as NMR relaxation times and Raman and IR lineshapes are affected by these types of forces. The time correlation function approach provides that the broadening of spectral lines and the change in NMR relaxation times with temperature (and other effects) be treated on a common basis.

The classical definition of a time correlation function for two dynamical properties A and B may be stated as

$$C_{AB} = \langle A(0) \cdot B(t) \rangle \qquad (1)$$

[illegible] proceed

[illegible] differe

[illegible] we [illegible]

[illegible]

[illegible] correlati

[illegible] at time

[illegible] the [illegible]

[illegible] is possi

[illegible] pro

[illegible] the [illegible]

[illegible] is [illegible]

[illegible] the [illegible]

[illegible] crossing

[illegible] lines.

[illegible] that is,

[illegible] proceed

[illegible].

[illegible] the corre

[illegible] tion is

[illegible] knowledge

[illegible] probabili

[illegible] observing the

[illegible] value y_1 a

[illegible] calculated fr

[illegible] is a fu

[illegible] be found to

where the brackets indicate an equilibrium ensemble average. When A and B are different properties C_{AB} is termed a cross-correlation function, when they are identical C_{AA} is termed an auto-correlation function.

A correlation function tells concisely how a given dynamical property at time t correlates with its value at time t=0. One could calculate the time correlation functions by this method: Imagine that it is possible to follow the motion of a single molecule and the dynamical property p(t) is the orientation of the molecular dipole moment. One measures its orientation at time t=0 and at time t; the correlation is the projection of p(t) on p(0). To get an average value for the function one repeats this experiment a large number of times choosing various reference times t=0, and averages over the starting times. If the usual assumption is made that the system is ergodic, that is, ensemble averages are the same as time averages, then this procedure will give a time correlation as defined by Equation (1).

A time correlation function can be calculated no matter what type of motion is occurring, however, usually the motion is random and the knowledge of its time dependence is in the form of a conditional probability function $P(y_2,y_1|t_2,t_1)$ which gives the probability of observing the dynamical variable with value y_2 at time t_2 if it had a value y_1 at time t_1. The time correlation function may then be calculated from P as follows: If y is a random function of time and f(y) is a function of y then the average value of f at time t_1 will be found to be

the average

when the pr

result is of

$$f(t_2-t_1)$$

introduce $P(y_1,$

time to the c

form

$$P(y_1,t_1$$

before

$$f(t_2-t_1) = \int$$

the carrier ass

that the ran

they are in

this process.

$$\overline{f(t_1)} = \int P(y_1,t_1)f(y_1)dy_1 \tag{2}$$

and the average value at time t_2 will similarly be

$$\overline{f(t_2)} = \int P(y_2,t_2)f(y_2)dy_2. \tag{3}$$

If we form the product $f(t_1)\cdot f(t_2)$ and then perform the averaging, the result is clearly a time correlation function,

$$G(t_2-t_1) = \overline{f(t_1)\cdot f(t_2)}$$

$$= \iint P(y_1,t_1)P(y_2,t_2)f(y_1)f(y_2)dy_1dy_2. \tag{4}$$

The product $P(y_1,t_1)\cdot P(y_2,t_2)$ is a joint probability function and is related to the conditional probability function P by the obvious relation

$$P(y_1,t_1)\cdot P(y_2,t_2) = P(y_1,t_1)P(y_1,y_2;t_1,t_2), \tag{5}$$

therefore

$$G(t_2-t_1) = \iint P(y_1,t_1)P(y_1,y_2;t_1,t_2)f(y_1)f(y_2)dy_1dy_2. \tag{6}$$

Some common assumptions made in the theory of random processes[6] are that the random functions are Gaussian and are stationary; that is, they are invariant to a shift of the time axis, and the process is a Markoff process. In a Markoff process the function P does not depend on

error to b
correlator
the correla
research
transform
or equati
also appear
ction of the
the only by
real transi
ment of the
the inform
the correla
sence of tr
tice the
tude too
the relsend
be obtained[2]
es for examp

$I(_$

the various
the spec
dependent s
to obtain t
her expansio

times prior to t_1. If, and only if, these assumptions hold, then the time correlation functions are exponential[7].

Time correlation functions appear in spectroscopy in two ways: in the Heisenberg description of the frequency spectrum as the Fourier transform of the appropriate time correlation function and also in an equation for the transition rate. The difference between these two appearances is that a spectrum is the complete Fourier transform of the time correlation function (the "spectral density") limited only by the resolution and sensitivity of the instrument, whereas a transition rate constant measures only a single frequency component of the spectral density. Obviously then, a spectrum gives much more information than a transition rate (relaxation time) about its time correlation function. While in principle the frequency dependence of transition rates would provide additional information, in practice the frequencies at which they are measured are orders of magnitude too low for any frequency dependence to be observed.

The Heisenberg expression for the shape of an absorption band may be obtained[2] from the corresponding Schrödinger expression, where for example the infrared absorption is given by

$$I(\omega) = 3 \sum_i \sum_f \rho_i |\langle f|\hat{\varepsilon}\cdot\vec{\mu}|i\rangle|^2 \delta(\omega_{fi}-\omega) \qquad (7)$$

and the various terms have their usual meaning. In the Schrödinger picture the spectrum is viewed as the set of transitions between the time-dependent states $|i\rangle$ and $|f\rangle$.

To obtain the Heisenberg expression from this we introduce the Fourier expansion of the δ-function

expressing

motion

In an isotr

I

Heisenberg p

the time corr

the ascending mo

An equivale

expression for t

W_{f}

where W_{f-i} is t

We let

$$\delta(\omega) = \frac{1}{2\pi}\int_{-\infty}^{\infty} e^{i\omega t}dt \tag{8}$$

and, expressing the dipole moment operator in the interaction representation,

$$\hat{\mu}(t) = e^{i\mathcal{H}t/\hbar}\hat{\mu}e^{-i\mathcal{H}t/\hbar}; \tag{9}$$

thus,

$$I(\omega) = \frac{3}{2\pi}\int_{-\infty}^{\infty} dte^{-i\omega t}\langle\hat{\varepsilon}\cdot\hat{\mu}(0)\hat{\varepsilon}\cdot\hat{\mu}(t)\rangle, \tag{10}$$

and for an isotropic system

$$I(\omega) = \frac{1}{2\pi}\int_{-\infty}^{\infty} dte^{-i\omega t}\langle\hat{\mu}(0)\cdot\hat{\mu}(t)\rangle. \tag{11}$$

The Heisenberg picture views the spectrum as the Fourier transform of the time correlation function for the dipole moment operator of the absorbing molecules.

An equivalent transformation can be done to the Schrödinger expression for the transition rate[5]

$$W_{f\leftarrow i} = \frac{1}{i\hbar^2}\left|\int_0^t \langle f|\mathcal{H}_1(t)|i\rangle e^{-i\omega_{fi}t}dt\right|^2, \tag{12}$$

where $W_{f\leftarrow i}$ is the average over some time interval t and $\omega_{fi} = (E_f-E_i)\hbar$. If we let

$$K_{fi}(t) = \langle f|\mathcal{J}C_1(t)|i\rangle,$$

Equation (12) becomes[5]

$$\langle W_{f\leftarrow i}\rangle = \frac{1}{\hbar^2}\int_{-\infty}^{\infty} d\tau G_{fi}(\tau)e^{-i\omega fi\tau}. \qquad (13)$$

This same type of expression was obtained by Callen and Welton[8] in an extension of the Nyquist relation for electrical circuits and is known as the fluctuation-dissipation theorem since it relates the power dissipated by the system, $I(\omega)$, to the function $\langle\mu(0)\cdot\mu(t)\rangle$ which describes the way spontaneous fluctuations return to equilibrium. The advantages of the Heisenberg picture have been thoroughly discussed by Gordon[2,9].

A. Calculation of Correlation Functions from Molecular Models

Two simple models of rotational motion exist and the time correlation functions calculated from these models may be considered as limiting cases for possible time correlation functions of real liquids. The parameters which emerge from any of these models which are pertinent to NMR relaxation theory are the correlation time for angular orientation, τ_θ, and the correlation time for angular momentum, τ_J.

An excellent physical picture which explains the relationship between τ_J and τ_θ has been given by Green and Powles[10] and bears repeating here. Consider a molecule undergoing rotational diffusion in a liquid. Since the rotational step size is very small,

a large number of diffusive steps will be required before an arbitrary vector with orientation Ω_o reaches orientation $\Omega_o + \delta\Omega$, where $\delta\Omega \approx 1$ radian. Consequently many diffusive steps will be necessary before the orientation becomes uncorrelated. But since the molecular angular momentum undoubtedly changes with each diffusive step, τ_J may be associated with the time between collisions and $\tau_J \ll \tau_\theta$. Now suppose the collisions occur less frequently and the step sizes begin to increase. The angular momentum correlation time increases while, since the path traversed by the orientation vector is shorter, τ_θ decreases. This trend continues until the step size is such that the orientation is uncorrelated after a single step, hence $\tau_J = \tau_\theta$.

The first model is the perturbed free-rotor model[11] in which the molecule is depicted as undergoing essentially free rotation, governed by the molecular inertia tensor, but is occasionally interrupted by a collision. The resulting time correlation function may be calculated from Equation (1). For example, for a linear molecule $G_n(t) = P_n(\cos\omega t)$, where n indicates which spherical harmonic the dynamical variable transforms as, and ω is the rotational frequency. Averaging over an ensemble of such molecules is accomplished by integrating over a Boltzmann distribution, so

$$\langle P_n(\cos\omega t)\rangle = \int_o^\infty P_n(\cos\omega t)\omega\exp(-\tfrac{1}{2}\omega^2)d\omega. \qquad (14)$$

This integral has been obtained numerically by Gordon[9]; also, the problem has been examined more generally[12]. The relationship between τ_θ and τ_J for this model is $\tau_\theta = \tau_J/(2J+1)$. One would not expect this description of rotational motion to be too good for

the liquid state, except perhaps as the critical point is approached.

A more liquid-like theory is the rotational diffusion theory originally formulated by Debye[13] to explain the anamolous dispersion of radiofrequency waves in liquids. In this model the molecular reorientation occurs through a large number of angular steps of vanishingly small size. The molecule is treated as a sphere embedded in a viscous fluid where the retarding force is given by Stokes' Law, $f = 8\pi a^3\eta$, where a is the molecular radius and η is the macroscopic viscosity. By analogy

$$\frac{\partial}{\partial t} P(\Omega_o,\Omega;t) = -D\nabla^2 P(\Omega_o,\Omega;t), \tag{15}$$

in the isotropic case with no external forces; here $P(\Omega,t)$ is the conditional probability function for the coordinates and time interval t, D is the rotational diffusion coefficient, and ∇^2 is the Laplacian operator. We examine the motion of a vector over the surface of a sphere by subjecting the Laplacian to the condition $\frac{\partial}{\partial r} = 0$. The coordinates Ω now become the polar angles θ and ϕ.

The solution can be written in terms of the eigenfunctions of ∇^2 (the spherical harmonics),

$$\nabla^2 Y_\ell^m(\Omega) = -\ell(\ell+1)Y_\ell^m\Omega, \tag{16}$$

as

$$P(\Omega_o,\Omega;t) = \sum_{\ell,m} Y_\ell^{m*}(\Omega_o)Y_\ell^m(\Omega)e^{-E_\ell t}, \tag{17}$$

$w(t) = L(t)$

$L(t)_0 = \int$

The graphical

σ_{max}, P_{max} cos

figure in

σ_{yd} will be

assessed in

$\dot{L}(t) = 0.$

The graphic

(1) The

(2) Ro

fi

re

fo

fo

(3) Th

is

co

in

wh

ti

The failur

stress, as was

where $E = \ell(\ell+1)D$. Then, from Equation (6)

$$G(t-t_o) = \iint P(\Omega_o)\sum_{\ell,m} Y_\ell^{m*}(\Omega_o)Y_\ell^m(\Omega)e^{-E_\ell t}f(\Omega_o)f(\Omega)d\Omega_o d\Omega. \qquad (18)$$

If the dynamical variable can be written in terms of a spherical harmonic $P_n(\cos\Omega)$ then, from the orthonormal properties of P_n, a single term in the sum in Equation (18) will be picked out, the integral will become trivial, and the time correlation function may be expressed in terms of a single exponential with time constant $\ell(\ell+1)D = \tau$.

The difficulties with the Debye treatment are:

(1) The particle is treated as a sphere.

(2) Rotation is described as a sphere turning in a viscous fluid, i.e., a "stick" boundary condition. (However, recently friction coefficients have been calculated[14] for a "slip" boundary condition, namely, zero friction for rotation about a symmetry axis.)

(3) The short time behavior of the time correlation function is not correct. The requirement that a classical time correlation function be symmetric with respect to time inversion implies[5] that

$$\left.\frac{d^nG}{dt^n}\right|_{t=0} = 0 \quad \text{for } n \text{ odd}, \qquad (19)$$

which is clearly at variance with the non-zero derivatives of an exponential function.

The failure of the Debye model is in not considering inertial effects, as was done in the perturbed free-rotor model, since even

which allow
correlation fu
The relation be
in Figure 1.
ridge model app
minimas when t_b
considered which on
very consistent
satisfaction both
Evidently, the

The correlation

The well-known

describes the
the time t, may b
the significantly
Theory in which
previous step[17].
considered the an
defined an expon
the previous sect
describe the r
derived in terms

models which allow large-step reorientation result in exponential time correlation functions[15,16].

The relation between τ_θ and τ_J for these two simple models is shown in Figure 1. In terms of the time between collisions (t_{bc}) the Debye model applies when $t_{bc} \ll \tau_\theta$ and the perturbed free rotor model holds when $t_{bc} \gg \tau_\theta$. In a later section a model will be considered which bridges the intermediate region between these two cases by considering the rotational time correlation function to be a function both of time and of the time between collisions (equivalently, the length of a diffusive step).

B. The Correlation Function for Anisotropic Rotational Diffusion

The well-known equation for isotropic translational diffusion

$$\frac{\partial}{\partial t} P(\vec{r},t) = -D\nabla^2 P(\vec{r},t), \tag{20}$$

which describes the probability P that a molecule will be at location $\vec{r}$ at time t, may be derived by a conservation of mass argument or, more significantly, by a random walk mechanism originally due to Einstein in which the particle completely loses the memory of the previous step[17]. In his monograph on polar molecules, Debye[13] considered the analogous case of isotropic rotational diffusion and obtained an exponential time correlation function as discussed in the previous section. This treatment was later generalized by Perrin[18] to describe the rotational diffusion of an ellipsoid and then re-derived in terms of the eigenfunctions and eigenvalues of a

Figure 1. The re
rotor

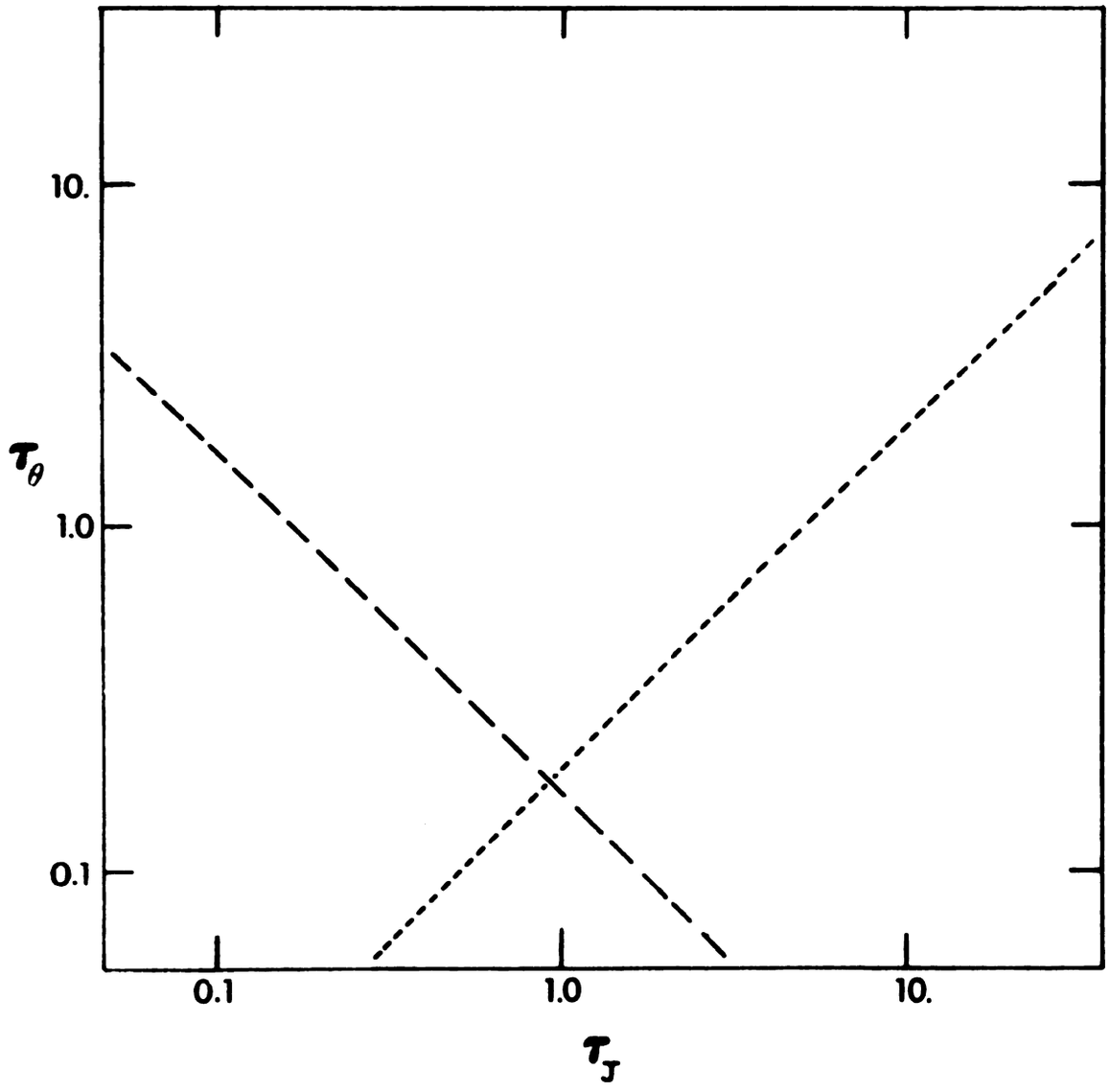

Figure 1. The relationship between τ_θ and τ_J for the perturbed free rotor model and the Debye model.

[illegible]-mechanical m[illegible]

[illegible]ure for NMR [illegible]

[illegible] have been [illegible]

[illegible] and [illegible]ness [illegible]

[illegible]'s paper.

[illegible]'s result [illegible]

$$\frac{\partial}{\partial t}$$

[illegible] is the dimen[illegible]

[illegible] molecule [illegible]

[illegible] tensor also [illegible]

[illegible] axes

[illegible]order to cal[illegible]

[illegible] is convenien[illegible]

[illegible] which are a c[illegible]

[illegible] angles $\Omega = \alpha,\beta$[illegible]

[illegible] of a linear co[illegible]

$$P(\Omega,t$$

[illegible] the expansion [illegible]

$$\alpha^{J}_{K,}$$

quantum-mechanical rigid rotor by Favro[19]. The correlation functions appropriate for NMR of a particle undergoing anisotropic rotational diffusion have been calculated by Woessner[20] using the notation of Perrin, and Huntress[21] has recently reviewed the relevant sections of Favro's paper.

Favro's result for a completely random process is[21]

$$\frac{\partial}{\partial t} P(\Omega,t) = -\hat{L}\cdot\bar{\bar{D}}\cdot\hat{L}\ P(\Omega,t), \tag{21}$$

where $\hat{L}$ is the dimensionless angular momentum operator. In a symmetric top molecule the coordinate system which diagonalizes the inertia tensor also diagonalizes the diffusion tensor, so Equation (21) becomes

$$\frac{\partial}{\partial t} P(\Omega,t) = -\sum_{i=1}^{3} D_{ii}\hat{L}_i^{\,2}P(\Omega,t). \tag{22}$$

In order to calculate a time correlation function from Equation (22) it is convenient to introduce the Wigner rotation matrices[22] $D^J_{KM}(\Omega)$ which are a complete orthonormal set spanning the space of Euler angles $\Omega = \alpha,\beta,\gamma$. Consequently, the probability function P in terms of a linear combination of rotation matrices becomes

$$P(\Omega,t) = \sum_{J=0}^{\infty} \sum_{K,M=-J}^{J} a^J_{K,M}(t)\ D^{J*}_{K,M}(\Omega)\,, \tag{23}$$

with the expansion coefficient

$$a^J_{K,M}(t) = \ d\Omega P(\Omega,t)D^J_{K,M}(\Omega)\left[\frac{2J+1}{8\pi^2}\right]. \tag{24}$$

all the time d

we place E

the quantum-me

ones are eigen

of one compo

$$\ldots_{(K,M)} = M^2 \ldots$$

omitting the firs

we have

$$\sum_{i=1}^{3} \ldots$$

$\ldots_{11} = D_{22} = D$

Thus, substitu

applying through

the rotation ma

$$\frac{\partial}{\partial t} a^J_{K,M}(t$$

equation is r

$$a^J_{K,M}(t) =$$

Since all the time dependence is now in the expansion coefficient $\alpha^J_{K,M}(t)$, we place Equation (23) in (22) to obtain

$$\sum_{J=0}^{\infty}\sum_{K,M=-J}^{J} D^{J*}_{K,M}(\Omega)\,\frac{\partial\alpha^J_{K,M}(t)}{\partial t} = -\sum_{i=1}^{3} D_{ii}L_i^2\sum_{J=0}^{\infty}\sum_{M,K=-J}^{J}\alpha^J_{K,M}(t)D^{J*}_{K,M}(\Omega). \quad (25)$$

From the quantum-mechanical rigid-rotor problem we know that the D matrices are eigenfunctions of the total angular momentum operator $\hat{L}^2$, and of one component, which we may choose to be $\hat{L}_z$;

$$\hat{L}^2 D^J_{K,M}(\Omega) = \hbar^2 J(J+1)D^J_{K,M}(\Omega) \quad \hat{L}_z D^J_{K,M}(\Omega) = -\hbar M D^J_{K,M}(\Omega). \quad (26)$$

Rearranging the first summation on the right-hand side of Equation (25) we have

$$\sum_{i=1}^{3} D_{ii}\hat{L}_i^2 = D_\perp \hat{L}^2 + (D_{||}-D_\perp)\hat{L}_z^2, \quad (27)$$

where $D_{11} = D_{22} \equiv D_\perp$, $D_{33} \equiv D_{||}$ and $L_3 \equiv L_z$.

Thus, substituting Equation (26) and (27) into Equation (25), multiplying through by $D^J_{K,M}(\Omega)$, and employing the orthogonal properties of the rotation matrices we obtain

$$\frac{\partial}{\partial t}\alpha^J_{K,M}(t) = -[D_\perp J(J+1) + (D_{||}-D_\perp)M^2]\alpha^J_{K,M}(t). \quad (28)$$

This equation is readily integrated; we then have

$$\alpha^J_{K,M}(t) = \alpha^J_{K,M}(0)\exp\{-[D_\perp J(J+1)+(D_{||}-D_\perp)M^2]t\}. \quad (29)$$

coefficient at

makes allows u

with a corr

Eqns 23) and (

$$\Omega_0 =$$

through the

Ω:

$$\Omega$$

from Equations

$$\Omega_0(\hat{\Omega}_0 t) = \sum_{J=}$$

$\Omega_0 = D_\perp J(J+$

To calculate a

$\langle \Omega_0 \rangle = \sigma^J_{K,M}(\Omega)\rangle$

Use $p(\Omega_0)$ with

rotation, and o

The coefficient at zero time is found from the initial condition

$$P(\Omega,0) = \delta(\Omega_o-\Omega), \tag{30}$$

which also allows us to replace the function P in Equations (22) and (23) with a conditional probability function $G(\Omega_o,\Omega;t)$. From Equations (23) and (30) we have

$$\delta(\Omega_o-\Omega) = \sum_{J=0}^{\infty}\sum_{M,K=-J}^{J} \alpha^J_{K,M}(0)D^{J*}_{K,M}(\Omega) \tag{31}$$

which, through the orthogonality properties of the D matrices, requires that

$$\alpha^J_{K,M}(0) = D^J_{K,M}(\Omega_o)\,\frac{2J+1}{8\pi^2}\,. \tag{32}$$

Also, from Equations (23), (29), and (32) we have

$$G(\Omega_o,\Omega;t) = \sum_{J=0}^{\infty}\sum_{K,M=-J}^{J} \frac{2J+1}{8\pi^2}\,D^J_{K,M}(\Omega_o)D^{J*}_{K,M}(\Omega)e^{-t/\tau_m}, \tag{33}$$

where $1/\tau_m = D_\perp J(J+1) + (D_{||}-D_\perp)\,M^2$.

To calculate an actual time correlation function such as $\langle D^{J*}_{K,M}(\Omega_o)\cdot D^J_{K,M}(\Omega)\rangle$ we substitute Equation (33) into Equation (6), replace $p(\Omega_o)$ with $1/8\pi^2$, which is equivalent to an initial isotropic distribution, and obtain

$$C^{J*}_{K,M}(\theta,\phi)C^{J}_{K,$$

$$\times\, C^{J}_{K,M'(\theta,$$

ely, for any gi

ernment from th

result for Raman

clarified out t

ymmetric rotor fi

ction. Equatio

$$C^{J*}_{K,M'(}$$

es the number of

e the molecular

II.

Site-lattice R

Nuclei with s

fraction of N su

degeneracy in the

ated. The pop

Bloch equatio

$$<D^{J*}_{K,M}(\Omega_o)D^{J}_{K,M}(\Omega)> = \frac{1}{8\pi^2}\iint d\Omega_o d\Omega \sum_{J=0}^{\infty}\sum_{K,M=-J}^{J} \frac{2J+1}{8\pi^2}$$

$$\times D^{J}_{K,M}(\Omega_o)D^{J*}_{K,M}(\Omega)D^{J*}_{K,M}(\Omega_o)D^{J}_{K,M}(\Omega)e^{-t/\tau_m}. \qquad (34)$$

Clearly, for any given value of J, only a certain number of terms will be non-zero from the orthogonality relations. Thus if J=2, which is the result for Raman and NMR correlation functions, only five terms will be picked out from the infinite series in (34), and for an asymmetric rotor five correlation times will be necessary to describe the motion. Equation (34) is simplified to

$$<D^{J*}_{K,M}(\Omega_o)D^{J}_{K,M}(\Omega)> = \sum_{M=-J}^{J} \frac{1}{2J+1} e^{-t/\tau_m}, \qquad (35)$$

where the number of terms in the sum of exponentials is seen to depend upon the molecular symmetry.

II. The Theory of NMR Relaxation

A. Spin-Lattice Relaxation

Nuclei with spin $I \neq 0$ possess a magnetic moment and when a collection of N such nuclei is placed in a magnetic field H_0 the degeneracy in the 2I+1 states of different spin quantum number is removed. The populations of the various states are given by the Boltzmann equation

exists the spin

tronics

temperatures hig

$\mu_B B_0/kT$, so

In addition to

ing from an un

k, a sample of

ment of elect

separation bet

$$P_m = \exp\{-E_m/kT\}$$

$$= \exp\{-\hbar\, mH_o/kT\}, \tag{36}$$

where m is the spin quantum number. Thus, the induced bulk magnetism becomes

$$M_o = N_\gamma \hbar \frac{\sum_{m=-I}^{I} mP_m}{\sum_{m=-I}^{I} P_m} . \tag{37}$$

For temperatures higher than a few millidegrees Kelvin, $\exp(-E_m/kT) \simeq 1 + \hbar_\gamma mH_o/kT$, so

$$M_o = N_\gamma \hbar \frac{\sum m + \frac{\gamma \hbar H_o}{kT} \sum m^2}{\sum 1 + \sum m}$$

$$= N_\gamma{}^2 \hbar^2 \frac{I(I+1)}{3kT} . \tag{38}$$

In addition to absorbing energy from the static (Zeeman) field in going from an unmagnetized state to a state described by Equation (38), a sample of nuclear magnets may interact with the magnetic component of electromagnetic radiation through resonant absorption. The separation between states ($\Delta m = \pm 1$) is

$$\Delta E = \gamma \hbar H_o . \tag{39}$$

being the energ

[illegible]

[illegible] is the basic e

the frequency o

The approach o

and M_g as the Z

the resonant

the constant T_1,

as follows.

Consider a sys

M_g. The diff

M_g is

[illegible]

M_{2c} is a tran

M_{2c} the stead

the purposes of

[illegible] for making

[illegible]ution, which

[illegible] can be ex

[illegible]

M_2

Expressing the energy difference in terms of frequency, $\Delta E = \hbar\omega$, we obtain

$$\omega = \gamma H_0, \tag{40}$$

which is the basic equation relating the strength of the static field and the frequency of the resonant radiation.

The approach of the magnetization to equilibrium, whether from zero to M_0 as the Zeeman field is turned on, or the return to M_0 after the resonant radiation is turned off, may be characterized by a time constant T_1, the spin-lattice relaxation time. This can be shown as follows.

Consider a system S characterized by eigenstates $|\alpha\rangle$ and populations P_α. The differential equation describing the time dependence of P_α is

$$\frac{dP_\alpha}{dt} = \sum_\beta W_{\alpha\beta}P_\beta - \sum_\beta W_{\beta\alpha}P_\alpha, \tag{41}$$

where $W_{\alpha\beta}$ is a transition rate of the form of Equation (12). Since $W_{\alpha\beta} = W_{\beta\alpha}$, the steady-state solution ($dP_\alpha/dt = 0$) of (41) is $P_\alpha = P_\beta$. For the purposes of this simple presentation we omit the <u>ad hoc</u> argument for making the steady-state populations follow the Boltzmann distribution, which is usually introduced at this point. The net magnetism can be expressed in terms of the time-dependent populations,

$$M_z(t) = \langle M_z(t)\rangle = N\hbar\gamma \sum_m mP_m(t), \tag{42}$$

ing the time

ing Equations

$\omega\tau = 1/2$,

$\omega\tau_1 = 2\omega$. How

ms arising fr

ngle time consta

ation (Equation

ssed by popula

ional. This res

ements as the

on-diagonal c

ent of nuclea

Density Matrix

Relaxation th

Bloch-Wangsnes

ear response th

the more common

ense approach

tively accep

and taking the time derivative,

$$\frac{dM_z(t)}{dt} = N\hbar\gamma \sum_m m \frac{dP_m(t)}{dt}. \tag{43}$$

Combining Equations (41) and (43), it is a simple matter to show that when m = 1/2,

$$\frac{dM_z(t)}{dt} = -\frac{1}{T_1} M_z(t), \tag{44}$$

where $T_1 = 2W$. However when $m \neq 1/2$ it is not apparent that the sum of terms arising from $\beta>1$ in Equation (41) will be expressible as a single time constant. An additional problem is that the master equation (Equation (41)) is applicable only when the system may be described by populations, that is, when the density matrix is diagonal. This restraint is commonly violated in NMR relaxation experiments as the spin system following a 90° pulse is characterized by a non-diagonal density matrix. Consequently a more rigorous treatment of nuclear relaxation is desirable.

B. Density Matrix Theory of NMR Relaxation

Relaxation theory has been developed through two formalisms; the Bloch-Wangsness-Redfield density matrix approach[23-25] and the linear response theory of Kubo and Tomita[26,27]. Although the former is the more commonly used, it has been argued[27] that the linear response approach is entirely equivalent, and in addition is the more intuitively acceptable theory, as the only approximations made are

behavior of

semiclass

here. In

mally but t

means that te

the lattice wi

correlation f

The equation

is

$$\frac{1}{T}\frac{d\sigma}{dt}$$

where $\Delta\Omega_0$ is the

correlation function of

the lattice.

In the interac

density matrix,

defined as

$$\sigma^*(t)$$

$$-\int_0^t dt$$

to the behavior of macroscopic variables.

The semiclassical density matrix theory of relaxation will be outlined here. In this approach the spin system is described quantum mechanically but the lattice is treated classically. This approximation means that terms in the interaction Hamiltonian which pertain to the lattice will be treated as random functions of time, describable as a correlation function.

The equation of motion of the density matrix σ for the system S is

$$\frac{1}{i}\frac{d\sigma(t)}{dt} = -[\mathcal{H}_0 + \mathcal{H}_1(t),\sigma], \tag{45}$$

where $\hbar\mathcal{H}_0$ is the Zeeman Hamiltonian and $\hbar\mathcal{H}_1(t)$ is a stationary random function of time describing the interaction of the spin system with the lattice.

In the interaction representation, Equation (45) becomes

$$\frac{1}{i}\frac{d\sigma^*(t)}{dt} = -[\mathcal{H}_1^*(t),\sigma^*]. \tag{46}$$

The density matrix, correct to second order, can then be formally solved as

$$\sigma^*(t) = \sigma^*(0)-i\int_0^t dt'[\mathcal{H}_1^*(t'),\sigma^*(0)]$$

$$-\int_0^t dt'\int_0^{t'} dt''[\mathcal{H}_1^*(t'),[\mathcal{H}_1^*(t''),\sigma^*(0)]] \tag{47}$$

the time deriva

$$\frac{d\sigma^{+}(t)}{dt} = -i[\sigma$$

the number of

time[26], an

$$\frac{d\sigma^{+}(t)}{dt} =$$

The interactio

the molecular m

by

$$J$$

σ_{α} is the uni

σ_{α} is effective

$$\frac{d\sigma^{+}(t)}{dt} = -\int_{0}^{\infty}$$

Equation (51) is t

expressions for th

follows is to

express the time d

the expectation va

and the time derivative of Equation (47) is

$$\frac{d\sigma^*(t)}{dt} = -i[\mathcal{H}_1^*(t),\sigma^*(0)]-\int_0^t dt'[\mathcal{H}_1^*(t),[\mathcal{H}_1^*(t'),\sigma^*(0)]]. \quad (48)$$

Making a number of approximations based on the shortness of the correlation time[28], and introducing the variable $\tau = t-t'$, Equation (48) becomes

$$\frac{d\sigma^*(t)}{dt} = -\int_0^\infty d\tau\langle[\mathcal{H}_1^*(t),[\mathcal{H}_1^*(t-\tau),\sigma^*(t)]]\rangle. \quad (49)$$

The interaction Hamiltonian, which is time dependent because of the molecular motion, can be related to its value at different times by

$$\mathcal{H}_1^*(t) = U^{-1}(\tau)\mathcal{H}_1^*(t-\tau)U(\tau), \quad (50)$$

where U is the unitary operator describing the molecular motion which is effective in changing $\mathcal{H}_1$. Thus, Equation (49) becomes

$$\frac{d\sigma^*(t)}{dt} = -\int_0^\infty d\tau\langle[\mathcal{H}_1^*(t),[U^{-1}(t-\tau)\mathcal{H}_1^*(\tau)U(t-\tau),\sigma^*(t)]]\rangle. \quad (51)$$

Equation (51) is the fundamental equation from which the explicit expressions for the relaxation time may be obtained. The procedure one follows is to choose the appropriate interaction Hamiltonian, express the time dependence in the evolution operator U, and calculate the expectation value $\langle I_z\rangle$ from the relation

ey cases a Bl

ite relaxatio

.... The

The orientati

ber of wo

important for

be the

Taylor series

$\bar{a}_1(t$

ere the summation

The term are ne

we employ the

the scattered

form of the p

I(

Substituting Equa

$$\langle I_z \rangle = \mathrm{Tr}(\sigma I_z). \tag{52}$$

In many cases a Bloch equation (Equation (44)) is obtained, showing that the relaxation is indeed expressible as an exponential decay.

III. The Theory of Reorientational Broadening

The orientational broadening of Raman lines has been discussed by a number of workers[2,3,29-32]; here we review the results which are important for this investigation.

Let $\bar{\bar{\alpha}}$ be the molecular polarizability tensor, which we expand in a Taylor series in the normal coordinates q(t),

$$\bar{\bar{\alpha}}(t) = \bar{\bar{\alpha}}^{\circ}(t) + \sum_{\nu} \bar{\bar{\alpha}}^{\nu}(t) q^{\nu}(t), \tag{53}$$

where the summation runs over all the normal coordinates and

$$\bar{\bar{\alpha}}^{\nu}(t) = \left. \frac{\partial \bar{\bar{\alpha}}(t)}{\partial q^{\nu}(t)} \right|_{q^{\nu}=0}; \tag{54}$$

higher term are neglected.

We employ the Heisenberg picture discussed in Section I to state that the scattered light intensity is proportional to the Fourier transform of the polarizability correlation function

$$I(\omega) = \frac{1}{2\pi} \int dt e^{-i\omega t} \langle \bar{\bar{\alpha}}(t)\ \bar{\bar{\alpha}}(0) \rangle. \tag{55}$$

*Subs*tituting Equation (53) into Equation (55) and labeling each tensor

superscript

ters, we have

$$\Gamma(\ ) = \frac{1}{[\ ]}$$

$$= \frac{1}{[\ ]}$$

$$+$$

we have made

are statisti

correlation fun

terms involvin

$$\phi(t) =$$

dropping both ter

the condition

tions on diff

are

$$\phi(t) =$$

$$+ \sum$$

can be ident

with a superscript capital letter indicating the molecule to which it refers, we have

$$I(\omega) = \frac{1}{2\pi}\int dt e^{-i\omega t} \{\sum_B <\bar{\bar{\alpha}}^A(t)\bar{\bar{\alpha}}^B(0)>\}$$

$$= \frac{1}{2\pi}\int dt e^{-i\omega t} \{\sum_B <\bar{\bar{\alpha}}^{0A}(t)\bar{\bar{\alpha}}^{0B}(0)>$$

$$+ \sum_v <\bar{\bar{\alpha}}^{vA}(t)\bar{\bar{\alpha}}^{vB}(0)><q^{vA}(t)q^{vB}(0)>\}. \qquad (56)$$

Here we have made the usual assumption that the vibrations and rotations are statistically independent. This may be rewritten in terms of correlation functions involving a single particle and correlation functions involving two particles

$$\phi(t) = <\bar{\bar{\alpha}}^A(t)\bar{\bar{\alpha}}^A(0)> + \sum_{B\neq A} <\bar{\bar{\alpha}}^A(t)\bar{\bar{\alpha}}^B(0) \ . \qquad (57)$$

Expanding both terms in Equation (57), just as in Equation (56), with the condition $<q^{vA}(t)\ q^{vB}(0)> = \delta_{AB}<q^{vA}(t)\ q^{vA}(0)>$, i.e., that vibrations on different molecules are uncorrelated, the remaining terms are

$$\phi(t) = <\bar{\bar{\alpha}}^{0A}(t)\bar{\bar{\alpha}}^{0A}(0)> + \sum_{B\neq A} <\bar{\bar{\alpha}}^{0A}(t)\bar{\bar{\alpha}}^{0B}(0)>$$

$$+ \sum_v <\bar{\bar{\alpha}}^{vA}(t)\bar{\bar{\alpha}}^{vA}(0)><q^{vA}(t)q^{vA}(0)>, \qquad (58)$$

which can be identified as the correlation functions responsible

single-particle

respectively.

three Raman s

high time

(SE),

scores

separate

art,

$a_{tr} = \frac{1}{3}(a_{xx}$

Equation

$$s(t) = \sum_{v}$$

the time cor

must be iden

before using

scattered lig

ure 2 (90° s

the polarizati

can be eithe

horizontally po

for single-particle Rayleigh, cooperative Rayleigh, and Raman scattering, respectively.

Since Raman scattering occurs displaced by a frequency ω^{v} from the Rayleigh line we may experimentally suppress the first two terms in Equation (58); we drop the superscripts and the time correlation function becomes

$$\phi(t) = \sum_{v} \langle \bar{\bar{\alpha}}(t)\bar{\bar{\alpha}}(0)\rangle\langle q(t)q(0)\rangle. \tag{59}$$

We separate the polarizability tensor into a trace and a traceless part,

$$\bar{\bar{\beta}} = \bar{\bar{\alpha}} - \alpha_{tr}\bar{\bar{1}}, \tag{60}$$

where $\alpha_{tr} = \frac{1}{3}(\alpha_{xx} + \alpha_{yy} + \alpha_{zz})$ and $\bar{\bar{1}}$ is the unit matrix. Consequently, Equation (59) may be written

$$\phi(t) = \sum_{v} \{\langle\beta(t)\beta(0)\rangle\langle q(t)q(0)\rangle + \langle q(t)q(0)\rangle\}, \tag{61}$$

since the time correlation function of a time independent quantity (α_{tr}) must be identically unity.

Before using Equation (55) and (61) to determine the equation for scattered light intensity we must consider the scattering geometry in Figure 2 (90° scattering). There are four possible arrangements for the polarization of the incident and detected light, each of which can be either vertically polarized (with reference to Figure 2) or horizontally polarized; stating the incident polarization first,

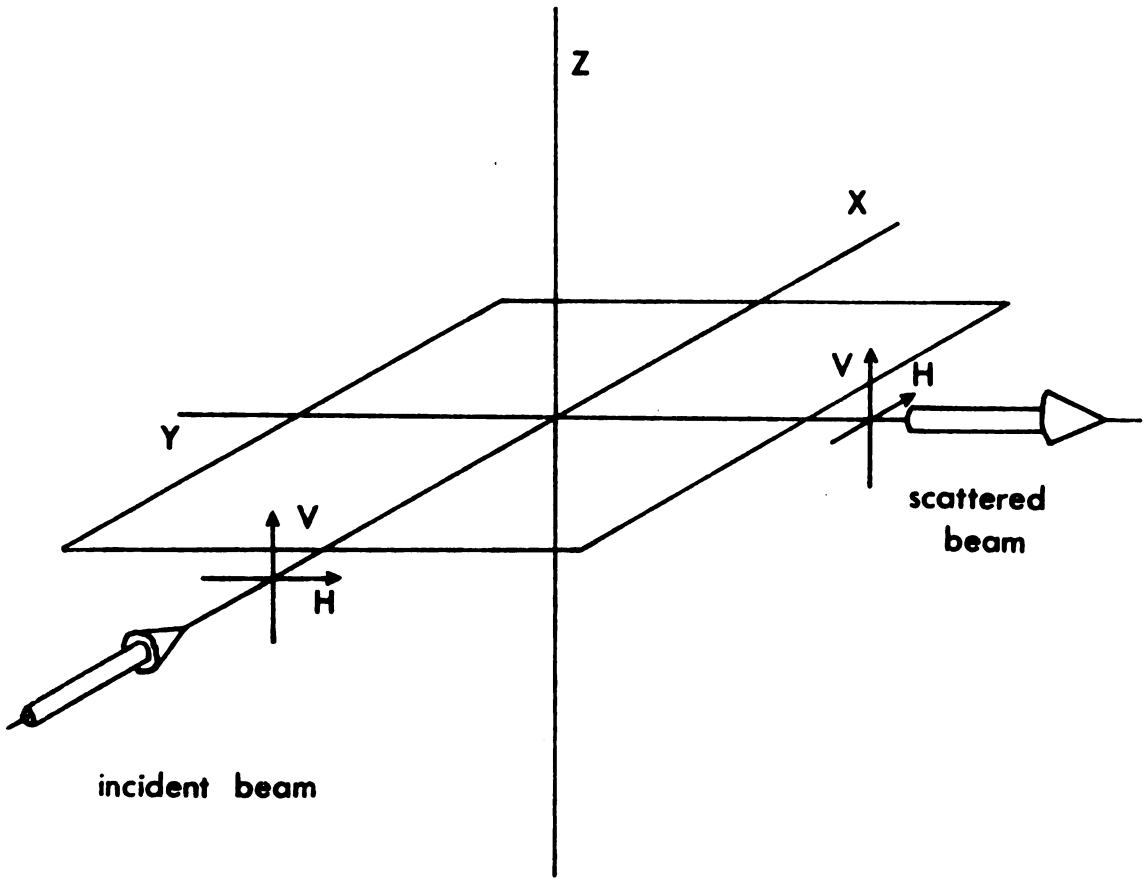

Figure 2. Raman 90° scattering geometry.

arrangements

spectroscopy the in

scattered light is

exists one of t

and equation re

polarizability

scale, for $\vec{r}$ ge

polarizability

laboratory f

"cut" a sing

becomes, for

$$\alpha(t) = \langle e_i \cdot \vec{E}$$

$$= \langle e_{ij}(t)$$

Similarly, the oth

these arrangements are referred to as VV, VH, HV, and HH. Thus with VH geometry the incident light is vertically polarized and the detected light is horizontally polarized. In a scattering experiment with one of these four types of polarization one replaces the general equation relating the incident and scattered light through the polarizability tensor with a scalar equation which is, for example, for VH geometry,

$$\hat{\varepsilon}_z \cdot \bar{\bar{\beta}} \cdot \hat{\varepsilon}_x = \beta_{zx}. \tag{62}$$

The polarizability tensor

$$\bar{\bar{\beta}} = \begin{pmatrix} \beta_{xx} & \beta_{xy} & \beta_{xz} \\ \beta_{yx} & \beta_{yy} & \beta_{yz} \\ \beta_{zx} & \beta_{zy} & \beta_{zz} \end{pmatrix} \tag{63}$$

is in laboratory frame Cartesian coordinates and the VH geometry "picks out" a single component. The time correlation function then becomes, for VH geometry,

$$\phi(t) = \langle \hat{\varepsilon}_i \cdot \bar{\bar{\beta}}(t) \cdot \hat{\varepsilon}_j \hat{\varepsilon}_i \cdot \bar{\bar{\beta}}(0) \cdot \hat{\varepsilon}_j \rangle \langle q(t)q(0) \rangle + \langle q(t)q(0) \rangle$$

$$= \langle \beta_{ij}(t)\beta_{ij}(0) \rangle \langle q(t)q(0) \rangle + \langle q(t)q(0) \rangle. \tag{64}$$

Similarly, the other geometries pick out other single components

appropriate to

we now wish to

the correlat

ion. We transf

phase (LF) to

using tr

α,β,γ, i

. If the mole

dependence w

is express

which the ro

ities,

$$\Omega^{LF}_{A}(\Omega)\cdot U$$

$$\gamma$$

is the

$$VV \rightarrow \beta_{zz} \qquad VH \rightarrow \beta_{zx}$$

$$HV \rightarrow \beta_{yz} \qquad HH \rightarrow \beta_{yx} \tag{65}$$

and appropriate time correlation functions can be written.

We now wish to express these tensor components, and consequently each time correlation function, in the molecule-fixed coordinate system. We transform an arbitrary Cartesian tensor A in the laboratory frame (LF) to the molecular frame (MF) through a unitary transformation using the (as yet unspecified) rotation operator R giving

$$\bar{\bar{A}}^{LF}(\Omega) = R^{-1}(\Omega)\cdot\bar{\bar{A}}^{MF}\cdot R(\Omega), \tag{66}$$

where $\Omega = \alpha,\beta,\gamma$, is the set of Euler angles specifying the orientation. If the molecule is rotating, then Ω is time-dependent and this time dependence will be contained in the rotation operator. If the tensor is expressed in the spherical basis, rather than the Cartesian basis, then the rotation operators are the familiar Wigner rotation matrices,

$$U^{-1}\cdot A^{LF}(\Omega)\cdot U = [U^{-1}\cdot R^{-1}(\Omega)\cdot U] \cdot U\cdot A^{MF}\cdot U^{-1} \cdot [U^{-1}\cdot R(\Omega)\cdot U], \tag{67a}$$

or

$$S^{LF}(\Omega) = D(\Omega) \cdot S^{MF} \cdot D^{-1}(\Omega), \tag{67b}$$

where S is the spherical tensor derived from the Cartesian tensor A

[illegible] is the ro[illegible]

[illegible]ments of a 3 [illegible]

[illegible] are given [illegible]

[illegible] we represe[illegible]

[illegible] then, from [illegible]

[illegible]rest among [illegible]

[illegible]metry argume[illegible]

[illegible] independent[illegible]

[illegible] that B_{xzxz} = [illegible]

[illegible]ation geome[illegible]

[illegible] correlation [illegible]

[illegible] we obtain f[illegible]

$$I_{in}(\omega) = [illegible]$$

[illegible] the second [illegible]

[illegible]ical element [illegible]

Similarly, [illegible]

[illegible]ce the scatt[illegible]

[illegible] incident [illegible]

and $D(\Omega)$ is the rotation matrix. The relationships between the components of a 3 × 3 Cartesian tensor and a second-rank spherical tensor are given in Table I for convenience.

If we represent the time correlation function $\langle\beta_{ij}(t)\beta_{k\ell}(0)\rangle$ by $\beta_{ijk\ell}$ then, from relation (65), there are four correlation functions of interest among the 81 possible combinations:

$$\begin{aligned} VV &\rightarrow \beta_{zzzz} \qquad & VH &\rightarrow \beta_{zxzx} \\ HV &\rightarrow \beta_{yzyz} \qquad & HH &\rightarrow \beta_{yxyx}. \end{aligned} \tag{68}$$

By symmetry arguments[32] it is possible to reduce these 81 combinations to two independent time correlation functions and, in the process, show that $\beta_{xzxz} = \beta_{zyzy} = \beta_{xyxy}$; consequently, the three "crossed"* polarization geometries, VH, HV, and HH all are measuring the same time correlation function. Substituting Equation (64) into Equation (55), we obtain for crossed polarization

$$I_{VH}(\omega) = \int dt e^{-i\omega t}\langle\beta_{xz}(t)\beta_{xz}(0)\rangle\langle q(t)q(0)\rangle, \tag{69}$$

where the second term in Equation (64) is clearly zero since off-diagonal elements of the unit matrix are zero.

Similarly, the polarized spectrum can be written

---

*Since the scattered polarization vector is rotated 90° with respect to the incident vector.

[illegible]. The re[illegible]

Componen[illegible]	
$T_{\pm}$	
$T_{\pm 2}$	
$T_{\pm 1}$	
T_0	
T_{xx} =	
T_{yy} =	
T_{zz} =	
T_{xy} =	
T_{zx} =	
T_{zy} =	

Table 1. The relationships between the Cartesian and spherical Components of a 3x3 tensor.

$$T_I \equiv \frac{1}{3}[T_{xx} + T_{yy} + T_{zz}]$$

$$T_{\pm 2} \equiv \frac{1}{2}[T_{xx} - T_{yy}] \mp iT_{xy}$$

$$T_{\pm 1} \equiv \mp[T_{zx} \pm iT_{zy}]$$

$$T_0 \equiv \frac{2}{\sqrt{6}}[T_{zz} - \frac{1}{2}(T_{xx} + T_{yy})]$$

$$T_{xx} = T_I - \frac{1}{\sqrt{6}} T_0 + (T_{+2} + T_{-2})/2$$

$$T_{yy} = T_I - \frac{1}{\sqrt{6}} T_0 - (T_{+2} + T_{-2})/2$$

$$T_{zz} = T_I + \frac{2}{\sqrt{6}} T_0$$

$$T_{xy} = (T_{+2} - T_{-2})/2i$$

$$T_{zx} = (T_{+1} - T_{-1})/2$$

$$T_{zy} = (T_{+1} - T_{-1})/2i$$

$L_{11}(\cdot) =$

are the coeffic

tively.

If we design

ity of the Ra

$L_{avg}(\cdot) = 1,$

x

Clearly, the

lineshapes.

of the coordi

$\Sigma(\cdot) = 1$ and ro

lineshape

line is bro

function

correlation f

the results

use the ro

$$I_{VV}(\omega) = b_1 \int dt e^{-i\omega t} \langle \beta_{zz}(t)\beta_{zz}(0)\rangle\langle q(t)q(0)\rangle$$

$$+ b_2 \int dt e^{-i\omega t} \langle q(t)q(0)\rangle, \qquad (70)$$

where the coefficients b_1 and b_2 have been shown[31] to be 4/3 and 1, respectively.

If we designate the depolarized and polarized components, respectively, of the Raman line as

$$I_{anis}(\omega) = I_{VH}(\omega) = \int dt e^{-i\omega t} \langle \beta_{xz}(t)\beta_{xz}(0)\rangle\langle q(t)q(0)\rangle, \qquad (71a)$$

and

$$I_{iso}(\omega) = I_{VV}(\omega) - \frac{4}{3} I_{VH}(\omega)$$

$$= \int dt e^{-i\omega t} \langle q(t)q(0)\rangle \qquad (71b)$$

then, clearly, these components may be determined by measuring the VV and VH lineshapes. Since the trace of a tensor is unchanged by rotation of the coordinate system, the time correlation function $\langle \alpha_{tr}(t) \cdot \alpha_{tr}(0)\rangle = 1$ and rotational motion contributes nothing to the isotropic lineshape $I_{iso}(\omega)$. On the other hand the anisotropic component of the line is broadened by the presence of the time-dependent correlation function $\langle \beta_{xz}(t)\beta_{xz}(0)\rangle$. The next step is to rewrite this time correlation function in terms of the rotation matrices in order to use the results of Section IB.

To use the rotation matrices we first must convert to a spherical

[illegible]

[illegible] the supers[illegible]

[illegible] system [illegible]

[illegible] molecular [illegible]

[illegible] (72, [illegible]

$$\varepsilon_{x}^{LF} [illegible]$$

[illegible] correlati[illegible]

$$\langle \varepsilon_{xz}^{LF}(t)\varepsilon_{xz}^{LF} [illegible]$$

[illegible] $= n(t)$ a[illegible]

[illegible] the fol[illegible]

[illegible]^3,

$$\langle D^{(2)}_{n,m} [illegible]$$

basis set

$$\beta_{xz}^{LF} = \frac{1}{2}(\beta_{+1}^{LF} - \beta_{-1}^{LF}), \tag{72}$$

where the superscripts remind us that we're still in the laboratory coordinate system. We then employ the rotation matrices to change to the molecular frame

$$\beta_{K}^{LF} = \sum_{M=-2}^{2} D_{K,M}^{(2)}(\Omega)\beta_{M}^{MF}. \tag{73}$$

Substituting (72) into (73),

$$\beta_{xz}^{LF} = \frac{1}{2} \sum_{M=-2}^{2} [D_{1,M}^{(2)}(\Omega) - D_{-1,M}^{(2)}(\Omega)]\beta_{M}^{MF}, \tag{74}$$

and the correlation function is

$$<\beta_{xz}^{LF}(t)\beta_{xz}^{LF}(0)> = \frac{1}{2} \sum_{M,M'=-2}^{2} <[D_{1,M'}^{(2)*}(\Omega') - D_{-1,M'}^{(2)}(\Omega')]$$

$$\times [D_{1,M}^{(2)*}(\Omega) - D_{-1,M}^{(2)}(\Omega)]\beta_{M'}^{MF*}\beta_{M}^{MF}>, \tag{75}$$

where $\Omega' = \Omega(t)$ and $\Omega = \Omega(0)$. We reduce the number of terms by employing the following relationship, valid for an equilibrium ensemble[3],

$$<D_{n,m}^{(2)}(\Omega')D_{j\ell}^{(2)}(\Omega)> = <D_{n\ell}^{(2)}(\Omega')D_{n\ell}^{(2)}(\Omega)>\delta_{nj}\delta_{m\ell} \tag{76}$$

are left with

$$\langle E_{xz}/t$$

$$+$$

ibution to a

case of rotat

exponenti

ing this res

$$\langle E_{xz}(0)E_{xz}(0)\rangle =$$

e that Equa

ion model

e time-depe

rotational c

decomposition

ter Raman vi

ficients $\mathcal{E}^{MF}$

symmetry.

For this sy

the A_1 and d

and are left with

$$<\beta_{xz}(t)\beta_{xz}(0)> = \frac{1}{2}\sum_{M=-2}^{2} <[D^{(2)*}_{1,M}(\Omega')D^{(2)}_{1,M}(\Omega)$$

$$+ D^{(2)*}_{-1,M}(\Omega')D^{(2)}_{1,M}(\Omega)]|\beta^{MF}_{M}|^2>. \qquad (77)$$

The solution to a time correlation function of rotation matrices for the case of rotational diffusion was seen in Section IB to be a sum of 2J+1 exponentials independent of the value of K (Equation (35)). Employing this result, we simplify Equation (77)

$$<\beta_{xz}(t)\beta_{xz}(0)> = \sum_{M=-2}^{2} |\beta^{MF}_{M}|^2 \frac{1}{2J+1} \exp\{-J(J+1)D_{\perp}+M^2(D_{||}-D_{\perp})\}t. \quad (78)$$

We note that Equation (77) is a model-independent result and that the diffusion model merely gives the specific form (decaying exponentials) for the time-dependent functions. From Equation (78) we have that the rotational component of the depolarized Raman line is, in general, a superposition of five Lorentzian lines. However the symmetry of a given Raman vibrational mode will allow us to set many of the coefficients $|\beta^{MF}_{M}|^2$ equal to zero[30], as we will show for the case of C_{3v} symmetry.

For this symmetry the polarizability tensor may be separated for the A_1 and doubly degenerate E vibrations[33] as follows:

$$\beta^{MF}_{A_1,i} = \begin{bmatrix} a_i & 0 & 0 \\ 0 & a_i & 0 \\ 0 & 0 & b_i \end{bmatrix} q_i(t) \qquad (79)$$

$$\begin{bmatrix} \mathrm{MF} \\ \mathrm{E}_{\pm 2} \end{bmatrix} = \begin{bmatrix} \mathrm{C}_{\mathrm{J}} \\ 0 \\ 0 \end{bmatrix}$$

ding to Tab

or (3), is for

$$\begin{bmatrix} \mathrm{MF} \\ \mathrm{E}_{\pm 2} \end{bmatrix}$$

for E modes

$$\begin{bmatrix} \mathrm{MF} \\ \mathrm{E}_{\pm 2} \end{bmatrix}$$

Consequently, for

$$\langle \mathrm{E}_{\mathrm{x}}$$

shows that

the symmetry a

the symmetry a

metry are affe

$$\mathrm{E}_{\mathrm{xz}}^{(+)}\mathrm{E}_{\mathrm{xz}}(0)\rangle_{\mathrm{E}}$$

In order to

extract the ro

and

$$\beta^{MF}_{E,j1} = \begin{bmatrix} c_j & 0 & 0 \\ 0 & -c_j & d_j \\ 0 & d_j & 0 \end{bmatrix} q_{j1}(t) \quad \beta^{MF}_{E,j2} = \begin{bmatrix} 0 & -c_j & -d_j \\ -c_j & 0 & 0 \\ -d_j & 0 & 0 \end{bmatrix} q_{j2}(t). \quad (80)$$

Referring to Table 1, it is clear that for A_1 modes $|\beta^{MF}_M|^2$ in Equation (78) is, for different M values,

$$|\beta^{MF}_{\pm 2}|^2 \equiv 0, \quad |\beta^{MF}_{\pm 1}|^2 \equiv 0, \quad |\beta^{MF}_0|^2 \neq 0 \qquad (81a)$$

and for E modes

$$|\beta^{MF}_{\pm 2}|^2 \neq 0, \quad |\beta^{MF}_{\pm 1}|^2 \neq 0, \quad |\beta^{MF}_0|^2 \equiv 0. \qquad (81b)$$

Consequently, for A_1 vibrations Equation (78) may be simplified to

$$\langle \beta_{xz}(t)\beta_{xz}(0)\rangle_{A_1} = \frac{1}{5} |\beta^{MF}_0|^2 e^{-6D_\perp t} , \qquad (82a)$$

which shows that A_1 lines are broadened only by rotations perpendicular to the symmetry axis ("tumbling") and are unaffected by motion parallel to the symmetry axis ("spinning"). On the other hand, lines of E symmetry are affected by both since

$$\langle \beta_{xz}(t)\beta_{xz}(0)\rangle_E = \frac{2}{5}[|\beta^{MF}_1|^2 e^{-(tD_\perp - D_{||})t} + |\beta^{MF}_2|^2 e^{-(4D_{||} - 2D_\perp)t}]. \quad (82b)$$

In order to test a model such as the diffusion model one needs to extract the rotational time correlation function from the

...ental spec...

...ated than E...

...ically b...

...ified to ac...

$I_{iso}(-) =$

$I_{ers}(-) = \int$

...es $\langle V \rangle$, $\langle R \rangle$ an...

...tion function...

...ction. There...

...period of Be...

...tic.

From the cor...

$\mathcal{F}[$

...

...es the * indic...

experimental spectra (Equation (71)). The problem is slightly more complicated than Equation (71) indicates since all real spectra will be additionally broadened by a slit function. Thus, Equation (71) is modified to account for instrumental effects

$$I_{iso}(\omega) = \int_{-\infty}^{\infty} d\omega \exp(i\omega t) \langle V(0)V(t)\rangle\langle S(0)S(t)\rangle$$

$$= \mathcal{F}[\langle V\rangle\langle S\rangle] \tag{83a}$$

$$I_{anis}(\omega) = \int_{-\infty}^{\infty} d\omega \exp(i\omega t)\langle V(0)(t)\rangle\langle R(0)R(t)\rangle\langle S(0)S(t)\rangle$$

$$= \mathcal{F}[\langle V\rangle\langle R\rangle\langle S\rangle], \tag{83b}$$

where $\langle V\rangle$, $\langle R\rangle$ and $\langle S\rangle$ are the vibrational, rotational and slit correlation functions, respectively, and $\mathcal{F}$ indicates a Fourier transformation. There are two alternatives for obtaining $\langle R\rangle$, the convolution method of Bartoli and Litowitz[30], and the Fourier inversion method.

From the convolution theorem we may write

$$\mathcal{F}[\langle V\rangle\langle R\rangle\langle S\rangle] = \mathcal{F}[\langle V\rangle\langle S\rangle] * \mathcal{F}[\langle R\rangle], \tag{84a}$$

or

$$I_{anis}(\omega) = I_{iso}(\omega) * I_{or}(\omega), \tag{84b}$$

where the * indicates a convolution and $I_{or}(\omega)$ is the Fourier

sum of the r

Alternatively

$$\frac{\mathcal{F}^{-1}\mathcal{F}_{\cdot}}{\mathcal{F}^{-1}\mathcal{F}_{\cdot}}$$

ly the Fourie

directional for

transform of the rotational correlation function.

Alternatively, we may write

$$\frac{\mathcal{F}^{-1}\{\mathcal{F}[\langle V\rangle\langle R\rangle\langle S\rangle]\}}{\mathcal{F}^{-1}\{\mathcal{F}[\langle V\rangle\langle S\rangle]\}} = \frac{\mathcal{F}^{-1}\{I_{anis}(\omega)\}}{\mathcal{F}^{-1}\{I_{iso}(\omega)\}} = \langle R\rangle. \tag{85}$$

Clearly the Fourier inversion method (Equation (85)) is superior when the functional form of $\langle R\rangle$ (or $I_{or}(\omega)$) is complex.

As was discus

mality per u

W

written in

W

are the i

amiltonian of th

ters.

Since the to

es of the form

fluction time c

Hamiltonian o

total. It is

each correl

Dipole-Dipole

The first i

shortly afte

HISTORICAL

I. NMR Relaxation Mechanisms

As was discussed in Section I, the perturbation expression for probability per unit time of an induced transition

$$W_{km} = \frac{2\pi}{\hbar} |\langle k|V|m\rangle|^2 \delta\{E_k - E_m - \hbar\omega\} \tag{86}$$

can be written in the Heisenberg representation as

$$W_{km} = \frac{1}{\hbar^2} \int_{-\infty}^{\infty} d\tau \langle V(t)V(0)\rangle e^{-i(m-k)\tau}, \tag{87}$$

where V are the interactions and are merely the various terms in the Hamiltonian of the system which are made time dependent by molecular motions.

Since the total relaxation rate is, in general, a sum of many terms of the form of Equation (87), the problem of interpreting the relaxation time comes down to the problem of deciding which terms in the Hamiltonian of the system give important contributions to $R_{1,total}$. It is possible to study $R_{1,total}$ and obtain information about each correlation function of the type defined by Equation (87).

A. Dipole-Dipole Relaxation

The first investigation into relaxation effects in NMR was done very shortly after the first nuclear resonance signal was observed

[illegible]. Biberbe[illegible]

[illegible]ects of [illegible]

[illegible]ar liqu[illegible]

[illegible]ctions. T[illegible]

[illegible]ted for

[illegible]interacti[illegible]

[illegible] can be w[illegible]

[illegible] the $p^{(q)}$ a[illegible]

[illegible]ons and th[illegible]

[illegible]ly, the t[illegible]

[illegible]ly contai[illegible]

[illegible]rical harmon[illegible]

$$p^{(0)} = (1-[illegible]$$

$$[illegible]^{(q)} = p(-q,[illegible]$$

[illegible]correlation [illegible]

[illegible]ergen, Pur[illegible]

in 1945. Bloembergen, Purcell and Pound published[34] in 1947 their measurements of proton relaxation times in water and a variety of hydrocarbon liquids, plus a few relaxation times for nuclei other than protons. They showed that the observed relaxation rates could be accounted for by two effects: inter- and intramolecular dipole-dipole interactions. A dipole-dipole interaction between two spins I and S can be written[28]

$$\mathcal{H}_1 = \sum_q F^{(q)} A^{(q)} \tag{88}$$

where the $F^{(q)}$ are random functions of the relative positions of the two spins and the $A^{(q)}$ are functions of the spin variables. Consequently, the time dependence of $\mathcal{H}$ produced by molecular motion is solely contained in the $F^{(q)}$, which are proportional to the Y_m^ℓ spherical harmonics

$$F^{(0)} = (1-3\cos^2\theta)r_{IS}^{-3},\ F^{(1)} = (\sin\theta\cos\theta e^{-i\phi})r_{IS}^{-3},$$

$$F^{(2)} = (\sin^2\theta e^{-2i\phi})r_{IS}^{-3} \tag{89}$$

and $F^{(q)} = F^{(-q)*}$. With the assumption of isotropic random motion the correlation of the $F^{(q)}$'s becomes

$$\langle F^{(q)}(0)F^{(q)*}(\tau)\rangle = \delta_{qq'}G(\tau). \tag{90}$$

Bloembergen, Purcell and Pound chose as a form for $G(\tau)$

xis xtained t

that the resc

ques to

$$J^{(i)}(-$$

ter evaluatin

Bergen, Pur

by consider

ersely on the

Numerical f

ssing) and c

$$G(\tau) = \langle |F^{(q)}|^2 \rangle e^{-|t|/\tau_c} \tag{91}$$

and so obtained the spectral density $J(\omega)$ as

$$J(\omega) \equiv \int_{-\infty}^{\infty} d\tau G(\tau) e^{-i\omega\tau}$$

$$= \langle |F^{(q)}|^2 \rangle \frac{2\tau_c}{1+\omega^2\tau_c^2} \, . \tag{92}$$

Since at the resonant frequencies used $\omega^2 t^2 << 1$, this expression reduces to

$$J^{(1)}(\omega) = \frac{4}{15} r_{IS}^{-6} \tau_c, \quad J^{(2)}(\omega) = \frac{16}{15} r_{IS}^{-6} \tau_c \tag{93}$$

(after evaluating the averages) and, consequently,

$$R_{1,dd} = 2\gamma^4 \hbar^2 I(I+1) r_{IS}^{-6} \tau_c \, . \tag{94}$$

Bloembergen, Purcell and Pound treated the intermolecular contribution by considering the correlation time for that process to depend inversely on the diffusion coefficient

$$\tau_t = \frac{r^2}{12D} \tag{95}$$

(the numerical factor is 12 rather than 6 because both spins are diffusing) and calculated

$$R_{1,trans} = \frac{3\pi\gamma^4 \hbar^2 N}{10Da} \, . \tag{96}$$

e and lated bo

hypogranic t

ing this the

ter good agree

is strongly r

the the visco

for qualitat

effects of d

error seems

study the ef

crease $R_{1,trans}$

δ, where $<\Delta^2$

the impurity a

Spin-Couple

For aqueous

T_2/T_1 was

was explaine

the form NA I·S

ds to T_1 and

P

They evaluated both of these correlation times by Debye's[13] application of hydrodynamic theory appropriate to spheres in a viscous fluid:

$$\tau_c = \frac{4\pi\eta a^3}{3kT}, \quad \tau_t = \frac{6\pi\eta a^3}{12kT} . \tag{97}$$

Applying this theory to water, Bloembergen, Purcell and Pound got rather good agreement because the jump mechanism is appropriate for such a strongly hydrogen-bonded system. In comparing the relaxation time to the viscosity for a number of hydrocarbons the results were only in qualitative agreement, undoubtedly because they neglected the effects of dissolved oxygen in shortening the relaxation times. This error seems rather ironic, as Bloembergen, Purcell and Pound did study the effect on R_1 of adding paramagnetic impurities, which increase $R_{1,trans}$ since γ^4 in Equation (96) is then replaced with $\gamma^2\langle\mu^2\rangle$, where $\langle\mu^2\rangle$ is the effective magnetic moment of the paramagnetic impurity and is about 10^3 larger than γ^2.

B. Scalar-Coupled Relaxation

For aqueous solutions of salts of Mn^{++} and Gd^{+++} it was found[35] that T_2/T_1 was less than unity and dependent on the proton frequency. This was explained as due to the presence of a scalar coupling of the form $\hbar A\, I\cdot S$ between the proton and the metal ion. The contributions to T_1 and T_2 from this term were shown to be

$$R_{1,sc} = \frac{2A^2}{3} S(S+1) \frac{\tau_S}{1+(\omega_I-\omega_S)^2\tau_S^2} \tag{98a}$$

$R_{2,sc}$ =

τ_c is the rela

strength low

$T_2 < T_1$.

found to b

much small

(S spin) re

coupling

such as SnCl

T_1 even at

Quadrupolar Re

Spanbergen, P

and D in 50% H

of deuterium

nuclear quadr

a fluctuati

$\vec{Q}$ is the q

gradient te

$\vec{Q}$ is quantiz

field while

rapid reorie

of the F tens

$$R_{2,sc} = \frac{A^2}{3} S(S+1) \left\{ \frac{\tau_S}{1+(\omega_I-\omega_S)^2\tau_S^2} + \tau_S \right\}, \qquad (98b)$$

where τ_S is the relaxation time of the electron spin. Clearly, at a field strength low enough so that $(\omega_I-\omega_S)^2\tau^2 << 1$, $T_1 = T_2$ but otherwise $T_2 < T_1$. The scalar coupling relaxation mechanism is also sometimes found to be important when S is a nuclear spin[36]. In this case the much smaller coupling constant is balanced by a much longer nuclear (S spin) relaxation time. In molecules for which nuclear spin-spin coupling constants are large and magnetic dipoles are small, such as $SnCl_4$, scalar coupling may give an important contribution to T_1 even at high fields.

C. Quadrupolar Relaxation

Bloembergen, Purcell and Pound also compared relaxation rates of H and D in 50% heavy water and realized that the faster relaxation of deuterium (although $\gamma_D < \gamma_H$) was due to an interaction of the nuclear quadrupole moment (present for all nuclei with I<1/2) with a fluctuating electric field. The Hamiltonian is

$$\mathcal{H}_1 = \bar{\bar{Q}} \cdot \bar{\bar{V}}(t), \qquad (99)$$

where $\bar{\bar{Q}}$ is the quadrupolar coupling tensor and $\bar{\bar{V}}$ is the electric field-gradient tensor. The time dependence of the interaction arises since $\bar{\bar{Q}}$ is quantized in the laboratory frame by the external magnetic field while $\bar{\bar{V}}$ is fixed in the molecular frame, which is undergoing rapid reorientational motions. The V tensor is exactly of the form of the F tensor in Equation (89), where now the θ in Equation (89)

ns to the angle

rel tensor. F

and intramolecu

$$R_{1,q} = \frac{}{}$$

the limit $\omega\tau_c \ll 1$

Non-Rotational

In gases, Bloe

ated that an in

ction between the

tical expressed a

ω_e indicates t

non-rotation tenso

ctions which al

the rotating ele

field. In the gas

ated to the rota

ole-dipole inter

refers to the angle between the Zeeman field and the symmetry axis of the V tensor. Proceeding through the same arguments as for the case of intramolecular dipole-dipole relaxation, we obtain

$$R_{1,q} = \frac{3}{40} \frac{2I+3}{I^2(2I-1)} \left(1 + \frac{\eta^2}{3}\right) \left(\frac{eQ}{\hbar} \frac{\partial^2 V}{\partial z^2}\right)^2 \tau_c \tag{100}$$

in the limit $\omega\tau << 1$.

D. Spin-Rotational Relaxation

In gases, Bloembergen, Purcell and Pound[34] and others[38-42] realized that an important relaxation mechanism would be the interaction between the nuclear spin and the overall rotation of the molecule expressed as

$$\hbar \mathcal{J} C = \bar{\bar{I}} \cdot \bar{\bar{C}} \cdot \bar{\bar{J}}(t), \tag{101}$$

where $\bar{\bar{J}}$ indicates the rotational quantum state and $\bar{\bar{C}}$ is called the spin-rotation tensor. This interaction is made time dependent by collisions which alter J. The magnetic field can be thought to arise as the rotating electron cloud produces a field opposing the Zeeman field. In the gas phase the time between collisions is directly related to the rotational correlation time τ_θ which governs the dipole-dipole interaction[11]

$$\tau_\theta = \frac{\tau_J}{2J+1}, \tag{102}$$

...ussed in Sec...

$$R_{1,total} = 4$$

...first term is t...

...the spin-rotat...

...ss. The second ...

...field at nucleus...

...34 gauss.

It was first t...

...ered in liquids,

...consistent wit...

...by Gutowsky a...

...that fluorine

...molecules su...

...dipole-dipole i...

...ed. Earlier mea...

...in liquid HF[4...

...ined on the ba...

...rine in an HF m...

...xation such as...

...act on the f...

...xation through...

...a study of th...

A number of y...

...relaxation tim...

as discussed in Section I, thus the total rate can be expressed as[34]

$$R_{1,total} = 2\gamma^2[\frac{1}{3} H'^2 J(J+1)+3H'^2 \frac{J(J+1)}{(2J-1)(2J+3)}]\tau_c. \qquad (103)$$

The first term is the spin-rotation contribution and for hydrogen gas, the spin-rotation constant H' was found to have the value 27 gauss. The second term is the intramolecular contribution with H" the field at nucleus 1 originating from nucleus 2 and for H_2 has the value 34 gauss.

It was first thought[43] that the spin-rotational relaxation was quenched in liquids, since relaxation rates in the early experiments were consistent with dipole-dipole interactions. However, measurements by Gutowsky and coworkers[44-46] on oxygen-free fluorocarbons showed that fluorine T_1's were consistently shorter than the proton T_1's in molecules such as $CHFCl_2$, where the correlation time τ_θ for the dipole-dipole interaction should surely be the same for the two nuclei. Earlier measurements of hydrogen and fluorine relaxation times in liquid HF[47] also gave $T_{1F} < T_{1H}$ but this inequality was explained on the basis of unequal correlation times for hydrogen and fluorine in an HF molecule. However, in the case of $CHFCl_2$ no easy explanation such as this was possible. The one known mechanism which would act on the fluorine nuclei more strongly than on the protons, relaxation through chemical shift anisotropy[48], was ruled out[44] from a study of the field dependence of T_{1F}.

A number of years after the initial observation of shorter ^{19}F relaxation times, it was proposed[46] that a different statistical

was responsi

tion. This m

as obtained unde

correct temp

model proposed

rotational mode

the molecu

another, wi

lar angular v

which descri

as does the a

shorter than t

ant to NMR is

Hubbard[49] exam

correlatio

tional Brownian

velocity ob

which is ofte

With the

able to obtain

tion times,

an expression

process was responsible for the extra contribution to the ^{19}F relaxation. This new approach was necessary because the relaxation times obtained under the assumption of rotational Brownian diffusion gave incorrect temperature dependence to the ^{19}F T_1's in $CHFCl_2$. The model proposed to account for the fluorine relaxation was a transient-jump model, where the mechanism became operative only during the time the molecule was making a rotational jump from one orientation to another, with an interactive strength proportional to the molecular angular velocity. The angular velocity correlation functions, which describe the time dependence of the angular velocity, decay as does the angular position correlation function in a time much shorter than the Larmor frequency, hence the measurable quantity important to NMR is the angular momentum correlation time.

Hubbard[49] examined this mechanism by calculating the angular velocity correlation function for a spherical molecule undergoing rotational Brownian diffusion and making the assumption that the angular velocity obeyed an equation analogous to the Langevin equation, which is often invoked to describe translational Brownian diffusion. With the condition that either $\tau_J \ll \tau_\theta$, or $\tau_J \gg \tau_\theta$, he was able to obtain a fundamental relationship between these two correlation times,

$$\tau_\theta \tau_J = \frac{I}{6kT} , \tag{104}$$

and an expression for the spin-rotational relaxation rate

$$R_{1,sr} = \frac{2IkT}{\hbar^2} C_{eff}^2 \tau_J , \tag{105}$$

is the mome

interactio

values a

τ_g. Thus, usi

as compared

the correct

increasing ra

quenching' of

τ_g) as

Spin-rotationa

important possi

^{19}F relaxat

SeF_6. These m

frequency-i

temperature decrea

rates. Since, in

be the dominant

ination of th

manner to su

Spin-rota

tic crystalli

in white phos

The reorient

in the solid

where I is the moment of inertia and C_{eff} is the effective spin-rotation interaction constant (in radians/sec)

$$C_{eff}^{2} = \frac{1}{3}\,(2C_{\perp}^{2} + C_{||}^{2})\ . \qquad (106)$$

Inserting values appropriate to the liquid state it is apparent that $\tau_J \ll \tau_\theta$. Thus, using a quite different model (rotational Brownian motion as compared to a transient-jump model), Hubbard was able to obtain the correct temperature dependence for spin-rotational relaxation (increasing rate with increasing temperature) and also explain the 'quenching' of the spin-rotation interaction in the liquid ($\tau_J = I/6kT\ \tau_\theta$) as opposed to the gas phase ($\tau_J = \tau_\theta\ (2J+1)$).

Spin-rotational relaxation in the solid state was not considered an important possibility until the observations of Blinc and Lahajner[50] of the ^{19}F relaxation in the liquid and solid phases of SF_6, TeF_6, and SeF_6. These molecules all have plastic crystalline phases and show a frequency-independent relaxation rate which decreases as the temperature decreases, both in the liquid and plastic crystalline phases. Since, in the case of SF_6, spin-rotation had been shown[51] to be the dominant relaxation mechanism in the liquid phase, the continuation of this relaxation curve into the solid phase led Blinc and Lahajner to suggest that spin-rotation is also important in the solid. Spin-rotation was later recognized to be important in the plastic crystalline phase for ^{19}F in MoF_6 and WF_6[52], ^{1}H in NH_4I[53,54], ^{31}P in white phosphorus[55,56], ^{1}H in NH_4ClO_4[57], and ^{31}P in phosphine[58].

The reorientational motion giving rise to spin-rotational relaxation in the solid phase may be described either as small-step

[53], as in

model[46],

in an n-fo

rotate the mo

, for plas

jumps fro

[55]

is the mear

expressio

(105)).

represented th

line white p

an eight-fol

calculati

orientation

have been re

II.

Modifications t

There were two

theory for no

the discont

diffusion[53], as in the Hubbard model[49] for liquids, or by a transient-jump model[46,52] in which molecular libration about an equilibrium position in an n-fold well is interrupted by random torque impulses which rotate the molecule to another potential well. At the Larmor frequency, for plastic phases, the contribution to τ_J comes mainly from the jumps from well to well[52] and the spin-rotation relaxation rate becomes[55]

$$R_{1,sr} = \frac{2IkT}{\hbar^2} C_{eff}^2 \phi^2 \tau_J \ , \tag{107}$$

where ϕ is the mean jump angle. This may be compared with the analogous expression for the case of isotropic rotational diffusion (Equation (105)). Boden and Folland[55] found that Equation (107) well represented the spin-rotational relaxation rate in plastic crystalline white phosphorus (P_4) when $\phi = 120°$. For most plastic solids an eight-fold (cubic) potential is more appropriate, and numerical calculations of the full time-correlation functions for angular orientation and angular velocity for the transient-jump model have been reported[59].

II. Rotational Motion in Liquids

A. Modifications to the Bloembergen, Purcell and Pound-Debye Treatment

There were two early attempts to correct the failure of the Debye theory for nonviscous fluids. Gierer and Wirtz[60] took into account the discontinuous nature of the liquid in a simple quasi-steady

calculation

neighbors and

$$\xi$$

where a is the ra

upper. For b

ratio is 1/6 the

b/a =100 (a sp

Hill[61] based

Debye's[62] theory

relaxation time wh

solvent pair. App

which may be compa

model predicts tha

5/5 than the De

for nearly spheri

segment, or a m

state calculation of the torques acting on a rotating molecule by its neighbors and obtained a friction constant

$$\xi = 8\pi\eta a^3[6(\frac{b}{a}) + (1 + \frac{b}{a})^{-3}]^{-1} , \tag{108}$$

where a is the radius of the molecule and b is the radius of the neighbor. For b = a,

$$\xi = \frac{8\pi\eta a^3}{6} , \tag{109}$$

which is 1/6 the value predicted by the Stokes-Einstein relation. For b/a ≃100 (a spherical macromolecule in solution)

$$\xi = 8\pi\eta a^3(0.970). \tag{110}$$

Hill[61] based her calculation of dielectric relaxation times on Andrade's[62] theory of viscosity and obtained an expression for the relaxation time which depended on the mutual viscosity of a solute-solvent pair. Applying this theory to pure polar liquids she obtained

$$\tau_c \cong \frac{3(3-\sqrt{2})}{2kT} \eta a^3 , \tag{111}$$

which may be compared with Debye's $\tau_c = 4\pi\eta a^3/kT$. Thus, the Hill model predicts that τ_c would be smaller by a factor of $3(3-\sqrt{2})/8 \approx 1/5$ than the Debye τ_c. Experimentally, dielectric relaxation times for nearly spherical molecules (for which one would expect the Debye treatment, or a modification, to work well) were found[63] that were

as eight c

Anisotropic Rot

The first exte
ment of rotat
appeared rou
ometer of ani
the solution, d
ation for a rig
These results showe
ured five time
Equation (35)) ap
tion functions
dielectric relaxat
single correlati
tion times. F

$$\tau_{\theta_{eff}} = \frac{(3}{}$$

where θ is the an
ow mechanism ar
is the perpend
show the rela
(K) $(K \equiv D_{||}/$
Boersgen, Pur
ated the rat

as small as eight one-thousandths of the predicted value.

B. Anisotropic Rotational Diffusion

The first extension of the Bloembergen, Purcell and Pound-Debye treatment of rotational motion was given in three independent papers which appeared roughly simultaneously. These authors[20,64,65] considered the problem of anisotropic rotational diffusion, basing their work on the solution, due to Perrin[18] and Favro[19], of the diffusion equation for a rigid ellipsoid, which was discussed in Section IB. These results showed that rotational diffusion of an asymmetric top required five time correlation functions for $\ell = 2$ spherical harmonics (Equation (35)) appropriate to magnetic relaxation or three time correlation functions for the $\ell = 1$ spherical harmonics appropriate to dielectric relaxation. The NMR relaxation time then depends not on a single correlation time but on a complex function of all the correlation times. For a symmetric top this function is[21]

$$\tau_{\theta_{eff}} = \frac{(3\cos^2\theta-1)^2}{24D_\perp} + \frac{3\sin^2\theta\cos^2\theta}{5D_\perp+D_{||}} + \frac{3\sin^4\theta}{4(2D_\perp+4D_{||})}, \qquad (112)$$

where θ is the angle between the vector interaction in the relaxation mechanism and the principal axis of the diffusion tensor, and $D_\perp$ is the perpendicular component of the diffusion tensor. In order to show the relation between the effective correlation time $\tau_{\theta_{eff}} = f(\theta,K)$ $(K \equiv D_{||}/D_\perp)$ and the correlation time obtained from the Bloembergen, Purcell and Pound-Debye treatment (τ_c), Shimizu[66] computed the ratio $\tau_{\theta_{eff}}/\tau_c$ as a function of axial ratio for prolate

ure 3a) and ob

is clear that f

anisotropic mo

ular relaxation

laxation times f

distinguishing

specially true fo

ding relaxati

relaxation rate

ed to nuclei w

intermolar mechan

molecules, inve

laxation rate fo

in Equatio

ties for the t

model chosen,

rotational diffus

ase symmetric-t

sor may be cal

(where I i

ortress disc

orientation, the

ation for rot

ment-of-inerti

components o

ling rotatio

verse componen

(Figure 3a) and oblate (Figure 3b) symmetric tops. From the figure it is clear that for many molecules, i.e., those with axial ratio ≤ 4, anisotropic motion does not make a large difference in the calculated relaxation times. Consequently, absolute calculations of relaxation times for a given nucleus in a molecule have little hope of distinguishing between anisotropic and isotropic motion. This is especially true for spin-1/2 nuclei, where several mechanisms, including relaxation through paramagnetic impurities, compete for the relaxation rate. Recognizing this problem, many investigators turned to nuclei with spin $I > 1/2$, with the understanding that the quadrupolar mechanism would dominate the relaxation rate. A number of molecules, investigated[67-81] by measuring the temperature-dependent relaxation rate for two quadrupolar nuclei in the same molecule, for which θ in Equation (112) is different, showed different activation energies for the two nuclei. This fact shows that, independent of the model chosen, the motion in these molecules is anisotropic. If rotational diffusion is used to describe the molecular motions in these symmetric-top molecules then the two components of the diffusion tensor may be calculated. Table 2 compares the ratio $D_{||}/D_{\perp}$ with $I_{\perp}/I_{||}$ (where I is the moment of inertia) for these and other molecules. As Huntress discusses[21] in his review of anisotropic molecular reorientation, the diffusion equation is equivalent to the Schrödinger equation for rotation with the diffusion tensor D replacing the moment-of-inertia tensor $\hbar^2/2I$. Since the relative magnitudes of the components of the inertia tensor determine the spinning and tumbling rotational velocities in the gas phase, by analogy the inverse components of the diffusion tensor determine the rate of

A

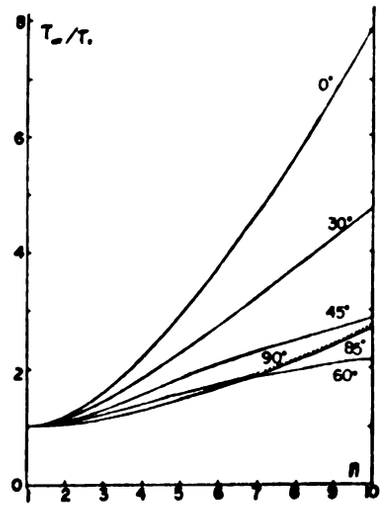

B

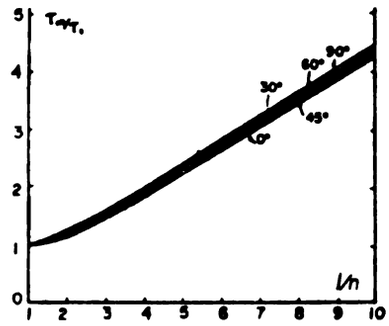

Figure 3. The effect of axial ratio n and the angle θ_0 upon the ratio τ_{eff}/τ_c: τ_{eff} is the effective correlation time obtained by assuming the molecule as (a) small prolate spheroid, (b) a small oblate spheroid; τ_c is the correlation time derived by the Debye-Bloembergen theory, assuming the molecule as a small sphere.

VI.2. Experime

Molecule	
[illegible]	
[illegible]	
[illegible]	
[illegible]	
[illegible]	
[illegible]	
[illegible]	
[illegible]	
[illegible]	
[illegible]	
[illegible]	
[illegible]-triazine	
[illegible]	

[illegible]pendicular mo
[illegible]pendicular mo
[illegible]cially deuter
[illegible]certainty due

Table 2. Experimental measurements of anisotropic motion in liquids.

Molecule	Temp. (°C)	$D_{\parallel}/D_{\perp}$	$I_{\perp}/I_{\parallel}$	$E_{a_{\perp}}$	$E_{a_{\parallel}}$	Ref.
CD_3CN	25	8.89	10.11	1.7 ±0.1	0.8 ±0.2	71
		10.35		2.00	0.73	74
$VOCl_3$	30	1.4	0.629	1.97±0.06	2.30±0.06	73
CCl_3CN	25	2.1	0.917	2.68±0.14	1.9 ±0.3	73
BCl_3	0	.75	0.500	1.28±0.02	1.66±0.14	73
$CDCl_3$	20	1.9	0.530	1.6 ±0.10	0.7 ±0.1	72
CD_3CCD	-30	14	10.1	1.7 ±0.2	0.5 ±0.1	75
PCl_3[a]	25	2.38	1.78	1.7	1.7	76
PBr_3[a]	25	3.16	1.89	2.3	1.7	76
$OPCl_3$[a]	25	3.32	1.35	2.3	----	76
C_6D_6[b]	57	4.6	0.500	2.7 ±0.3	0.3	77
C_5H_5N[c]	-1	2.1	0.498	3.1 ±0.3	1.0 ±0.3	78
d_3-s-Triazine	152	2.3	0.498	3.4 ±1	0.3 ±1	79
CD_3I	25	∿15[d]	20.32	1.9[a]	0.8 ±0.1	80
	20	22±3[d]		2.1[b]	0.4 ±0.1	81

[a]Perpendicular motion estimated by microviscosity theory.

[b]Perpendicular motion determined by Raman lineshape analysis.

[c]Partially deuterated molecules were studied.

[d]Uncertainty due to estimate of deuteron quadrupole coupling constant.

rotation abou

the componen

to the com

diffusion limi

dipolar interact

mentally this

rotate more r

the symmetry ax

related to the

isotropic interm

Rapid motion

one to quest

the spinning m

magnetic or die

as CH_4 or CCl

Non-Diffusional

Isotropic Bro

relaxation ra

rotational diffus

molecule such as

field as a descri

The calculat

spherical molecu

coworkers 82-8

rotational motion are

reorientation about the different molecular axes in the liquid phase. Since the components of the diffusion tensor can be shown to be related to the components of the inertia tensor[21] as $D_i \sim kT/I_i$ in the diffusion limit, then in liquids with sufficiently weak intermolecular interactions we would expect to find $D_{||}/D_{\perp} \propto I_{\perp}/I_{||}$. Experimentally this is not the case, as all molecules in Table 2 except BCl_3 rotate more rapidly about their symmetry axis than perpendicular to the symmetry axis. The fact that the diffusion tensor is not at all related to the inverse inertia tensor shows the importance of anisotropic intermolecular forces in the liquid.

Rapid motion about the symmetry axis, as in $CD_3C{\equiv}CD$ or CD_3CN leads one to question the validity of small-step rotational diffusion for the spinning motion. Alternatively, one may consider the problem in magnetic or dielectric relaxation with much more symmetric molecules, such as CH_4 or CCl_3Br.

C. Non-Diffusional Models

Isotropic Brownian diffusion gives correlation times (and therefore relaxation rates) which are much too large. Clearly, if isotropic rotational diffusion is not a valid description of the motion in a molecule such as CH_4, then rotational diffusion will not likely be valid as a description of the spinning motion in a CH_3X molecule.

The calculation of correlation times for isotropic rotation in spheroidal molecules was the subject of a series of papers by Steele and coworkers[82-84]. They observed that the forces governing translational motion are quite different from those restricting free rotation

the liquid, and

ship betwee

, and rela

friction.

be well r

experimental

Bergen, Purce

Steele's re

lation based

as determin

lar interact

ant time cor

non-Markovia

ammonia[86]. Th

dal molecul

recently, wh

rate should i

of rotation,

ent observatio

spectrum of a r

long-lived r

The Extended

Gordon's[93] m

provide a smoo

is, very sma

in the liquid, and one should not in general expect to find any relationship between the viscosity, which depends on the translational friction, and relaxation times, which usually depend on the rotational friction. The calculated time correlation functions were found to be well represented by a Gaussian function and comparisons[84] with experimental data showed better agreement than the Debye-Bloembergen, Purcell and Pound model had shown. Atkins[85] has obtained Steele's result as the classical limit to a quantum-mechanical calculation based on a model wherein the molecules rotate in the liquid as determined by their free-rotor Hamiltonian. The intermolecular interactions enter the model as a Gaussian damping of the resultant time correlation functions. This theory was modified to allow non-Markovian process in order to analyze the relaxation data for ammonia[86]. The effects of spin-rotational relaxation in these spheroidal molecules was not considered for this inertial model until quite recently, when it was shown[87] that the spin-rotational relaxation rate should increase as $T^{1/2}$. The importance of an inertia model of rotation, at least for small molecules, is evident from recent observations[88-92] of rotational fine structure in the far ir spectrum of a number of molecules dissolved in SF_6, which indicate that long-lived rotational states are present in these systems.

D. The Extended Diffusion Model

Gordon's[93] model of rotational motion of molecules was an attempt to provide a smooth transition between strictly diffusive motion, that is, very small step size, and motion characterized by large

lar steps. The
ed by Ivanov[1]
s of arbitrary
ver[34]. The fur
of Gordon is
ng the reorie
ach the molec
quently in th
ngs exponential
tion functions
the inertial mo

The primary v
ar time between
lar momentum c
s been generaliz
ss, although the
as studied in t
e theory as it a
ant features a
e results for th
necessary.

The correlati
ic time evolut
tzmann distri
ods of free ro
rupted by col
ectum vector wi

angular steps. The problem of large step reorientation has been treated by Ivanov[16] and a general theory of reorientation through steps of arbitrary size by Cukier and Lakatos-Lindenberg[15] and Cukier[94]. The fundamental difference between these approaches and that of Gordon is that Ivanov, and Cukier et al., employ a model wherein the reorientations occur instantaneously, whereas in Gordon's approach the molecule rotates as governed by its inertia tensor. Consequently in the "jump" models the correlation functions are always exponential while in the extended diffusion model the time correlation functions are Gaussian for an initial portion of time due to the inertial motion of the molecules between collisions.

The primary variable in the extended diffusion model is the mean time between collisions, which may be identified with the angular momentum correlation time. The extended diffusion model has been generalized to include spherical[95-98] and symmetric[99,100] tops; although the symmetric-top treatment is required for the molecules studied in this investigation, in this section we will consider the theory as it applies to linear molecules, where all of the important features are present but little of the mathematical complexity. The results for the symmetric-top case will then simply be stated as necessary.

The correlation function is calculated by following the microscopic time evolution of a single molecule and then averaging over a Boltzmann distribution of velocities. The motion is pictured as periods of free rotation, during which the molecule behaves classically, interrupted by collisions which instantaneously randomize the angular momentum vector without affecting the orientation of the molecule.

In the M-diff

vector is

ation and th

is inappropr

for a molec

ation of M- a

molecular for

Following Gor

vector (linea

first diffusiv

t_1 the mol

ntation of J;

on U(0) is,

is the an

ated to ran

In the M-diffusion model only the orientation of the angular momentum vector is randomized; in the J-diffusion model both the orientation and the magnitude are randomized. Clearly the M-diffusion limit is inappropriate for real systems, as the angular momentum vector for a molecule must change through collisions, but the consideration of M- and J-diffusion limits allow the strength of the intermolecular forces to vary.

Following Gordon[93], we now calculate the correlation function of a vector (linear molecule) undergoing extended diffusion. During the first diffusive step the molecule is rotating with velocity ω_1 so

$$U(0) \cdot U(t) = \cos\omega_1 t. \tag{113}$$

At time t_1 the molecule undergoes a collision which changes the orientation of J; at the end of this diffusive step the projection of U on U(0) is, from spherical geometry,

$$U(0) \cdot U(t) - \cos\omega_1 t_1 \cos\omega_2 (t-t_1)$$

$$- \cos\alpha \sin\omega_1 t_1 \sin\omega_2 (t-t_1) , \tag{114}$$

where α is the angle between J_1 and J_2. Since the collision is postulated to randomize this angle,

$$\langle\cos\alpha\rangle = 0, \tag{115}$$

ves the average

$$<U($$

ra the first c

rnal t we mus

ies of t_1

$$<U(0)U$$

e can generalize

ticles in the

$$<U(0)U(t)>_{n+1} =$$

$$x \ldots x \int_0^{t_3}$$

he correlation f

n the first, sec

stribution of r

nal time t is r

ter the contrib

y this probabil

where the average is taken over many molecules. Therefore

$$\langle U(0)U(t)\rangle_2 = \cos\omega_1 t_1 \cos\omega_2 (t-t_1). \tag{116}$$

Since the first diffusive step may be terminated at any time in the interval t we must properly average this projection over different values of t_1

$$\langle U(0)U(t)\rangle_2 = t^{-1} \int_0^t dt_1 \cos\omega_1 t_1 \cos\omega_2 (t-t_1). \tag{117}$$

We can generalize this result to an arbitrary number of steps; for molecules in the (n+1)th diffusive step

$$\langle U(0)U(t)\rangle_{n+1} = \frac{n!}{t^n} \int_0^t dt_n \cos\omega_{n+1}(t-t_n) \int_0^{t_n} dt_{n-1} \cos\omega_n (t_n - t_{n-1})$$

$$\times \ldots \times \int_0^{t_3} dt_2 \cos\omega_3 (t_3 - t_2) \int_0^{t_2} dt_1 \cos\omega_2 (t_2 - t_1) \cos\omega_1 t_1. \tag{118}$$

The correlation function will be a sum of contributions from molecules in the first, second,...,n^{th} diffusive steps. If we represent the distribution of number of steps by a Poisson distribution, since the total time t is not long compared to the time between collisions,

$$f(n) = \frac{1}{n!} \left(\frac{t}{\tau}\right)^n e^{-t/\tau}, \tag{119}$$

then the contribution from molecules in the nth step is weighted by this probability that n steps will occur, and therefore

$$\langle U(0)U(t$$

$$\int_0^{t_n} dt_{n-1} \cdots$$

$$\times$$

For the M-di

The correlation

distribution of r

$$\langle U(0)U$$

In the J-dif

it each must be

In terms o

$$F_0(t) =$$

The J-diffusion c

$$\langle U(0)U$$

$$\times \int_0^{t_n} d$$

$$\langle U(0)U(t)\rangle = e^{-t/\tau}\sum_{n=0}^{\infty}\tau^{-n}\int_0^t dt_n \cos\omega_{n+1}(t-t_n)$$

$$\times\int_0^{t_n} dt_{n-1}\cos\omega_n(t_n-t_{n-1})\times\ldots\times\int_0^{t_3} dt_3\cos\omega_3(t_3-t_2)$$

$$\times\int_0^{t_n} dt_2\cos\omega_2(t_2-t_1)\cos\omega_1 t_1. \qquad (120)$$

For the M-diffusion limit $\omega_{n+1} = \omega_n = \ldots = \omega_2 = \omega_1$, and the time correlation function is Equation (120) averaged over a Boltzmann distribution of rotational velocities $\omega\exp(-\frac{1}{2}\omega^2)$

$$\langle U(0)U(t)\rangle_m = \int_0^{\infty} d\omega\exp(-\tfrac{1}{2}\omega^2)\langle U(0)U(t)\rangle. \qquad (121)$$

In the J-diffusion limit the rotational velocities are not equal and each must be separately averaged over a Boltzmann thermal distribution. In terms of the free-molecule dipole correlation function $F_0(t)$,

$$F_0(t) = \langle\cos\omega t\rangle = \int_0^{\infty}\cos(\omega t)\omega\exp(-\tfrac{1}{2}\omega^2)d\omega, \qquad (122)$$

the J-diffusion correlation function is

$$\langle U(0)U(t)\rangle_J = e^{-t/\tau}\sum_{n=0}^{\infty}\tau^{-n}[\int_0^t dt_n F_0(t-t_n)$$

$$\times\int_0^{t_n} dt_{n-1}F_0(t_n-t_{n-1})\times\ldots\times\int_0^{t_3} dt_2 F_0(t_3-t_2)$$

$$\times\int_0^{t_2} dt_1 F_0(t_2-t_1)F_0(t_1)]. \qquad (123)$$

both the M- a

ly in Gordon's

The M- diffus

ributions othe

ules when sphe

the replacement

ances.

A number of

ve appeared whi

ses[102-104] or

ve published, b

rrose theory b

reorientational

non-diffusion

Experimental

As yet, ther

total, in spite

are probably rel

ilation rate

to be separated

system to stu

the type of nucl

through the quad

which have been

these in order

Both the M- and J- correlation functions were evaluated numerically in Gordon's paper[93].

The M- diffusion limit has been examined[101] for collision distributions other than Poisson. The primary change in these formulas when spherical[95] or symmetric-top[99] molecules are considered is the replacement of the various $\cos\omega t$ terms with the $D(\Omega)$ rotation matrices.

A number of other papers on the subject of extended diffusion have appeared which have treated Gordon's M- and J- diffusion models[102-104] or a similar model[105]. Also a series of papers has been published, based on the projection operator treatment of linear response theory by Mori[106,107], which attempts a more general approach to reorientational relaxation by including both extended diffusion and non-diffusional reorientation as limiting cases[108-111].

E. Experimental Tests of Extended Diffusion

As yet, there have been few tests of the extended diffusion model, in spite of countless relaxation studies in which the data are probably reliable. This is so because in the usual case the relaxation rate has contributions from several mechanisms which cannot be separated. Since one wishes to know τ_θ and τ_J, the best type of system to study would be a linear or spherical-top molecule with one type of nucleus relaxing through spin-rotation and a second type through the quadrupolar mechanism. Table 3 lists those molecules which have been investigated by NMR or NMR-Raman methods as a fluid phase in order to test the applicability of the extended-diffusion

Table 1. Experimental tests of extended diffusion.

Molecule	Nuclei Monitored	Methods Used	Temp.[a] Range	Value[b] of C	Anisotropy Considered?	Conclusions	Ref.
	^{13}-	T C	pl	C	----	J	112

Table 3. Experimental tests of extended diffusion.

Molecule	Nuclei Monitored	Methods Used	Temp.[a] Range	Value[b] of C	Anisotropy Considered?	Conclusions	Ref.
CS_2	^{13}C	T_1[c]	PL	C_σ	----	J	112
HCl	H,^{35}Cl	T_1,T_2	EL	C_{MB}	----	anomalous[d]	113-119
HBr	H^{31}Br	T_1,T_2	EL	C_{MB}	----	anomalous[d]	116,119
F_2	^{19}F	T_1	PL		----	large-jump reorientation	120
CH_4	^{1}H	T_1,D	EL	C_{MB}	----		121-124
CF_4	^{19}F	T_1,Ram.	DF	C_{MB}	----	J	125
CCl_4	$^{13}C^{35}Cl$	$T_1(^{19}F)$,$T_2(^{35}Cl)$	PL	C_σ	----	J	126
$PbCl_4$	^{205}Pb	T_1,T_2	PL	C_{NMR}	----	anomalous[d]	127
$SnCl_4$	^{119}Sn	T_1,T_2	PL	C_{NMR}	----	J	37
$SnBr_4$	^{119}Sn	T_1,T_2	PL	C_{NMR}	----	inertial	128
SnI_4	^{119}Sn	T_1,T_2	PL	C_{NMR}	----	inertial	128
PD_3	^{31}P,^{2}D	T_1		C_{MB}	no	J	129
ClO_3F	^{19}F,^{35}Cl	$T_1(^{19}F)$,$T_2(^{35}Cl)$	EL	C_σ	no	J	130

Table 4 - Continued.

Molecule	Nuclei Monitored	Methods Used	Temp. Range[a]	Value of C[b]	Anisotropy Considered	Conclusions	Ref.
					T_{1J} T_{1I}		

Table 3 - Continued.

Molecule	Nuclei Monitored	Methods Used	Temp.[a] Range	Value[b] of C	Anisotropy Considered	Conclusions	Ref.
CCl_3F	$^{19}F, ^{35}Cl$	$T_1(^{19}F), T_2(^{35}Cl)$	EL	C_σ	$\frac{\tau_{J\perp}}{\tau_{J\parallel}} = \frac{I_{\parallel}}{I_{\perp}}$	J	131
C_6D_5F	$^{19}F, ^{2}D$	T_1	El,DF		no	J	132,133

[a]PL-partial liquid range (usually from the melting point to the boiling point), EL-entire liquid range from the melting point to the critical point, DF-dense fluid (the temperature region about the critical point).

[b]C_σ is derived from the chemical shielding data, C_{MB} is measured in a molecular beam experiment, and C_{NMR} is obtained from NMR relaxation data using the Hubbard relation.

[c]T_1 was measured in different Zeeman field strengths to separate $R_{1,csa}$ from $R_{1,sr}$.

[d]But at the critical point $\tau_J^* \simeq \tau_\theta^* \simeq 0.7$.

[illegible]112-133.

[illegible]sed to inve[illegible]

[illegible] that J-diffu[illegible]

[illegible]les, the ma[illegible]

[illegible]ch. In all [illegible]

[illegible]lar symmetr[illegible]

[illegible] not importa[illegible]

[illegible]135, may be [illegible]

[illegible]les is off-a[illegible]

[illegible] complicated. [illegible]

[illegible]ied to a mole[illegible]

[illegible]dered.

[illegible] Investigation [illegible]

[illegible]troscopy

Classical fo[illegible]

[illegible] considered to [illegible]

[illegible] full rotation [illegible]

[illegible] this τ_θ and [illegible]

[illegible]tisfactory in [illegible]

[illegible]dependently. [illegible]

[illegible] only indepen[illegible]

[illegible]cussed[134,135] [illegible]

[illegible]mining time [illegible]

[illegible]ce generally [illegible]

[illegible]shape. In a[illegible]

model[37,112-133]. Table 3 shows that a variety of techniques have been used to investigate the temperature dependence of τ_θ and τ_J and also that J-diffusion has been remarkably successful for these small molecules, the majority of which are spherical tops (or were analyzed as such). In all of these cases the spin -1/2 nucleus is on the molecular symmetry axis; so if anisotropic motion was not considered, or is not important for reason of symmetry, as in CCl_4 or CS_2, Equation (105) may be used to obtain τ_J. Naturally, if the spin -1/2 nucleus is off-axis or if the motion is anisotropic, the analysis is more complicated. In only one case[131] (CCl_3F) was extended diffusion applied to a molecule of lower symmetry and the effects of anisotropy considered.

F. Investigations of Extended Diffusion by Visible and Infrared Spectroscopy

Classical forms of spectroscopy (Raman, Rayleigh, and IR) can be considered to test the extended diffusion model directly since the full rotational correlation function is, in principle, measured; from this τ_θ and τ_J may be extracted. These experiments are less satisfactory in that the two correlation functions are not determined independently. At the present time NMR relaxation experiments are the only independent measure of τ_J, although other methods have been discussed[134,135]. The difficulty with spectroscopic methods of determining time correlation functions is shown by Equation (83), since generally it is not possible to simply Fourier invert the bandshape. In addition, Raman scattering experiments suffered from

pre-defined sc

ge as a light

Raman[2,9,31,

e discussed in

ower Raman and

been pointed

clear relaxatio

ments a result

perimentally.

he reorientation

cribed in deta

the zeroth mo

been shown t

nes[14] except

number of meas

the IR techni

procedure is to

ber of Rayleig

he problem of t

Rayleigh effect.

NMR-IR[158,

experiments repo

an ill-defined scattering geometry before the introduction of the laser as a light source.

Raman[2,9,31,93,136] and infrared[2,9,93,137-137] band shapes have been discussed in terms of molecular motions, also the relationship between Raman and nuclear spin relaxation has been examined and it has been pointed out that Raman bandshapes can be used to predict nuclear relaxation times[140]. That this has not been exploited is perhaps a result of the ease of measuring nuclear relaxation times experimentally. Recently the experimental techniques for isolating the reorientational broadening component of Raman lines have been explored in detail with a number of systems studied[125,141-157], and the zeroth moment of the Raman rotational correlation function has been shown to agree satisfactorily with the NMR correlation times[141] except in the case of chloroform at high pressures[155]. A number of measurements of the rotational time correlation function by the IR technique have been reported[152,153,157-166]; the usual procedure is to neglect other broadening mechanisms[158,159]. A smaller number of Rayleigh experiments have appeared[149-151,167-171], due to the problem of the uncertain contribution of the intermolecular Rayleigh effect. In addition, there have been a small number of joint NMR-IR[158,172], NMR-Raman[77,81,125,155], and NMR-Rayleigh[174,175] experiments reported.

Phase Transitions

A solid-solid p
through[176] states
calorimetric metr
thermal anomaly i
earlier is a solid-
charges to cr
highly spherical or
ability, originally,
transition signals
this model it is
potential contain
kT. In an alt
barriers are greate
tion to another occ
entropies of transi
these reasonably we
where n, the number
the crystal symmetr
plastic crystal str
molecule of C_{3v} sy
by a predicted tra
of molecules of thi
due to the rotation

III. Plastic Crystals

A. Phase Transitions in the Solid

A solid-solid phase transition is a not uncommon phenomenon; McCullough[176] states that of 300 organic compounds studied in detail by calorimetric methods, more than one-third exhibited some sort of thermal anomaly in the solid. The most obvious cause for such behavior is a solid-solid phase transition wherein crystal structure A changes to crystal structure B. When the molecules are roughly spherical or possess an axis of high symmetry another possibility, originally suggested by Pauling[177], is that the phase transition signals the onset of molecular rotation in the solid. In this model it is helpful to think of a molecule as rotating in a potential containing n wells, with the barrier between wells less than kT. In an alternative model, proposed by Frankel[178], the barriers are greater than kT and a jump from one preferred orientation to another occurs through thermal fluctuations. The observed entropies of transition for many molecules which have plastic phases agree reasonably well[179] with entropies calculated from $\Delta S = R \ln n$ where n, the number of preferred orientations, is determined by the crystal symmetry and the molecular symmetry. For example, in a cubic crystal structure there are eight potential wells, and a molecule of C_{3v} symmetry will have eight distinguishable orientations for a predicted transition entropy of 4.13 e.u. Crystals made up of molecules of this type should have quite unusual physical properties due to the rotational freedom; quite early it was recognized that

g solids where the
entropies of fus
ly by the follo
-plastic) solid
translational a
ellipsoidal mo
already gained
solid will only
T_m, so ΔS_m =
lastic solid will b
since a plast
characteristic
vapor pressures
lastic solids ofte

The early meas
thermodynamic, a
ic data are on
ve no indication
thermodynamic
high-barrier, the
ntinuous-rotation

Spectroscopic S

In order to un
in plastic so
quilibrium proper

many solids where the molecules were of spherical shape had unusually low entropies of fusion[180]. That this should be so may be seen quite readily by the following argument. The entropy of fusion for a normal (non-plastic) solid consists of the entropy gained as the molecules gain translational and orientational freedom upon melting. For a rigid ellipsoidal molecule this is $3R/T_m$. However, molecules which have already gained orientational freedom at a phase transition in the solid will only gain the translational freedom at the melting point T_m, so $\Delta S_m = 1.5R/T_m$. Furthermore, the melting point of a plastic solid will be higher than the melting point of a non-plastic isomer since a plastic crystal process more degrees of freedom. Other characteristic properties of plastic solids are relatively high vapor pressures in the solid, small liquid temperature range (plastic solids often sublime) and a soft, waxy solid state.

The early measurements on the nature of plastic solids were all thermodynamic, and as Darmon and Brot[181] point out, thermodynamic data are only a measure of the disorder of the system and give no indication of the dynamics of this disorder. Consequently, from thermodynamic data alone one is unable to distinguish between a high-barrier, thermally-activated jump model and a low-barrier continuous-rotation model.

B. Spectroscopic Studies of Phase Transitions

In order to understand the dynamics of the thermodynamic disorder in plastic solids it is necessary to study more than the equilibrium properties. Dielectric relaxation studies[182] have

ow that the rotat
ization is unaf
the dielectric
over the liquid a
ation requires
-polar molecules
ized. Since the
electric relaxati
the other hand, do
more complete i
use this method.
ing both continuo
ow the temperatu
astic crystal; th
ent discontinuitie
ical a phase tran
for the change in
the energy for the
dependence of the l

where $a = (8/\ln 2)^{-1}$
B is the line wid
with before, and B
been to drop at

shown that the rotational motion contributing to the dielectric polarization is unaffected upon freezing a plastic solid[13,184]; both the dielectric constant and the activation energy change little between the liquid and the solid[183,184]. However since dielectric relaxation requires the presence of a reorientating electric dipole, non-polar molecules or rotations about the dipolar axis cannot be studied. Since these are precisely the cases of special interest, dielectric relaxation has proven of limited use. NMR studies, on the other hand, do not require a permanent dipole moment, and most of the more complete investigations into motion in plastic solids have used this method. NMR studies of plastic solids have been performed using both continuous wave (cw) and pulse techniques. Figure 4 shows the temperature-dependent second moment M_2 for a characteristic plastic crystal; the linewidth behaves similarly. In the cw experiment discontinuities in the second moment, or in the linewidth, signal a phase transition. The nature of the motion may be deduced from the change in the value of the second moment[185] and the activation energy for the process may be determined from the temperature-dependence of the linewidth through the semi-emperical relation[34]

$$\tau_d = \frac{\tan[\frac{\pi}{2}(\frac{\delta H^2-B^2}{C^2-B^2})]}{\alpha\gamma\delta H} . \qquad (124)$$

where $\alpha = (8/\ell n2)^{-1}$, γ is the magnetogyric ratio of the resonant spin, δH is the line width in the transition region, and C is the line width before, and B after, the narrowing. In Figure 4 the second moment is seen to drop at T_t from a value consistent with a rigid lattice

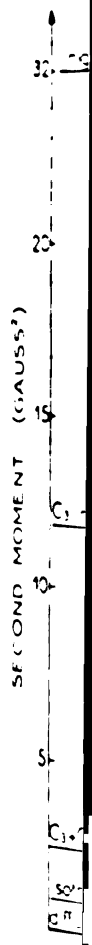

Figure 4. The te
resona
hexame
calcu
Refere

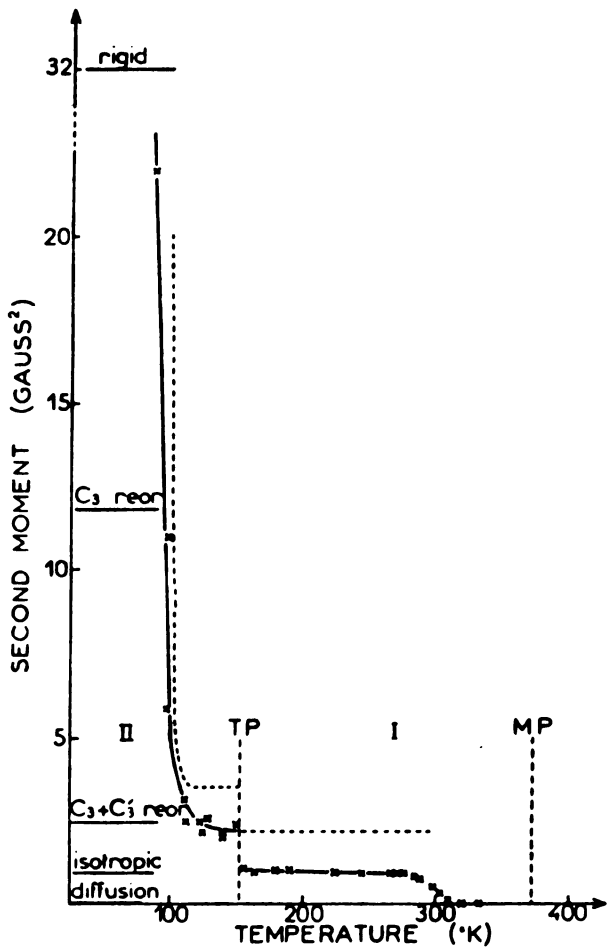

Figure 4. The temperature dependence of the second moment of the resonance line for a typical plastic crystalline solid hexamethylethane. Also shown are the second moments calculated for different types of motions. From Reference 197.

value in agr

second moment

rapid translat

in T_1 indic

dence of T_1,

ating frame) c

ive jumps and

to Torrey[186],

The Pople-Kar

NMR determina

xation ($E_{a,dd}$

onal diffusion

ystalline phase

for isotropic

$E_{a,dd}$. The rela

translation and ro

Gerasz theory of m

transition tempera

ich is a measure

elative to those

Gerch[191,202], we as

for molecular reor

respectively; thus

to a value in agreement with quasi-free isotropic rotation. At T_{sd} the second moment undergoes a smooth decline to zero, an indication of rapid translational diffusion. In pulse experiments discontinuities in T_1 indicate a phase transition and strong temperature dependence of T_1,T_2 and $T_{1\rho}$ (the spin-lattice relaxation time in the rotating frame) can be used to determine the mean time between diffusive jumps and the activation energy for diffusion using the theory due to Torrey[186,187], as corrected by Torrey and Resing[188].

C. The Pople-Karasz Theory of Melting

NMR determinations of activation energies for dipole-dipole relaxation ($E_{a,dd}$), spin-rotational relaxation ($E_{a,sr}$), and translational diffusion ($E_{a,trans}$) for compounds which exhibit a plastic crystalline phase[50-58,189-206], are summarized in Table 4. Recall that for isotropic rotational diffusion one predicts that $E_{a,sr} = - E_{a,dd}$. The relationship between the activation energies for translation and rotation may be studied on the basis of the Pople-Karasz theory of melting[207-209]. In this theory the melting and transition temperatures are shown to depend on the parameter v, which is a measure of the energy barriers for molecular rotation relative to those for a jump to an interstitial site. Following Smith[191,202], we associate these barriers with the activation energies for molecular reorientation ($E_{a,dd}$) and molecular diffusion ($E_{a,trans}$), respectively; thus

$$v \propto \Gamma \equiv \frac{E_{a,dd}}{E_{a,trans}} . \qquad (125)$$

Table 4. Activation Energies in the Plastic Crystalline Phase

Molecule	T_t	T_m	T_B[a]	$E_{a,dd}$	$E_{a,sr}$	$E_{a,trans}$	$D_S \times 10^{19}$[a]	Ref.
P_4	196	317	553	5.7	-6.0			55,56
				4.0		12.1		188
C_6F_6	168	336	---	0.430 (high T)		14.1±0.2	2.1	189

Table 4. Activation Energies in the plastic crystalline phase

Molecule	T_t	T_m	T_B[a]	$E_{a,dd}$	$E_{a,sr}$	$E_{a,trans}$	$D_S \times 10^{+9}$[a]	Ref.
P_4	196	317	553	5.7	-6.0			55,56
				4.0		12.1		188
C_6F_{12}	168	336	---	0.430 (high T)		14.1±0.2	2.1	189
				1.2 (low T)		14.5±0.4	4.2	190
$C(CH_2OH)_4$	461	539	∿573	25.2±1.0		24.3±0.5		191
Adamantane	209	540	∿540	3-6		36.5	1.0	192
$C(CH_3)_4$	140	257	283	1.0		66.0	4.1	193
Camphor	250	449	482	2.8		14.6		194
NH_4ClO_4	<80	d	---	0.70±0.1	-1.1			57
Pivalic acid	280.1	309.7	437.0	8.6±0.7		15.1±1.4	1.6	195
$Cl_3CC(CH_3)_2Cl$	210.8	442	---	2.8±0.2		18 ±2		196
$(CH_3)_3CC(CH_3)_3$	152.5	374	380.0	2.2±0.1		19.6±0.5	14	197
				1.5		18 ±2		198
				2.2		19.6		199
$(CH_3)_3SiSi(CH_3)_3$	221.7	288	---	2.20±0.10		8.7±0.4		198
				1.2		10		199
MoF_6	263.6	290.6	308.2			12.9	5.2	52
WF_6	264.7	275.7	292.7			12.7	3.6	52
Norbornylene	---	320	---	∿1.0		11.6		199
Norbornadiene	---	254	---	1.91		9.54		199

Molecule	T_t	T_m	T_B [a]	$E_{a,dd}$	$E_{a,sr}$	$E_{a,trans}$	$D_S \times 10^{9n}$	Ref.
$C(CH_3)_3Cl$	183	245	324	~1.5		5		193,201
$C(CH_3)_2Cl_2$	187	238	343	~3		6		193,201
$Si(CH_3)_4$		174	300	7.2		6.2		202

Table 4 - Continued.

Molecule	T_t	T_m	T_B[a]	$E_{a,dd}$	$E_{a,sr}$	$E_{a,trans}$	$D_S x10^{+9}$[a]	Ref.
$C(CH_3)_3Cl$	183	245	324	∿1.5		5		193,201
$C(CH_3)_2Cl_2$	187	238	343	∿3		6		193,201
$Si(CH_3)_4$	---	174	300	7.2		6.2		202
NF_3	56.6	66	153.2	0.98±0.08		1.93±0.11		203,204
PD_3	88	139	---	0.5	∿-0.5	4.5	1.0	58
D_2S	126.2	187.6	211.4	<1.0		7.4 0.4		205
DCl	105	161	189.5	0.85		3.9		206
DBr	121	184.7	206.2	1.09		6.2		206
DI	128	222.4	---	0.97		6.1		206

[a]T_t - temperature of the transition to the plastic crystalline phase; T_m - melting point; T_b - boiling point.

[b]The value of the self-diffusion coefficient at the melting point.

In Figure 5 we

temperatures,

$$T_m^* = C$$

where T_b is the boil

lines are from Re

with the pred

In Figure 5 we plot Γ versus reduced melting (T_m^*) and transition (T_t^*) temperatures, where

$$T_m^* = 0.72(T_m/T_b) \qquad T_t^* = 0.72(T_t/T_b) \tag{126}$$

and T_b is the boiling point at one atmosphere pressure. The smooth curves are from Reference 191, Figure 6, and give qualitative agreement with the predictions of the Pople-Karasz theory[208].

Figure 5. Plot
melti
Solid

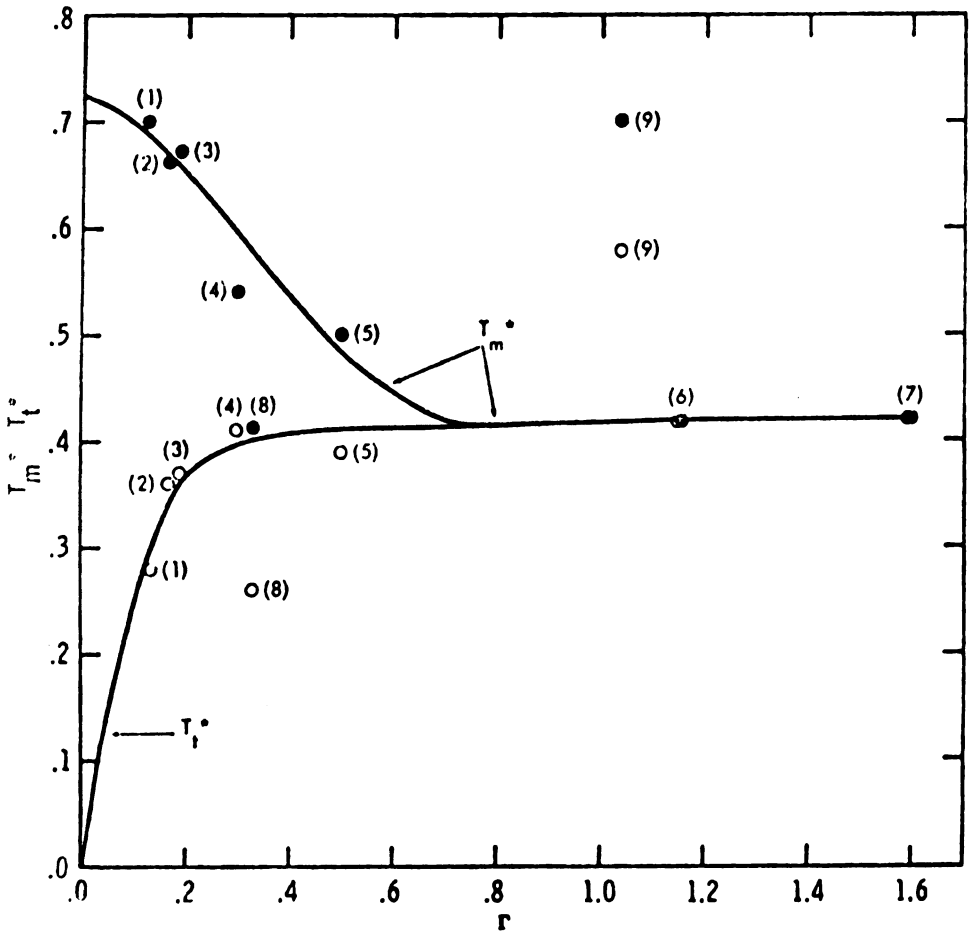

Figure 5. Plot of reduced transition temperature (T_t^*) and reduced melting temperature (T_m^*) versus Γ for molecular crystals. Solid points are T_m^* data, open circles T_t^* data.

I. Introduction

Although seve
time saving in
nes in liquids [3]
has the advanta
mode detection) a
H_1 homogeneity
experiments. Howe
detection becomes
free induction dec
signal-noise ratio. P
this difficulty by
this advantage is
a larger uncerta
the more elaborate

For very shor
sequence remains t
stringent require
$T_1 \gg nT_s$, where
the magnetization
pose of the multi
magnetization man
Thus, even pulse

EXPERIMENTAL

I. The NMR Spectrometer

A. Introduction

Although several multiple-pulse sequences have been suggested for time saving in the measurement of long spin lattice relaxation times in liquids [37,210-214], the 180°-τ-90° method is still useful. It has the advantages that only two pulses and one rf channel (hence, diode detection) are needed, and the requirements on pulse lengths and H_1 homogeneity are not as stringent as in the multiple-pulse experiments. However, if T_1 is much longer than one second, data collection becomes tedious, particularly if the addition of several free induction decays (FID) is necessary for a satisfactory signal-to-noise ratio. Progressive saturation methods[213,214] alleviate this difficulty by not waiting for the return to equilibrium but this advantage is offset by the smaller value of M_0-M_∞, which leads to larger uncertainties in the calculated relaxation times, and by the more elaborate calculations necessary.

For very short relaxation times ($<10^{-2}$ sec) the 180°-τ-90° sequence remains the preferred method. In addition to the less stringent requirements on the spectrometer, the assumption that $T_1 \gg n\tau_s$, where τ_s is the length of pulse(s) necessary to sample the magnetization, becomes valid only for n small whereas the purpose of the multiple-pulse experiment is to sample the decay of the magnetization many times in the span of a few relaxation times. Thus, even pulse sequences which average out errors in phasing and

ogeneity[37] ar

al control of t

operator cannot

m to equilibr

By interfacin

ferencies in th

ments have r

partially-rela

ing amounts of

ly employ a type

ribed below bu

resent approach s

r studying sing

ectrometers and

Measurement o

med convenient

lse method for

the shape of

s in the case of

rovide a useful

mical exchange

here scalar coup

$T_{1S} \ll T_{1I}$), J

determined[220] fro

A slight dis

ge measurements

ward manner.

H_1 homogeneity[37] are not adequate for short relaxation times. However, manual control of the 180°-τ-90° experiment is now inefficient since the operator cannot collect the data at the rate allowed by the rapid return to equilibrium.

By interfacing a computer to the pulse spectrometer these inefficiencies in the two-pulse experiment may be minimized. Commercial instruments have recently become available which include a capability for partially-relaxed Fourier transform (PRFT) experiments with varying amounts of data reduction[215,216]. These systems presumably employ a type of computer-controlled timing similar to that described below but no details appear to have been published. The present approach should provide a useful and less expensive alternative for studying single-spin systems and is applicable to a variety of spectrometers and minicomputers.

Measurement of $T_{1\rho}$ (T_1 in the rotating frame) may also be performed conveniently by the method described here. Since the only pulse method for $T_{1\rho}$ measurement requires many repetitions to trace out the shape of the relaxation curve, the same inefficiencies apply as in the case of the 180°-τ-90° T_1 experiment. Such measurements provide a useful method for studying ultra-slow motions in solids[217], chemical exchange rates[218] and spin-spin relaxation times[219]. Also, where scalar coupling exists between a resonant nucleus I and a spin S ($T_{1S} << T_{1I}$), J_{IS}, the scalar coupling constant, and T_{1S} can be determined[220] from T_{1I}.

A slight disadvantage to this simple scheme for relaxation time measurements is that T_2 cannot be determined in a straightforward manner. The two-pulse experiment for measuring T_2

should
correla
shall be
turn to
over tra
acute ca
difficult
and tra
computer
"built"
define a

Comp
filtered a
"Gaussian"
shortage
"electroni
ability
is an ac

The
then, wi
substitu
noise an
in Figur
The de
an "rec
check o
This vis

($90°-\tau-180°-\tau$) is affected by diffusion[221] and may not give an exponential decay; the Meiboom-Gill modification[222] to the Carr-Purcell method B[221] removes this effect and produces an exponential return to equilibrium but requires more than two pulses. Therefore, either the computer-controlled two-pulse experiment may be performed and the data analyzed as discussed in Section II to determine the self-diffusion coefficient, or the timing of the Carr-Purcell spin-echo train may be arranged externally and the data collected by the computer and analyzed on-line. The program and procedure for analyzing multiple-pulse T_2 experiments is fast and efficient but entirely routine and is discussed in Appendix A.

Computer-controlled data collection may in one sense be considered a convenience, although in repetitive experiments, like the $180°-90°T_1$ sequence, the convenience can be substantial. The true advantage to the procedure described herein lies in the interactive relationship between the experimenter and the experiment. The ability to evaluate an experiment immediately as it is performed is an advantage which cannot be stressed too strongly.

The components of a modified NMR Specialties MP-1000 spectrometer, with a Nicolet 1082 computer[216] and a home-built interface substituted for the pulse programmer, are shown in Figure 6. The pulse and timing sequences for both T_1 and $T_{1\rho}$ measurement are shown in Figure 7(a). In addition to providing the necessary pulses and time delays, the computer provides on-line data analysis, giving an immediate numerical value for the relaxation time and a visual check of the fit to the expected log (M_z-M_∞) vs. time relationship. This visual check is useful in tracing the cause of a large standard

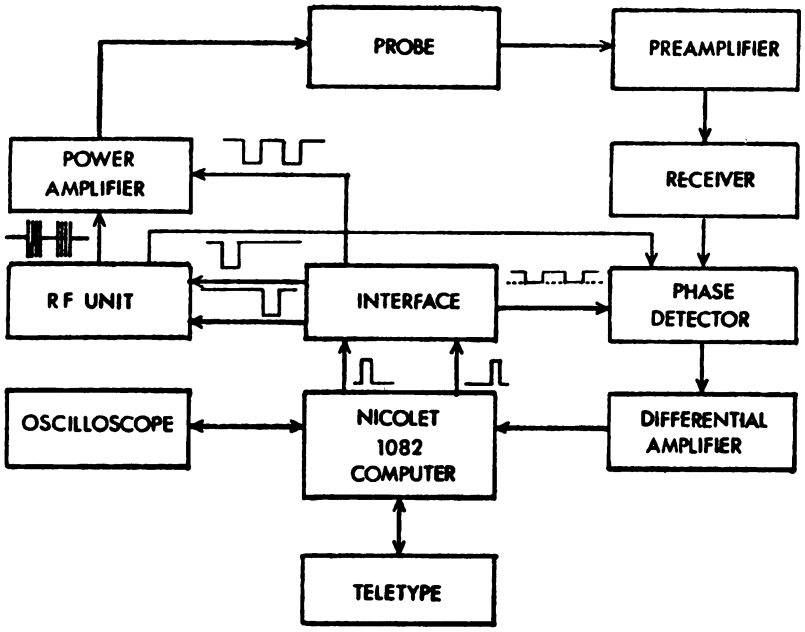

Figure 6. Block diagram of computer-interfaced pulsed NMR spectrometer.

[a]

T_1

CO
PU

$T_{1\rho}$

[b]

1in
2i
M
M
M
M
FF
FF
M
M
FF

[c]

$T_1[T_2]$

PHASE D

$T_{1\rho}$

PHASE

Figure 7.

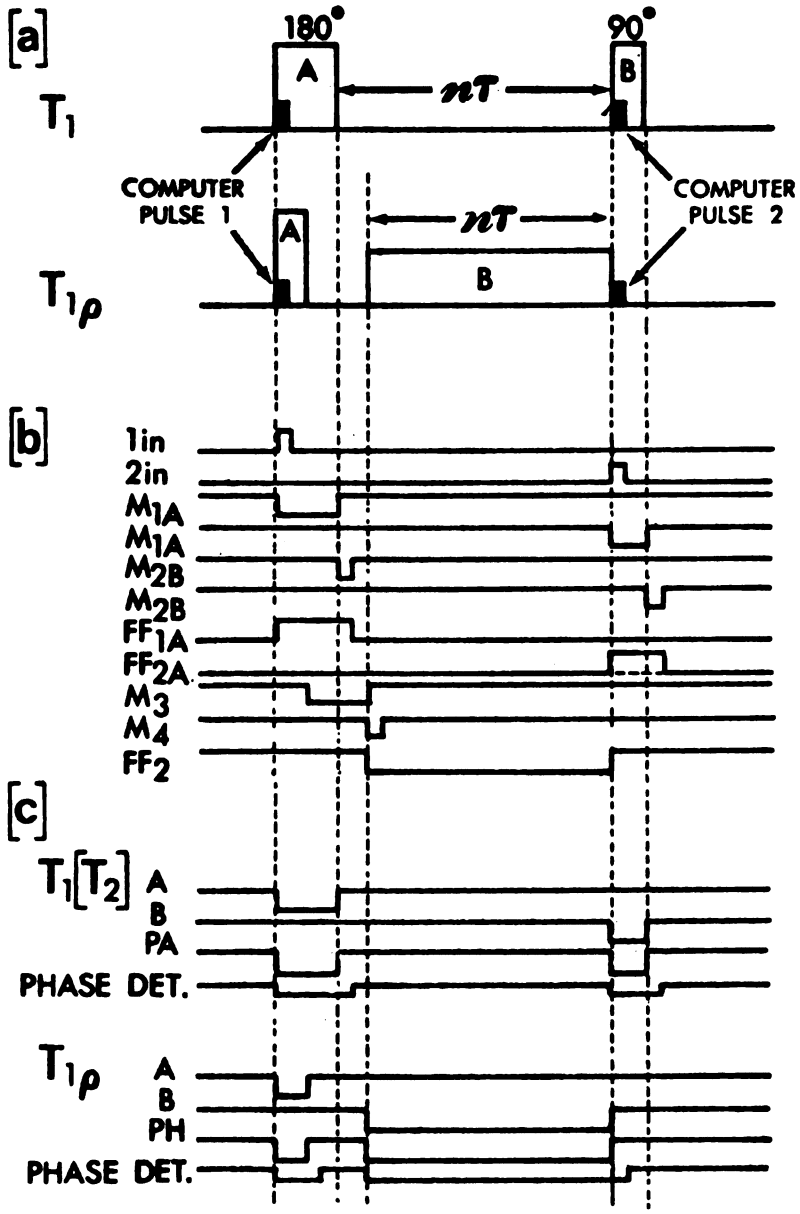

Figure 7. Timing diagram (x axis to scale). (a) Timing of rf pulses. (b) Internal timing in the interface. The levels are 0 V and +5 V. (c) Timing of the interface output. Positive voltages are ∿2 V, negative voltages -15 V.

ation since,

ne inhomogeneit

ar choice of b

reasing a sig

ver the course

The only mo

sitive detect

measure descri

ise in channel

as shown in Figu

ring pulse fo

ata collection

n both T_1 and

3. The Pulse S

The spectr

specialties MP-

used is shown i

15.00 MHz qua

phase control,

and a phase-sen

operate at 56.4

at 14.11 MHz an

convenient to u

as the frequenc

also allowed sa

deviation since, for systems in which $T_1 \cong T_2$, it has been shown[223] that inhomogeneties in H_1 produce a non-exponential relaxation. A poor choice of baseline will also produce systematic deviations, indicating a significant drift from optimum operating conditions over the course of the experiment.

The only modification to a spectrometer employing phase-sensitive detection required to perform $T_{1\rho}$ experiments by the procedure described here is a variable attenuation for the locking pulse in channel B. The timing for the two experiments is identical, as shown in Figure 7 (a), with pulse 2 serving to terminate the locking pulse for $T_{1\rho}$ measurements. The procedure for more efficient data collection and reduction in two-pulse experiments applies directly to both T_1 and $T_{1\rho}$ experiments.

B. The Pulse Spectrometer

The spectrometer used in this work was a highly modified NMR Specialties MP-1000. A block diagram of the components which were used is shown in Figure 6. The rf unit originally consisted of a 15.00 MHz quartz crystal, two doubler stages, the delay lines for phase control, an rf amplifier consisting of two nuvistor tubes, and a phase-sensitive detector. This unit was first modified to operate at 56.4 MHz by exchanging the crystal for one which oscillated at 14.11 MHz and retuning all of the stages, but it proved more convenient to use a frequency synthesizer operating at 56.4 MHz as the frequency source and bypassing the two doubler stages. This also allowed samples to be brought to resonance by changing the rf

heavy rather t

The power am

on the second s

ge that was use

al configuratior

for load.

The probe was

tation between

arter-wave (λ/4

both the tra

for maximum

this applicat

all voltages

pedance while

conductors. C

ets of diodes

attenuation bu

from rising m

appears as an

arter-wavel

to present a

the transmitte

impedence when

eight pairs of

The preamp

to 36.4 MHz. Th

rf pulse was

frequency rather than changing the magnetic field.

The power amplifier was a two-stage, high-power unit but for this work the second stage of amplification was not necessary. The one stage that was used contained two 3E29 tubes operating in a push-pull configuration and delivering an output of 350 V p-p across a 50 ohm load.

The probe was of the single-coil design described in Section ID. Isolation between the transmitter and receiver was achieved with quarter-wave ($\lambda/4$) cables and crossed diodes[244,245] shown in Figure 8. Both the transmitter-probe and probe-receiver distances were $\lambda/2$ for maximum transmitted voltage. The useful properties of diodes in this application is their non-linear voltage-current curve. For small voltages (<0.5 V) a set of crossed diodes will present a high impedence while for large voltages (>0.5 V) they will behave as conductors. Consequently, when an rf pulse is being delivered both sets of diodes conduct; the pulses arrive at the probe with little attenuation but set D2 prevents the input voltage to the preamplifier from rising much above 0.5 V. The effective short circuit at D2 appears as an open circuit at D1 since the two sets of diodes are a quarter-wavelength apart. After the pulse is over both sets D1 and D2 present a high impedence to the nuclear signal, thus isolating the transmitter from the receiver circuit. In order to lower the impedence when the diodes are conducting, each set was made up of eight pairs of diodes.

The preamplifier and receiver were standard components, tuned to 56.4 MHz. The recovery time of the receiver system following an rf pulse was 7 microseconds, consequently the total dead-time

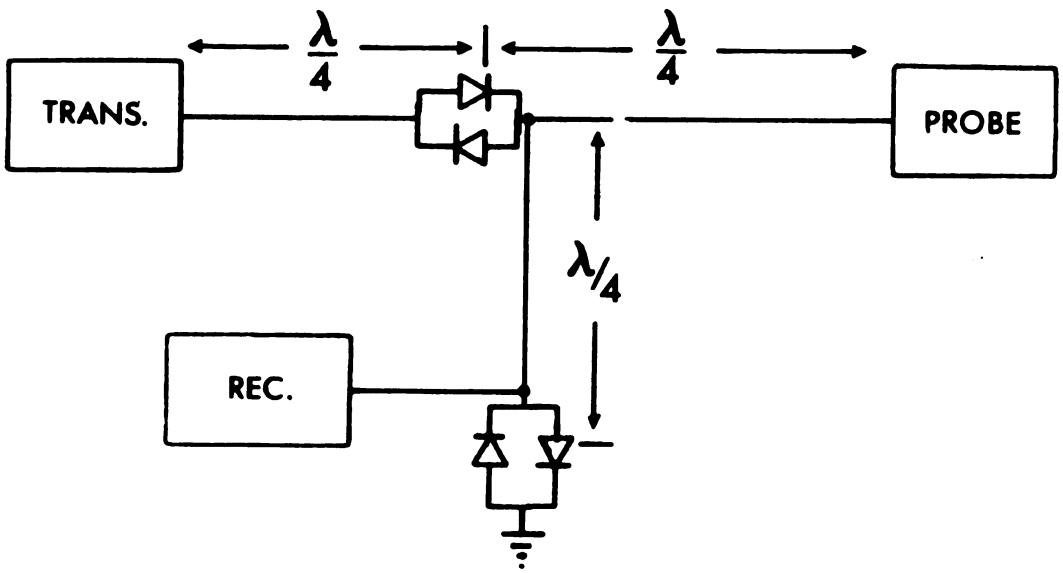

Figure 8. The arrangement of crossed diodes and tuned cables for the purpose of isolating the transmitter from the receiver.

the 90° pulse

The timing

the NMRS puls

sources and mu

ses per subco

ains three

ing sequence

this investi

introducing

which were c

which may be c

ses, are dis

In order

its frequency

ange 5-30 MHz

ower amplifi

[228]. This

the probe cha

changed.

The Inte

In orde

interface mu

generated tr

the +5 V and

spectrometer

the section

the interfa

for a 90° pulse was 11 μsec.

The timing for various pulse sequences was originally supplied by the NMRS pulse programmer which is capable of generating two pulse sequences and multiple pulse sequences with up to four different pulses per subcycle (for example, the triplet T_1 sequence[210,212] contains three pulses per subcycle, and the basic Waugh dipolar narrowing sequence[226,227] contains four pulses per subcycle). As a part of this investigation, a major improvement was made to the spectrometer in introducing the option of computer-controlled timing, the advantages of which were discussed in Section IA. The different pulse sequences which may be computer-controlled, and their respective computer programs, are discussed in Section II.

In order to measure the spin-lattice relaxation times for deuterium at a frequency of 9.21 MHz, this system was modified to operate in the range 5-30 MHz with the addition of an rf mixing network and broadband power amplifier, probe and preamplifier as described by Traficante et al[228]. This modification, shown in Figure 9, affects the discussion of the probe characteristics only; the rest of the basic spectrometer is unchanged.

C. The Interface

In order to perform the function of the pulse programmer, the interface must provide pulses of varying lengths from the computer-generated trigger pulses[229] and must shift the logic levels from the +5 V and 0 V used by the computer to those required by the spectrometer. The circuit diagram is shown in Figure 10 with the sections responsible for the different outputs identified. The interface is switched from T_1 to $T_{1\rho}$ mode by a single control

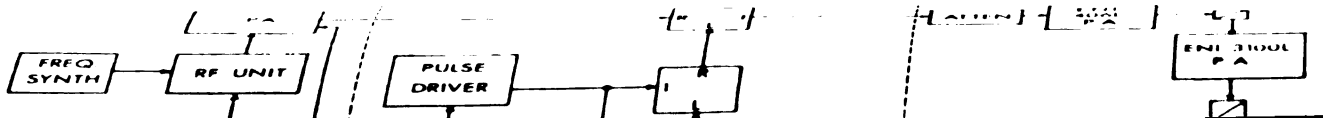
FREQ SYNTH
RF UNIT
PULSE DRIVER

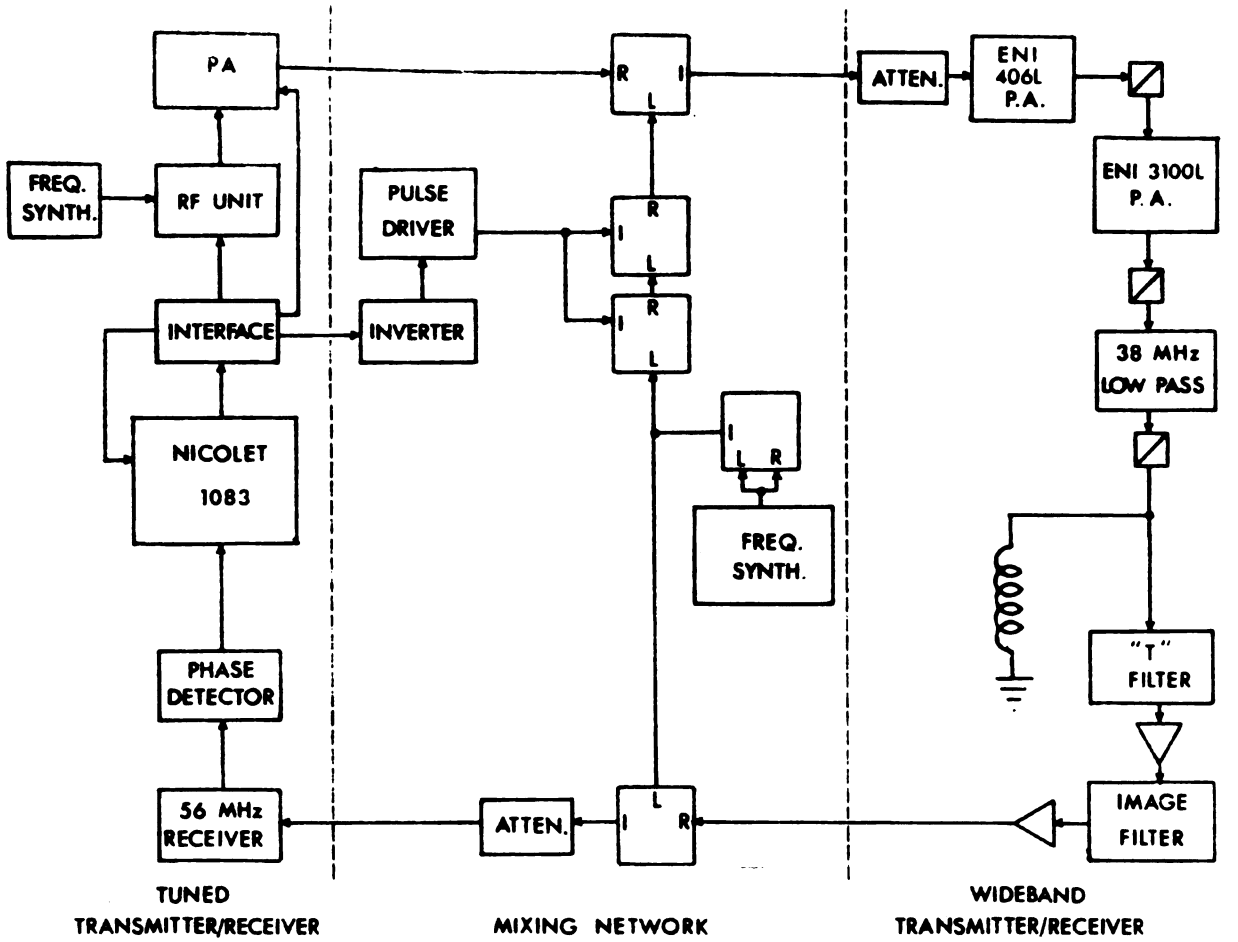

Figure 9. Modification of the tuned spectrometer to allow nuclei to be observed in the frequency range 4-30 MHz. Crossed diodes are denoted by ⊠, low-noise amplifiers are denoted by ▷.

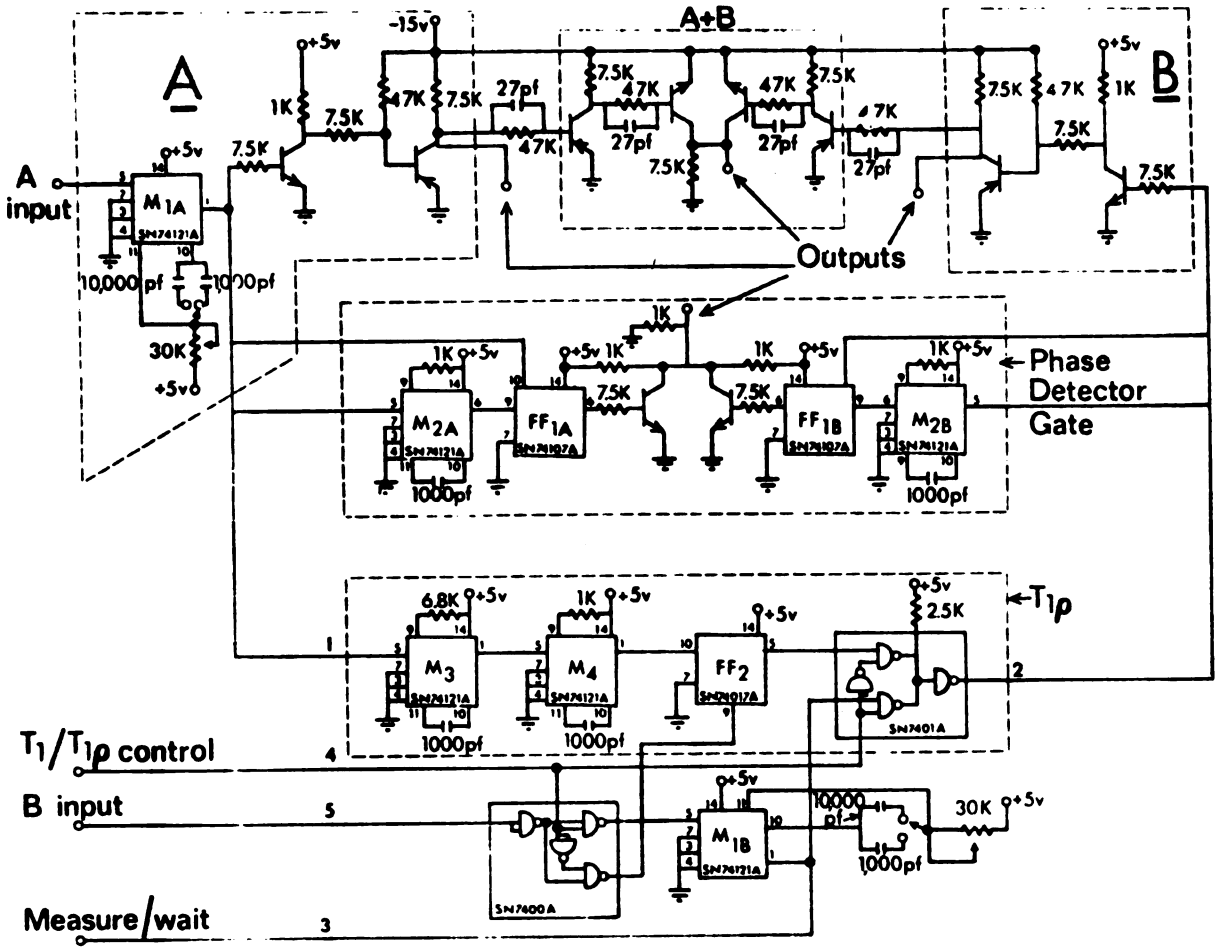

Figure 10. Interface circuit diagram. All npm transistors are T1S98; all pnp are 2N3645. All resistors are 1/4 w, 7.5 kΩ except where noted; all capacitors are 10,000 pfd 500 VDC mica except where noted.

leading to a

NAND gates w

wiring for th

mode the i

consisting

from thes

produce the ou

the multivib

were two mor

A to clear

from the c

the spectrome

this flipflo

level 1)

output of th

circuit B.

The length

mode) is var

potentiomet

rators M_{1A} ar

switching to the

90°.

The NMR Spe

oscillator an

logical OR betwe

circuit may be p

biased on at

line leading to a front panel SPDT switch. This line controls two quad NAND gates which are connected to function as SPDT switches. The wiring for the $T_{1\rho}$ section is given fully in Figure 11. In the T_1 mode the input pulses from the computer gate identical circuits consisting basically of a monostable multivibrator M_1. The outputs from these monostables are then level-shifted and combined to produce the outputs required by the spectrometer. In the $T_{1\rho}$ mode the multivibrator circuit B (M_{1B}) is replaced as shown in Figure 10, where two monostables (M_3 and M_4) produce a pulse 6 μsec after pulse A to clear the flipflop FF_2 (1 and 2 are used here for the pulses from the computer while pulse A and pulse B [Figure 7(a)] are the spectrometer pulses). Input pulse 2 is used as the clock for this flipflop, and since the J and K inputs are unconnected (logic level 1) the outputs change state after the clock pulse. The output of this flipflop (Q of FF_2) replaces the output of M_{1B} in circuit B.

The length of each pulse in the T_1 mode (and of pulse A in the $T_{1\rho}$ mode) is varied manually from 1-100 μsec in two steps by three-turn potentiometers in the timing circuits of the two primary multivibrators M_{1A} and M_{1B}. The use of a calibrated dial facilitates switching to the $T_{1\rho}$ mode, as the A pulse must be changed from 180° to 90°.

The NMR Specialties MP-1000 requires -15 V pulses to gate the rf oscillator and power amplifier, with the output to the PA a logical OR between A and B pulses. The phase detector in this circuit may be protected from feed-through by a diode gate which is biased on at all times except during, and 2 μsec after, the PA

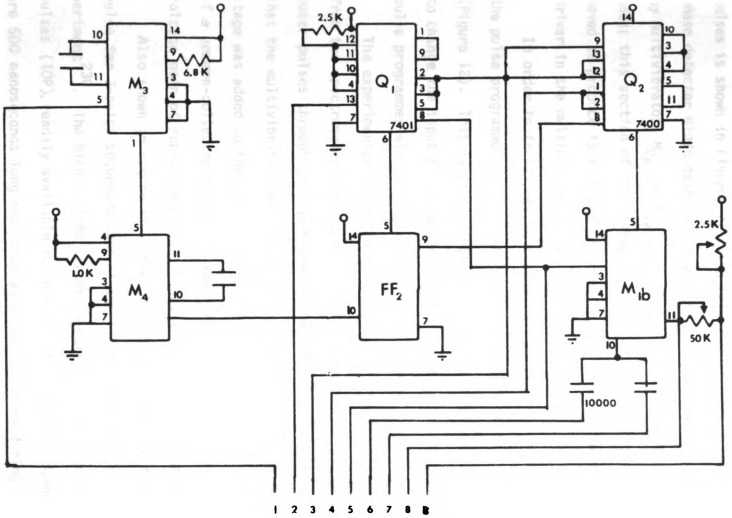

Figure 11. Details of the switching circuit for T_1/T_{1_ρ} control.

ulse. T

ses is shown

ase detector

multivibrato

ae, this sect

ned to produc

ver in the m

In order t

e pulse progr

igure 12). T

change the

ulse programm

The exper

m the spect

ser pulses t

at the multi

stage was adde

f a common-c

oltage gain

Also sho

ulse for 3-p

periment[230].

ulses (IOP),

the 500 nanos

sec allotted

OP1 and IOP2

ogical OR op

output pulse. The internal timing and the timing of the output pulses is shown in Figures 7(b) and (c); the ON voltage for the phase detector diode gate is 2 V and the 2 μsec delay is produced by multivibrators M_{2_A} and M_{2_B}. Currently, this protection is not used; this section of circuitry, with the 1 kΩ output resistor removed to produce +5 V pulses, is used as the input to the pulse driver in the multinuclear system (Figure 9).

In order to facilitate switching control from the computer to the pulse programmer an additional board was added to the interface (Figure 12). This is simply a series of NAND gates wired as switches to change the input to the power amplifier from the computer to the pulse programmer with a single front panel switch.

The experimental setup placed the computer about 20 feet away from the spectrometer and it was found that attenuation of the computer pulses through the approximately 40 feet of cable was so great that the multivibrators would not trigger. Consequently an amplifier stage was added to the computer output (Figure 13) which consisted of a common-collector transistor amplifier for each pulse with a voltage gain of approximately unity but a large current gain.

Also shown in Figure 13 is the circuitry to generate the trigger pulse for 3-pulse sequences such as the pulsed-field-gradient experiment[230]. The Nicolet 1080 series computer has two input/output pulses (IOP), readily available for control of an experiment, which are 500 nanoseconds long and occur at different times during the 4 μsec allotted to the associated commands. The commands which generate IOP1 and IOP2 (4102 and 4104, respectively) may be combined in a logical OR operation to produce a command (4106) which causes both

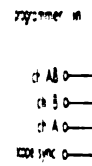

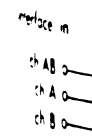

Figure 12.

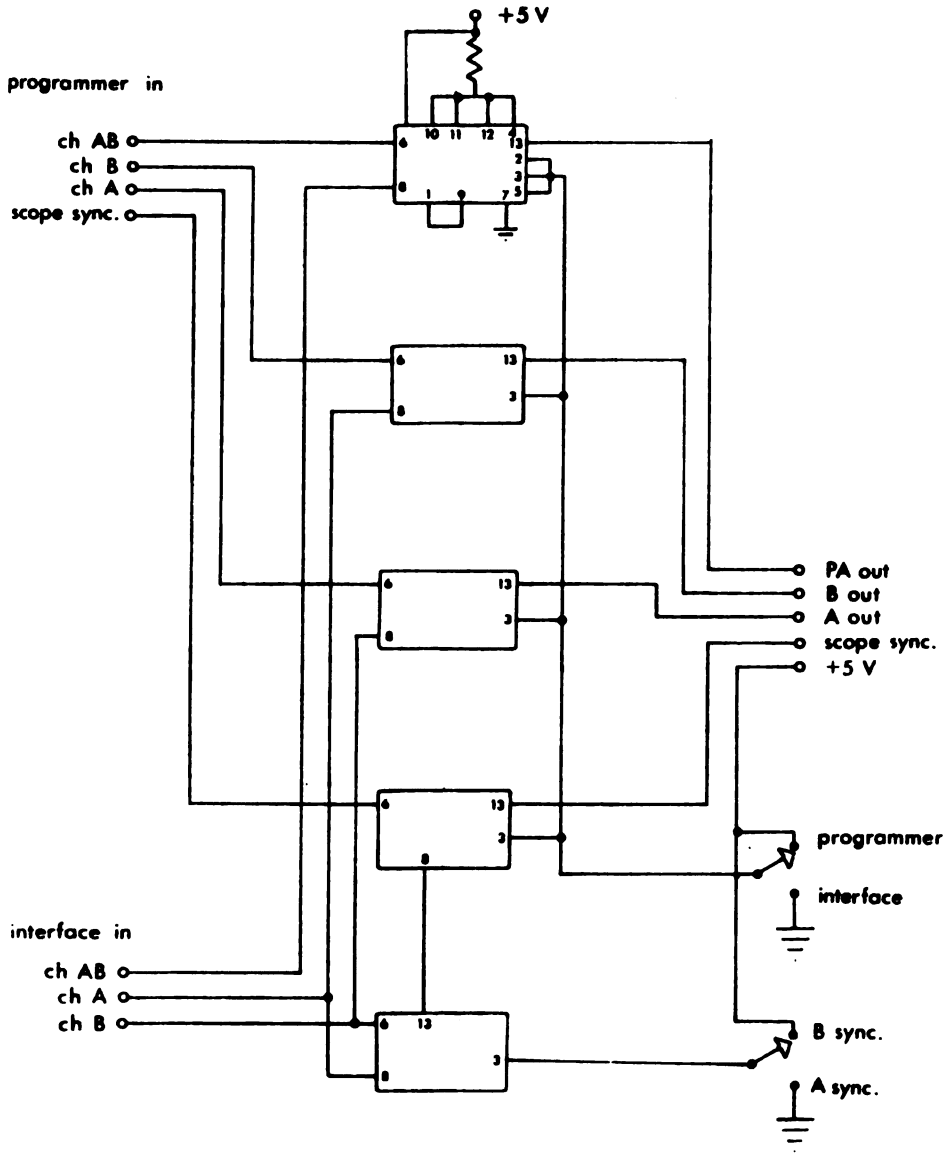

Figure 12. The circuit diagram of the switch for transferring control of the spectrometer from the pulse programmer to the computer. The other wiring details of all IC's are identical with those shown on the top IC.

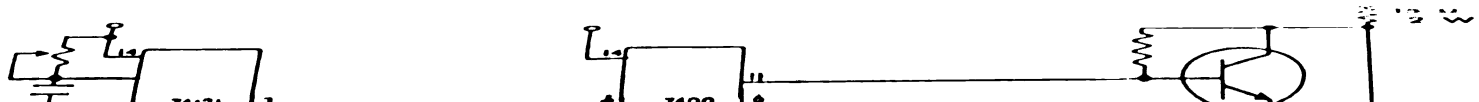

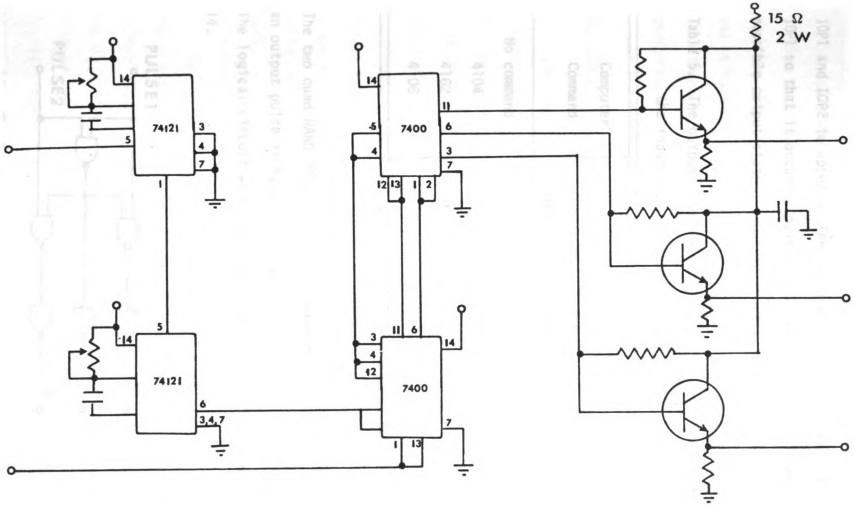

Figure 13. The pulse booster circuit and the circuit for generating a third pulse. All resistors are 1 kΩ, 1/4 W, except as noted.

ack 1092 to

so that it c

sible output

ble 5. The o

the f

Computer Command
No command
4134
4132
4136

he two qua

output p

he logical

4.

PULSE1

PULSE2

Figure 14. Th

IOP1 and IOP2 to appear. The two multivibrators in Figure 13 delay IOP1 so that it occurs simultaneously with IOP2. Now there are four possible output states, shown in Table 5.

Table 5. The output from the "pulse booster" unit as determined by the input from the computer

Computer Command	Resulting pulse				
	Out from computer		Out to spectrometer		
	IOP1	IOP2	A	B	C
No command	0	0	0	0	0
4104	1	0	1	0	0
4102	0	1	0	1	0
4106	1	1	0	0	1

The two quad NAND IC's distinguish between these states to produce an output pulse at A, B, or C under the condition shown in the table. The logical circuit which performs this function is shown in Figure 14.

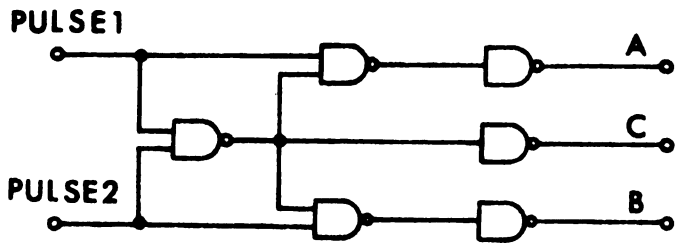

Figure 14. The logical circuit for generating the third pulse.

These contro

with Model 29

ever, that op

as performed.

ar three diff

formed using

1. The Probe

The prob

conventional

a piece o

This is the

difficulty

spectrometer

make tube

shown in Fi

coils, mach

block, provi

of thermal

The co

found that

MHz becau

the H_1 homoge

make tunin

(0.356") apar

simultaneously

These control pulses could equally well be generated with the Nicolet Model 293 I/O Controller and some software modifications; however, that option was not available at the time most of this work was performed. More complex pulse sequences (those requiring more than three different types of pulses) will certainly be more easily performed using the 293 controller.

D. The Probe

The probe which was designed and built for this work was of the conventional single-coil design (Figure 15). The coil was wound on a piece of 8" long, 0.250" i.d. quartz tubing (Wilmad Glass Co.). This is the same size as the standard Varian insert so there was no difficulty in using a standard Varian Dewar salvaged from an A56/60 spectrometer. The only modification made to the Dewar was in the gas intake tube. The complete probe, with one side panel removed, is shown in Figure 16. Note that the support for the field gradient coils, machined from Delrin, also serves as a holder for the external lock, providing the necessary electrical insulation and some amount of thermal insulation as well.

The coil consisted of seven turns of #26 magnet wire. It was found that if more turns were added, the coil could not be tuned to 56 MHz because the inductance was too large. In order to increase the H_1 homogeniety, and at the same time decrease the inductance to make tuning possible, the turns were spaced three wire diameters (0.056") apart. This was done by winding three strands of wire simultaneously and then removing two after the coiled wire had been

Figure 15.

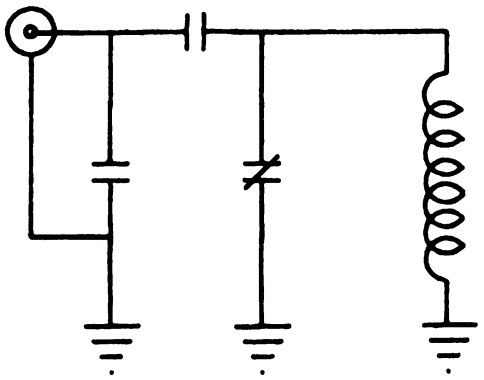

Figure 15. Circuit diagram of the probe.

Figure 16.

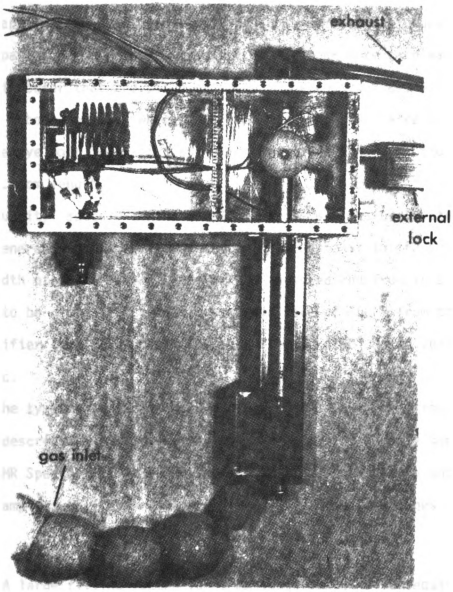

Figure 16. Photograph of the probe showing the placement of the Dewar, the field gradient coils and the external lock.

ngerated down

carefully affix

ts were wo

as to be app

ext the spac

ecessary in

he quartz tu

ext to the e

.4 and 0.9

The qual

sweep gene

The bandwidth

as found to

ower amplifi

f 3.5 μsec.

For the

he probe des

lled by NMR

ccepted samp

are:

(1) A

fo

(2) Ve

st

su

(3) Eas

od

cemented down with Duco cement. The remaining wire was then permanently affixed to the quartz tube with Epoxy cement. A number of coils were wound and inspected carefully before the Epoxy cement was to be applied. The technique of winding three strands insured that the spacing between turns was exact, but rather more care was necessary in order that the pitch of the wire be constant all around the quartz tube. The coil which was finally selected appeared perfect to the eye both in spacing and pitch and had dimensions of 0.250" i.d. and 0.9 cm length.

The quality factor Q of the completed probe was measured with an rf sweep generator and a small search coil to couple it to the probe. The bandwidth of the probe at 56.4 MHz was measured and from this Q was found to be 30. With a peak-to-peak voltage of 350 V from the power amplifier (the 3E29 tubes) this resulted in a 90° pulse length of 3.5 μsec.

For the types of experiments performed in this investigation the probe described here has several advantages over the probe supplied by NMR Specialties, which was of the crossed-coil design and accepted sample tubes up to 15 mm in diameter. These advantages are:

(1) A large filling factor for 5 mm tubes (which were required for reasons stated in Section V).

(2) Very short pulse lengths without needing the high power stage of the PA (which was somewhat tempermental and subject to expensive breakdowns).

(3) Ease of construction - no paddles are necessary and no oddly shaped coils need be wound.

(4) Lots

exte

his design ha

ence the 90°

ecoulse len

varied. A

ulse T_1 exce

time T^{222} se

sperse of in

the Dewar. F

ulse length

would be acce

made; however

Field Gr

ried in gene

of a spin sys

and of many

investigated

The sim

of disadvant

it was feare

effects on t

groundless a

factory for

is most simp

from its opt

(4) Lots of empty space in the probe for such things as the external-lock and the field-gradient coils.

This design had one disadvantage, though, that was not anticipated, since the 90° pulse length proved to be slightly temperature dependent and pulse lengths had to be constantly readjusted as the temperature is varied. Adjusting the pulse length is not difficult for the two-pulse T_1 experiment but proves rather more bothersome for the Carr-Purcell[222] sequence. This disadvantage could be removed at the expense of increasing the pulse length by placing the coils outside the Dewar. For relaxation times of spin-1/2 nuclei in liquids, a pulse length 10-20 times the value currently attained (3.5 μsec) would be acceptable and for this case the modification should be made; however, for solids a 100 μsec pulse would not be acceptable.

Field Gradients for Diffusion Measurements - Several methods were tried in generating field gradients for diffusion studies. The response of a spin system under the influence of a steady[221] field gradient, and of many types of time-dependent field gradients[230-232], has been investigated.

The simplest method, employing a steady gradient, has a number of disadvantages which have been discussed elsewhere[233]; in addition it was feared that a steady, inhomogeneous field would have adverse effects on the stability of the external lock. This fear proved groundless and the steady gradient method proved perfectly satisfactory for measuring diffusion constants in liquids. The gradient is most simply generated by changing the current in the z-shim coil from its optimum value. This typically amounted to a change in the

ment to the
dimensions
the gradient a
ase due to th

Although
alternative m
the first inv
5-100 msec
discussed in
the shim coil
ed, the c
current, resu
ed. Adding a
of the gradie
as was done
carefully en
that this ar
since the gr
sample, but
that one cou
ent was kep
switch and t
length and a
2 msec; th
to die away.
even in liqu
to destroy t

current to the z-shim coil of ∿20 mA. A rough calculation based on the dimensions of the coil gives a gradient G = 0.1 Gauss cm^{-1}. The gradient across the sample volume may be considered linear in this case due to the relative size of the z-shim coils and the sample.

Although the steady-gradient method proved satisfactory, two alternative methods which used a pulsed field gradient were explored. The first involved simply pulsing the z-shim coils with pulse lengths of 1-100 msec triggered by the C output of the "pulse booster" unit (discussed in Section IC). Figure 17 shows the circuit for pulsing the shim coils. Since the normal current range in these coils is ±25 mA, the circuit was designed to add 25 mA to the steady state current, resulting in a current during the pulse of between 0 and 50 mA. Adding a constant known current should improve the reproducibility of the gradient, as opposed to simply turning the z-shim potentiometer as was done in the steady gradient method, but this was not checked carefully enough to permit drawing a conclusion. (It might be noted that this argument is not directed toward the accuracy of the results, since the gradient was always determined by calibration with a known sample, but rather toward the ease of performing the experiment in that one could dispense with these numerous calibrations.) The current was kept extremely low to avoid damaging the shim coils. A switch and trimpot, shown in Figure 17, were used to vary the pulse length and a pulse of 10 msec duration produced an effective T_2^* of ∿2 msec; the field transients produced by the pulse took ∿17 msec to die away. This performance is not adequate for measuring D, even in liquids, although this field-gradient pulse worked very well to destroy the magnetization in the x-y plane for the "homospoil"

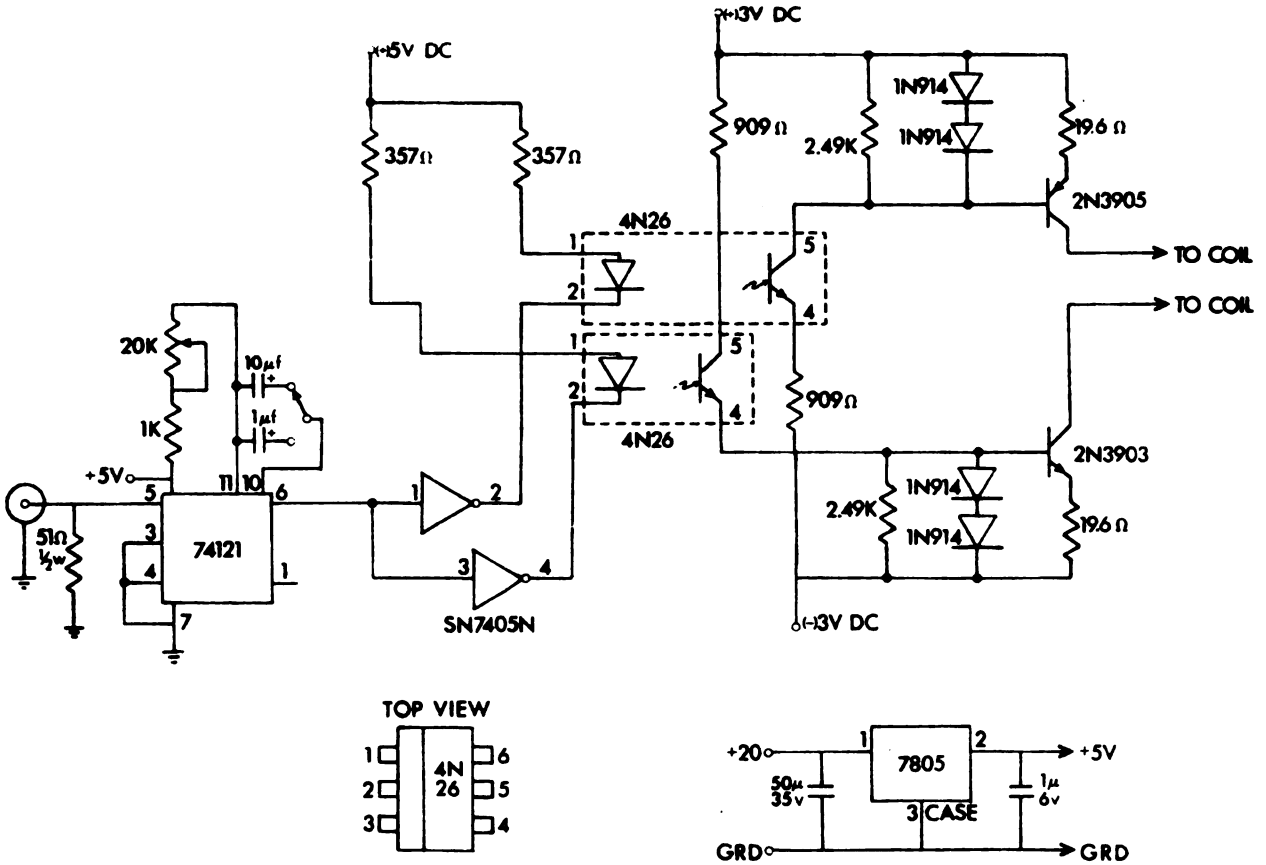

Figure 17. The circuit for providing a variable-length field-gradient pulse by means of altering the current to the z-shim coils.

acement

In order t
o reduce the
rrent coils
ere wound ac
e most line
s Figure 1,
for the micr
e distance
distance fro
ldin form
field gradie
tal coil
s capacit
e coil sh
ality.

The p
ransistor
oil was c
n this Fig

Temp
tandard
ble usin
temperatu
s long a
ge. H

T_1 experiment[234].

In order to produce a larger field gradient during the pulse and reduce the pulse rise and fall times, a separate set of field-gradient coils were wound, shown in Figure 16 and 18. The coils were wound according to the calculations of Tanner[230] to produce the most linear gradient at the sample. Using the nomenclature of his Figure 1, $0.32<z/\ell<0.43$ and $0.337<r/\ell<0.60$, where ℓ is the distance from the midplane of the magnet gap to the face of the magnet, z is the distance from the midplane to turn i of the coil, and r is the distance from the coil axis to turn i. The coils were wound on a Delrin form to reduce the amount of metal in the vicinity of the field gradient. Each coil consisted of 15 turns of #30 wire for a total coil resistance of 0.86 ohms. The steady-state current carrying capacity of #30 wire is 10 amperes, so with wire of this gauge the coil should handle up to 30 A at a duty cycle of 1% with no difficulty.

The power supply is a pair of 12 V lead-acid batteries and the transistor switch to allow these batteries to discharge through the coil was copied from the circuit of Tanner[230] with transistor Q4 in his Figure 2,an MHT 1808, replaced with a more common 2N4048.

Temperature Control and Measurement - Since the Dewar was of standard Varian design, temperature regulation was readily available using the standard Varian heater-sensor and V-4343 variable temperature controller. This system provided quite stable temperatures as long as the indicating meter of the V-4343 was in the regulation range. However, it was found that although the temperature was

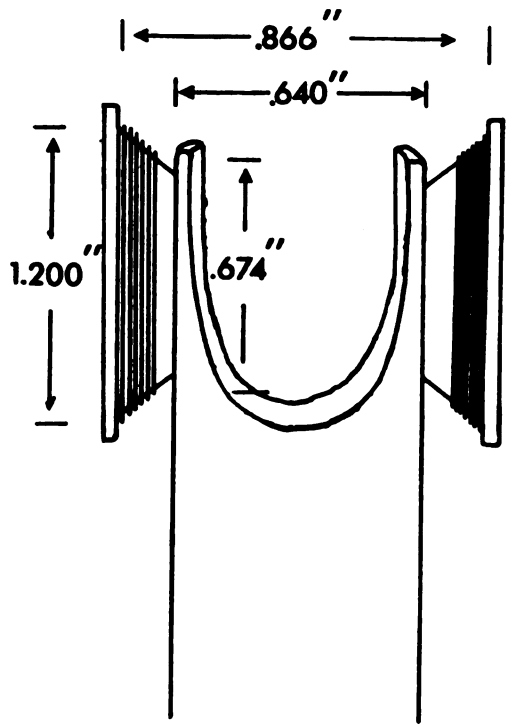

Figure 18. Details of the coils and coil form for generating a pulsed field gradient.

ily held to
ize on the
ry-constant
he thermoco
rode, with
ell past th
reactivity
not reproduc
and subsequ
ntained by
within a sa
table cali
n the usu
melting po
was closer
the same
that the
the top o
calibrat
Unf
calibrat
discrepa
according
calibrat
of melt-
point wa
field wa

easily held to ±0.50°K, the actual value of the temperature as indicated on the dial could be incorrect by ±50°K. Consequently, an iron-constantan thermocouple was added to measure the temperature. The thermocouple was first placed in the Plexiglas cap on top of the probe, with the sensing end extending into the gas stream at a point well past the receiver coil. It was found that the cap's thermal conductivity was too great and temperatures below about 130°K were not reproducible with the thermocouple in this position. (This, and subsequent calibration curves discussed in this section, were obtained by an indirect method. A second thermocouple was placed within a sample tube and inserted into the probe and the first thermocouple calibrated against the second. The second was then calibrated in the usual fashion using materials with well-known freezing or melting points.) The second location tried for the thermocouple was closer to the sample. The thermocouple wire was inserted through the same hole in the Dewar as used for the leads to the rf coil so that the sensing end projected into the gas stream about 1 cm above the top of the coil. With the thermocouple in this position a linear calibration curve was obtained from 100°K to 420°K.

Unfortunately, melting and critical points obtained using this calibration did not agree exactly with the literature values, the discrepancy becoming distressingly large at the lower temperatures. Accordingly, the indirect calibration procedure was abandoned and a calibration curve determined directly from experimental observations of melting points. A number of compounds for which the true melting point was well established were chosen; for hydrocarbons the magnetic field was lowered to detect proton resonances and T_2^* was monitored

as a function o

the dramati

sed in Tabl

correcting

plying know

sults of th

served and

he fluorocar

ceptable.

Thermal

ve by plac

ode, such

as 4 cm ab

temperature

and was ne

n sample.

A. The C

The

divided

sequence

propriat

the rela

provided

as a function of thermocouple reading. The melting point was detected by the dramatic change in T_2^*. The results of this calibration are listed in Table 6 with the experimental temperatures calculated by correcting the measured potential with $mV_{act} = mV_{exp} - .083$, and employing known e.m.f-temperature conversion tables[235]. Using the results of this final calibration the discrepancies between the observed and literature values of melting and critical points of the fluorocarbons studied in this investigation were found to be acceptable.

Thermal gradients in the probe were also measured. This was done by placing a thermocouple in a sample tube, and the tube in the probe, such that one junction was inside the coil while the other was 4 cm above the first. The gradient, given in Table 7 at different temperatures, was not strongly dependent on the actual temperature and was never greater than 2.20° in 4.0 cm, or 0.27° across a 0.5 cm sample. The average gradient was smaller than this, about 0.20°.

II. Measurement of Relaxation Times

A. The Computer Program

The computer-controlled measurement of relaxation times may be divided into two sequential operations: (1) generating the correct sequence of rf pulses and measuring the nuclear signal at the appropriate times, and (2) analyzing the resultant data to determine the relaxation time. The latter operation is of little interest provided it is done correctly, so a full discussion of that portion

Table 6. A com

with

Compo
CF_3Br
CF_3CC
CF_3CF
Neop

[a] $W_{act} = mV_e$

Table 6. A comparison of experimentally determined temperatures with accepted literature values.

Compound	MP	CP	Observed[a]	Literature
CF_3Br	x		-175.5	-174
		x	70.8	67
CF_3CCl_3	x		13.5	13.2
CF_3CF_3	x		-98.2	-100
		x	18.1	23
Neopentane	x		-159.6	-159.6

[a] $mV_{act} = mV_{exp} - 0.083$.

Table 7. Me

ar

Ta, a	
-0.386	
-0.325	
-0.351	
-0.390	
-1.253	
-1.772	
-2.049	
-2.527	
-2.749	
-3.096	
-3.358	
-3.600	
-3.888	

[a]Copper-co

[b]Iron-cons
gradient

Table 7. Measured values of temperature gradients across the sample area of the probe for temperatures below 300° K.

TC_1(mV)[a]	T(°C)	TC_2(mV)[b]	Gradient (°C/cm)
-0.088	-2.3	0.035	0.175
-0.225	-5.9	0.083	0.415
-0.551	-13.2	0.078	0.390
-0.990	-26.6	0.105	0.525
-1.263	-34.2	0.091	0.455
-1.772	-49.0	0.103	0.515
-2.049	-57.4	0.103	0.515
-2.527	-72.3	0.094	0.470
-2.749	-79.5	0.088	0.440
-3.096	-91.2	0.110	0.550
-3.358	-100.3	0.071	0.355
-3.600	-109.0	0.097	0.485
-3.888	-120.0	0.079	0.395

[a]Copper-constantan, measuring the actual temperature.

[b]Iron-constantan, leads separated by 4.00 cm, measuring the temperature gradient within the sample area.

the experim

may be u

more int

A flow c

bes is sho

estimate c

the nurse

and to s

[ST - pu

where n is

$= 4T/N_p$; t

Figure 7(a),

tions of gos

measurement

attached to

after pulse

4 V on the

rate possib

In the case

second $n\tau$.

the signal

integrated

This t

similar sec

of the experiment will be found in Appendix A. The pulse sequences which may be used to measure various relaxation times are of somewhat more interest and will be thoroughly discussed.

A flow chart of the program for generating the time delays and pulses is shown in Figure 19. The operator enters, via the teletype, an estimate of the relaxation time T, the number of points desired N_p, and the number of repetitions N_s required for each point. On the command to start, data are collected with $N(= N_p x N_s)$ sequences

[6T - pulse 1 - $n\tau$ - pulse 2 - ($n\tau$) - measure signal],

where n is varied by the computer from $\simeq 0$ to 4T ($1 \leq n \leq N_p$) and $\tau = 4T/N_p$; the second n may or may not be present. As seen in Figure 7(a), if pulse 1 and pulse 2 correspond to appropriate combinations of 90° and 180° rf pulses, the usual sequences for T_1 and T_2 measurement may be obtained; when a slightly different meaning is attached to pulse 2, the timing sequence will measure $T_{1\rho}$. Immediately after pulse B in T_1 experiments (signalled by the transition 0 V → +5 V on the measure/wait line) the FID is digitized at the maximum rate possible (20 μsec per point) and integrated to a preset limit. In the case of T_2 measurements, signal acquisition is delayed by the second $n\tau$. Since the measure/wait line is normally high (+5 V) the signal is digitized immediately after the second delay and is integrated as in the T_1 experiment.

This basic timing sequence is readily modified to produce other, similar sequences. This has been done for the following cases:

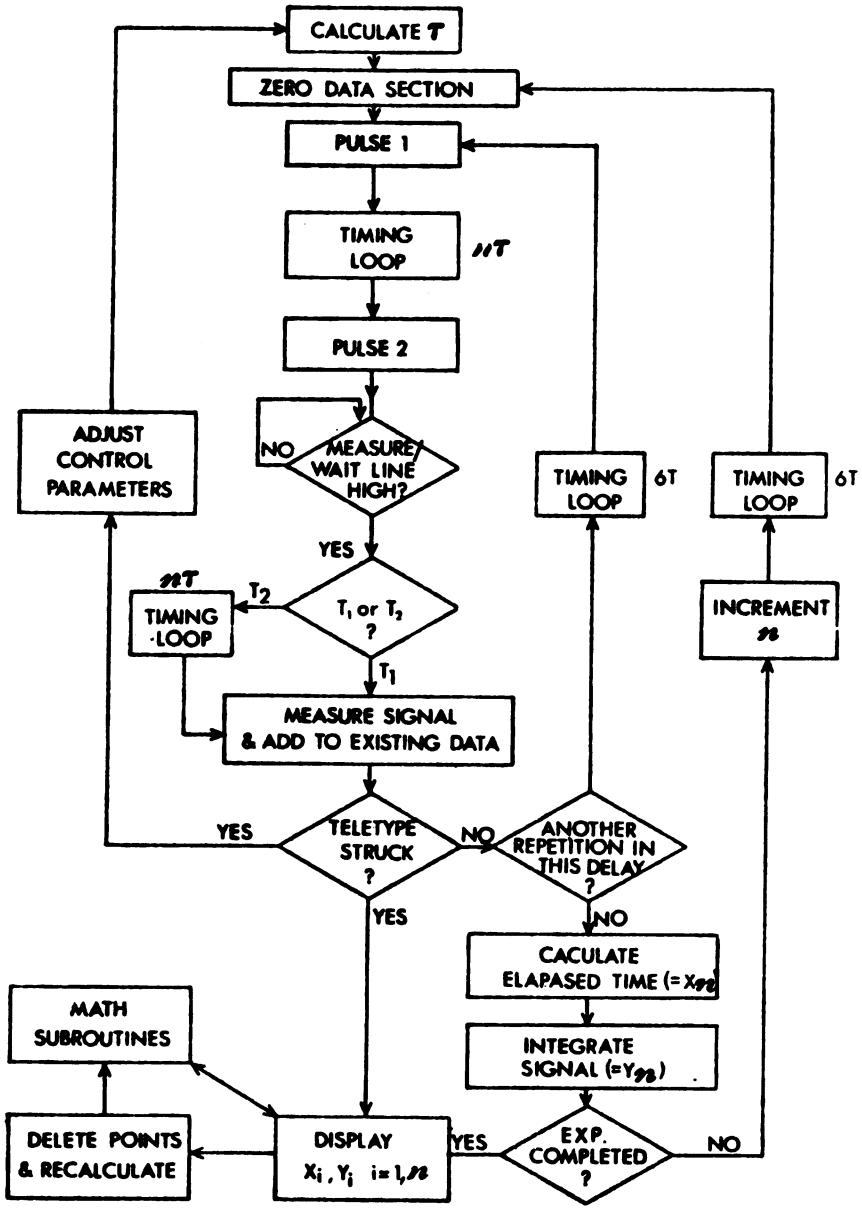

Figure 19. Generalized flow diagram of the software for timing and measurement control.

(1) The
roduced by c
s variant
xt start ea
rx) rather
(2) Th
E wait and
rm IE) pri
(3) Th
sequence for
he two-puls
urring symm
Figure 20a.
conceptually
ussed in de
The ba
tent to p
sequence).
Figure 20b
3. This pr
sequences,
altered to
The da
ussed abov
he experim
by compu
is only obt

(1) The 90°-τ-90° sequence for measuring T_1 in solids may be produced by omitting the $8T_1$ wait at the onset of each cycle. This is a variant of the so-called "homospoil" T_1 sequence[234] in that both start each pulse sequence with zero net magnetization (saturation) rather than from equilibrium.

(2) The homospoil sequence[234] is produced by omitting the $8T_1$ wait and inserting a field-gradient pulse (as described in Section IE) prior to pulse 1.

(3) The final sequence is that used in the pulsed field-gradient sequence for measuring the diffusion coefficient. This is simply the two-pulse spin-echo experiment with field-gradient pulses occurring symmetrically about the 180° refocusing pulse as shown in Figure 20a. The modification necessary for this sequence, although conceptually straightforward, is somewhat more involved and is discussed in detail in Appendix B.

The basic timing program has been modified to a somewhat greater extent to produce multiple-pulse sequences (such as the triplet T_1 sequence). The basic timing for this type of sequence is shown in Figure 20b and a complete listing of the program is given in Appendix B. This program should provide the basic timing for a number of sequences, since within certain limits the subsequence may be readily altered to include an arbitrary number of pulses and time delays.

The data which have been collected by one of the sequences discussed above are displayed on an oscilloscope at the completion of the experiment and may be punched or typed out for analysis by hand or by computer. However, the full benefit of an on-line computer is only obtained when an immediate calculation for the desired parameter

Figure 20.

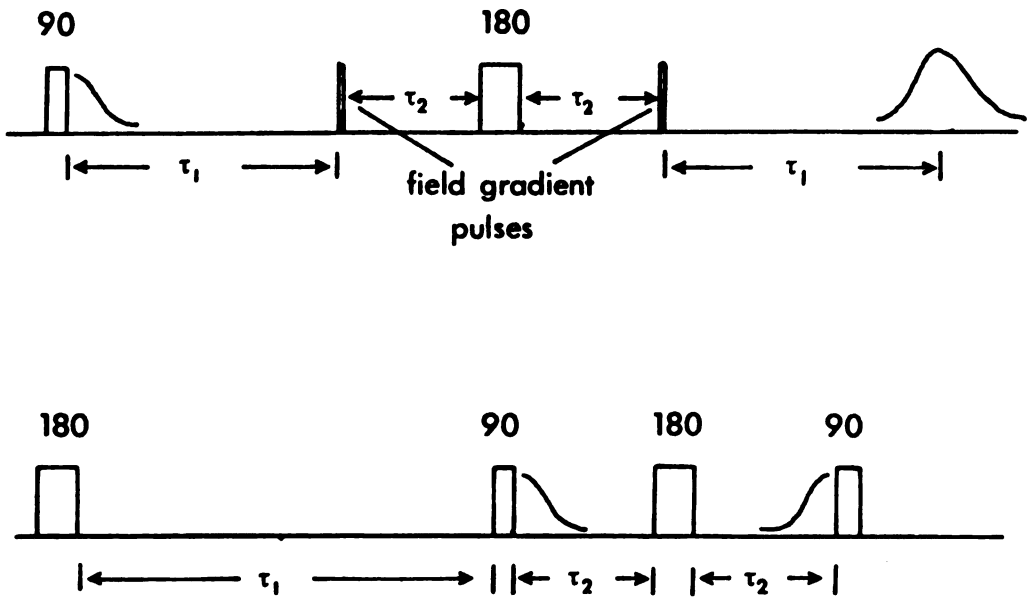

Figure 20. Basic timing for sequences involving more than two pulses. (a) the pulsed field-gradient sequence, and (b) generalized multiple-pulse sequence.

xactly
experi
the Wi
necess
ighted
he differ
culated
that sp
culated
rity val
alue for
squares ca

4. Perfor

An im
instrument
f the ins
sible lim
between th

The r
he speed
xecute a
sec, and
he shorte
accuracy i
tially no

(relaxation time, diffusion coefficient) is performed, in order that the experiment may be redone if necessary. Additional subroutines for the Nicolet 1083 have been written (Appendix A) which perform the necessary arithmetic operations, such as baseline correction and weighted least-squares fit to an equation of the form $\ln M_z = At + B$. The differences between the experimental values of $\ln M_z$ and those calculated from the least-squares slope and intercept are displayed so that spurious points may be detected and the time constant re-calculated. The common error of a poor choice of the baseline (infinity value), which produces a large standard deviation (but a good value for the relaxation time, if weights are used in the least-squares calculation) may also be easily detected and corrected.

B. Performance of the Computer-Controlled NMR System

An important consideration in interfacing a computer to an instrument is that the computer does not restrict the capabilities of the instrument. Computer control in this case provides two possible limitations of performance. These are the allowable intervals between the 180° and 90° pulses, and roundoff errors in calculations.

The minimum value of τ, the time between pulses, depends on the speed of the computer and the number of commands required to execute a timing loop. With the computer employed here τ is 16 μsec, and the minimum delay to the first 90° pulse is 42 μsec, so the shortest relaxation time which can be measured with reasonable accuracy is about 100 μsec, adequate for liquids. There is essentially no limit on long relaxation times as the timing loop can

ent 2^46 .

ser writ

n less t

Roun

gile as

h the N

n double

A no

n the si

gal valu

n error

It would

time more

work. Fi

the accur

2. Adjus

The

descending

or NMRS s

considere

The

by settin

restricti

sequence

strongly

count 2^{42} μsec (1200 hours). A simpler version of the program has been written which reduces the minimum delay to 26 μsec but limits T_1 to less than one second.

Roundoff errors in the calculations should be completely negligible as an accuracy of greater than three parts in 10^7 is claimed for the Nicolet floating-point routine. Fixed-point multiplication is double precision integral (40 bits) with, of course, no roundoff.

A more important roundoff error occurs in the time delay assigned to the signal following the 90° pulse. This time is given an integral value between zero and 4096 and in a typical experiment is ∿0.3% in error for the first point and ∿0.03% in error for later points. It would not be difficult to reduce this error by specifying the time more exactly but this refinement was not necessary in the present work. Field inhomogeneities and spectrometer noise still determine the accuracy obtainable.

C. Adjustments for Various Pulse Sequences

The method for adjustment of pulse lengths and phases differs depending on whether the spectrometer is under computer control or NMRS Sequence Synthesizer control. The latter condition will be considered first.

The pulse length required to give a 90° nutation is adjusted by setting a train of n identical pulses $(p\text{-}\tau)_{4m}$, $1 \leq m$. Under this restriction, when p is a 90° pulse the magnetization vector ends the sequence at equilibrium, consequently saturation effects do not strongly affect the signal amplitude. When the pulse length is

nearly a

ise is

homogeni

gain the

The homog

re seen

be devia

The

izer com

hen usin

zing a

To s

djust th

o comput

and-wait

an be do

differen

turning

Maximize

djusted

Dependin

than the

only be

length

throughou

properly adjusted the signal appears as shown in Figure 21. A 180° pulse is obtained in the same manner but now n is a multiple of two. A properly adjusted pulse length results in no nuclear signal and again the sequence ends with the magnetization vector at equilibrium. The homogeniety of the 5 mm probe is not good enough that these decays are seen when n is large, so the pulse lengths are adjusted such that the deviation is minimized at the start of the sequence.

The phasing is most conveniently done under sequence synthesizer control using a single 90° pulse to phase each channel in turn, then using a closely spaced Carr-Purcell sequence to make the fine phasing adjustments.

To set up the two-pulse spin-echo sequence one should first adjust the phases under sequence synthesizer control, then switch to computer control and adjust the pulse lengths by the slow pulse-and-wait method. The 180°-τ-90° sequence is easier, since everything can be done under computer control. The phases are adjusted to 180° difference by running two pulses (SE command) of 90° or less and turning the phasing knobs until the two free induction decays are maximized and in opposite directions. Then the first pulse may be adjusted to 180° by increasing its length until no decay is seen. Depending on the T_1 of the sample it may be necessary to wait longer than the SE mode allows between repetitions. The second pulse need only be set to approximately 90°, since it is easily shown that its length is not important to the experiment as long as it is constant throughout the measurement.

Figure

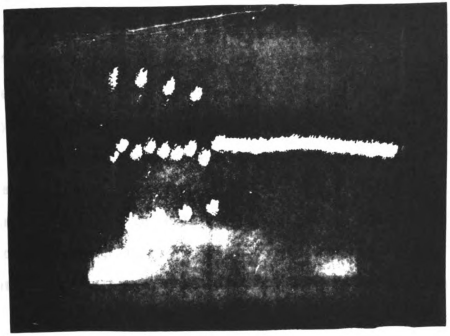

Figure 21. Correctly adjusted phasing as shown by a train of 90° pulses.

Some
carefu
stabilize
control p
shift was
ers. A
freque
frequency
The
muscle a
constr
also be c
force, put
sample.
writer, r
small pro
with only
receiver
through t
coil was
d.d. thir
turns of
capillary
snug fit

III. The External Lock

Some experiments were done without a field/frequency lock by carefully minimizing the field drift with the V-K3506 Super Stabilizer and using a small value for the integration limit (a control parameter in RELAX2 described in Appendix A). However, field drift was obviously limiting the accuracy of relaxation-time measurements. Although corrections offsetting the drift, either in the time or frequency[236] domain, were considered, it seemed that a field/frequency lock would provide the greatest benefits.

The most obvious procedure was to use the entire (unused) DP-60 console as the lock circuit. This meant that it would be necessary to construct a probe which could operate from the V-4311 rf unit and also be compact enough to be within, or ride piggy-back on, the pulse probe, putting the lock sample in close proximity to the experimental sample. Varian probes normally have three sets of coils - the transmitter, receiver, and modulation coils. Winding three coils in a small probe seemed too difficult, so an attempt was made to get by with only two. The first configuration had separate transmitter and receiver coils with the modulation riding on the transmitter coil through the external modulation input on the V-4311. The transmitter coil was two turns of #30 wire square-wound on a 1" section of 0.25" o.d. thin-wall quartz tubing. The receiver coil consisted of five turns of #36 wire wound two diameters apart on a 3 mm o.d. quartz capillary. The smaller tube was wound with tape so that it made a snug fit in the larger one but could still be rotated to adjust the

null. The capillary was filled with water doped with $CuCl_2 \cdot 2H_2O$ to give a linewidth of ∿4 Hz. This configuration worked poorly because the two coils were not sufficiently rigid with respect to each other to minimize the leakage. Consequently the signal-to-noise was very poor and a lock signal could not be obtained.

The second configuration that was tried was with the transmitter and receiver using the same coil and a separate coil for the modulation. A diagram of the probe circuitry is shown in Figure 22. The transmitter-receiver coil is five turns of #36 wire wound on the outside of the 3 mm sample tube. A small Plexiglas block was machined (Figure 23) to support the modulation coils. These were wound and the strands glued together while supported on a jig before being glued to the supporting block. Winding the coils on a jig made it a simple matter to obtain the forty-turn coil of the proper dimensions (radius 3.5 mm, separation 5 mm), and gluing the turns together on the jig made transferring the coils, which were rather small, easy. The coils were deformed somewhat during the process of gluing them to the Plexiglas support block but this made little difference since extremely high resolution was not needed. It had been determined that such a large number of turns was necessary in order that the coil impedance match the output impedance of the V-3521A modulation unit. More than 40 turns would have been desirable, as the impedance was still too low, but with this number of turns sufficient modulation power to saturate the lock signal was available.

The receiver and transmitter were coupled to the single coil by a 1:1:1 transformer which consisted of five turns of #26 wire wound on a ferrite toroid. The circuit for this device, shown in

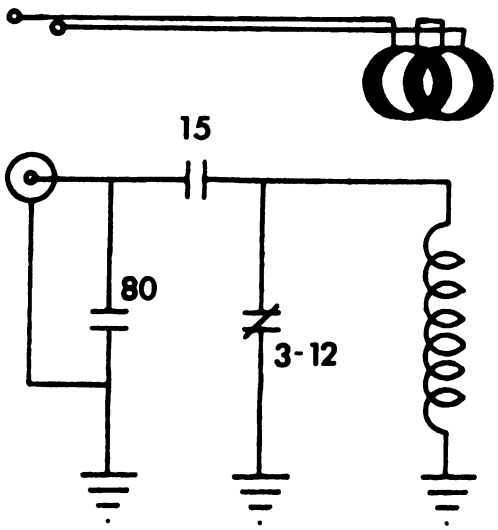

Figure 22. The probe circuit for the external lock.

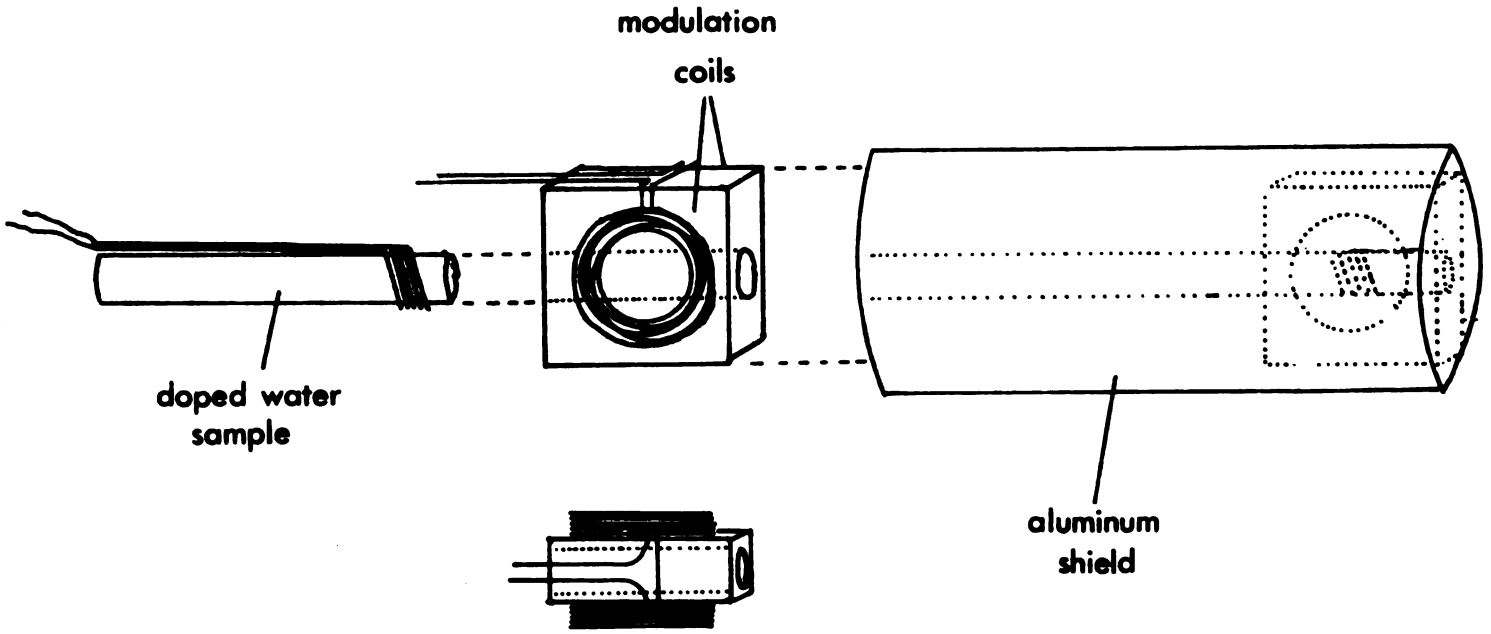

Figure 23. The arrangement of modulation coils and transmitter/receiver coil in the external lock.

Figure 24, was copied almost exactly from the Varian hybrid box circuit for the Varian V-4354 audio phase detector. The entire external lock circuit is shown in Figure 25. The capacitor on the receiver input was necessary since this line is normally at +250 VDC for the Varian preamplifier contained in the standard probe. The preamplifier used here was a Vanguard dual-gate MOSFET (Vanguard Electronic Labs, Hollis, New York) tuned to 60.0 MHz.

Little power was needed for such a small transmitter coil. Generally the V-4311 rf unit would operate with all but ∿30 dB of attenuation. The amount of leakage was critical to the S/N and should be adjusted to less than 40 μA by varying the gain on the preamplifier. Other than that adjustment, operating the DP-60 console as an external lock is exactly the same as operating in HA mode.

The lock probe slides into the back of the pulse probe, as can be seen in Figure 16. The separation between lock and sample can be as small as 1.4 cm but the homogeneous region of the field is so large that the S/N for the lock was adequate even when it was well back in the field. Since the lock probe was not thermally insulated, it would tend to some extent to follow the temperature of the experimental sample. For relaxation studies this is important only in that extremely high or low lock temperatures may cause the lock sample to explode. With the lock slid to its fullest extent into the pulse probe, it was determined that the lock sample attained a temperature of 0.1° C when the experimental sample was at a thermocouple reading of -6.14 mV, or approximately -170° C. In order to go to lower temperatures while still using the lock, the lock probe must be partially withdrawn from the pulse probe to decrease the thermal

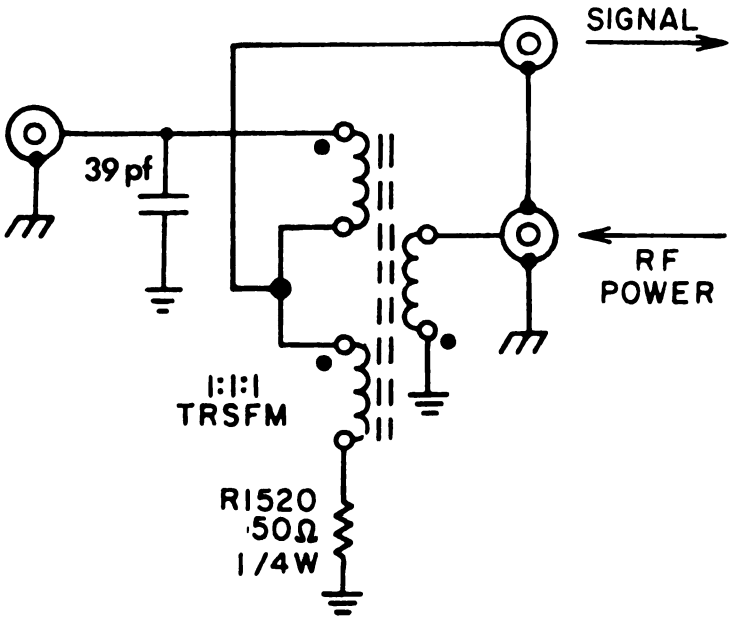

Figure 24. The circuit for coupling the transmitter and receiver in the external lock.

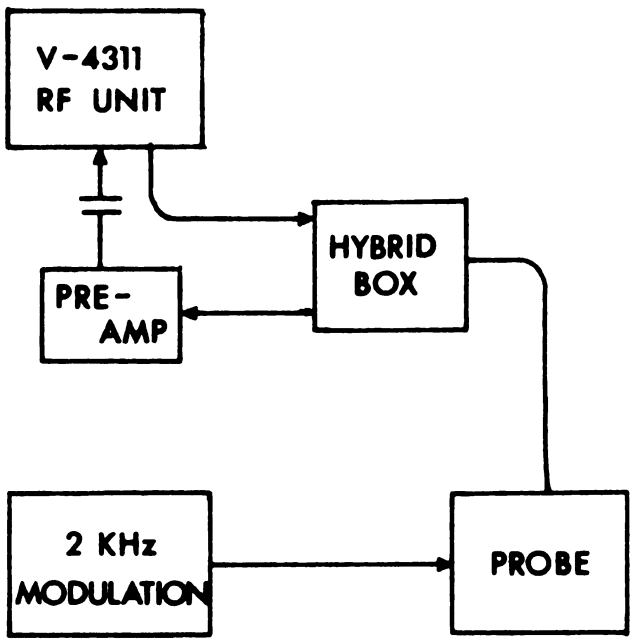

Figure 25. A block diagram of the external lock circuit.

contact. In this manner locked operation was possible down to the lowest attainable temperature. The stability of the field lock has not been determined precisely but the drift is less than ±2.5 Hz in eight hours.

IV. The Raman Spectrometer

Raman spectra were obtained with a Spex model 1401 Ramalog spectrometer equipped with a double grating monochromator, a 1 W He-Ar laser operating at 5145 Å, and photon counting electronics. A diagram of the optics used in this experiment is shown in Figure 26. The third monochromator was removed for this application in order to increase the throughput to the photomultiplier tube. The polarization scrambler prior to the first slit is required because the grating efficiency is polarization dependent, favoring the strong I_{VV} spectrum. Lines of $\sim$5 cm^{-1} width were measured at a slit width of 70 μ, which corresponds to 1.5 cm^{-1} resolution at 5145 Å, while broader lines were recorded at 2.0 cm^{-1} resolution. The sample temperature was not controlled, so the laser power was kept low to avoid heating the sample by the well-known lens effect. At 350 mW, the power setting at which all spectra were recorded, the temperature was measured as 27° C by placing a thermocouple within the capillary containing the sample and as close as possible to the laser beam ($\sim$1 mm). Since the Ramalog is a departmental instrument, more than usual care was taken prior to each run to ensure that the system was operating properly and that the throughput was maximized. Spectra were digitized with a Varian C-1024 time-averaging computer (CAT)

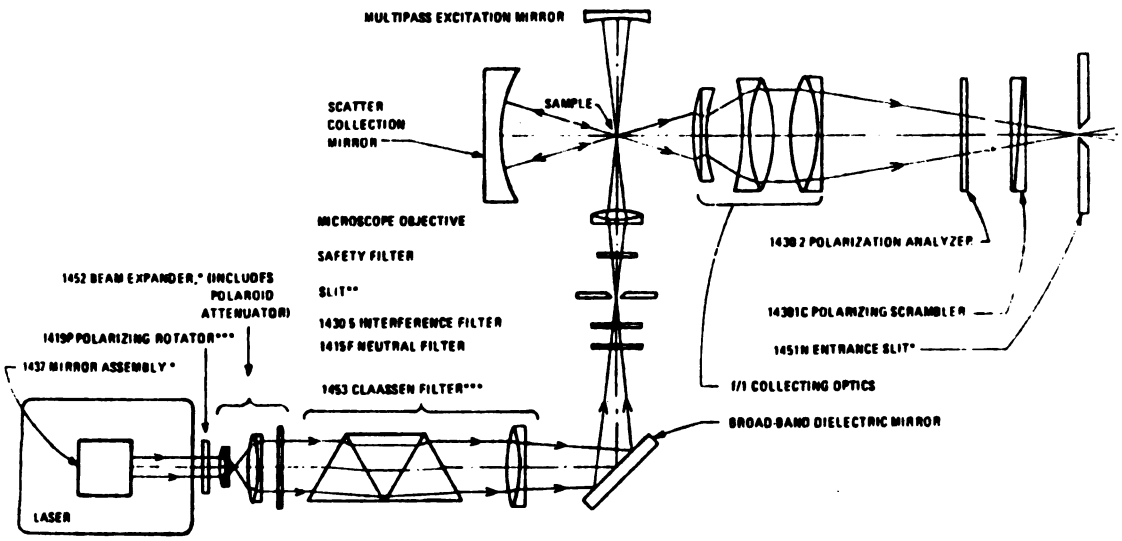

Figure 26. The optical train for the Raman scattering experiment.

and transferred to cards on an IBM 526 keypunch equipped with a Varian C-1001 coupler. The basis for control of data collection with the CAT was the output available from the Spex marker/encoder circuitry which provided pulses every wavenumber or every 0.1 wavenumber. Either of these pulse rates may be used for CAT address advance, thus spectra may be digitized at a resolution of 1.0 or 0.1 wavenumbers per point with a maximum sweep width of 1024 cm^{-1}. The trigger for the start of a scan was obtained from the pulse per wavenumber output, with the autostop of the CAT set at 1 to inhibit further trigger pulses. This experimental arrangement is shown in Figure 27.

The polarized component of a line was almost always measured in a single scan while the depolarized component usually required averaging two to nine scans for satisfactory signal-to-noise. No significant difference was observed in the analysis of an averaged or a single-scan spectrum.

In order to correct for the errors introduced by the Polaroid analyzer and the polarization scrambler, the depolarized spectra were corrected for different absolute transmissions for different polarizations, and for leakage of the much stronger polarized component through the analyzer. These corrections were made by comparing the observed depolarization ratios of the 314 cm^{-1} and 459 cm^{-1} lines of CCl_4 with the reported values[237]. The experimentally determined transmission correction c_1 and leakage factor c_2

$$I^{act}_{depol} = c_1 I^{exp}_{depol} - c_2 I^{exp}_{pol} \qquad (127)$$

were measured frequently and are given by 0.91±.01 and 0.0024±.0003,

SPEX

INTERFACE

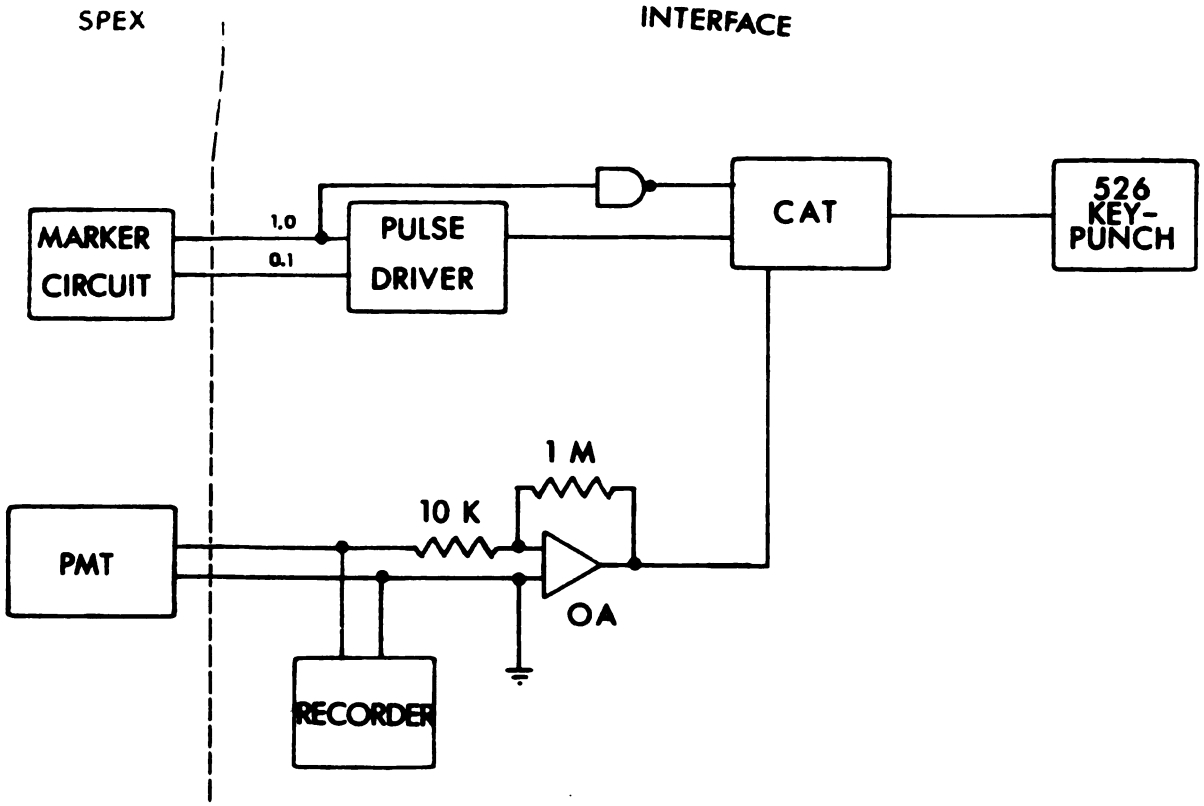

Figure 27. A block diagram of the apparatus for digitally recording Raman lineshapes.

respectively.

A FORTRAN computer program was written to extract the reorientational correlation time from the experimental spectra and is discussed in Appendix C. Basically, the analysis is as follows. After the correction described above was made, the spectra were digitally smoothed using the method of Savitzky and Golay[238]. The best value for the orientational half-width was obtained by a simple iterative procedure in which the width of the Lorentzian orientational function was varied so as to minimize the chi-squared error between the experimental depolarized spectrum and the calculated convolved spectrum.

Uncertainties in ω_{or} were estimated in the following manner. The residual

$$R(\omega_{or}) = \sum_{\omega}^{N}\{I_{depol}(\omega) - I_{convolution}(\omega)\}^2 \qquad (128)$$

was determined as a function of ω_{or} and was a parabola with the minimum occurring at the value of ω_{or} listed in each line in Table 24. The uncertainty in ω_{or} was taken to be the range of ω_{or} values for which the residual was less than twice the minimum residual. The minimum residual depended on the limits of summation since the difference $(I_{depol} - I_{conv})$ for points far in the wings was practically independent of the value of ω. Therefore the residual was computed out to four half-widths. Repeated measurement of ω_{or} for the 221 cm^{-1} line of $CDBr_3$ verified that the uncertainties determined by this method were realistic.

V. Sample Preparation

A. NMR Samples

Since measurements were to be made up to the critical point for many samples, the ability to withstand large pressures was a primary consideration in choosing the type of sample tube to be used. Since smaller tubes are inherently stronger than larger ones, and vacuum seal-offs could be made with less difficulty with smaller tubes, it was decided to use 5 mm sample tubes. The critical pressure in the substituted ethanes and methanes which were to be studied is ∿40 atmospheres and an unflawed standard-wall pyrex tube can withstand that easily.

The design of the sample tubes is shown in Figure 28. The restriction at point A serves both to reduce diffusion to the liquid-vapor interface, which provides an additional source of relaxation through spin-rotation in the vapor phase[239], and also to restrict the sample to the most homogeneous region of the H_1 field. The seal-off when the sample is filled on the vacuum line is done at point C, and if the critical temperature is higher than room temperature an additional seal-off is done at point B, after the sample has been carefully frozen in the bottom of the tube, in order that approximately uniform temperature be maintained at all portions of the sample when it is in the probe. The region of the sample which is immersed in the gas flow in the probe is indicated in the figure. This second seal-off was found to be necessary to prevent the sample, when at higher than ambient temperature, from rapidly distilling

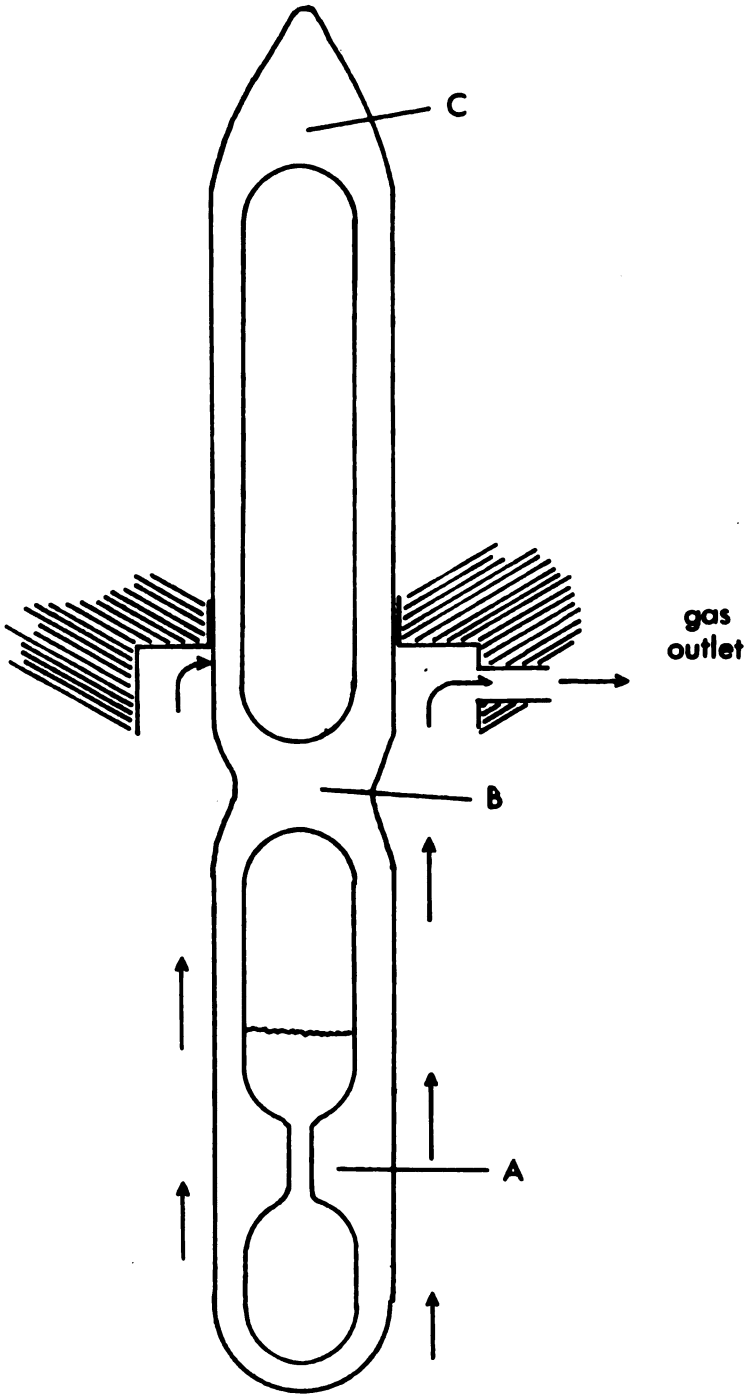

Figure 28. The design of 5 mm NMR sample tubes for relaxation time measurements up to the critical temperature.

from the bottom to the top of the tube causing bumping and large thermal currents.

All samples were degassed with several cycles of the freeze-pump-thaw procedure. Compounds which boiled at room temperature or above showed little affinity for oxygen and reproducible relaxation times could be obtained whether the degassing was done with the aid of a diffusion pump or only a rough pump. Low-boiling compounds showed a much greater affinity for oxygen and it was found that rough pumping was not sufficient to remove the dissolved oxygen. All of the compounds, however, were degassed using a diffusion pump, but for the low-boiling compounds the pressure was monitored during the "pump" part of the cycle and these samples were cycled until the pressure dropped to 5×10^{-6} torr.

Since an explosion of a sample tube while it is in the probe is to be avoided at all costs, all tubes were carefully tested after they had been filled. Each tube was heated (inside a closed oven or behind a protective shield) to a temperature 20° higher than it would ever be subjected to inside the probe. If the tube survived this temperature for ∿10 minutes it was considered acceptable. About one tube in six exploded during testing, presumably due to flaws in the glass which arose through the seal-off.

B. Raman Samples

Samples for Raman measurements were sealed into melting-point capillary tubes. Occasionally the laser beam caused the haloform samples to decompose, as indicated by a black spot forming at that

point on the inner wall of the tube which was illuminated by the beam. When this happened the sample was discarded.

C. Preparation of Materials

Deuterobromoform was prepared by agitating a mixture of $CHBr_3$ and D_2O, made basic with $NaCO_3$, at 50° C for 2 hours. This exchange was repeated five times with fresh D_2O until the proton NMR spectrum showed deuteration to be 97% complete. The $CDBr_3$ was distilled prior to sealing in a capillary tube but the $CDCl_3$ (Aldrich Chemical Company, Milwaukee, Wisconsin, 99.6+ % purity) and the fluorocarbons (Pierce Chemical Company, Rockford, Illinois and Columbia Organic Chemicals Company, Inc., Columbia, South Carolina) were used without further purification (except the degassing step for NMR samples).

RESULTS

All relaxation times were measured at a magnetic field strength of 14.1 kilogauss except for a few measurements of T_1 and T_2 in CF_3CCl_3 at 15.87 MHz, which corresponds to a resonant magnetic field of 2.52 kG for fluorine nuclei. The following tables (8-21) comprise the raw data from which the temperature dependence of the relaxation times was determined. These tables list the thermocouple reading in millivolts with a reference ice-water bath, the temperature and inverse temperature calculated as discussed in Section I.F of the Experimental portion of this work, the number of points (NP) taken to define the relaxation curve, and the weighted least-squares relaxation rate (R_1 or R_2) and standard deviation as calculated by the program RELAX2 and discussed in Appendix A. For measurements of R_1, the spin-lattice relaxation rate, the decay of the magnetization was monitored for the time interval $0<t<4T_1$ (T_1 is the relaxation time) and usually about thirty points in this time interval were collected. For measurements of R_2, generally more points were taken, but the time interval was shorter. The only data points deleted from these tables were those for which the observed temperature drift was unacceptable (greater than two degrees). At all but the lowest temperatures, the observed drift in temperature during the course of an experiment was less than 0.5° K after the system had reached thermal equilibrium.

I. Measurements of Spin-Lattice Relaxation Rates

Table 8. Spin-lattice relaxation rates in CF_3CCl_3.

TC(mV)	T(°K)	10^3/T(°K)	NP	R_1(sec^{-1})
4.760	362.3	2.760	40	0.2105±.0026
6.780	399.5	2.503	34	0.2730±.0066
8.613	432.7	2.311	27	0.3772±.0077
4.874	364.4	2.744	22	0.2088±.0107
-5.558	147.4	6.784	27	0.5765±.0324
-5.659	144.7	6.911	35	0.1565±.0442
-5.627	145.5	6.873	41	0.0626±.0031
-5.078	159.9	6.254	33	0.4976±.0272
-3.176	205.0	4.878	42	0.1464±.0029
-3.867	189.4	5.280	37	0.1828±.0052
-4.519	173.9	5.150	44	0.2611±.0057
-5.230	156.1	6.406	34	0.4389±.0082
-5.890	138.4	7.225	34	0.0796±.0043
-4.918	163.9	6.101	45	0.3278±.0068
-1.653	237.9	4.203	21	0.1084±.0058
-2.100	228.5	4.376	32	0.1244±.0029
-2.677	216.0	4.630	31	0.1549±.0082
-3.424	199.5	5.013	20	0.1777±.0068
0.634	284.1	3.520	13	0.1372±.0018
-0.150	268.7	3.722	10	0.1111±.0008
0.723	285.8	3.499	17	0.1360±.0038
0.520	281.9	3.547	14	0.1361±.0026
0.013	271.8	3.679	14	0.1132±.0031
-0.634	258.9	3.862	14	0.1031±.0011
-1.168	248.0	4.032	13	0.1000±.0032
1.073	292.6	3.418	16	0.1333±.0047
1.320	297.5	3.361	17	0.1361±.0044
2.060	312.1	3.204	16	0.1553±.0063
4.940	365.7	2.734	23	0.2201±.0116
1.755	305.8	3.270	16	0.1453±.0070

Table 8 - Continued.

TC(mV)	T(°K)	10^3/T(°K)	NP	R_1(sec^{-1})
1.155	294.2	3.399	20	0.1339±.0272
0.160	274.7	3.640	13	0.1236±.0029
4.745	362.0	2.762	14	0.2028±.0018
3.738	343.3	2.913	17	0.1782±.0029
2.996	329.4	3.036	21	0.1669±.0015
2.120	312.8	3.197	16	0.2086±.0017
1.180	294.7	3.393	20	0.1970±.0031
-1.000	251.3	3.979	23	0.1005±.0005
-1.722	236.5	4.228	22	0.1081±.0046
7.208	407.3	2.455	15	0.2636±.0063
6.165	388.2	2.576	14	0.2475±.0048
4.632	359.0	2.786	17	0.2170±.0052
5.673	379.2	2.637	27	0.2322±.0040
1.520	301.3	3.319	24	0.1427±.0011
1.576	302.4	3.307	15	0.1545±.0010
-3.276	202.7	4.933	26	0.1353±.0086
-3.605	195.2	5.123	27	0.1403±.0086
-3.970	186.9	5.350	21	0.1614±.0108
-4.272	179.8	5.562	20	0.2013±.0135
-4.516	174.0	5.747	24	0.2438±.0140
-4.903	164.3	6.086	25	0.3422±.0155
-5.105	159.2	6.281	17	0.3374±.0154
-5.342	153.1	6.532	30	0.4714±.0303
-5.360	152.6	6.553	22	0.4794±.0125
-5.648	144.9	6.901	5	0.1122±.0269
-5.631	145.4	6.878	25	0.0696±.0063
-5.784	141.3	7.077	25	0.0405±.0082
-5.500	149.1	6.707	30	0.0790±.0086
-5.237	155.9	6.414	23	0.4967±.0315

Table 9. Spin-lattice relaxation rates in CF_3CCl_3 at 15.87 MHz.

T(°K)	10^3/T(°K)	NP	R_1(sec^{-1})
288.2	3.470	40	0.1566±.0035
277.5	3.604	23	0.3667±.0138
280.5	3.565	22	0.4368±.0080
283.9	3.522	22	0.5135±.0097
286.7	3.488	23	0.5587±.0163
276.2	3.621	27	0.2783±.0168
272.4	3.671	22	0.2245±.0088
269.2	3.715	16	0.2017±.0056
257.5	3.883	14	0.1060±.0042
232.2	4.307	22	0.1021±.0051
204.0	4.902	22	0.0638±.0063
196.2	5.097	17	0.1060±.0087
260.3	3.842	24	0.1570±.0043
262.7	3.807	24	0.1629±.0027
258.5	3.868	26	0.1315±.0045
256.1	3.905	27	0.1149±.0030

Table 10. Spin-lattice relaxation rates of ^2D in $CDBr_3$

T(°K)	$10^3/T$(°K)	$R_1 sec^{-1}$
281.2	3.556	3.087±.160
283.8	3.524	3.64 ±.12
289.5	3.454	2.850±.031
293.2	3.411	2.751±.047
296.5	3.373	2.636±.041
298.0	3.356	2.606±.081
300.6	3.327	2.479±.035
303.6	3.294	2.27 ±.035
304.1	3.288	2.360±.032
305.0	3.279	2.317±.045
310.3	3.223	1.911±.024
333.2	3.001	1.416±.188
340.7	2.935	1.45 ±.029
354.5	2.821	1.38 ±.031

Table 11. Spin-lattice relaxation rates of ^{19}F in CF_3Br

TC(mV)	T(°K)	$10^3/T$(°K)	NP	R_1(sec^{-1})
-3.267	202.9	4.929	35	0.3836 ±.0046
-1.437	242.4	4.125	32	0.5195 ±.0085
+0.258	276.7	3.614	34	0.6965 ±.0125
1.205	295.2	3.388	34	0.8642 ±.0117
2.430	318.7	3.138	35	1.153 ±.031
2.947	328.5	3.044	22	1.315 ±.012
3.075	330.8	3,023	33	1.320 ±.034
3.438	337.7	2.961	23	1.576 ±.033
3.600	340.5	2.937	35	1.627 ±.076
3.774	344.0	2.907	31	2.022 ±.071
3.986	348.0	2.874	24	3.162 ±.081
2.380	317.7	3.148	35	1.123 ±.018
-7.343	98.5	10.15	21	0.8713 ±.0101
-7.396	96.8	10.33	27	0.5578 ±.0390
-7.134	100.0	10.00	14	0.6578 ±.0292
-6.945	106.3	9.407	26	0.8646 ±.0389
-7.100	101.1	9.891	34	1.071 ±.0241
-6.863	109.0	9.174	35	0.8688 ±.0090
0.398	279.5	3.578	33	0.7441 ±.0135
-3.693	193.3	5.173	33	0.3226 ±.0098
-6.530	119.8	8.347	15	0.4766 ±.0136
-3.118	206.4	4.845	35	0.3857 ±.0073
-3.061	207.7	4.815	31	0.3907 ±.0082
-3.975	186.7	5.356	31	0.3340 ±.0082
-4.283	179.7	5.565	27	0.3386 ±.0063
-5.037	160.9	6.215	32	0.3289 ±.0091
-5.347	152.9	6.540	26	0.3498 ±.0082
-5.588	146.7	6.817	31	0.3997 ±.0068
-5.846	139.6	7.163	34	0.4189 ±.0074
-6.275	127.3	7.855	32	0.4906 ±.0085

Table 11 - Continued.

TC(mV)	T(°K)	10^3/T(°K)	NP	R_1(sec^{-1})
-6.856	109.2	9.158	33	0.6919 ±.0087
-7.000	104.4	9.579	24	0.9948 ±.0161
-7.291	94.4	10.59	11	0.7461 ±.0366
-7.335	92.6	10.80	21	0.6113 ±.0228
-7.269	95.1	10.52	17	0.6600 ±.0183
-6.690	114.8	8.711	33	0.6170 ±.0082
-6.850	109.4	9.141	30	0.6561 ±.0143
-6.954	106.0	9.434	20	0.8408 ±.0219
-6.641	116.1	8.613	21	0.6423 ±.0108
-4.780	167.4	5.974	30	0.2958 ±.0035
-5.286	154.6	6.468	32	0.3151 ±.0097
-5.562	147.3	6.789	33	0.3220 ±.0041
-5.861	139.1	7.189	35	0.3690 ±.0089
-6.040	134.1	7.457	31	0.4261 ±.0118
-3.122	206.3	4.847	34	0.3852 ±.0088
-2.540	219.1	4.564	34	0.4212 ±.0112
-2.540	219.1	4.564	34	0.4190 ±.0112
-1.865	233.4	4.284	27	0.4819 ±.0130
-0.515	261.2	3.828	35	0.6048 ±.0038
+0.212	275.8	3.626	34	0.6851 ±.0062
0.842	288.2	3.470	33	0.7752 ±.0176
1.566	302.3	3308	35	0.8966 ±.0207
1.973	310.0	3.226	34	0.9995 ±.0171
1.993	310.4	3.222	35	0.9959 ±.0228

Table 12. Spin-lattice relaxation rates of ^{19}F in CF_2Br_2

TC(mV)	T(°K)	$10^3/T$(°K)	NP	$R_1(sec^{-1})$
-5.757	142.2	7.032	35	0.6813 ±.0038
-5.037	160.9	6.215	23	0.3542 ±.0020
0.804	287.4	3.479	23	0.3251 ±.0033
-3.893	188.8	5.297	42	0.2389 ±.0031
-4.818	166.4	6.010	40	0.3532 ±.0075
-5.316	153.7	6.506	41	0.6289 ±.0096
-5.540	147.9	6.761	45	0.8596 ±.0068
-5.597	146.4	6.831	47	1.026 ±.0102
-2.588	218.0	4.587	50	0.1895 ±.0020
+1.639	303.5	3.295	33	0.3603 ±.0018
1.668	304.1	3.288	27	0.3717 ±.0015
1.675	304.2	3.287	30	0.3754 ±.0019
2.755	3.24.8	3.079	35	0.4321 ±.0034
4.138	350.8	2.851	32	0.5150 ±.0055
5.328	372.8	2.682	34	0.6391 ±.0471
6.631	396.7	2.521	35	0.7188 ±.0091
7.824	418.4	2.390	32	0.8503 ±.0116
9.383	446.6	2.239	35	1.017 ±.0187
7.385	410.4	2.437	35	0.8077 ±.0087
4.973	366.2	2.731	32	0.5803 ±.0070
-4.547	173.2	5.774	35	0.2726 ±.0036
1.305	297.2	3.365	32	0.3466 ±.0051
0.385	279.2	3.582	30	0.2987 ±.0019
-0.356	264.4	3.782	32	0.2736 ±.0033
-1.218	247.0	4.049	32	0.2393 ±.0017
-2.453	220.9	4.527	31	0.1981 ±.0056
-5.070	160.1	6.246	32	0.3500 ±.0050

Table 13. Spin-lattice relaxation rates of ^{19}F in CF_2ClCCl_3

TC(mV)	T(°K)	10^3/T(°K)	NP	R_1(sec^{-1})
2.304	316.2	3.163	16	0.1259 ±.0119
-1.622	238.6	4.191	14	0.08295±.00487
-0.552	260.5	3.839	22	0.08250±.01476
0.45	280.5	3.565	14	0.08820±.00087
1.722	305.2	3.277	15	0.1039 ±.0019
6.413	392.7	2.546	16	0.2814 ±.0394
5.165	369.8	2.704	16	0.1676 ±.0072
4.105	350.2	2.856	15	0.1356 ±.0110
3.104	331.4	3.018	17	0.1425 ±.0013
2.225	314.8	3.177	16	0.1602 ±.0037
1.808	306.9	3.259	47	0.1121 ±.0045
0.857	288.5	3.466	37	0.09093±.00169
0.108	278.2	3.595	47	0.08346±.00035
-0.999	251.4	3.978	47	0.08959±.00114

Table 14. Spin-lattice relaxation rates of ^{19}F in $CFCl_2CFCl_2$

TC(mV)	T(°K)	$10^3/T$(°K)	NP	R_1(sec^{-1})
1.120	293.5	3.407	14	0.09027±.00095
2.187	314.1	3.184	34	0.1049 ±.00085
3.979	347.8	2.875	32	0.1397 ±.0009
5.445	374.9	2.667	42	0.1548 ±.0010
6.923	402.1	2.487	45	0.1815 ±.0014
8.007	421.8	2.371	47	0.2118 ±.0045
2.182	314.0	3.185	33	0.1028 ±.0020
2.358	317.3	3.152	101	0.1020 ±.0090
0.856	288.5	3.466	30	0.04468±.0019
1.260	296.3	3.375	23	0.09312±.0015
4.997	3.667	2.727	22	0.1472 ±.0032
3.026	329.9	3.031	35	0.1295 ±.0059
1.378	298.5	3.350	14	0.09736±.0060
-0.646	258.6	3.867	12	0.05097±.00054
-1.725	236.4	4.230	17	0.04727±.00055
-2.975	209.7	4.773	14	0.04574±.00120
-4.437	175.8	5.688	23	0.07510±.00400
-5.655	144.7	6.911	10	0.6477 ±.0325
-5.655	144.7	6.911	21	0.4829 ±.0275

Table 15. Spin-lattice relaxation rates of ^{19}F in CF_3I

TC(mV)	T(°K)	$10^3/T$(°K)	NP	$R_1(sec^{-1})$
1.168	294.5	3.396	35	0.6094 ±.0086
2.110	312.7	3.198	31	0.7172 ±.0168
2.162	313.6	3.189	35	0.7126 ±.0207
0.475	281.0	3.559	34	0.5521 ±.0059
-3.623	194.7	5.136	27	0.3632 ±.0050
-4.897	164.4	6.083	32	0.4534 ±.0067
-5.075	160.0	6.250	32	0.4969 ±.0064
-4.537	173.4	5.767	35	0.3863 ±.0037
-2.726	215.0	4.651	35	0.3474 ±.0056
-1.100	249.2	4.013	35	0.4358 ±.0025

Table 16. Spin-lattice relaxation rates of ^{19}F in CF_3CF_3

TC(mV)	T(°K)	10^3/T(°K)	NP	R_1(sec^{-1})
0.677	284.9	3.510	35	0.5132 ±.0029
0.523	282.0	3.546	35	0.4840 ±.0023
-4.000	186.1	5.373	15	0.2029 ±.0032
-4.312	178.8	5.593	16	0.2097 ±.0139
-4.312	178.8	5.593	34	0.1978 ±.0061
-0.198	267.6	3.737	35	0.4022 ±.0013
-1.153	248.3	4.027	35	0.3159 ±.0015
-1.755	235.8	4.241	31	0.2557 ±.0038
-2.406	220.0	4.505	25	0.2237 ±.0035
-2.859	212.2	4.713	45	0.2080 ±.0019
-3.672	193.8	5.160	43	0.1965 ±.0026
-4.496	174.5	5.731	32	0.2000 ±.0052
-4.610	171.6	5.828	34	0.1752 ±.0018
-4.757	167.9	5.956	36	0.1541 ±.0024
1.200	295.1	3.389	11	1.159 ±.018
1.226	295.7	3,382	17	1.374 ±.024
0.936	290.1	3.447	23	0.5859 ±.0052
-4.842	165.8	6.031	34	0.1411 ±.0014

II. Measurements of Spin-Spin Relaxation Rates

Table 17. Spin-spin relaxation rates of ^{19}F in solid CF_3CCl_3

TC(mV)	T(°K)	$10^3/T$(°K)	NP	$R_2(sec^{-1})$
0.768	287.6	3.489		8.31
-0.168	268.2	3.729		57.9
-1.097	249.4	4.001		450.
-1.988	230.9	4.331		2138.
-3.516	197.2	5.071		4770.
-3.089	207.0	4.831		12900.
	285.2	3.506	77	9.461± .259
	280.2	3.569	77	12.53 ± .35
	276.2	3.621	101	23.50 ± .55
	273.3	3.659	73	59.35 ± 1.89
	268.2	3.729	50	70.93 ± 2.05
	263.2	3.799	50	109.2 ± 8.2
	258.2	3.873	21	346.8 ± 35.2
	253.2	3.949	310	433.8 ± 8.5
	248.2	4.029	310	679.5 ± 12.3
	243.2	4.112	226	1349. ± 73.
	238.2	4.198	144	2163. ±106.
	233.2	4.288	62	4068. ±138.
	223.2	4.480	36	10740. ±843.
	213.2	4.690	17	24320. ±6710.

Table 18. Spin-spin relaxation rates of ^{19}F in liquid CF_3CCl_3

TC(mV)	T(°K)	$10^3/T$(°K)	NP	$R_2(sec^{-1})$
0.671	284.8	3.511	36	7.876 ±.241
0.760	286.5	3.490	36	6.464 ±.200
0.860	288.5	3.466	56	0.1888±.0062
1.133	302.5	3.306	56	0.2218±.0079
1.634	303.4	3.296	56	0.1843±.0048
1.663	304.0	3.289	54	0.1873±.0051
2.345	317.0	3.155	53	0.2054±.0070
3.200	333.3	3.000	53	0.2239±.0065
4.223	352.4	2.838	47	0.2711±.0146
5.046	367.6	2.720	46	0.2906±.0110
6.352	391.6	2.553	51	0.4668±.0258
6.436	393.1	2.544	54	0.4260±.0157
	288.2	3.470	200	0.1594±.0062

Table 19. Spin-spin relaxation rates of ^{19}F in CF_2Br_2

T(°K)	$10^3/T$(°K)	$R_2(sec^{-1})$
301.5	3.317	0.3785±.0089
326.7	3.061	0.5680±.0187
344.2	2.905	0.6557±.0193 0.6040±.0153
364.2	2.746	0.7138±.0120
367.2	2.723	0.9568±.0240
383	2.611	1.291 ±.063
400	2.500	2.019 ±.087

Table 20. Spin-spin relaxation rates of ^{19}F in CF_3CF_3

TC(mV)	$10^3/T(°K)$	$R_1(sec^{-1})^a$	$R_2(sec^{-1})$
291.7	3.428		0.6562±.0208
280.6	3.564	0.4986±.0263	0.5290±.0090
266.7	3.750	0.4022±.0013	0.4007±.0080
249.9	4.002	0.3159±.0015	0.3042±.0070
227.2	4.401	0.2237±.0035	0.2476±.0037
214.2	4.669		0.2131±.0041
195.1	5.126	0.2028±.0032	0.2170±.0031
191.0	5.236	0.2097±.0131	0.2274±.0031

[a]From Table 16.

Table 21. Spin-spin relaxation rates of ^{19}F in CF_2ClCCl_3

TC(mV)	T(°K)	10^3/T(°K)	NP	$R_2(sec^{-1})$
2.492	320.0	3.125	40	0.5572± .0260
2.939	328.3	3.046	40	0.5865± .0286
3.441	337.8	2.960	40	0.6176± .0360
3.984	347.9	2.874	31	0.6869± .0475
4.536	358.1	2.793	40	0.5806± .0269
5.127	369.1	2.709	40	0.6602± .0287
3.512	239.2	2.948	40	0.4939± .0139
4.023	348.6	2.869	40	0.4841± .0144
5.164	369.8	2.704	40	0.5770± .0129
6.488	394.1	2.537	34	0.6403± .0214
7.583	414.1	2.415	40	0.7434± .0317
8.547	431.5	2.317	36	0.9435± .0572
2.467	319.5	3.129	40	0.3636± .0129
	∿313	∿3.20	104	5.592 ± .211
0.586	283.2	3.531	46	54.10 ± 1.94
-0.015	271.2	3.687	24	139.0 ± 6.4
-0.420	263.2	3.799	26	268.6 ± 6.5
-0.974	251.9	3.970	34	1660.2 ± 35.8
-2.623	217.3	4.602	17	6124. ± 319.
-4.175	182.1	5.491	11	10820. ±2461.

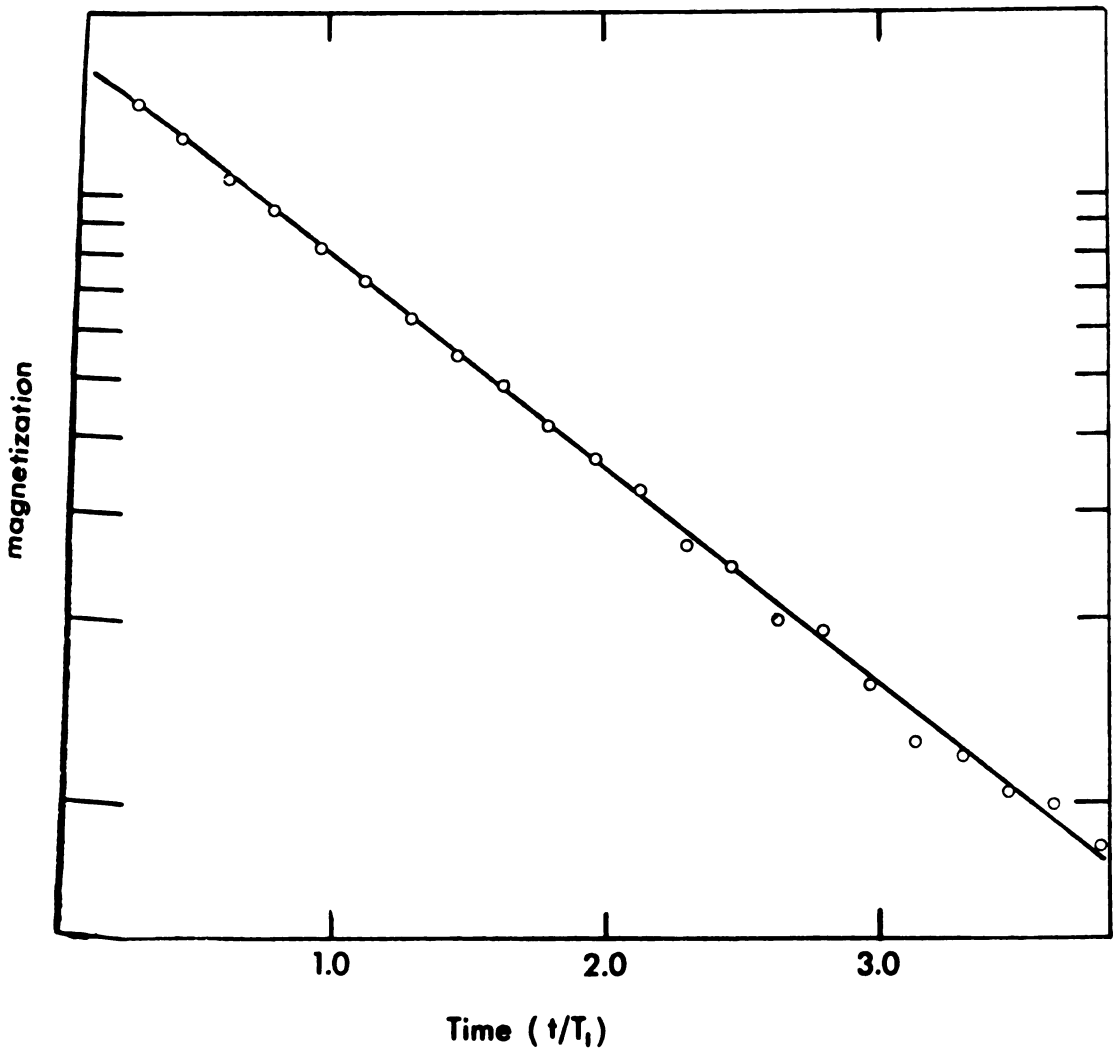

Figure 29. A semi-logarithmic plot of magnetization versus time in the 180°-τ-90° T_1 measuring sequence, showing the typical linearity and degree of scatter observed.

III. Self-Diffusion Coefficients

Table 22. Determination of the field gradient and measurement of the self-diffusion coefficient in CF_3CCl_3

Compound	TC(mV)	T(°C)	Slope[a]	T_2(sec)	G(gauss cm^{-1})	$D_S(cm^2/sec)x10^5$
$CFCl_3$	-1.040	-22.7	13.38 ± .85	0.958	0.135	1.38[b]
$CFCl_3$	0.542	9.1	23.71 ±1.28	0.846	0.144	2.16[b]
$CFCl_3$	1.577	29.3	25.49 ±1.25	0.792	0.128	2.93[b]
					0.136 average	
CF_3CCl_3	0.674	11.6	8.790± .912	5.95		0.902±.094
CF_3CCl_3	1.513	28.0	16.71 ±3.95	5.85	0.136	1.72 ±.41
CF_3CCl_3	2.689	50.4	28.92 ±2.14	5.00		2.97 ±.22

[a]KINFIT results.

[b]Reference 131.

Table 23. Determination of the field gradient and measurement of the self-diffusion coefficient in CF_3Br

TC(mV)	1/T (10^3°K/T)	T (°K)	T_2[a] (sec)	Slope[b]	D_S(cm^2/sec)x10^5	G(gauss cm^{-1})
1.284	3.40	294	0.71	8.60± .71	2.63[c]	0.0787±.0056[d]
0.000	3.693	270.8	0.80	9.40± .63	1.93[c]	0.0960±.0093
-0.820	3.914	255.5	0.83	9.10± .78	1.53[c]	0.1061±.0123
					weighted av.	0.0898
0.455	3.582		0.971	27.5 ±1.1	6.45	
-0.842	3.922	1.39	1.39	37.2 ±2.3	8.73	
-1.945	4.300		1.64	34.0 ±2.6	7.98	
-3.138	4.75		1.92	17.2 ±2.7	4.04	
-3.957	5.23		2.08	22.8 ±1.9	5.26	
-4.850	5.80		2.17	23.2 ±1.8	5.45	
-6.355	7.42		1.09	10.5 ±1.0	2.46	
-6.808	8.22		0.714	4.14± .54	0.972	
-7.030	8.67		0.571	4.44± .90	1.04	

[a]Estimate.
[b]KINFIT results.
[c]$CFCl_3$ values $D_S = 9.5 \cdot 10^{-4}$ exp (2.11 kcal/kT).
[d]Estimated uncertainty of D_S is 3%.

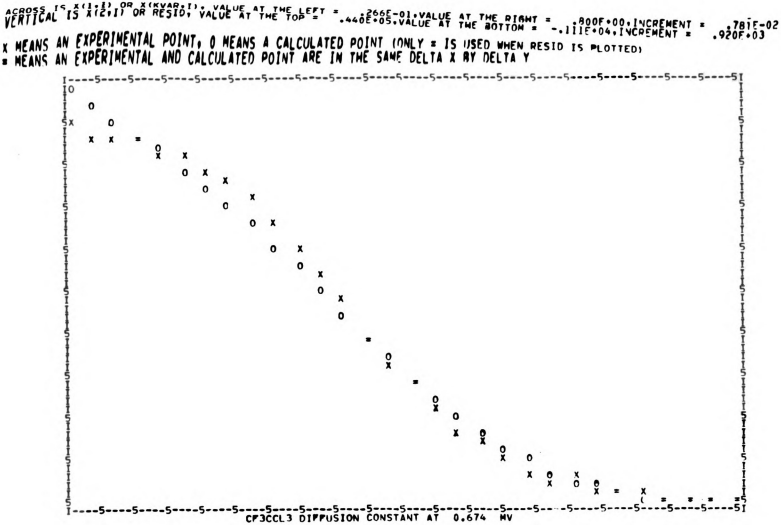

Figure 30. A typical KINFIT plot of experimental and theoretical values of magnetization versus time in the two-pulse spin echo experiment, from which the diffusion coefficient is calculated.

Table 24. Raman linewidth measurements

Molecule	Freq. (cm^{-1})	ρ^a	$\omega_{intr}{}^a$	$\omega_{or}{}^a$	$R(\omega_{or})$	%Corr[b]
$CDCl_3$	650	0.017	3.3	2.87	.24	12
	2256	0.088	2.8	2.70	.093	2
$CDBr_3$	222	0.063	1.8	0.997	.023	3
	521	0.011	2.0	1.29	.24	17
	2250	0.13	3.3	1.07	.78	1
CF_3CCl_3	714	0.027	2.5	2.09	.41	7

[a] ω_{intr} = intrinsic half-width at half-height; ω_{or} = half-width at half-height of the orientational component; ρ = depolarization ratio.

[b] Percent intensity of the depolarized spectrum subtracted to correct for leaked polarized light.

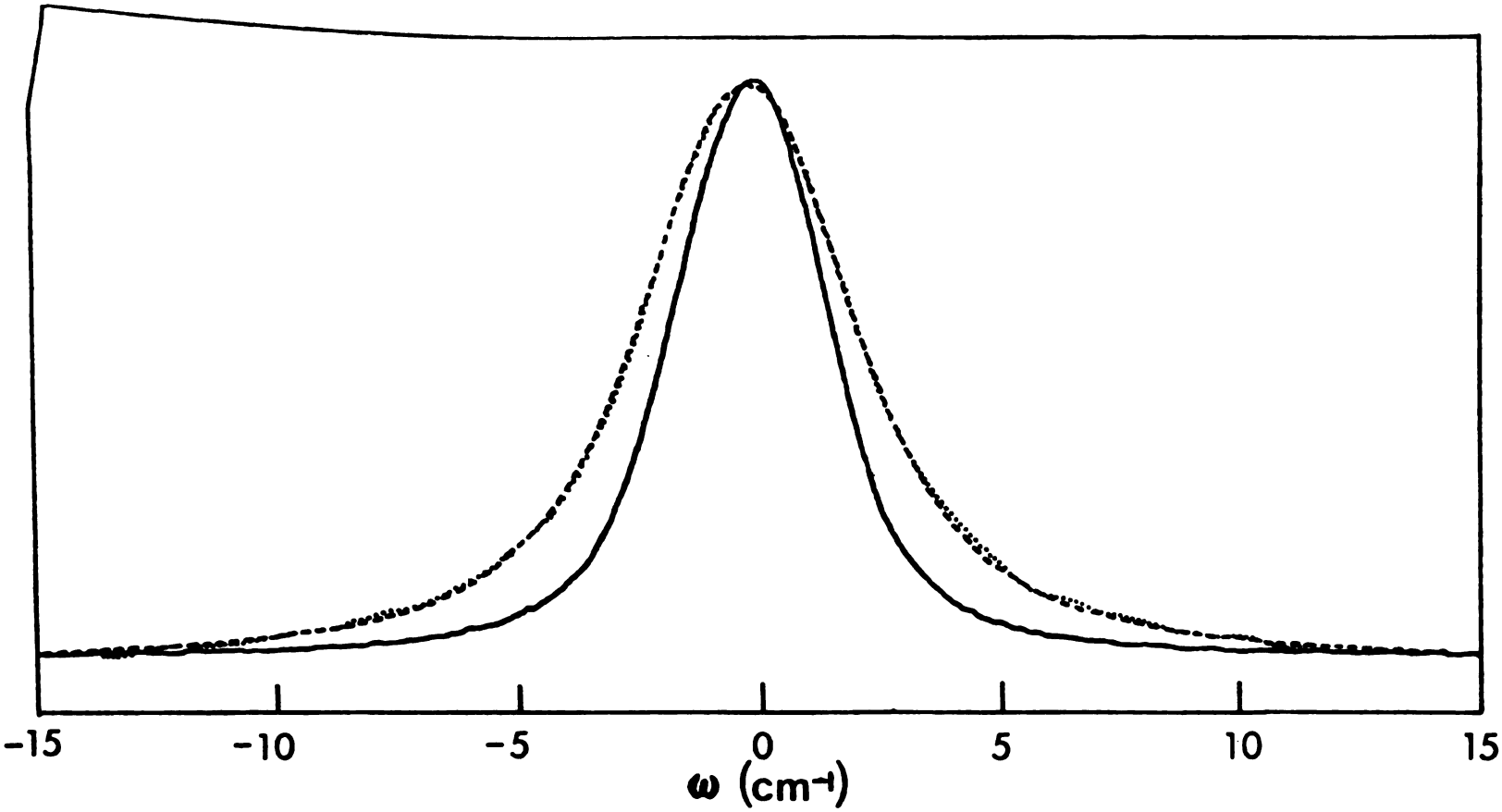

Figure 31. Polarized spectrum (___), depolarized spectrum (· · ·), and calculated convolution of the polarized component with a Lorentzian reorientational spectrum (- - -), for the 222 cm^{-1} line of $CDBr_3$.

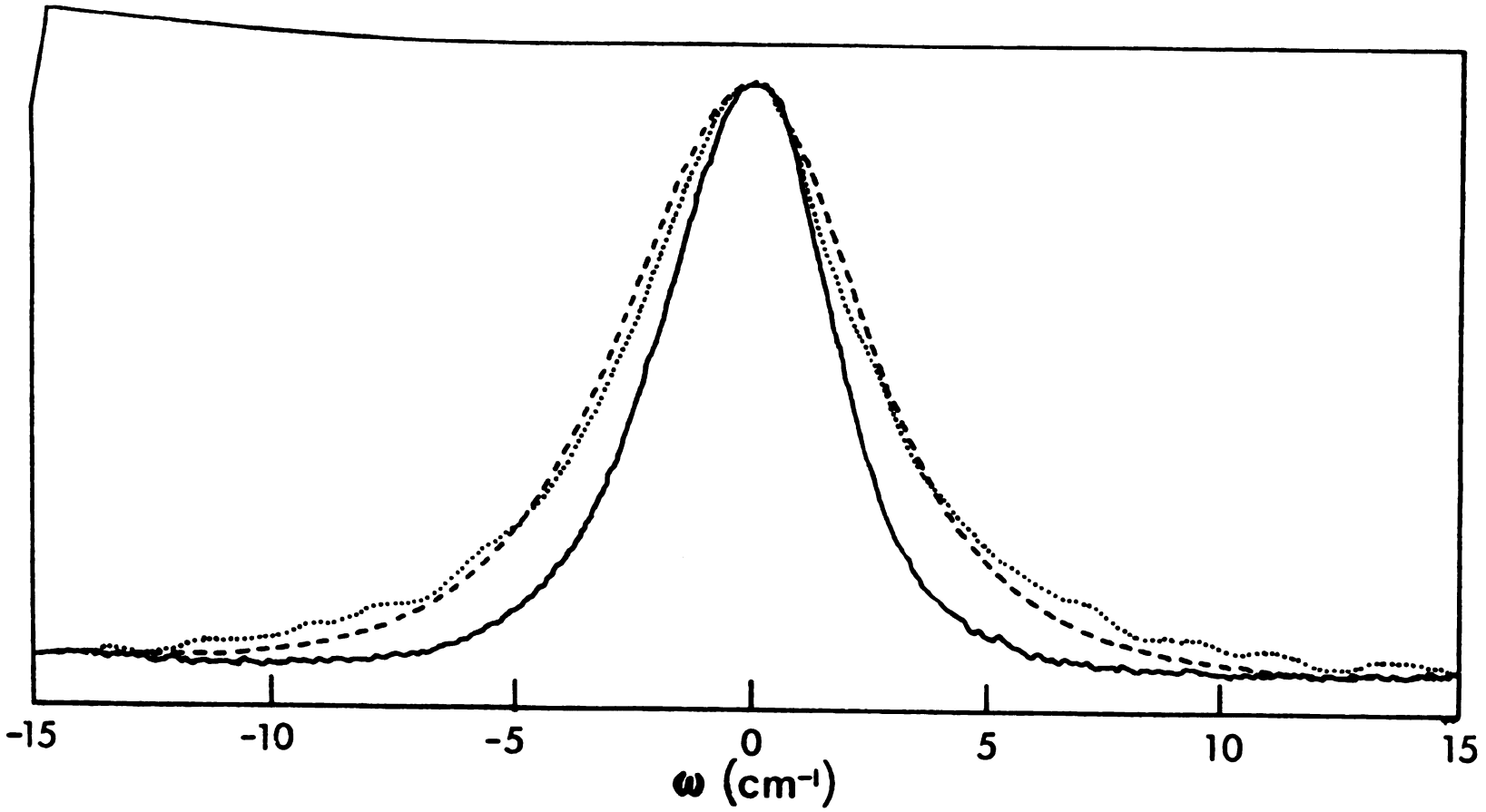

Figure 32. Polarized spectrum (——), depolarized spectrum (· · ·), and calculated convolution of the polarized component with a Lorentzian reorientational spectrum (- - -), for the 521 cm^{-1} line of $CDBr_3$.

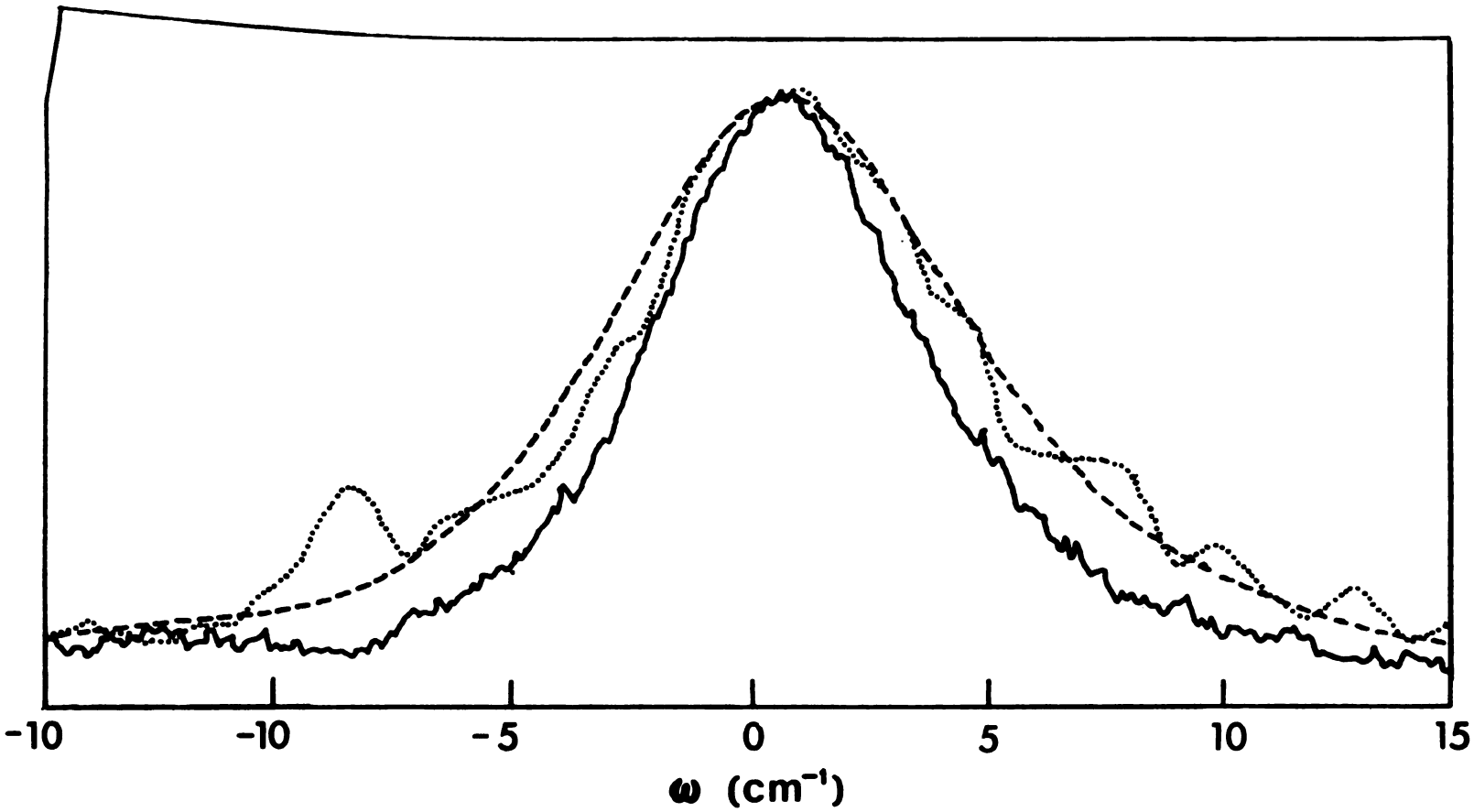

Figure 33. Polarized spectrum (——), depolarized spectrum (· · ·), and calculated convolution of the polarized component with a Lorentzian reorientational spectrum (- - -), for the 2250 cm^{-1} line of $CDBr_3$.

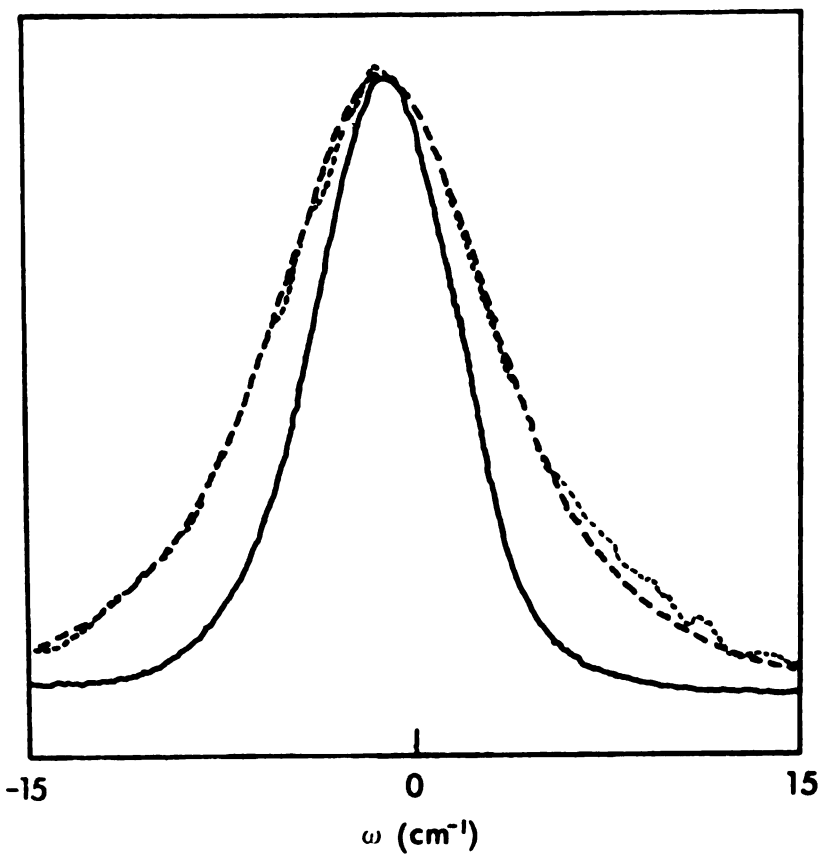

Figure 34. Polarized spectrum (——), depolarized spectrum (· · ·), and calculated convolution of the polarized component with a Lorentzian reorientational spectrum (- - -), for the 650 cm^{-1} line of $CDCl_3$.

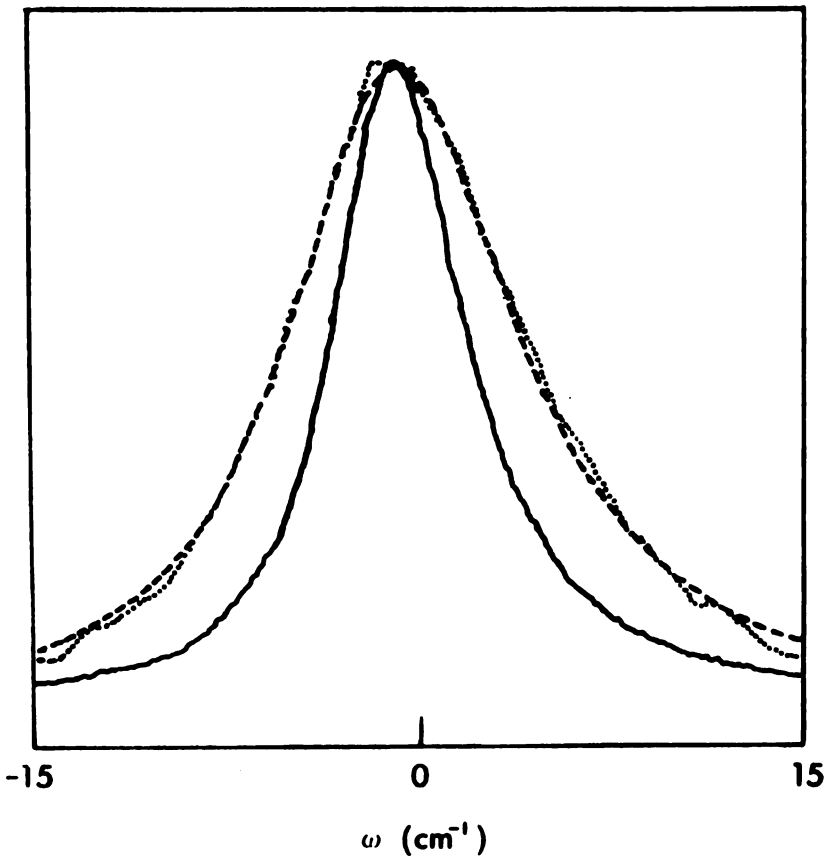

Figure 35. Polarized spectrum (——), depolarized spectrum (· · ·), and calculated convolution of the polarized component with a Lorentzian reorientational spectrum (- - -), for the 2256 cm^{-1} line of $CDCl_3$.

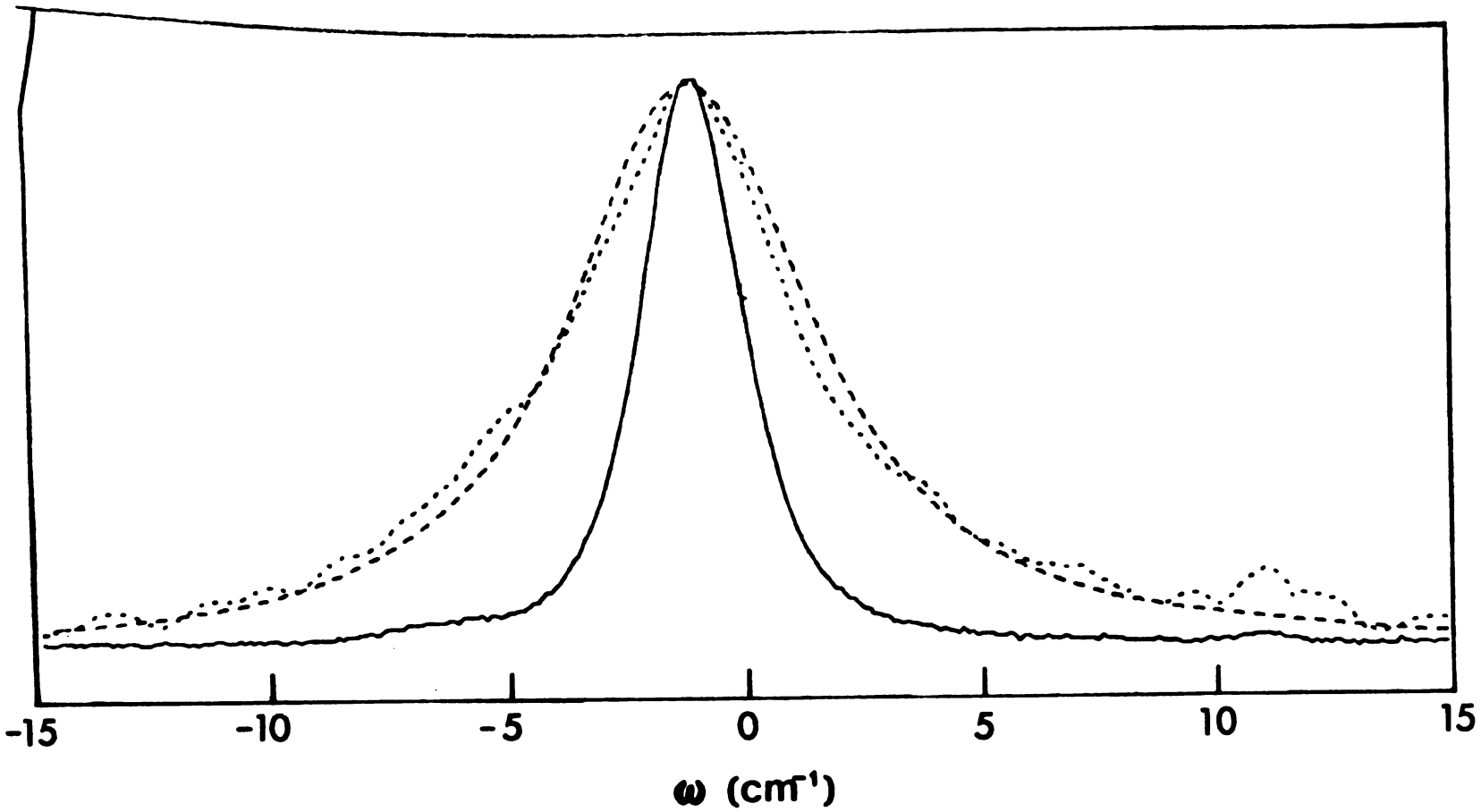

Figure 36. Polarized spectrum (——), depolarized spectrum (· · ·), and calculated convolution of the polarized component with a Lorentzian reorientational spectrum (- - -), for the 714 cm^{-1} line of CF_3CCl_3.

DISCUSSION

I. Raman and NMR Relaxation Studies of $CDCl_3$ and $CDBr_3$

A. Introduction

Nuclear quadrupole coupling constants are not directly measurable in the liquid phase since the rapid molecular motions broaden the pure quadrupole resonance lines. They may be estimated from the solid and/or gas phase values or else obtained indirectly from various NMR experiments.

In the absence of strong intermolecular interactions in the solid phase, such as hydrogen bonding or Lewis acid-base interactions, it has been shown that quadrupole coupling constants from microwave gas studies are about 5-10% larger than those obtained from NQR spectra of solids[240] and the liquid-phase value may then be presumed to lie somewhere between these two. When there are important intermolecular interactions, as is often the case for ^{2}D and ^{14}N, an investigation[241] has indicated that the solid-phase value should be the best approximation unless the structure is considerably deformed from that in the liquid, as in ammonia[242]. Unfortunately, deuterium pure NQR spectra are not in general observed in solids because of the low sensitivity at the low frequencies necessary and one must therefore obtain them from NMR spectra of solids[243-245] where there may be complications from molecular motions[245].

NMR studies of solutes in liquid-crystal solvents have been used to obtain deuterium quadrupole coupling constants with uncertainties ranging from 3-10%[246-248]. Alternatively, quadrupole

coupling constants may be obtained from liquid-phase measurements of T_1 for the quadrupolar nucleus by use of the equation[28]

$$\frac{1}{T_1} = \frac{1}{T_{1Q}} = \frac{3(2I+3)\ \pi^2}{10I^2(2I-1)}\ (1 + \frac{\eta^2}{3})(\frac{e^2Qq}{h})^2\tau_\theta, \qquad (129)$$

if the angular correlation time for reorientation of the X-D bond, τ_θ, is known. Where the asymmetry parameter η is unknown it may be taken as zero without too great error. Values of τ_θ have been estimated from viscosity data using the Debye relationship $\tau_\theta = 4\pi\xi a^3/3kT$, (where ξ is the viscosity coefficient and a the molecular radius)[249,250], from viscosity data combined with structural parameters[251], and, in the case of deuterium quadrupole coupling constants, from proton relaxation times of the protonated analogue[252-253]. For a few molecules of special geometry it has been possible to determine τ_θ rather accurately from NMR data[241,254].

We assume here that the Raman correlation time from Raman line-shape analysis can be used to obtain τ_θ in Equation (129) and describe a new procedure for determining quadrupole coupling constants in liquids which yields the coupling constants directly for molecules with the quadrupolar nucleus on an axis of threefold or higher symmetry. Values of T_{1Q} are then obtained directly from NMR data and used to solve for e^2qQ (Equation 129 above); η is identically zero for this geometry. The analysis is less satisfactory for molecules of lower symmetry or nuclei not on the symmetry axis, as has been pointed out for benzene[171].

As a result of the theoretical and experimental difficulties mentioned above, few "experimental" values of quadrupole coupling

constants in liquids have been reported. The present method should be useful in providing additional data, which may be used, for example, to investigate environmental effects of deuterium quadrupole coupling constants by comparison with recent gas phase[255-258] and solid phase[243,244,259] values. Although the method is an indirect one the uncertainties are reduced since we are determining the square of the quadrupole coupling constant.

Since the quadrupolar relaxation mechanism dominates, elaborate purification of the samples, chemically or isotopically, is not important. Since T_{1Q} and τ_θ are strictly related via Equation (129), making both Raman and NMR measurements on the same sample will eliminate the effects of impurities, other than paramagnetic ones.

In contrast to pure quadrupole resonance spectroscopy, where quadrupole coupling constants below about 1 MHz are experimentally inaccessible, small quadrupole coupling constants are easier to obtain than large ones by the present method since the NMR relaxation time becomes longer. Of course, as the quadrupole coupling constant approaches zero other relaxation mechanisms become important and the interpretation becomes more complex. However, even deuterium quadrupole coupling constants, which are among the smallest studied, are large enough that other mechanisms do not compete as we demonstrate here for the case of deuterobromoform. The importance of other mechanisms may be estimated from the proton relaxation rate ($1/T_1$) of $CDBr_3$, which is found[260,261] to be 0.0461 sec^{-1} at 25° C. For the various other interactions which may be of importance (intermolecular dipole-dipole, spin rotation, scalar coupling to bromine) the contribution to the deuterium relaxation rate will be

smaller by a factor of ∿40 due to the dependence on gyromagnetic ratio (γ^2) or on spin-rotation interaction constant (C^2). Thus, we estimate $1/T_{1(other)} \cong 0.001\ sec^{-1}$, which is certainly negligible compared to $1/T_{1Q} = 2.68\ sec^{-1}$.

The correlation time associated with NMR relaxation is the zeroth moment of the rotational correlation function

$$\tau_\theta = \int_{-\infty}^{\infty} \langle R(t)R(0)\rangle dt \ . \qquad (130)$$

When the correlation function is exponential (i.e., the orientational spectrum $I_{or}(\omega)$ is Lorentzian) the correlation time is the half-width at half-height of $I_{or}(\omega)$.

For symmetric-top molecules the motion can be described by two correlation functions describing the motions parallel to and perpendicular to the symmetry axis. Consequently, through Equation (130) there are two rotational correlation times $\tau_{\theta_\perp}$ and $\tau_{\theta_{||}}$. It was shown that for symmetric molecules the Raman line of A_1 symmetry is affected only by rotation perpendicular to the symmetry axis and thus gives information only concerning $\tau_{\theta_\perp}$. Other lines contain information about both parallel and perpendicular rotations, but $\tau_{\theta_{||}}$ is more difficult to extract. In the case of symmetric-top molecules with the quadrupolar nucleus on the symmetry axis this presents no problem as only motion perpendicular to the symmetry axis is effective in relaxing the nuclear spins. Since both the NMR and Raman data refer in this case to reorientation of the same vector they may be compared directly, or Equation (129) may be used to examine the liquid-phase quadrupole coupling constant.

B. Analysis of Raman Spectra of $CDBr_3$ and $CDCl_3$

In Figures 31 and 32 are shown the normalized polarized and depolarized spectra, and the calculated convolution of the polarized spectrum with the Lorentzian orientational spectrum for the 222 cm^{-1} and 521 cm^{-1} lines of $CDBr_3$. The calculated lineshape for the 222 cm^{-1} line matches the experimental as far into the wings as the signal may be distinguished from the noise ($\sim$6 half-widths). The 521 cm^{-1} line, on the other hand, clearly does not conform to a Lorentzian orientational spectrum. The depolarized component is too narrow at the center and too broad in the wings. The polarized line is slightly asymmetric on the low frequency side, while the depolarized component shows a distinct shoulder on the high frequency side. The presence of fine structure on both sides of the absorption makes analysis difficult, as Bartoli and Litovitz discuss[30], but it is not clear that the unresolved weaker components of the 521^{-1} cm line are responsible for the large discrepancies between the calculated and observed line shape. The low-frequency asymmetry in the polarized spectrum, which was presumed to be due to a "hot" band, was successfully described by an absorption band with fractional intensity of 0.14 and frequency offset 2.6 cm^{-1} (with reference to the main band).

Since the Fourier inversion method of determining $\tau_{\theta_\perp}$ makes no assumptions concerning line shape, it must be used when the convolution method fails. Figure 37 shows the correlation functions obtained via Equation (85) for the 222 and 521 cm^{-1} lines plotted on a logarithmic scale. The 521 cm^{-1} function is arbitrarily shifted

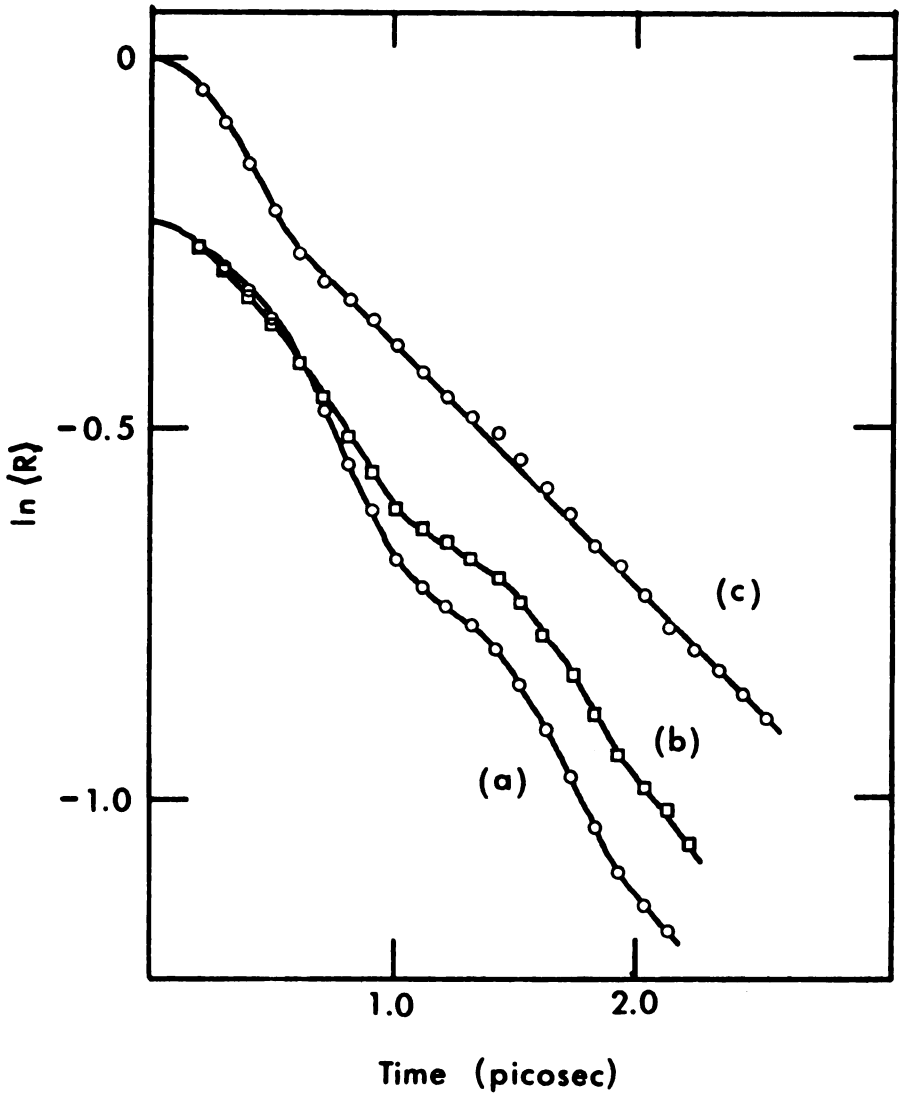

Figure 37. Correlation functions calculated from $CDBr_3$ Raman lines; (a) uncorrected low-frequency side of the 521 cm^{-1} line, (b) low-frequency side of the 521 cm^{-1} line corrected for the presence of a hot band, and (c) low-frequency side of the 222 cm^{-1} line.

downward for clarity. The correlation function labeled 521a was obtained by Fourier inversion of the low-frequency sides of both components of the spectrum, while the one labeled 521b was obtained from the low-frequency sides after correcting for the presence of the hot band. It was necessary to assume that the depolarization ratio of the hot band is the same as that of the main band in order to make the correction to the depolarized component. From Figure 37 it is clear that the hot-band correction brings the correlation time for the 521 cm^{-1} line into closer agreement with $\tau_{\theta_\perp}$ for the 222 cm^{-1} line (although this number was not calculated). However, it is equally clear that both correlation functions derived from the 521 cm^{-1} line contain the same features and both deviate from exponential (linear on the logarithmic scale) behavior at times when the 222 cm^{-1} line correlation function is well described by an exponential decay.

Since all A_1 lines in a given molecule must show the same reorientational broadening in the absence of vibration-rotation coupling (which is not possible in this case), we conclude from this discrepancy between the 521 cm^{-1} line and the other two A_1 lines in $CDBr_3$, that as many lines as possible should be studied for each molecule and that conclusions (especially any conclusion that there is nonexponential correlation behavior at long times) not be drawn on the basis of a measurement of a single line.

The remaining Raman lines of A_1 symmetry for $CDBr_3$ and $CDCl_3$ are all adequately fit with a Lorentzian orientational spectrum, although smaller depolarization ratios or smaller absolute intensities result in larger uncertainties in ω_{or}. These lines are listed in

Table 24 with their observed intrinsic (vibrational plus slit broadening) and orientational widths, plus the percentage correction to the depolarized line for leakage from the strong component, and the measured depolarization ratios. Literature values of the depolarization ratios are much larger since they were measured before the advent of the laser as a light source and consequently the scattering geometry was not well defined. The 365 cm^{-1} line of $CDCl_3$ is not included in Table 24 because the chlorine isotope splitting (expected intensity ratios 27:27:9:1) was resolved, making analysis more difficult. The bromine isotope splitting (expected intensity ratios 1:2:2:1) was not observed for any of the $CDBr_3$ A_1 lines. Table 25 lists the correlation times obtained from these measurements plus results from Raman experiments in other laboratories. Table 26 lists the observed deuterium NMR relaxation times and the Raman correlation times, along with the quadrupole coupling constants calculated from them by use of Equation (129). Other measurements[72,236] of the ^2D relaxation time in $CDCl_3$ agree very well with our result of 1.47 ± 02 seconds, which was obtained at 27° C; however, the range of Raman correlation times $\tau_{\theta_\perp}$ for $CDCl_3$[143] or $CHCl_3$[141,155] is much larger than the quoted uncertainties and seems to be independent of the vibrational band or the isotopic species studied. The solid-phase values of the coupling constants are included for comparison. It was noted[245] that the solid-state value of the quadrupole coupling constant of $CDBr_3$ was abnormally low, perhaps as a result of molecular rotation.

Table 25. Raman correlation times reported for $CDCl_3$ and $CDBr_3$[a]

Molecule	Line (cm^{-1})	$\tau_{\theta_\perp}$ (psec)	Method[b]	Temp.	Ref.
$CHCl_3$	667	1.4 ±.3	C	22°	c
	3019	1.5 ±.3	C	22°	c
	3019	1.97±.17[d]	FT	23°	e
$CDCl_3$	650	1.85±.31	C	27°	f
	2256	1.96±.14	C	27°	f
	2256	1.59±.03	FT	RT	g
$CHBr_3$	222	5.3 ±2	C	22°	c
$CDBr_3$	221	5.33±.22	C	27°	f
	521	4.1±1.2	C	27°	f
	2250	5.0±2	C	27°	f

[a]Obtained from the relation $\tau_\theta = [2\pi c\omega_{or}]^{-1}$.

[b]C = convolution method [Equation (84)]; FT = Fourier inversion method [Equation (85)].

[c]Reference 141.

[d]Uncertainty estimated from Reference 155, Figure 2.

[e]Reference 155.

[f]This laboratory.

[g]Reference 143.

Table 26. NMR and Raman results and deuteron quadrupole coupling constants in $CDCl_3$ and $CDBr_3$.

Molecule	NMR T_1(sec)	Raman $\tau_{\theta_\perp}$ (psec)	QCC(kHz) Solid	QCC(kHz) Liquid
$CDCl_3$	1.47 ±.02	1.85±.31	166.9[a]	158±14
		1.96±.14		153±7
$CDBr_3$	0.403±.006	5.33±.22	122[b]	177±5

[a]Reference 244.

[b]Reference 245.

C. Effect of ^2D on Diffusional Motion

According to Gordon's[93] extended diffusion model the effect of isotopic substitution on the rotational correlation times will depend on the ratio of moments of inertia for the axis in question, taken to the one-half power. NMR relaxation experiments, such as T_1 measurements of ^{14}N in ammonia[86] which give $T_1(NH_3)/T_1(ND_3) = 1.42$, independent of temperature, while $[I\ (ND_3)/I\ (NH_3]^{1/2} = 1.39$, tend to confirm this prediction but Raman results are less conslusive. For example, one would expect that deuteration of methyl iodide would strong affect $\tau_{\theta_{||}}$ but have very little effect on $\tau_{\theta_{\perp}}$. Goldberg and Pershan[142] examined Raman lines sensitive to $\tau_{\theta_{\perp}}$ for both of these molecules and, although they claimed reasonable agreement for the different A_1 lines, their results were somewhat inconclusive in that $\tau_{\theta_{\perp}}$ for CD_3I and CH_3I agreed within experimental error for the v_3 line but not for the v_2 line. This may result from the smaller depolarization ratio for the v_2 line, evident in their Figure 1, but they do not give uncertainties on a line-by-line basis. Gillen and Griffiths[77] observed that $\tau_{\theta_{\perp}}$ in C_6D_6 is 10% larger than $\tau_{\theta_{\perp}}$ in C_6H_6, which is approximately correct for the change in the moment of inertia for that axis. In view of the utility of joint NMR-Raman experiments involving a quadrupolar nucleus such as deuterium, both to obtain coupling constants and to determine complete diffusion tensors[77,81,173], it would be useful to investigate more fully the effect of deuteration, especially in light of the discrepancies in the Raman $\tau_{\theta_{\perp}}$ of $CHCl_3$ and NMR $\tau_{\theta_{\perp}}$ of $CDCl_3$ observed by Campbell and Jonas[155].

D. Deuterium Quadrupole Coupling Constants

Table 27 lists the reported ^2D quadrupole coupling constants for molecules of the type DCX_3, plus other relevant data. To a good approximation the contributions to the total field gradient, $\underline{q}^{tot}$, may be considered to arise wholly from the directly-bonded nucleus (q^{nuc}) and the electrons in the bonding orbital (q^{el}). There are two reasons for this. First, the contributions to the field gradient depend on r^{-3}, so directly-bonded nuclei are much more important than more distant nuclei and electrons. Second, the two contributions q^{nuc} and q^{el} for more distant atoms tend to cancel as can be seen in theoretical calculations of the field gradient in polyatomic molecules[262].

The electronic contribution is calculated from the relation $q^{el} = q^{tot} - q^{nuc}$ where $q^{nuc} = 2Z_i/r^3_{CH}$, Z_i is the nuclear charge (= +6), and r_{CH} is the carbon-hydrogen bond length. We assume here that $r_{C-H} \cong r_{C-D}$ since these values are usually equal within the experimental errors.

Salem[263] has demonstrated that the relationship $k \sim eq^{tot}$ exists for diatomic molecules, where k is the force constant of the bond. That relationship seems to be appropriate for polyatomic molecules as well[264,265] and can be seen in Table 27 to be valid for this series, although the proportionality constant (in a.u.) is somewhat larger than the 0.70 predicted by the covalent model. We note that if the C-D vibrations result solely in motion of the deuteron, while the rest of the nuclei and the electron cloud remain fixed, then the theory predicts k = eq. Various values of k have been reported

Table 27. The relations between coupling constants, force constants and structure for sp^3 hybridized carbon.

Molecule	e^2qQ(kHz)	r_{C-H}(Å)	q^{nuc} (a.u.)	q^{el}(a.u.)	q^{tot}(a.u.)[a]	$k \times 10^5$ ($\frac{dynes}{cm}$)	$\frac{eq}{k}$ (a.u.)	X[b]
CDH_3	191.48± .77[c]	1.091[d]	1.3693	-1.0858	0.2835	5.92	0.746	2.15
CDF_3	170.8 ±2.0	1.098±.02	1.3433	-1.0905±.0274	0.2528±.0030	5.00	0.787	3.95
$CDCl_3$	166.9 ± .1	1.100±.004	1.3360	-1.0889±.0050	0.2471±.0002	5.00	0.769	3.0
$CDBr_3$	177 ±5	1.068±.02	1.4597	-1.1972±.0546	0.2625±.0073	5.08	0.804	2.8

[a]Calculated using $Q = 2.875 \times 10^{-27}$ cm^2 [R. V. Reid and M. L. Vaida, Phys. Rev. lett. 29, 494 (1972)].

[b]Electronegativity values X selected by Gordy and Thomas from those derived by four different methods [J. Chem. Phys. 24, 439 (1956).]

[c]The value of e^2qQ for CDH_3 is from S. C. Wofsy, J. S. Muenter, and W. Klemperer, J. Chem. Phys. 53, 4005 (1970); values for CDF_3 and $CDCl_3$ are from References 255 and 244, respectively, while the value for $CDBr_3$ is from the present work.

[d]The value of r_{C-H} for CH_4 is from D. J. R. Boyd and H. W. Thompson, Proc. Roy. Soc. (London) A126, 143 (1953); those for CHF_3, $CHCl_3$ and $CHBr_3$ are from References 271, 272 and 270, respectively.

[e]The value of k for CH_4 is from P. Pulay, Mol. Phys. 21, 329 (1971) and that for CHF_3 from D. A. Long, R. B. Gravenor, and D. T. L. Jones, Trans. Faraday Soc. 60, 1509 (1964); values for $CHCl_3$ and $CHBr_3$ are from References 267 and 268, respectively.

for $CDCl_3$ and $CDBr_3$[266-268] but the ratio $k(CDCl_3)/k(CDBr_3) \approx 1.02$.

Bersohn[269] has presented a qualitative argument to show that the deuterium quadrupole coupling constant should decrease with an increase in substituent electronegativity. His argument considers only the charge distribution in the C-D bonding orbital but it is clear from Table 27 that a more important effect in determining the quadrupole coupling constant is the C-D bond length. The value of r_{C-D} for $CDBr_3$ is somewhat suspect because of the large uncertainty (0.02 Å) associated with the early microwave determination[270]. In the case of $CHCl_3$ the early value[271] $r_{C-H} = 1.073 \pm 0.02$ Å was later redetermined[272] and the more precise value $r_{C-H} = 1.100 \pm 0.0004$ Å found. It seems likely that the value of r_{C-D} in $CDBr_3$ should also be larger and we prefer to use the same value (1.100 Å) as found for $CHCl_3$, which leads to $q^{nuc} = 1.3360$ and $q^{el} = -1.0735 \pm .0122$. In all of these molecules the uncertainties in q^{el} are dominated by the uncertainties in the C-H bond length.

E. The Rotational Diffusion Tensor in $CDBr_3$

From the correlation function obtained from the 222 cm^{-1} line it can be seen that, at 27° C, rotational motion perpendicular to the symmetry axis is well described by a diffusional process. Additional information on molecular motion in $CDBr_3$ can be obtained from studies of the temperature dependence of NMR relaxation times. Table 10 gives relaxation data for the deuterium nucleus, and Farrar et al.[239] have studied the temperature dependent ^{13}C relaxation in 60% enriched $^{13}CHBr_3$, which is given in Table 28. Ordinarily, to extract both

Table 28. The temperature dependence of ^{13}C spin-lattice relaxation in $^{13}CHBr_3$

T(°C)	$10^3/T$(°K)	$R_{1,total}$[a] (sec^{-1})	$\tau_{\theta_\perp} \cdot 10^{12}$[b] (sec)	$R_{1,dd}$[c] (sec^{-1})	$R_{1,sc}$[d] (sec^{-1})
124	2.52	0.90	2.01	0.0362	0.864
107	2.63	0.86	2.28	0.0411	0.819
90	2.75	0.79	2.62	0.0472	0.743
69.3	2.92	0.70	3.20	0.0576	0.642
50.4	3.09	0.61	3.89	0.0700	0.536
30.8	3.29	0.61	4.91	0.0884	0.518
10.9	3.52	0.61	6.42	0.116	0.490

[a]Reference 239, uncertainty ±3%.

[b]From ^2D relaxation.

[c]$R_{1,dd} = 1.801 \times 10^{10}\ \tau_{\theta_\perp}$.

[d]$R_{1,sc} = T_{1,total} - R_{1,dd}$.

$\tau_{\theta_\perp}$ and $\tau_{\theta_{||}}$ one must measure relaxation rates of two nuclei, one on and one off the symmetry axis. However $^{13}CHBr_3$ is a special case in that the carbon relaxation rate at high temperatures is dominated by scalar coupling to the three bromines and consequently ^{13}C relaxation data is sensitive to the relaxation rate of the bromines. The value of this is that one can indirectly measure the bromine relaxation time, which is inaccessible to direct measurement by virtue of the large quadrupole coupling constant.

Evaluation of $\tau_{\theta_\perp}$ - The perpendicular correlation time may be obtained from ^2D relaxation data as long as hydrogen bonding is not appreciable, which would make the ^2D quadrupole coupling constant temperature dependent. VanderHart[236] has recently summarized the data for the case of $CDCl_3$ and concluded that hydrogen bonding is at most of minor importance. The experimental data which supported this conclusion for $CDCl_3$ are not all known for $CDBr_3$, but NMR proton chemical shifts upon dilution in an inert solvent are very similar for both chloroform and bromoform[273]. If the ^2D quadrupole coupling constant is temperature independent then $\tau_{\theta_\perp}$ may be calculated, and the best fit to the experimental points gives

$$\tau_{\theta_\perp} = 4.842 \times 10^{-14} \exp(2.80 \text{ kcal mol}^{-1}/RT). \qquad (131)$$

Separation of the ^{13}C Relaxation Mechanisms in $^{13}CHBr_3$ - Of the various mechanisms which can contribute to $1/T_1$, we can calculate exactly only the intramolecular dipole-dipole contribution. We calculate this from the $\tau_{\theta_\perp}$ values determined from the ^2D relaxation

measurements by use of the relation

$$1/T_{1,intra} = \hbar^2\gamma_C^2\gamma_H^2 r_{CH}^{-6}\tau_{\theta_\perp}$$

$$= 1.801 \times 10^{10}\tau_{\theta_\perp}, \qquad (132)$$

where $r_{CH} = 1.100 \times 10^{-8}$ cm, as discussed previously. The contribution from the dipole-dipole interaction with the three bromines may be neglected since the product $\gamma_{Br}^2 r_{CBr}^{-6}$ is about 0.002 that of $\gamma_H^2 r_{CH}^{-6}$. The dipolar contribution at 25° C calculated from Equation (2), 0.095 sec^{-1}, agrees well with the value 0.10 sec^{-1} obtained from the nuclear Overhauser enhancement[239]. In Figure 38 are plotted the relaxation rates of ^{13}C in $^{13}CHBr_3$ and ^2D in $CDBr_3$, plus the intramolecular dipole-dipole contribution to the total ^{13}C relaxation rate as calculated from Equations 132 and 131, and the sum of the remaining contributions to the ^{13}C relaxation rate, $R_{1,total} - R_{1,dd}$. Of the remaining possible mechanisms for ^{13}C relaxation, we neglect the intermolecular D-D contribution, as is the usual procedure in ^{13}C relaxation studies[224]. We also neglect the spin-rotation mechanism, since for chloroform it was at most 10% of the total rate[275] and should be less for a more massive molecule. Relaxation through chemical shift anisotropy is also negligible at the low field used in the ^{13}C studies (14.1 kG). An anisotropy of 200 ppm results in

$$(1/T_1)_{csa} = 2.4 \times 10^7\tau_{\theta_\perp}, \qquad (133)$$

which is clearly negligible with respect to $1/T_{1,intra}$. The final

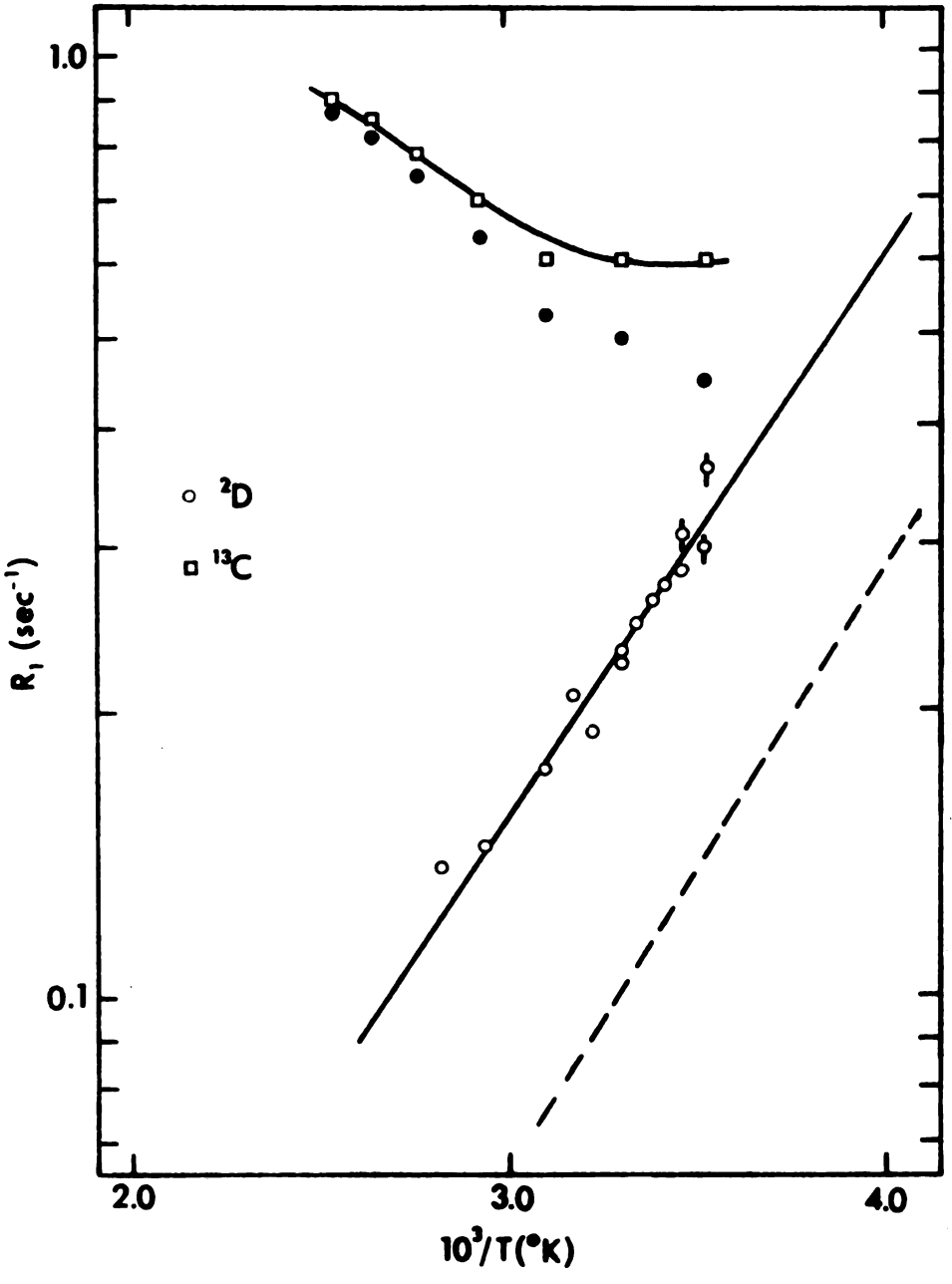

Figure 38. Spin-lattice relaxation rates as a function of temperature for ^{2}D in $CDBr_3$(o), and ^{13}C in $^{13}CHBr_3$ (□). Also shown are the calculated dipole-dipole contribution to the ^{13}C relaxation rate (- - -), and $[R_{1,total}(^{13}C)-R_{1,dd}(^{13}C)]$(●).

possibility is relaxation through scalar coupling to the bromines, which Farrar et al.[239] concluded is the dominant relaxation mechanism in $CHBr_3$. The expression for this mechanism is

$$(1/T_1)_{sc} = \frac{3A^2}{3} S(S+1) \frac{\tau}{1 + \Delta\omega^2\tau^2} \qquad (134)$$

where $A = J/2\pi$ is the scalar coupling constant in radians per second, S is the spin of the other nucleus (Br in this case), τ is the relaxation time of the S spin, and $\Delta\omega$ is the difference in Larmor frequencies of the two spins. This expression is further complicated in this case by the presence of two isotopes of bromine, each of ~50% abundance. The total rate for the scalar-coupled interaction is then the sum of the individual rates for the various combinations present multiplied by their fractional abundance,

$$(1/T_1)^{tot}_{sc} = \frac{1}{8} (R^{818181}_{1,sc} + R^{797979}_{1,sc}) + \frac{3}{8} (R^{798181}_{1,sc} + R^{797981}_{1,sc}), \qquad (135)$$

where the superscripts indicate the isotopic species present and

$$R^{ABC}_{1,sc} = (1/T_{1,sc})^A + (1/T_{1,sc})^B + (1/T_{1,sc})^C. \qquad (136)$$

From Equations (135) and (136) we obtain

$$(1/T_1)^{tot}_{sc} = \frac{3}{2} [1/T_{1,sc}(^{79}Br) + 1/T_{1,sc}(^{81}Br)]. \qquad (137)$$

For values of the correlation time on the order of 5×10^{-12}, $\Delta\omega^2\tau^2 << 1$ for ^{79}Br; however, for ^{81}Br, $\Delta\omega^2\tau^2 \approx 1$. Therefore the

total scalar-coupled rate is

$$(1/T_{1,sc})^{tot} = \frac{3}{2}\left[\frac{2A^2(^{79}Br)}{3}S(S+1)T_1(^{79}Br)\right.$$

$$\left. + \frac{2A^2(^{81}Br)}{3}S(S+1)\frac{T_1(^{81}Br)}{1+\Delta\omega^2T_1^2(^{81}Br)}\right] . \qquad (138)$$

The number of unknowns may be reduced by the relations $\gamma_{79}/\gamma_{81} = A(^{79}Br)/A(^{81}Br) = 0.928$, and $Q_{79}^2/Q_{81}^2 = T_1(^{81}Br)/T_1(^{79}Br) = 1.474$, but there are still more unknowns than equations. Therefore we cannot calculate $(1/T_{1,sc})^{tot}$ or, conversely, obtain $(1/T_{1,sc})^{tot}$ from the total rate and then calculate $T_1(^{79}Br)$ and τ_θ'. What we can do, though, is vary the values and activation energy of τ_θ' in order to best fit the experimental data. This may be readily done graphically. In Figure 39 we plot as functions of inverse temperature $(1/T_1(^{79}Br))/\frac{2A^2}{3}S(S+1)$, $(1/T_1(^{81}Br))/\frac{2A^2}{3(0.928)^2}S(S+1)$, and $(1/T_{1,sc})^{tot}/\frac{2A^2}{3}S(S+1)$, (where $A = A(^{79}Br)$) for the case of isotropic rotational diffusion. We see that $(1/T_{1,sc})^{tot}$ at very high and very low temperatures is linear (on the log scale) with activation energy $E_a^{sc} = E_a^{dd}$, while at intermediate temperatures the curve smoothly varies from one linear region to the next with an inflection point occurring at $\Delta\omega^2T_1^2(^{81}Br) = 1$, which occurs at 317° K. The effect of anisotropic reorientation will be that this inflection point will occur at higher or lower temperature and the high- and low-temperature activation energies will have a value different than E_a^{dd}. We graphically vary E_a^{sc} and τ_θ' by rotating this curve and attempting to fit any section of it to the experimental data. Obviously the right-most half of the curve is not suitable, no matter what E_a^{sc} is chosen, as the curvature is in the wrong sense.

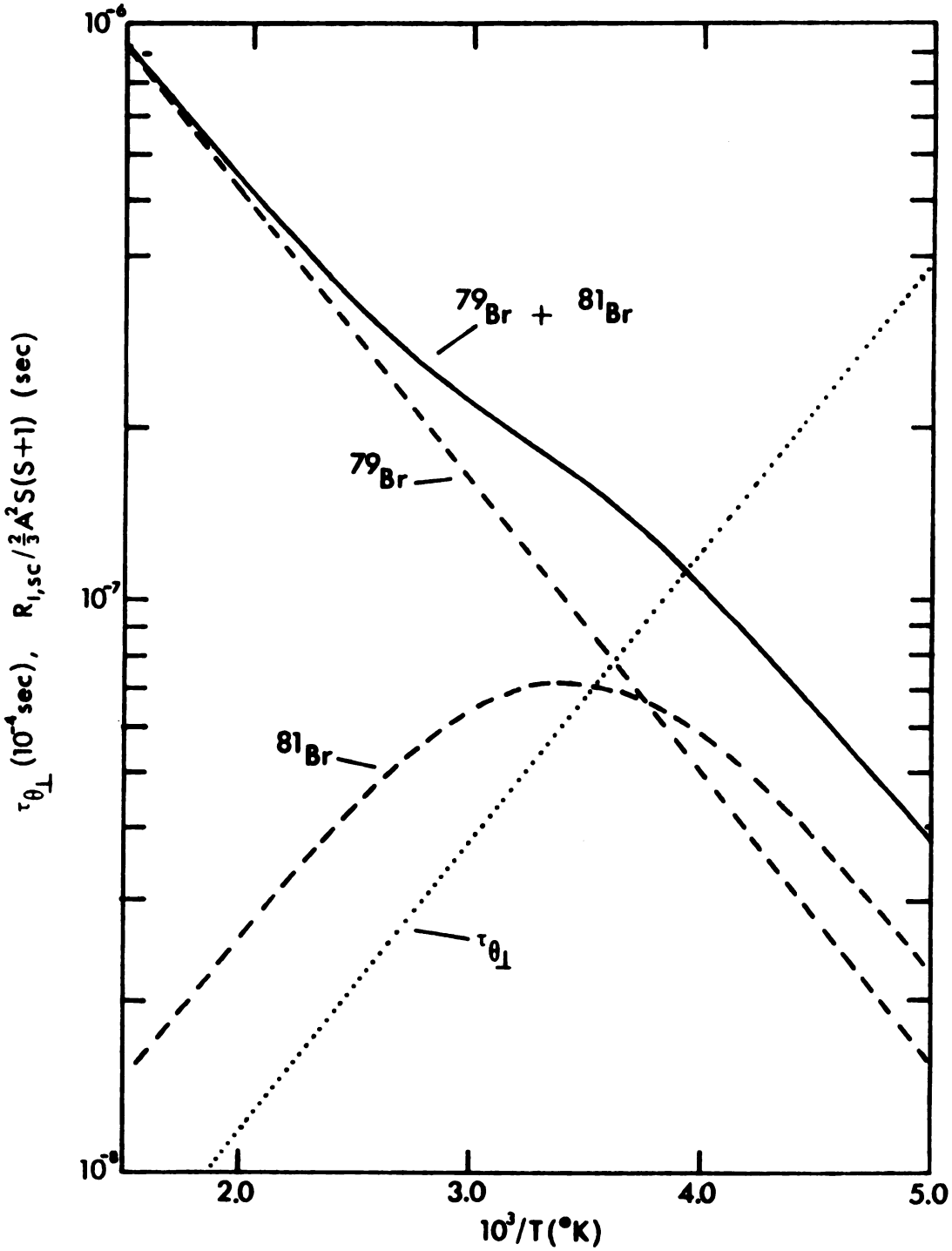

Figure 39. The temperature dependence of the contribution to the ^{13}C relaxation rate in $^{13}CHBr_3$ from scalar coupling to ^{79}Br and ^{81}Br, assuming isotropic reorientation.

Therefore we can conclude that $E_a^{sc} \geq E_a^{dd}$ and consequently $E_{a||} \geq E_{a\perp}$, which is what has been found for other symmetric tops. The curve fits the experimental data reasonably well with values at one extreme of $E_a^{sc} = E_a^{dd}$ and J_{CBr} = 91 Hz (isotropic reorientation), and at the other extreme E_a^{sc} = 1.59 kcal/mole and J_{CBr} = 55 Hz (from which $D_{||}/D_{\perp}$ = 1.49 at 20° C). The comparison of theory with experiment in these two cases is shown in Figure 40.

Discussion of the Experimentally-Derived Diffusion Tensor - The uncertainties associated with the activation energy for the spinning motion and the ratio $D_{||}/D_{\perp}$ are so large that a detailed discussion would be out of place. It is, however, worthwhile to call attention to two points. The first is the comparison of bromoform with chloroform, summarized in Table 29. Huntress[72] found that for $CDCl_3$ at 20° C $D_{||}/D_{\perp}$ = 1.98, while the χ-test[72] gave that the tumbling motion is diffusional but the spinning motion is approaching free-rotor behavior. In the case of bromoform all that can be said is that $E_{a,||} \leq E_{a,\perp}$. Raman lineshape studies reported previously show clearly that the tumbling motion is diffusional, so $\chi_{\perp}$ = 4.1 and $\chi_{||}$ lies between 4.1 and 2.1. The second point to be made is concerning J_{CBr}. Farrar et al.[239] have argued that J_{CI} in CH_3I must not be greater than 60 Hz by virtue of the very minor importance of scalar relaxation for ^{13}C in $^{13}CH_3I$. Since ^{13}C-Br coupling constants would be expected to be smaller than ^{13}C-I couplings an anisotropic reorientation is favored, as it results in a smaller J_{CBr}.

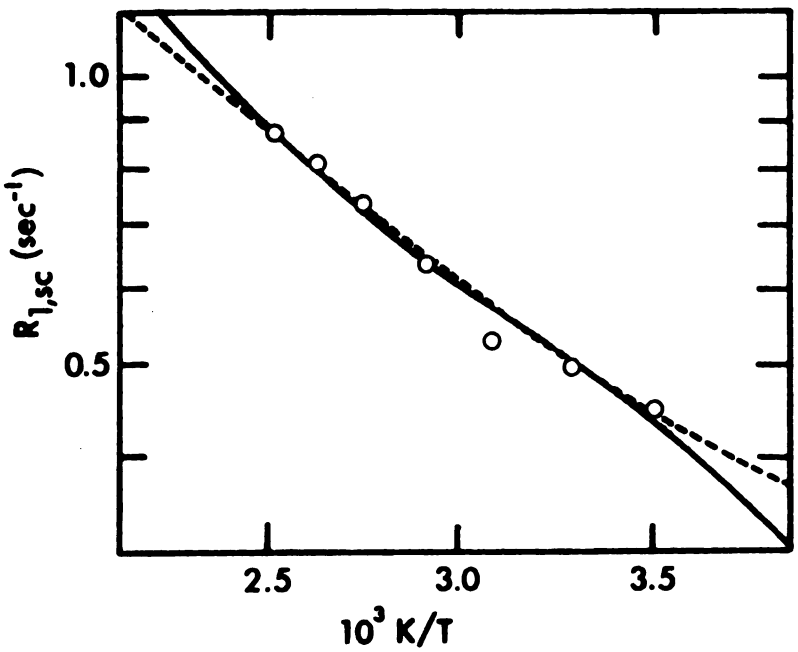

Figure 40. The temperature dependence of the contribution to the ^{13}C relaxation rate in $^{13}CHBr_3$ from scalar coupling to bromine predicted by (a) isotropic reorientation with J_{CBr} = 91 Hz (——), and (b) anisotropic reorientation with $E_{a,sc}$ = 1.59 kcal/mole, J_{CBr} = 55 Hz and $D_{||}/D_{\perp}$ = 1.49 at 20° C (- - -).

Table 29. Physical properties of $CDBr_3$ and $CDCl_3$

Physical Property	$CDBr_3$	$CDCl_3$
$I_{\perp}$, g-cm^2	$686 \cdot 10^{-40}$	$264 \cdot 10^{-40}$[a]
$I_{\parallel}$, g-cm^2	$1202 \cdot 10^{-40}$	$498 \cdot 10^{-40}$[a]
$(e^2qQ)_D$, kHz	177	167[b]
$(e^2qQ)_{^{79}Br}$, MHz	550[c]	79[c]
r_{C-D}, Å	1.100	1.100[d]
$\tau^*_{\theta\perp}$	4.1	2.2[a]
$\tau^*_{\theta\parallel}$	4.1-2.1	0.84[a]
$E_{a,\perp}$	2.80	1.6[a]
$E_{a,\parallel}$	2.80-1.6	1.2[a]

[a]Reference 72.

[b]Reference 244.

[c]Reference 240.

[d]Reference 272.

II. NMR and Raman Studies of CF_3CCl_3

Very little physical data have been reported for CF_3CCl_3, the most symmetrical of the fluorochloroethanes. But from the melting point (13.2° C as compared to -35° C for its unsymmetrical isomer), high vapor pressure in the solid[276] and approximately spherical shape, this substance may be expected to form a plastic phase in the solid. If this can be shown to be the case, then the usual temperature-dependent relaxation time study may be enhanced in two ways: (1) If the rotational motion in the solid and liquid occurs by the same process, that is, if there isn't a distinct rotational transition at the melting point, then the effective range for studying rotational motion is extended down to the phase transition, and the separation of the total spin-lattice relaxation rate into contributions from different mechanisms is easier, and (2) The contribution to T_1 from translational diffusion in the solid may be separated, from which the diffusion coefficient may be determined.

From Figure 41 it can be seen that the plastic crystalline phase extends down to 157° K, at which temperature the relaxation time exhibits a discontinuous and reversible change. This discontinuity presumably signals a phase change in which the high temperature form has the cubic symmetry typical of plastic solids, and permits either rotation about a molecular axis or isotropic rotation. The low value measured for the second moment in the high-temperature phase is consistent only with isotropic rotation, as will be discussed.

The most striking feature of the relaxation curve is that the melting transition causes very little change in T_1, at least at 56 MHz.

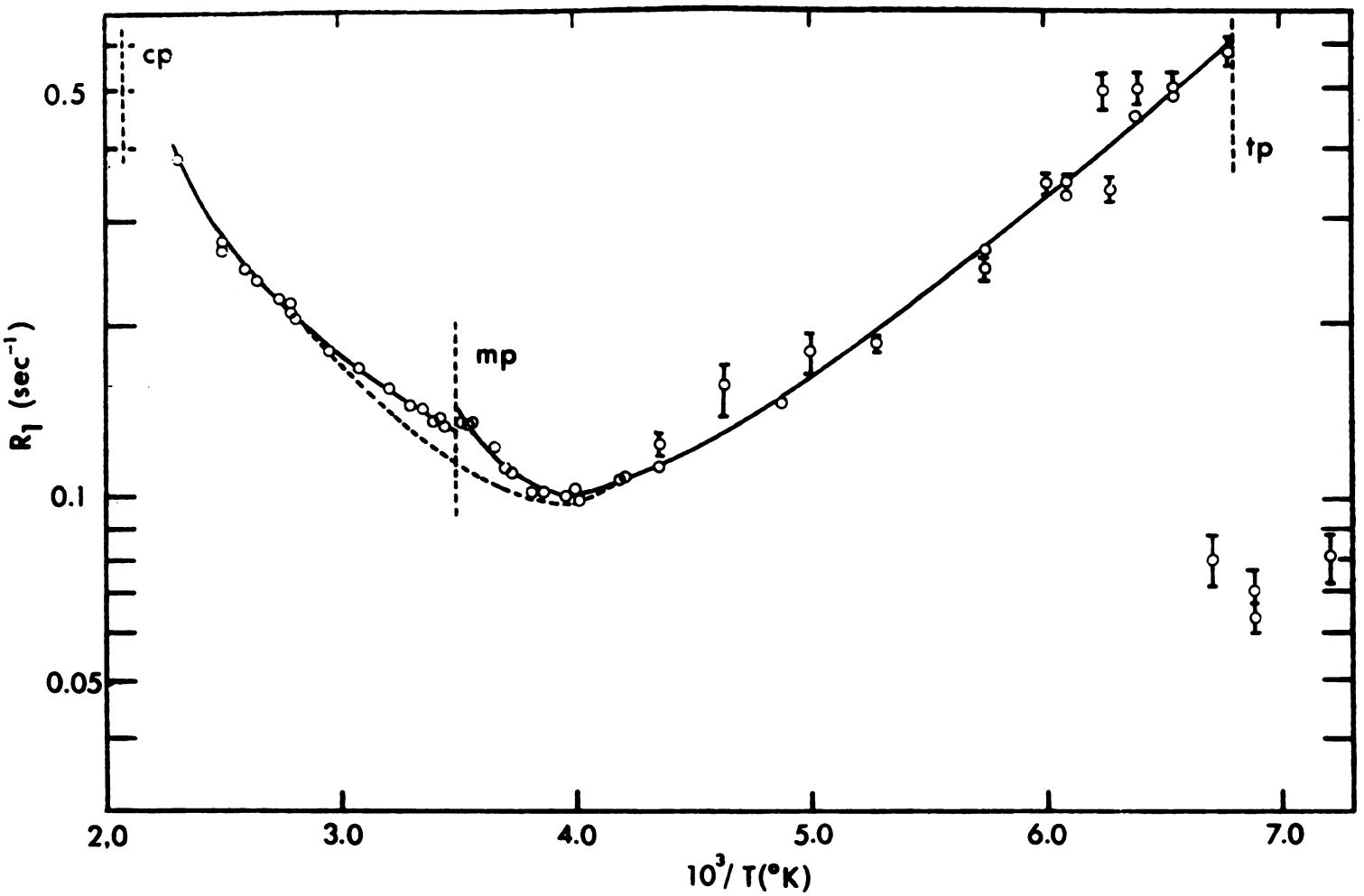

Figure 41. Spin-lattice relaxation of ^{19}F in liquid and solid CF_3CCl.

This behavior is common to all members of the series $C_2F_nCl_{6-n}$ which were studied in the course of this investigation. Since this is so, the results will be presented in terms of the translational and rotational contributions to T_1^{-1} over the whole temperature range studied.

A. Determination of the Second Moment

For the case of isotropic rotation the intramolecular contribution to the second moment averages to zero. The total second moment then arises from intermolecular contributions and can be quite simply calculated as[277]

$$M_2 = 358.1\ N_0 \sum r^{-6}$$

$$= 3581\ N_0 N_1 a^{-6}\ , \qquad (139)$$

where N_0 is the number of spins per molecule and the lattice sum N_{1a}^{-6} has been calculated[278] for body-centered (bcc) and face-centered (fcc) cubic lattices as 23.045 a^{-6} and 115.631 a^{-6}, respectively.

Unfortunately the crystal structure of CF_3CCl_3 is not known. By analogy with similar compounds which form a plastic phase[279], the structure is almost certainly cubic, but it is not possible to distinguish between face-centered or body-centered. The shape of this molecule might be considered to be slightly distorted from that of carbon tetrachloride, which would imply fcc symmetry. On the other hand, the majority of the substituted ethanes which form a plastic phase, and for which the crystal structure is known, have a

bcc structure.

However, this ambiguity is not serious, as Resing[188] has shown that the reduced second moment is the same within 0.5% for bcc and fcc structures of the same density. We measure the density of CF_3CCl_3 at -10° C as 1.71 g/cm^3. This corresponds to a lattice constant of 9.0 Å (CCl_4 has a = 8.34 Å) or 7.14 Å ($Me_2ClC\text{-}CCl_3$ has a = 7.4 Å) for fcc and bcc lattices, respectively. The corresponding second moments are 0.234 G^2 and 0.235 G^2. We experimentally obtain a value of $0.25\left\{\begin{matrix}+ & .10\\ - & .05\end{matrix}\right\}$ G^2 just prior to the rapid drop in M_2 which signals the onset of rapid translational diffusion. The uncertainty in our experimental value is large for a number of reasons, so it is reassuring to find agreement as good as this. Since neither the density-derived M_2 nor the directly-measured M_2 are very precise we will choose a value which gives the best agreement for the τ_d values from the T_1 and T_2 measurements. This adjusted value, though, must certainly be in the neighborhood of 0.24 G^2.

B. Translational Diffusion in the Solid

In the solid, the relaxation function is linear on the $\ln(T_1^{-1})$ vs. 1/T(°K) plot only for the lowest temperatures, showing a distinct curvature to shorter relaxation times as the melting point is approached. In order to understand the origin of this curvature more clearly, T_2 measurements at 56.4 MHz and T_1 measurements at 56.4 and 15.87 MHz were performed. The results of all of these measurements in the solid (T_1,T_2 at 56.4 MHz, T_1 at 15.87 MHz) are shown in Figure 42. The frequency dependence of T_1 near the melting point, and the rapid increase in T_2, are both indicative of rapid translational

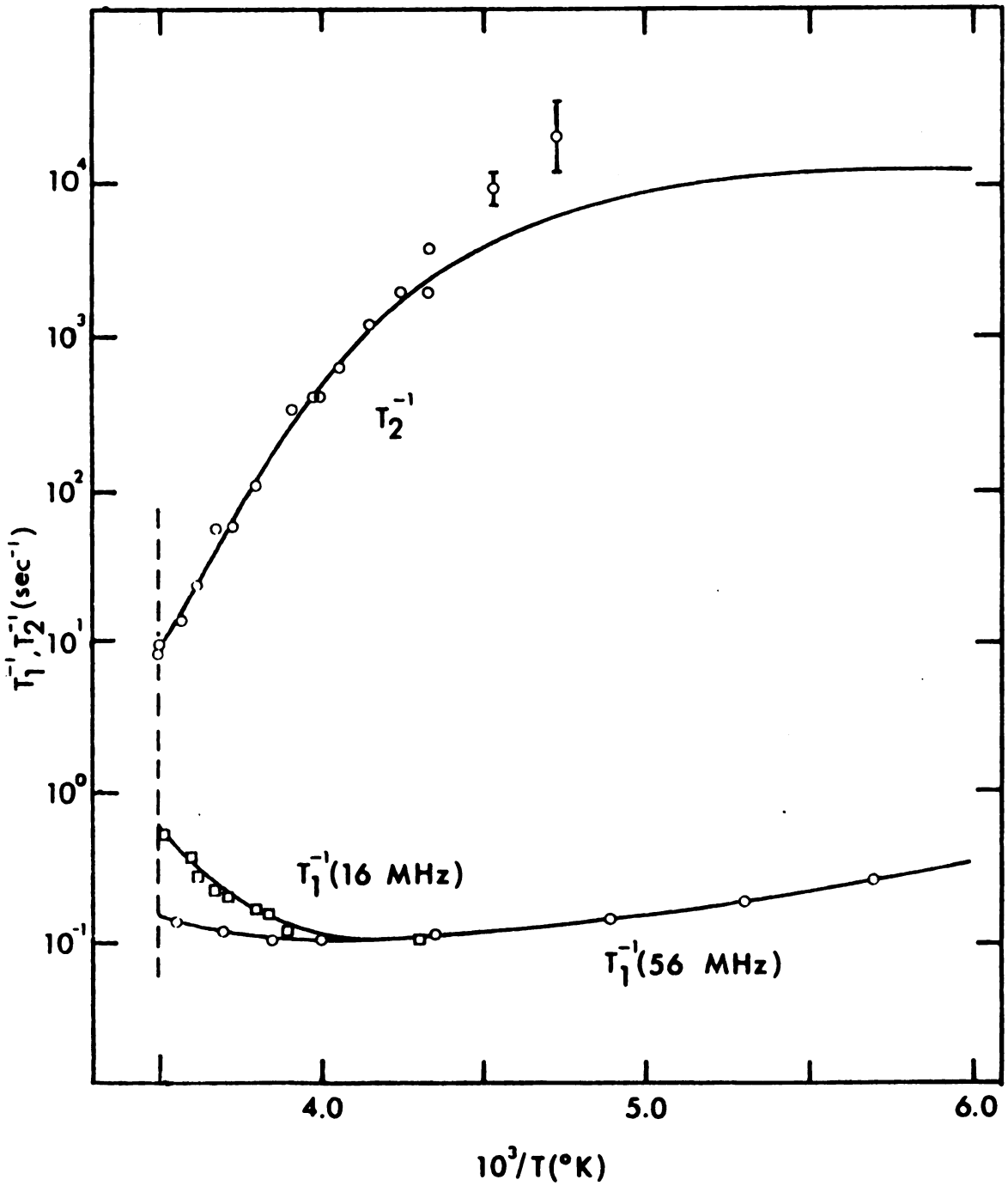

Figure 42. The temperature dependence of spin-spin relaxation and the temperature and frequency dependence of spin-lattice relaxation in solid CF_3CCl_3.

diffusion. The temperature dependence of T_2, and T_1 at 15.87 MHz near the melting point, are similar (ΔE are 13.7±0.5 and 12.8±0.5 kcal/mol, respectively), supporting this conclusion. Further evidence is given by linewidth measurements, both high-resolution (on a Varian A56/60) and pulse FT, which show a rapid narrowing of the width from ∿0.8 gauss at 208° K to a value not much greater than the width in the liquid phase at 283° K, two degrees below the melting point. We do not observe the "pre-melting" phenomena reported in other studies[190,194,202,280] on plastic solids. Even though the observed linewidths in the solid and liquid phases are very similar near the melting point this effect, if it occurred, could easily be detected as the solid-liquid chemical shift is 33.9 Hz and this resolution is easily achieved during pulse experiments (although the sample is not spun).

So there is no doubt that translational diffusion narrows the resonance line and shortens T_1 at 15.87 MHz, but does it account for all the curvature at 56.4 MHz? We decide this by separating the translational contribution from the total relaxation rate at the two frequencies:

$$R_{1,other} = R^{56}_{1,total} - R^{56}_{1,trans} \tag{140a}$$

and

$$R^{15}_{1,other} = R^{15}_{1,total} - R^{15}_{1,trans} \cdot \tag{140b}$$

In order to solve these equations from the experimental knowledge

of R_1 at 56 and 15 MHz we need two more relationships. From the discussion of rotational diffusion we have that $R^{56}_{1,other} = R^{15}_{1,other}$.

To get the second relationship we must choose a model for translational diffusion. Torrey[186,187] considered a diffusion mechanism in which the molecules execute a random walk from a lattice site to a neighboring one with an average jump frequency $1/\tau_d$. In terms of the spectral density functions G for which numerical results are available[188], the relaxation rates due to diffusion are

$$\frac{1}{T_1} = \frac{8\pi}{5}\gamma^4\hbar^2 I(I+1)\frac{n}{k^3\ell^3\omega}\, y[G(k,y) + 4G(k,2y)] \qquad (141a)$$

$$\frac{1}{T_2} = \frac{8\pi}{5}\gamma^4\hbar^2 I(I+1)\frac{n}{k^3\ell^3\omega}\, y[\tfrac{3}{2}G(k,0) + \tfrac{5}{2}G(k,y) + G(k,2y)], \qquad (141b)$$

or

$$\frac{1}{T_1} = \gamma^2 M_{2r}\,\tau_d[G(k,y) + 4G(k,2y)] \qquad (142a)$$

$$\frac{1}{T_2} = \gamma^2 M_{2r}\,\tau_d[\tfrac{3}{2}G(k,0) + \tfrac{5}{2}G(k,y) + G(k,2y)], \qquad (142b)$$

where n is the number of spins per unit volume, k and ℓ are constants depending on the crystal structure, $y = \frac{\omega\tau_d}{2}$, γ is the magnetogyric ratio, ω is the resonance frequency, and M_{2r} is the reduced second moment, measured between the phase transition and the onset of rapid translational diffusion. Use of the second moment in this manner has been justified by Resing[192].

In the temperature range between the phase transition and the T_1 minimum (which is not observed here, as the sample melts while

T_1 is decreasing) the expression for T_2 reduces to

$$\frac{1}{T_2} = \frac{3}{2}\gamma^2 M_{2r} G(k,0)\tau_d \ . \qquad (143)$$

We adjust M_{2r} to give agreement for τ_d calculated from T_2 and T_1^{15} data, and adjust $R_{1,other}$ such that Equations (140a) and (140b) are satisfied. For the initial value of M_{2r} we choose the average of our experimental values, 0.24 G^2. The justification for this procedure is that the temperature dependence of T_1^{15} and T_2 show the same process to be active in both; also the total adjustment results in an optimized value of M_{2r} = 0.22 G^2, which is certainly not a major change. Correlation times τ_d obtained from this procedure, along with τ_d calculated from linewidth measurements (Figure 43) by Equation (124), are shown in Figure 44. Table 30 gives the values of τ_d calculated from the T_1 and T_2 measurements, plus the calculated contribution of relaxation through translational diffusion to the total relaxation rate at 56 MHz. This adjustment leaves some curvature in the temperature dependence of T_1^{-1}, shown in Figure 41 as the dotted portion, but if all the experimental curvature as the melting point is approached is attributed to translational diffusion Equation (140) cannot be satisfied, τ_d values do not agree with the values from linewidth measurements, and the temperature dependence of τ_d is non-linear. We also note that the presence of this extra curvature, indicative of another relaxation mechanism acting in the solid, does not depend on the reliability of the second moment value. Determining τ_d from the frequency dependence of T_1 gives a result which is practically independent of the value of M_{2r}.

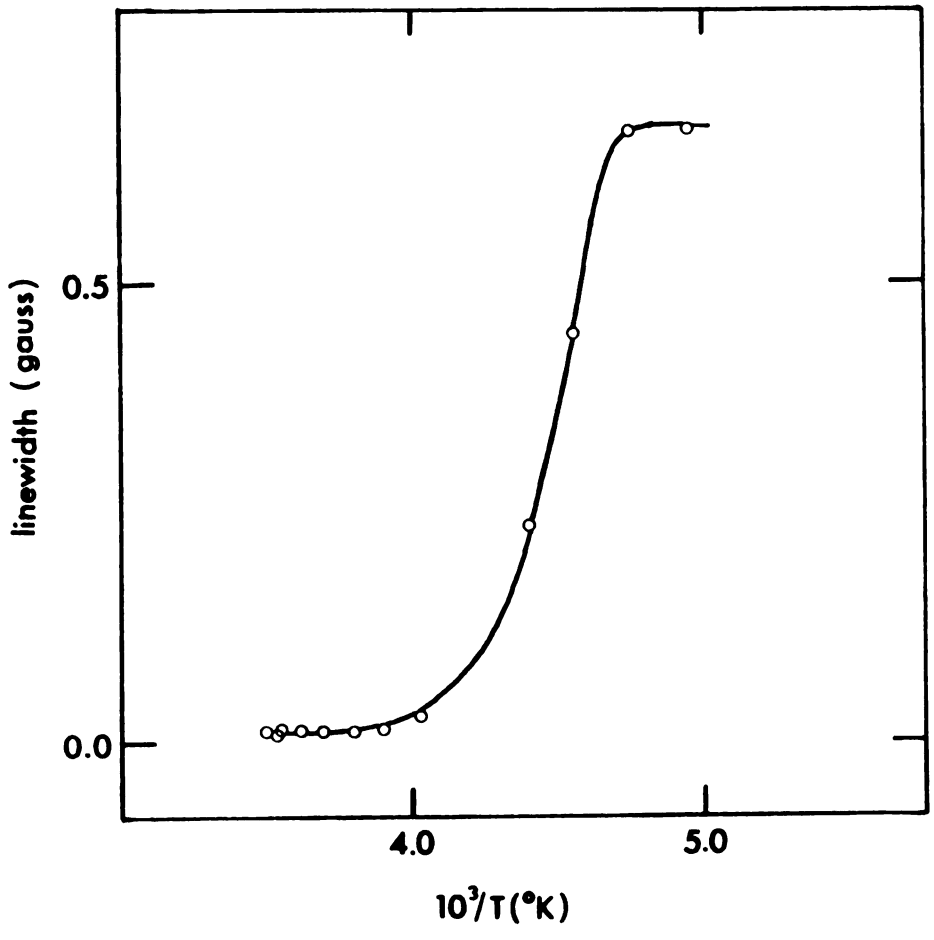

Figure 43. The temperature dependence of the width of the ^{19}F resonance line in solid CF_3CCl_3.

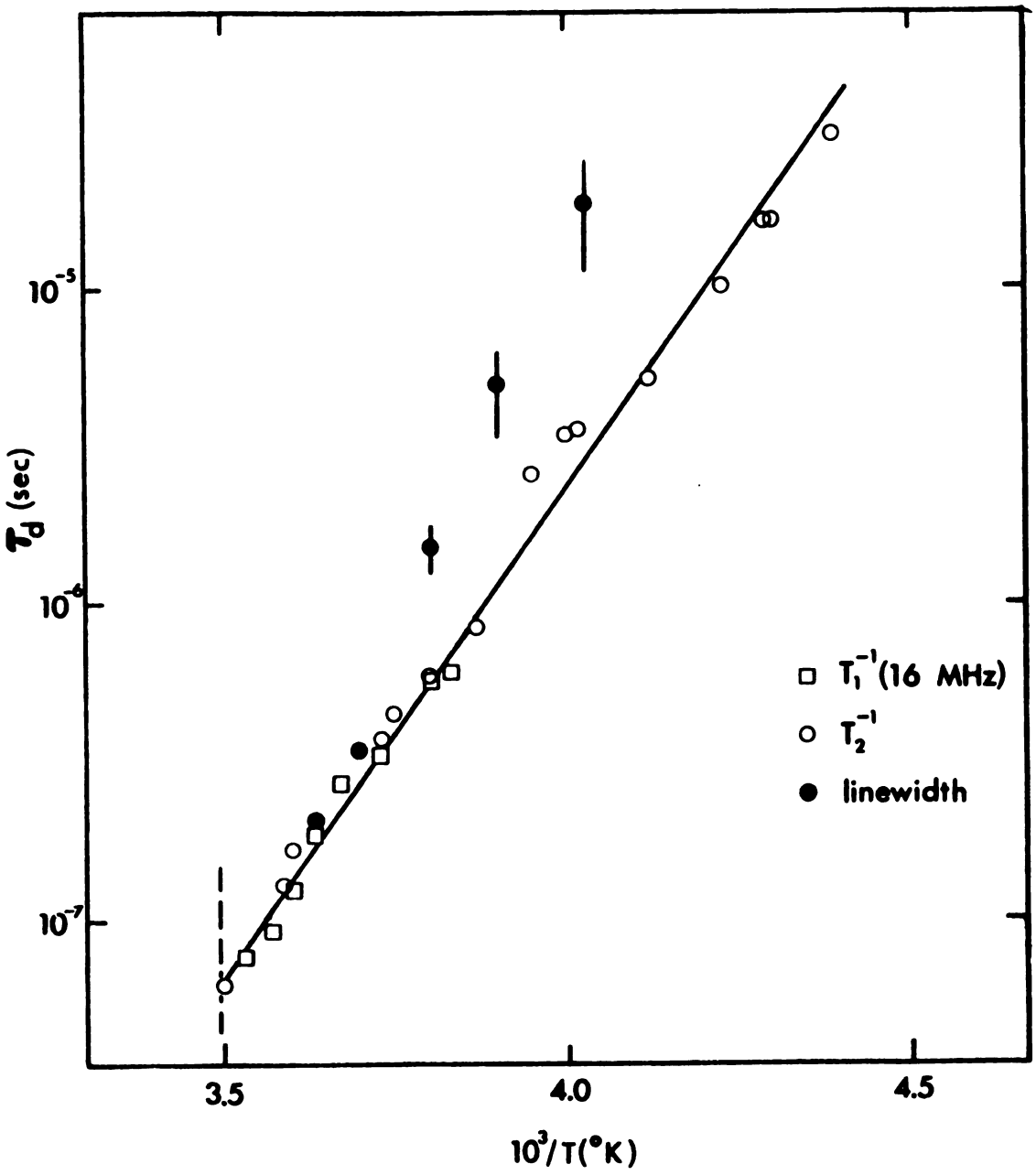

Figure 44. The temperature dependence of the mean jump time for translational diffusion in solid CF_3CCl_3.

Table 30. The contribution of translational diffusion to spin-lattice relaxation in solid CF_3CCl_3 and the derived values of the mean jump time, τ_d.

1/T	$R^{15}_{1,total}$ [a]	$R^{56}_{1,total}$ [b]	$R^{15}_{1,trans}$	$\tau_d \cdot 10^8$	$R^{56}_{1,trans}$ [c]
3.495	0.5587	0.143	0.445	6.50	0.0391
3.53	0.5135	0.138	0.403	7.54	0.0334
3.57	0.4368	0.132	0.338	9.16	0.0309
3.605	0.3667	0.125	0.257	12.1	0.0210
3.62	0.2783	0.124	0.174	18.2	0.0139
3.67	0.2245	0.118	0.118	27.0	0.0088
3.718	0.2017	0.114	0.098	33.1	0.0080
3.81	0.1629	0.107	0.059	55.0	0.0058
3.84	0.1570	0.106	0.055	58.0	0.0055

[a]Experimental points.

[b]Smoothed values.

[c]Calculated from τ_d.

We will demonstrate in the next section how this curvature is consistent with the presence of spin-rotational relaxation in the solid. We will show that the rotational relaxation rate, $R_{1,total} - R_{1,trans}$, varies smoothly across the melting transition, supporting the assumption that rotational motion in this molecule is unaffected by freezing.

C. Translational Diffusion in the Liquid

When the diffusion equation is solved without requiring the molecules to be at fixed lattice points, the spectral density functions thus obtained are appropriate for translational diffusion in a liquid, and the contribution to T_1 is[28]

$$R_{1,trans} = \frac{\pi N \hbar^2 \gamma^4}{5Da}, \qquad (144)$$

where the effect of the chlorine moment may be neglected since $\gamma_F^2/\gamma_{Cl}^2 \approx 100$. In this equation N is the number of spins per unit volume, D is the translational diffusion coefficient, and a is the molecular radius. The fact that the spins are not located at the centers of the molecules will cause a small change to this equation[181], which we ignore. In order to use Equation (144) we must determine the diffusion coefficient, which can be measured directly[221] or estimated from the macroscopic viscosity. We consider the latter method first.

The Stokes-Einstein relationship between the translational diffusion coefficient and the shear viscosity

$$D = \frac{kT}{6\pi a\eta} \tag{145}$$

is obtained from hydrodynamic theory. If we estimate the molecular radius a by considering a liquid to consist of close-packed spheres occupying 74% of the total volume this becomes

$$D = 2.20 \times 10^{-9} \frac{T}{\eta}\left(\frac{\rho}{MW}\right)^{1/3} . \tag{146}$$

Table 31 gives the reported values of ρ[282], η[283], N, and D calculated from Equation (146) for a temperature of 25° C. Table 31 in addition lists the values of D measured by the two-pulse spin-echo method[221]. The static field gradient in the spin-echo method was produced by changing the current to the x-shim coils and the system was calibrated by measuring the echo attenuation in a fluorocarbon sample for which D, T_1, and T_2 were reported accurately[131]. The gradient was determined to be 0.136 g/cm and the diffusion constants are believed to be accurate to ±10%. The results of this calibration are given in Table 22. Using the directly measured values of the diffusion coefficient and the known values of the density we calculate values of $R_{1,trans}$ listed in Tables 31 and 33. Figure 41 shows this correction made to the total relaxation rate. For comparison the contribution $R_{1,trans}$ calculated from the macroscopic viscosity is 0.00695 at 1/T = 0.00335. Clearly the agreement is very good. It is also gratifying to observe that after making the corrections for translational diffusion in the solid and liquid by completely independent experimental procedures, the relaxation rate $R^{56}_{1,other}$ (Equation 140a) shows no discontinuities, or changes in slope, through the melting

Table 31. The contribution of translational diffusion to spin-lattice relaxation in liquid CF_3CCl_3 calculated from the self-diffusion coefficient or the macroscopic viscosity.

$D(cm^2/sec)$	$\rho^b(g/cm^3)$	$N \cdot 10^{22}$	T(°C)	$10^3/T(°K)$	$R_{1,trans}(sec^{-1})$
0.902±.094	1.61	1.55	11.6	3.51	0.0147 ±.0015
1.72 ±.41	1.55	1.50	28.0	3.32	0.00747±.0018
2.97 ±.22	1.52	1.47	50.4	3.09	0.00424±.0031
1.85[a]		1.50	25.0	3.35	0.00695

[a]Obtained by use of Equation (146); η is from Reference 283.

[b]Reference 282.

Table 32. Physical properties of CF_3CCl_3

$I_{\parallel}$	$655 \cdot 10^{-40}$ g cm^2
$I_{\perp}$	$448 \cdot 10^{-40}$ g cm^2
σ_{av}	+298 ppm
$\Delta\sigma$	$\mp$76 ppm
C_{σ}	1.79 kHz
ρ_{25}	1.559 g cm^{-3}
η_{25}	0.720 centipoise
M_{2r}	0.22 G^2

Table 33. Smoothed relaxation rates in CF_3CCl_3

1/T	$R_{1,total}$	$R_{1,trans}$ [a]	$R_{1,dd}$ [b]	$R_{1,sr}$ [c]	τ_θ^* [d]	τ_J^* [e]
2.31	0.379	----	0.0142	0.365	1.15	0.558
2.50	0.274	----	0.0168	0.257	1.31	0.409
2.75	0.213	----	0.0207	0.192	1.53	0.321
3.00	0.174	0.004	0.0254	0.145	1.80	0.253
3.25	0.148	0.011	0.0312	0.106	2.13	0.192
3.50	0.129	0.015	0.0387	0.075	2.54	0.141
3.75	0.112	0.010	0.0476	0.054	3.02	0.105
4.00	0.103	0.004	0.0586	0.040	3.60	0.081
4.25	0.110	----	0.0722	0.038	4.30	0.079
4.50	0.122	----	0.0889	0.0331	5.15	0.071
4.75	0.138	----	0.110	0.028	6.20	0.061
5.00	0.162	----	0.135	0.027	7.42	0.061
5.25	0.190	----	0.166	0.024	8.90	0.055
5.50	0.224	----	0.203	0.021		
5.75	0.269	----	0.251	0.018		
6.00	0.323	----	0.310	0.013		
6.25	0.391	----	0.382	0.009		
6.50	0.478	----	0.469	----		
6.75	0.585	----	0.583	----		

[a] From self-diffusion measurements in the liquid and $R_1^{15\ MHz}$, R_2 measurements in the solid.

[b] Extrapolated from low temperature linear region and room temperature Raman $\tau_{\theta_\perp}$.

[c] $R_{1,sr} = R_{1,total} - R_{1,trans} - R_{1,dd}$.

[d] $\tau_\theta^* = 7.519 \cdot 10^{-11}\ R_{1,dd}(kT/I)^{1/2}$.

[e] $\tau_J^* = 6.162 \cdot 10^{-10}\ R_{1,sr}/T \cdot (kT/I)^{1/2}$.

point. This behavior of $R^{56}_{1,other}$ is entirely to be expected as long as molecular rotation is unaffected through the melting point.

D. Rotational Motion

The relaxation data shown in Figure 41 make it obvious that completely different mechanisms dominate the relaxation rate at the two temperature extremes. We identify these mechanisms as follows. An R_1 which increases with increasing temperature is indicative of relaxation through the spin-rotational ($R_{1,sr}$) or scalar coupling ($R_{1,sc}$) interactions. From the difference R_2-R_1, and the rotational correlation time determined by Raman lineshape analysis, it will be shown that J_{FCl} = 1.7 Hz and that $R_{1,sc}$ is completely negligible. Therefore, the mechanism dominant at high temperatures is spin-rotation. At the other temperature extreme R_1 increases with decreasing temperature. At low temperatures in the solid translational diffusion is not an important contribution, while at other temperatures it is of minor importance at 56 MHz as discussed previously; the dashed line in Figure 41 gives R_1 corrected for this effect. Other mechanisms which give the right temperature dependence at low temperatures are the intramolecular dipole-dipole interaction ($R_{1,dd}$) and relaxation through anisotropic chemical shift coupled with molecular rotation ($R_{1,csa}$). We now proceed to calculate the interaction constants for these mechanisms.

Relaxation through Intramolecular Dipole-Dipole Interaction - For isotropic rotational diffusion the intramolecular contribution to the fluorine relaxation is given by[28]

$$R_{1,dd} = \hbar^2\gamma_F^2[\tfrac{3}{2}\gamma_F^2 \sum_{F'} r_{FF'}^{-6} + \gamma_{Cl}^2 \sum_{Cl} r_{FCl}^{-6}]\tau_\theta \ . \qquad (147)$$

The second term is completely negligible and, using the intermolecular distances of Ward and Ward[284],

$$R_{1,dd} = 1.33 \times 10^{10}\tau_\theta \ . \qquad (148)$$

It will be shown in a later section that the reorientation is isotropic within experimental error and is diffusional over all but the highest temperatures studied, therefore Equation (148) is appropriate to describe $R_{1,dd}$.

<u>Relaxation through Chemical Shift Anisotropy</u> - Again employing the assumption of isotropic rotational diffusion, the contribution to R_1 of the anisotropic shielding-molecular rotation interaction is[28]

$$R_{1,csa} = \frac{2}{15}\Delta\sigma^2\omega^2\tau_\theta \qquad (149)$$

for axially symmetric molecules. The chemical shift anisotropy $\Delta\sigma = \sigma_{||} - \sigma_{\perp}$ refers to the molecular symmetry axis and has been measured[285] as ±76 ± 3 ppm for CF_3CCl_3. Accordingly, the relaxation rate is calculated as

$$R_{1,csa}^{56} = 2.92 \times 10^8\tau_\theta \ , \qquad (150a)$$

$$R_{1,csa}^{15} = 2.31 \times 10^7\tau_\theta \ . \qquad (150b)$$

Comparing these rates with the dipole-dipole rate it can be seen that $R_{1,csa}$ is completely negligible at 15 MHz and is just on the edge of detectability (2% of $R_{1,dd}$) at 56 MHz.

Relaxation through Spin-Rotation Interaction Hubbard[49] obtained an expression for the contribution to R_1 from the spin-rotation interaction for the case of nuclei occupying identical positions in a spherical top molecule undergoing isotropic rotational diffusion (Equation (105)). Wang[286] calculated the relaxation rate for the more general case of anisotropic reorientation with a non-diagonal spin-rotation tensor and obtained

$$R_{1,sr} = \frac{2kT}{3\hbar^2} \{I_{||}(C_{||} + \beta\sin^2\theta)^2 \frac{\tau_{||}}{1+2D_\perp\tau_{||}} + I_\perp\beta^2(\sin^2\theta\cos^2\theta)$$

$$\times [\frac{\tau_\perp}{1+2D_\perp\tau_\perp} + \frac{\tau_{||}}{1+(D_\perp+D_{||})\tau_{||}}]$$

$$+ I_\perp[(C_\perp-\beta\sin^2\theta)^2 + C_\perp^2] \frac{\tau_\perp}{1+(D_\perp+D_{||})\tau_\perp}\} , \qquad (151)$$

where the τ's refer to τ_J and the D's to $1/6\tau_\theta$, and $\beta = C_\perp - C_{||}$ with $C_{||}$ and $C_\perp$ the principal components of the spin-rotation tensor along and perpendicular to the bond axis.

For the case of CF_3CCl_3 ($D_\perp\tau_\perp, D_\perp\tau_{||}, D_{||}\tau_{||} \ll 1$) Equation (151) reduces to

$$R_{1,sr} = \frac{2kT}{3\hbar^2} \{[I_{||}(C_{||}+ \sin^2\theta)^2 + I_\perp(\beta^2\sin^2\theta\cos^2\theta)]\tau_{||}$$

$$+ I_\perp[(C_\perp-\beta\sin^2\theta)^2 + C_\perp^2 + \beta^2\sin^2\theta\cos^2\theta]\tau_\perp\} . \qquad (152)$$

Since $C_{\perp}$ and $C_{||}$ are not known, and calculating them from $\Delta\sigma$ requires neglecting off-diagonal elements, Equation (105) will be used initially and the attempt to calculate the components of the spin-rotation tensor will be discussed later. Thus,

$$R_{1,sr} = 1.62 \times 10^{9}\ T\tau_{sr}\ , \qquad (153)$$

or, since this equation will actually be used to calculate τ_{sr}, after determining

$$R_{1,sr} = R_{1,total} - R_{1,dd} - R_{1,trans} - R_{1,csa}\ , \qquad (154)$$

we have

$$\tau_{sr} = 6.16 \times 10^{-10}\ \frac{R_{1,sr}}{T}. \qquad (155)$$

In Figure 46 are plotted the reduced correlation times τ_{θ}^{*} and τ_{J}^{*} ($\tau^{*} = \tau(kT/I)^{1/2}$) obtained from Equations (148) and (155) for comparison with the predictions of Gordon's extended diffusion model as applied to spherical top molecules[95]. It can be seen that the data obtained through an isotropic diffusion model and an "effective" spin-rotation interaction constant ($2C_{\perp}^{2}+C_{||}$) conform to the general features of the model and lie between the M- and J-diffusion limits. The fact that the data lie closer to the M-diffusion limit, which is physically unrealistic for liquids in that it does not allow the magnitude of the angular momentum vector to change with collisions, indicates that the simplifying assumptions which went into the

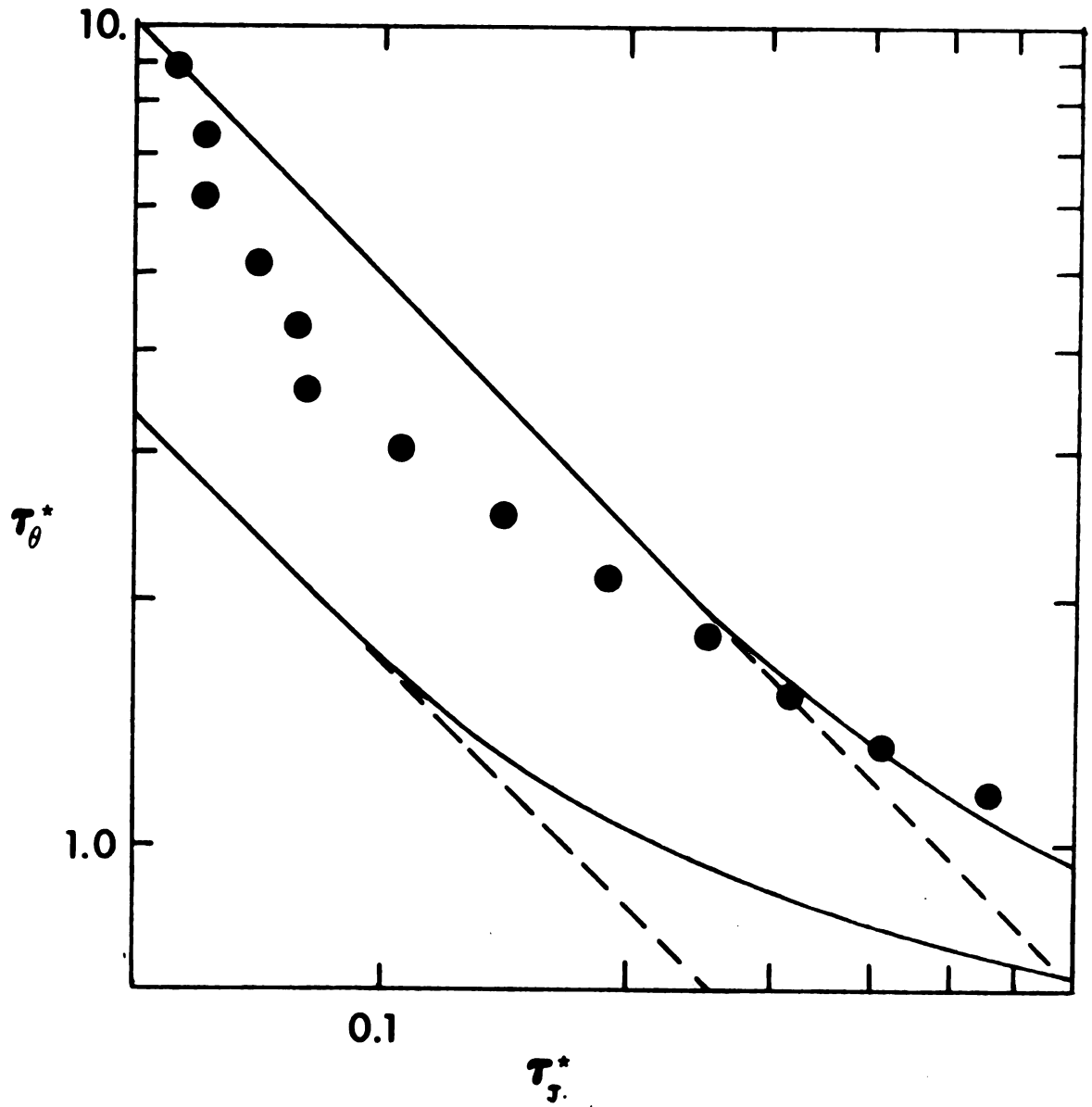

Figure 45. A comparison of the experimental relations between τ_θ^* and τ_J^* with the predictions of the extended diffusion model.

derivation of Equations (148) and (155) are not permissible for CF_3CCl_3. The reason for this is that in CF_3CCl_3, contrary to other molecules which have been studied in terms of the extended diffusion model (CCl_4[126], ClO_3F[130], CS_2[112], and CCl_3F[131]) and have been found to follow J-diffusion, the spin-rotation tensor is not diagonal in the molecular symmetry axis and, consequently, off-diagonal elements must be included in the calculation of $R_{1,sr}$. However before making this calculation we will show that, while in the case of CF_3CCl_3 it may be assumed that the reorientational motion is isotropic from the spherical shape of the molecule, this fact can also be demonstrated experimentally.

E. Demonstration of Isotropic Motion from Raman Data

If it is assumed that the temperature dependence of τ_θ is given by an Arrhenius-type equation throughout the temperature range studied, then τ_θ in the liquid may be extrapolated from the values obtained in the solid. This correlation time is an "effective" correlation time τ_θ' which, for a symmetric-top molecule, depends on $\tau_{\theta\perp}$ and $\tau_{\theta\parallel}$ as previously discussed. In order to separate the parallel and perpendicular motion the reorientational broadening of a Raman line of A_1 symmetry, which is sensitive only to $\tau_{\theta\perp}$, is measured. Although CF_3CCl_3 has five A_1 lines only one, at 714 cm^{-1}, is of sufficient intensity and also devoid of fine structure. The parameters appropriate to the Raman experiment are given in Table 24, and Figure 40 shows the polarized and depolarized bandshape with the calculated convolution of the polarized band with a Lorentzian orientational

component of half-width ω_{or} = 2.08 cm^{-1}. Employing the relation $\tau_{\theta_\perp} = (2\pi c\omega_{or})^{-1}$, a value $\tau_{\theta_\perp}$ = 2.54±0.81 psec is obtained at 27° C. From Table 33 we have that τ'_θ = 2.20 psec at 27° C., and conclude from this that $\tau_{\theta_\perp} = \tau_{\theta_{||}} = \tau'_\theta$, at least at 27° C. For comparison, the relaxation time calculated using the Debye relation $\tau_c = 4\pi\eta a^3/3kT$ is 25.5 psec at 27° C., and the Hill model[61] gives τ_c = 5.10 psec.

III. Relaxation of ^{19}F in CF_3Br and CF_2Br_2

Spin-lattice relaxation times were measured for CF_3Br and CF_2Br_2 from the melting point to the critical point (these were 99° and 340° K for CF_3Br (Figure 46) and 131° and 471° K for CF_2Br_2 (Figure 47), respectively). Both of these curves show the same general features, a minimum in the rate at intermediate temperatures, indicative of dipole-dipole dominated relaxation at low temperatures and spin-rotation dominated relaxation as the critical point is approached. The most obvious difference in relaxation for these two molecules is the much more pronounced curvature in R_1 of CF_3Br at high temperatures. This may be presumed to arise from the increasingly important free rotation about the symmetry axis (spinning) which cannot occur in the asymmetric top CF_2Br_2. In the case of fluorochlorocarbons additional information could be obtained from measurement of R_2, the spin-spin rel xation rate, due to scalar coupling with the chlorine; however, the much larger bromine quadrupole coupling constants in CF_3Br and CF_2Br_2 (∿500 MHz[240] versus ∿70 MHz[240]), along with a reasonable guess as to the scalar coupling constant (J_{FBr} ≃ 20-40 Hz vs.

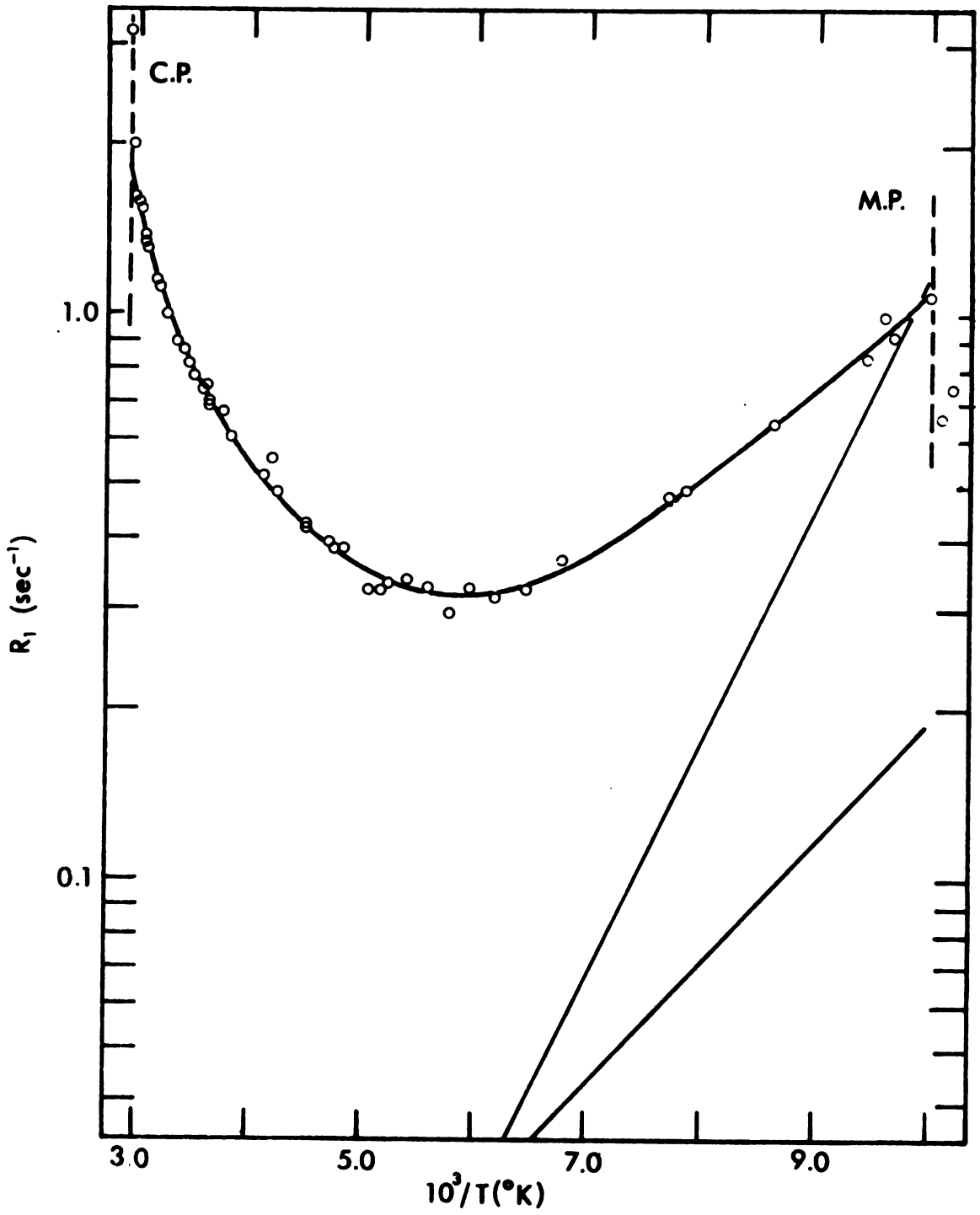

Figure 46. The temperature dependence of spin-lattice relaxation in CF_3Br, and the calculated contribution from translational diffusion.

Figure 47. The temperature dependence of spin-lattice and spin-spin relaxation in CF_2Br_2, showing a separation into different contributions based on the calculated contribution from translational diffusion and equal but opposite temperature dependence of $R_{1,dd}$ and $R_{1,sr}$. The dipole-dipole relaxation rate predicted from dielectric relaxation data is given by (●).

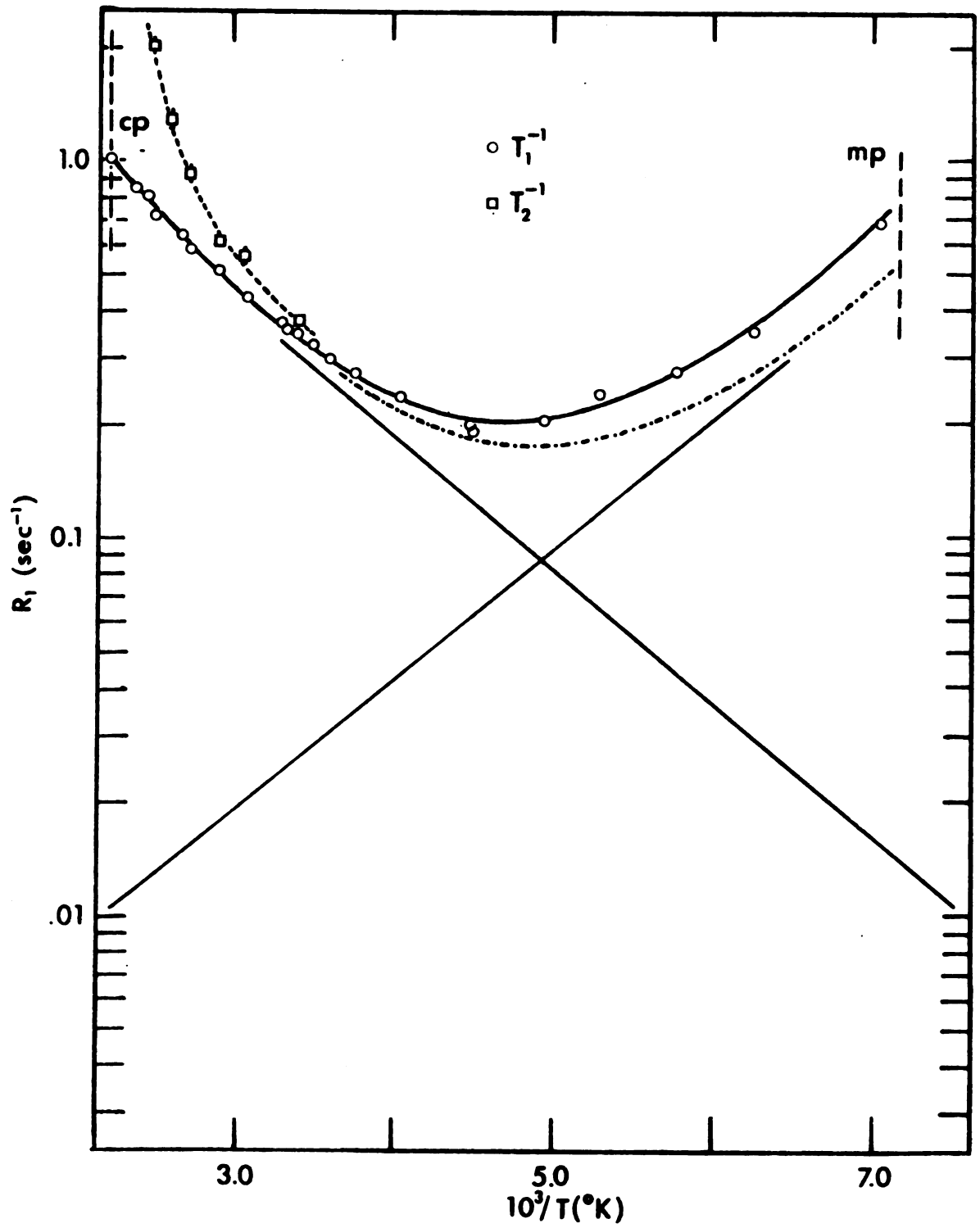

Figure 47

$J_{FCl} \approx 10\text{-}15$ Hz[131,287]), result in a scalar coupling contribution which is very minor ($R_{1,sc} \approx 0.025$ sec^{-1}) in the fluorobromocarbons. This has been verified by measuring T_2 in CF_2Br_2 (Figure 47), from which the value $R_{1,sc} = 0.028$ is obtained at 286° K. The much greater curvature evident in the temperature dependence of T_2 as opposed to T_1 will be discussed later.

Using the same arguments as applied to CF_3CCl_3 (but noting here that the total rate is ∿3 times larger), we conclude that the possibly important relaxation mechanisms are spin-rotation and the intermolecular and intramolecular dipole-dipole interactions. The main problem in these instances is separating the contributions from the two dipole-dipole interactions.

To estimate the diffusion coefficient and the intermolecular contribution to the total rate in these two molecules we use Equation (144)

$$R_{1,trans} = \frac{\pi N \hbar^2 \gamma^4}{5Da}$$

and (146)

$$D = 2.20 \times 10^{-9} \frac{T}{\eta}\left(\frac{\rho}{MW}\right)^{1/3}.$$

The densities and viscosities of these two fluids have been measured from -80° C to +40° (CF_3Br)[288] and -70° - +20° (CF_2Br_2)[289,290]. These experimental data, plus the results of calculations using Equations (144) and (146), are shown in Tables 34 and 35 for CF_3Br and

Table 34. Calculation of intermolecular contribution to T_1 in CF_3Br

$10^3/T(°K)$	T°C	ρ g cm^{-3}	η cp	$Dx10^{+5}$	$T_{1,inter}^{-1}$ sec^{-1}
518	-80	2.05	0.58	1.75	0.00306
469	-60	1.98	0.400	2.78	0.00864
429	-40	1.90	0.295	4.06	0.00568
395	-20	1.82	0.235	5.46	0.00404
366	0	1.71	0.200	6.77	0.00306
341	20	1.58	0.165	8.58	
319	40	1.41	0.150*	9.71	

Table 35. Calculation of intermolecular contribution to T_1 in CF_2Br_2

$10^3/T(°K)$	T°C	ρ^a g cm^{-3}	η^b CP	$D \times 10^{5c}$ $cm^2 sec^{-1}$	$T_{1,inter}^{-1}{}^d$ sec^{-1}
4.92	-70	2.584	1.594	0.635	0.02113
4.69	-60	2.551	1.346	0.7858	0.01679
4.48	-50	2.517	1.152	0.9570	0.01354
4.29	-40	2.484	1.003	1.143	0.01113
4.11	-30	2.450	0.08796	1.354	0.009233
3.95	-20	2.415	0.7788	1.584	0.007743
3.80	-10	2.380	0.6969	1.831	0.006567
3.66	0	2.344			
3.53	10	2.307	0.5664	2.399	0.004808
3.41	20	2.268	0.5130	2.727	0.004135

[a] Reference 290.

$$\rho = 2.3440 - 3.67 \cdot 10^{-3} t - 5.75 \cdot 10^{-6} t^2 - 3.3 \cdot 10^{-8} t^3$$

[b] Reference 289.

[c] $D = 2.20 \cdot 10^{-9} \frac{T}{\eta} \left(\frac{\rho}{MW}\right)^{1/3}$ MW = 221.82

[d] $T_1^{-1} = 11550 \cdot \left(\frac{n}{MW}\right)\left(\frac{\rho\eta}{T}\right)$ n = spins/molecule

CF_2Br_2, respectively, and have been subtracted from the total relaxation rate in Figure 47.

In the case of CF_2Br_2 the intermolecular dipole-dipole mechanism can be seen in Figure 47 to be a minor contribution to the total rate. The total rate may be then separated into the spin-rotational and intramolecular dipole-dipole contribution, with equal and opposite temperature dependence except for a slight curvature in the spin-rotational contribution at high temperatures. This separation is also shown in Figure 46 and the separate contributions to the total rate are given in Table 35. Miller and Smyth[63] have measured the dielectric relaxation times at 0° and 20° C as 2.60 and 2.28 psec, respectively; if we assume that the reorientation is isotropic and diffusional, and remembering that $\tau_{NMR} = \tau_{diel}/3$, then $R_{1,dd}$ = .0058 at 0° C and $R_{1,dd}$ = .0051 at 20°. The intramolecular dipole-dipole contribution calculated from dielectric relaxation is shown in Figure 46. The two points are not really sufficient to determine the temperature dependence but the dielectric-derived τ_θ values are clearly too small by a factor of ∿5 to account for the NMR relaxation. At 20° C the motion is probably not fully diffusional, so the ratio of three between $\tau_{\theta_\perp}$ and $\tau_{\theta,2}$ should be replaced by a factor of ∿2.4 which is appropriate for a spherical molecule undergoing isotropic orientation of finite-step size. This is obviously not the whole answer. In order to discuss anisotropy effects, we first consider Figure 48 and the different vectors studied by NMR and dielectric relaxation. If the coordinate system is chosen as in Figure 48, the NMR experiments are insensitive to motion about the y axis while dielectric measurements are insensitive to motion about

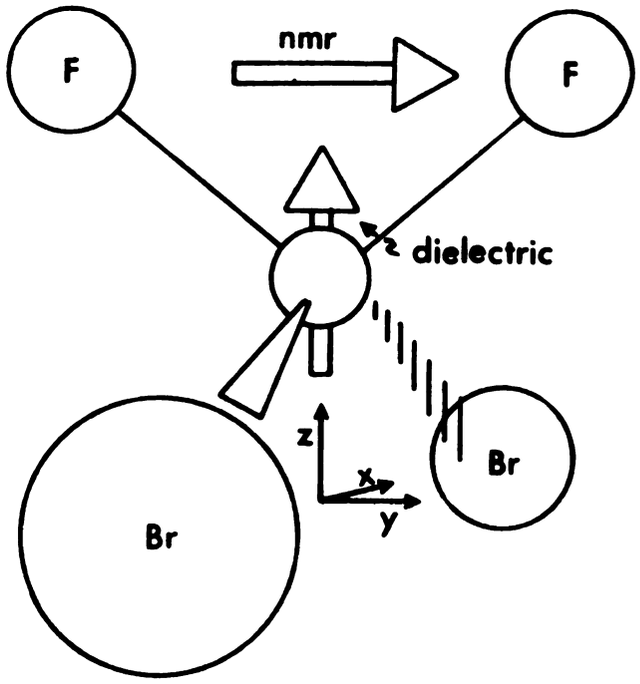

Figure 48. Choice of axes for the CF_2Br_2 molecule.

the z axis. However, $I_{zz} \approx I_{yy} >> I_{xx}$ and, since most discussions of anisotropic reorientation relate $\tau_{\theta_{ii}}$ to I_{ii}^{-1}, it seems that even if the motion in CF_2Br_2 is found to be highly anisotropic, the correlation times for motion about the y and z axis should be very similar. Since the CF_2Br_2 samples were not degassed with the care accorded the CF_3Br samples, there exists the unfortunate possibility that the CF_2Br_2 samples still contained a small amount of dissolved oxygen.

In the case of CF_3Br, the values of $R_{1,trans}$ were calculated by use of Equations (144) and (146) which employ the reported density and viscosity data[204]. The results do not agree with the measured relaxation times, as can be seen from Figure 46. The calculated values of $R_{1,trans}$ become equal to the total rate at the melting point, which is of course not possible. In fact, by analogy with CF_2Br_2, $R_{1,dd}$ should be an appreciable fraction of the total rate at low temperatures. In an attempt to resolve this problem, the self-diffusion coefficient was experimentally determined in the low-temperature region (Table 23). The experimental results are plotted along with the ("theoretical") viscosity-derived diffusion coefficient in Figure 49. The scatter in the points is embarrassingly large; however, the experimental data clearly do not fit the "theoretical" curve. Since the field gradient used to measure D was not directly determined at the lowest temperatures, there exists the possibility that the gradient is temperature dependent. Since the echo attenuation depends on DG^2, an increase in G by a factor of three will account for the discrepancy. Clearly, further work is needed to understand the low-temperature relaxation behavior in CF_3Br, but it seems likely from the other fluorocarbons studied that the true

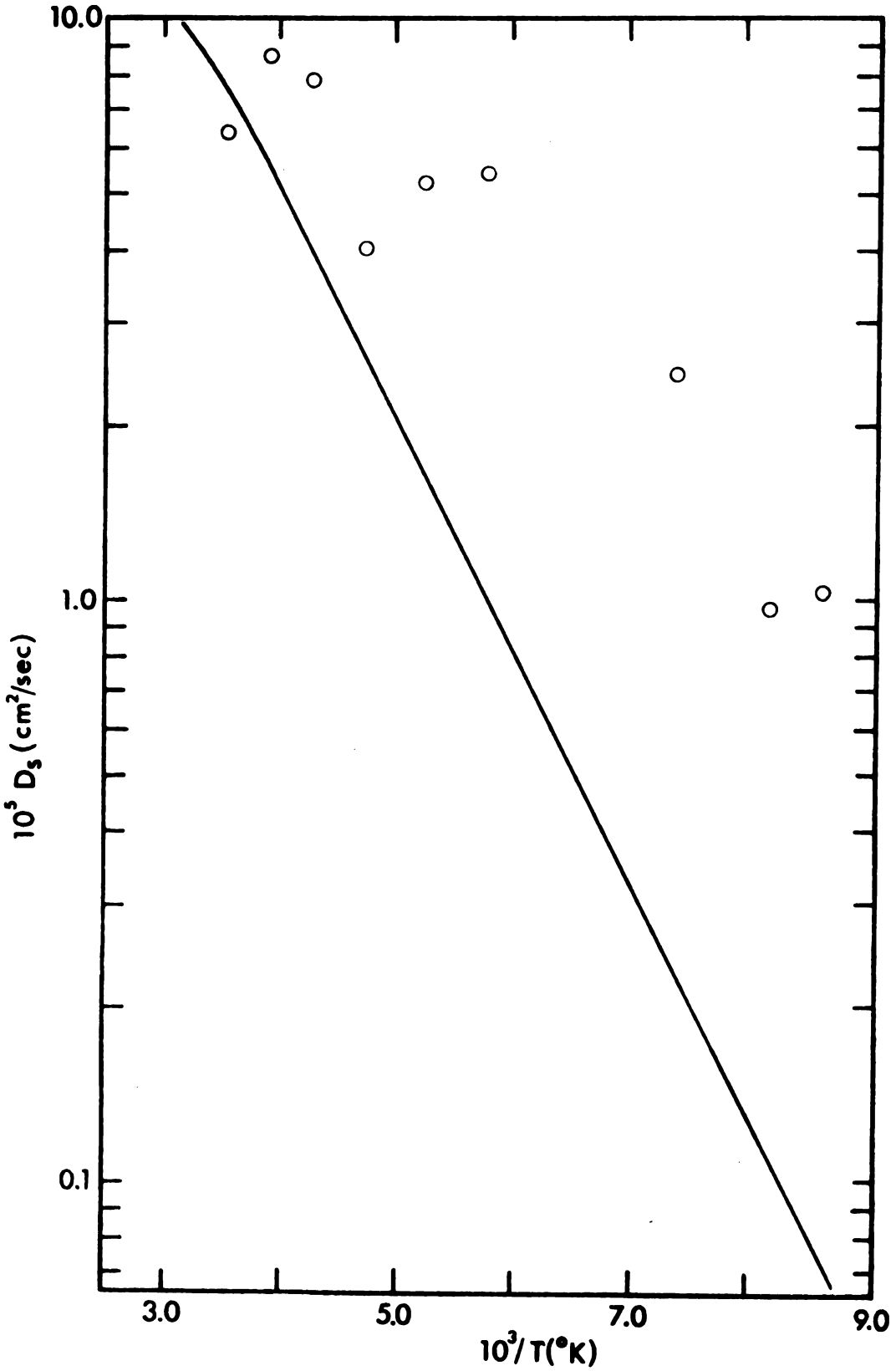

Figure 49. The temperature dependence of the self-diffusion coefficient (D_S) measured by the two-pulse, steady gradient, spin-echo method, compared with the temperature dependence of D_S as derived from the macroscopic viscosity and density, for CF_3Br.

size of the intermolecular contribution to R_1 lies between the two possibilities discussed here.

IV. Other Systems

A number of other fluorocarbons were investigated with varying degrees of thoroughness. In general, the reason for not analyzing these systems to the extent which CF_3CCl_3 has been examined is the much lower symmetry of these other molecules, making both the Raman and NMR analysis much more complex. Figure 50 shows T_1 in the liquid and solid and T_2 in the liquid as functions of temperature for CF_2ClCCl_3; Figure 51 shows the same parameters for $CFCl_2CFCl_2$, and Figure 52 shows T_1 in liquid and solid $CFCl_2CFCl_2$. Only in the case of perfluoroethane were the measurements done at temperatures up to the critical point. Figure 53 shows the temperature dependence of T_1 in liquid CF_3I, and Figure 54 shows T_2 in the solid for CF_2ClCCl_3. It is immediately obvious that the behavior of these systems is very similar to that of CF_3CCl_3 in all respects. T_1 and T_2 are dominated by spin-rotation and there is little change in R_1 across the melting point, indicating that the contribution of $R_{1,trans}$ is minor both in the liquid and solid phase. The curvature of T_1 with temperature in the solid probably indicates a spin-rotational contribution, although the effect of $T_{1,trans}$ must be determined, as was done in CF_3CCl_3, to verify this. Furthermore, all three systems form plastic phases and show a rapid drop of R_2 as the melting point is approached in the solid from translational diffusion. From the difference $R_2 - R_1$ in the liquid, information about J_{FCl} and the rotational correlation

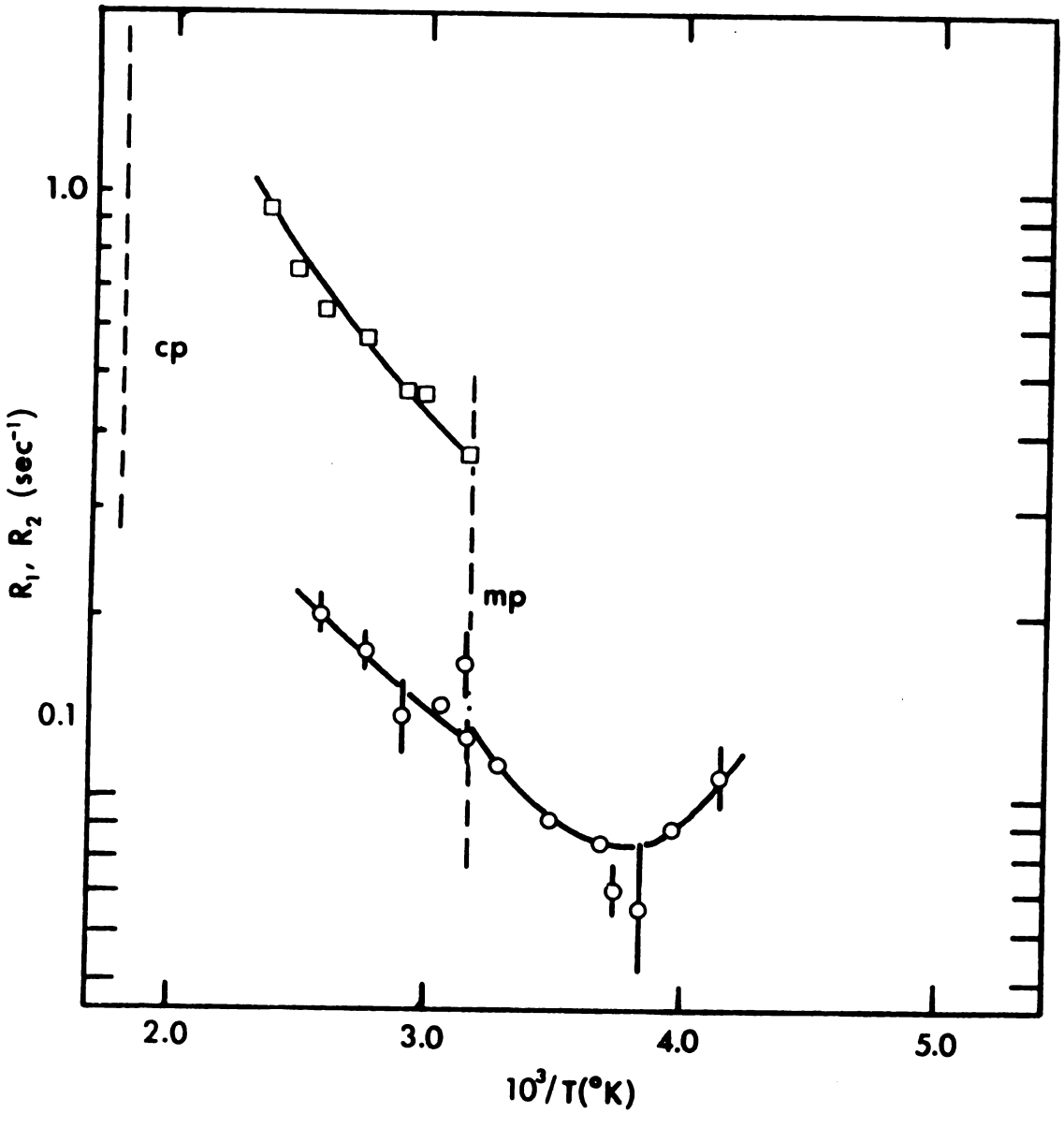

Figure 50. The temperature dependence of the spin-lattice relaxation rate of ^{19}F in liquid and solid CF_2ClCCl_3 and the spin-spin relaxation rate in the liquid.

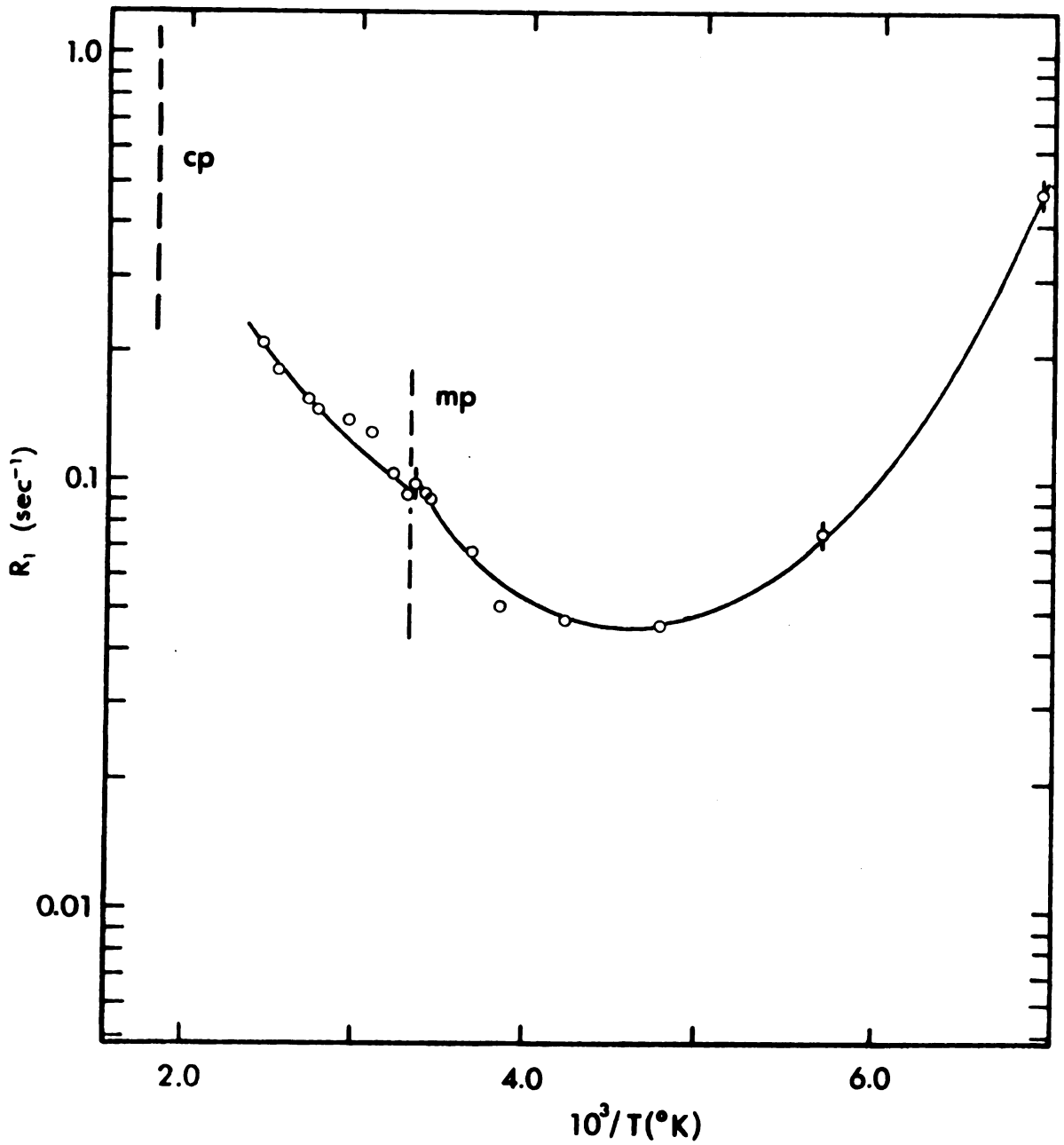

Figure 51. The temperature dependence of the spin-lattice relaxation rate of ^{19}F in solid and liquid $CFCl_2CFCl_2$.

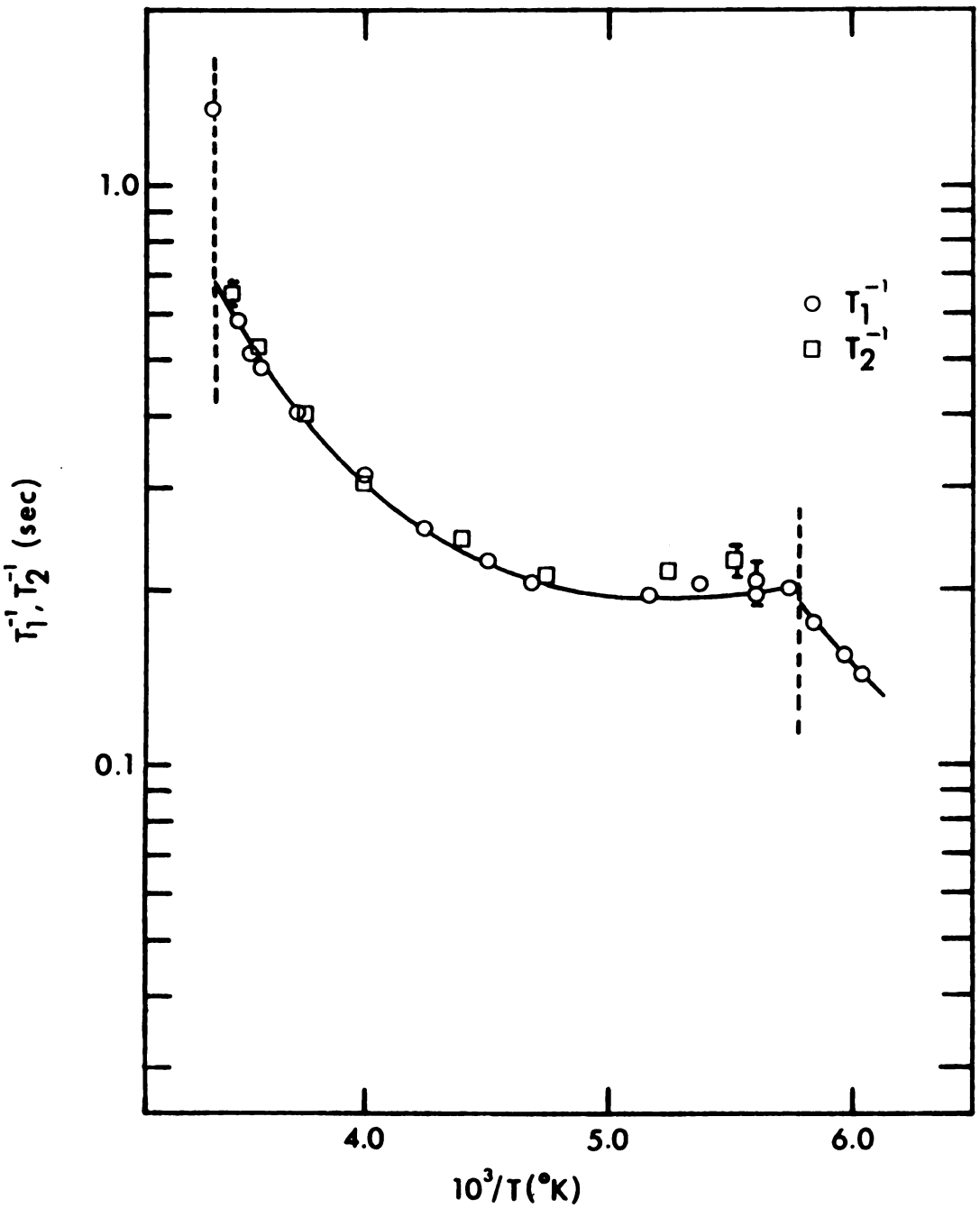

Figure 52. The temperature dependence of the spin-lattice and spin-spin relaxation rate of ^{19}F in CF_3CF_3.

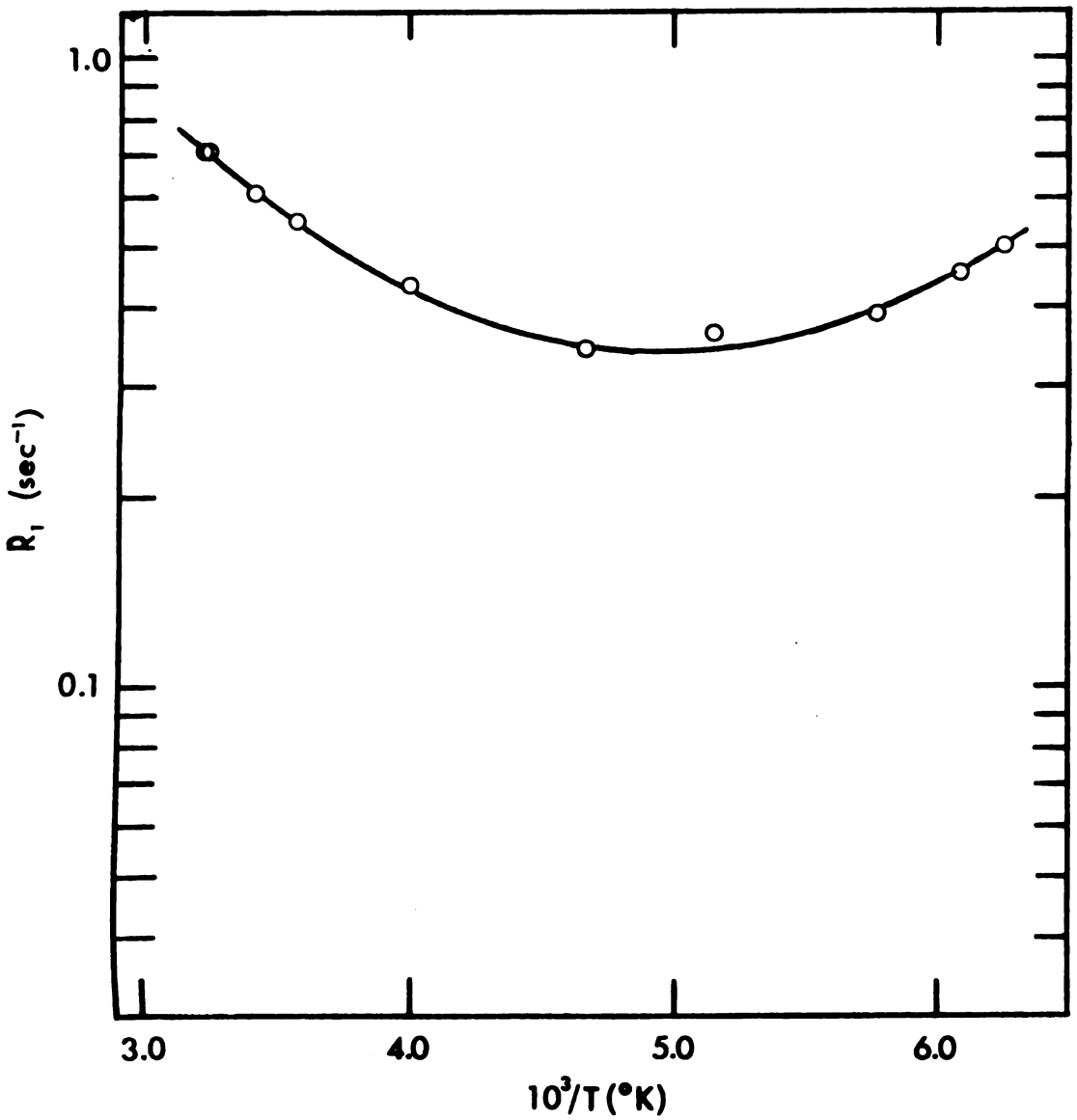

Figure 53. The temperature dependence of the spin-lattice relaxation rate of ^{19}F in liquid CF_3I.

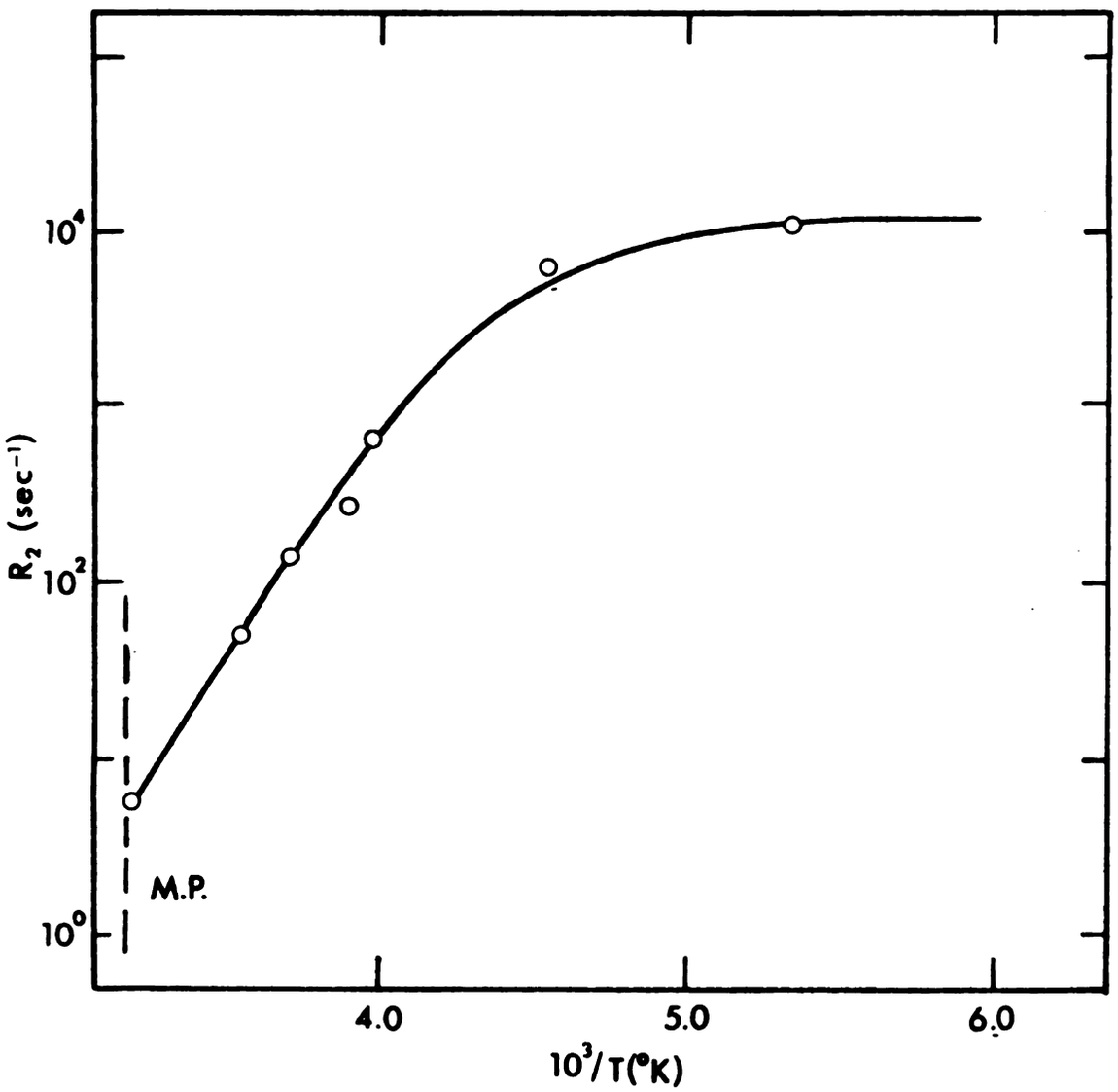

Figure 54. The temperature dependence of the spin-spin relaxation rate of ^{19}F in solid CF_2ClCCl_3.

time should be obtained; this will be discussed later. However, note that experimentally $T_1 = T_2$ in the liquid phase of CF_3CF_3, indicating that the T_2 experiments, which are much more susceptible to error, are measuring the true T_2 in these systems.

V. Spin-Spin Relaxation

A. Anomalous T_2 Behavior

For all but one case in which the temperature dependence of T_2 in the liquid was measured the results were anomalous in that the linear dependence on τ_θ, expected from Equation (98) for $R_2 - R_1$, was not observed. The spin-spin relaxation rate invariably increased faster than theory predicts as the critical point is approached. This curvature can be seen in Figure 55 (which plots $\ln(R_2 - R_1)$ versus T_c/T, where T_c is the critical temperature) to vary from a very slight effect for CF_2ClCCl_3 to a very large effect for most other systems. Although the uncertainty for many of the values is large due to the near equality of T_1 and T_2, the curvature is greater than this uncertainty would allow. In order to learn more about possible experimental errors in determining T_2, measurements were made on CF_3CF_3, for which $T_1 = T_2$ due to the absence of the scalar coupling interaction. Results of these measurements are shown in Figure 52, and it can be seen that, indeed, $T_1 = T_2$ in CF_3CF_3. Although longer T_2's are measured with perhaps a slight bias toward too short a value, all T_2's obtained are essentialliy in agreement with observed T_1's. This small systematic error for long T_2's is very probably the cause

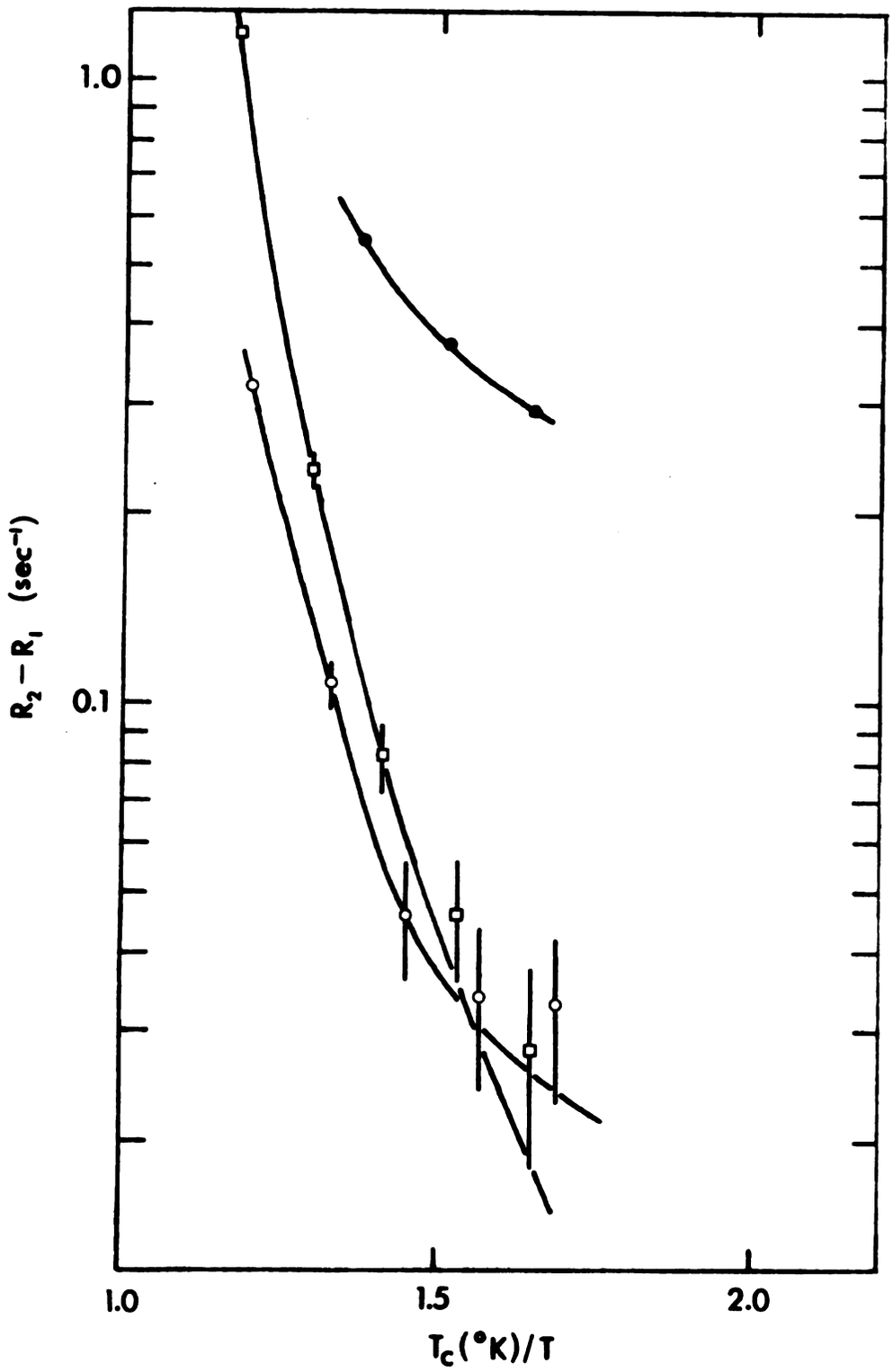

Figure 55. The temperature dependence of the difference R_2-R_1 for various fluorohalocarbons. (o) CF_3CCl_3, (□) CF_2Br_2, and (●) CF_2ClCCl_3.

of the extra curvature in the ΔR versus T_c/T plot (Figure 55) for CF_3CCl_3. No explanation is known for this anomalous behavior of T_2, but it is clear that ΔR cannot be used to calculate τ_θ, and it is also clear that the value of J_{FX} derived will depend on the temperature at which T_2 is measured.

VI. ^{19}F Spin-Rotation Tensors

In order to obtain quantitative information concerning molecular motion from nuclear relaxation times of spin 1/2 nuclei, the spin-rotation tensor must usually be known. This is particularly important for ^{19}F relaxation data, since spin-rotational relaxation often dominates the relaxation rate, as was found for the compounds studied here.

There are three methods in use for determining spin-rotation tensors (actually, usually only a spin-rotation constant). For a number of simple molecules, C has been measured from molecular beam (MB) experiments[291] and, more recently, molecular beam results have been reported for larger molecules[255,256,292-296]. The number which comes out of this type of experiment is an average value $C_{MB} = \frac{1}{3}(2C_\perp + C_{||})$ although the full tensor can, in theory, be determined by analyzing results for different rotational states. Molecular beam measurements provide probably the most reliable technique for measuring spin-rotation tensors, but are clearly not applicable to large, complex molecules.

The second method utilizes the relationship between the spin-rotation tensor and the paramagnetic component of the chemical

shift[297,298]. If we decompose the shielding tensor into diamagnetic and paramagnetic terms

$$\sigma = \sigma^d + \sigma^p \tag{157}$$

then, as Ramsey shows[297],

$$\sigma^{(k)} = \frac{e^2}{3mc^2}\langle\psi^\circ|\sum_i \frac{1}{r_i}|\psi^\circ\rangle - \frac{e^2}{6mc^2}\left\{2\sum_\ell \frac{Z_\ell}{r_{k\ell}} - \frac{\hbar c}{2e\mu_n g_k}\sum_{j=1}^{3} C_{jj}I_{jj}\right\} \tag{158}$$

where the I_{jj} are the principal moments of inertia and the other terms have the usual meaning with k and ℓ referring to nuclei and i to the electrons. The procedure is to establish an absolute shielding scale by comparing known spin-rotation constants with chemical shifts (such as in HF) to obtain a value for the diamagnetic terms. A number of workers[299,300] have considered this problem; for ^{19}F shifts the sum of the first two terms in Equation (158) is assigned the value 471 ppm and

$$\sigma_{av} = 471 \times 10^{-6} + 0.2091 \times 10^{-6}\sum_j C_{jj}I_{jj}. \tag{159}$$

If we replace I_{jj} with the average value of the inertia tensor I_{av} then

$$\sigma_{av} = 471 \times 10^{-6} + 0.2091 \times 10^{-6} C_\sigma I_{av} \tag{160}$$

and C_σ is the average spin-rotation constant from chemical shift data.

Furthermore, Chan and Dubin[300] have shown that, although the first two terms in Equation (158) are not in general isotropic, to a good approximation their sum is, thus we can write for the individual components of σ

$$\sigma_j = 471 \times 10^{-6} + 0.2091 \times 10^{-6} C_{jj} I_{jj} \qquad (161)$$

and, consequently, if the trace and anisotropy of a symmetric shielding tensor are known then the individual components of C can be calculated. If just the trace is known then the spin-rotation constant calculated is of the same form as from the molecular beam experiment: $C_\sigma = \frac{1}{3}(2C_\perp + C_{||})$.

The final method of obtaining C is by estimating it from NMR relaxation times. Other workers[76,299,301] have employed Equation (105) and estimated τ_J by various means which include rotational diffusion; however, it should also prove possible to use the value of R_1 at the critical point and make the assumption $\tau_J^* = 1.0$. Since the largest deficiency of the NMR method for calculating C is the uncertainty in the correct value of τ_J, this new approach should prove at least as good as previous methods. This argument is supported by two points: (1) The extended diffusion model, which predicts that $\tau_J^* = 1.0$ at the critical point, has been found to give an excellent description of the reorientational process in most cases which have been carefully studied (see page 60) and (2) at the critical point contributions to the rate by other mechanisms may always be neglected for fluorocarbons from which paramagnetic impurities have been removed.

The spin-rotation constant measured by the NMR method is given

by $C^2_{eff} = 2C^2_{\perp} + C^2_{||}$, which is related to C_σ or C_{MB} by

$$C^2_{eff} = C^2_{av} + \frac{2}{9}\Delta C^2 \qquad (162)$$

where $C_{av} = C_\sigma = C_{MB}$. Accordingly, $C^2_{eff} \geq C^2_{av}$, and if the anisotropy in C is large C_σ (or C_{MB}) values will not be useful in interpreting NMR relaxation data.

Table 36 lists the majority of molecules for which the ^{19}F spin-rotation constant is known. It can be seen that agreement is good between C_σ and C_{MB} for those molecules for which both are known. Contrary to previous discussions[298], agreement of C_σ or C_{MB} with C_{eff} is also generally good. The two exceptions to this are the molecules OPF_3 and AsF_3; it may be pointed out that C_{eff} calculated here is for the C tensor in the inertial coordinate system and, as discussed previously, this includes the off-diagonal terms which are neglected in C_{av}.

The two molecules CH_3F and CHF_3 have been intensively studied[208, 209,213,219-225]; in the case of CH_3F the ^{19}F shift anisotropy of -66 ppm[220] seems[208] to be the correct value, giving $C_{||}$ = -38.5 kHz and $C_\perp$ = +3.67 kHz, which agree better with the MB values[208] of -51 kHz and 4 kHz, respectively, than do the $C_{||}$ and $C_\perp$ values from the liquid crystal determination[221] of $\Delta\sigma$ = -157 ppm. In the case of CHF_3 the chemical shift-derived value of C_σ may be used to reject two of the molecular beam measurements as inaccurate. In this molecule C_{eff} may be expected to be larger than C_{av} as the ^{19}F spin-rotation tensor is not diagonal in the inertial axis system. From a consideration of these two molecules it is clear that there will be a great deal of

Table 36. Spin-rotation constants for ^{19}F in various molecules as determined from molecular beam (MB), chemical shielding (σ), or NMR relaxation (NMR) data.

Molecule	C_σ [a]	C_{MB}	C_{eff}	$\sigma_{absolute}$ [b]	$\Delta\sigma^{MF}$	$I_{\parallel}$	$I_{\perp}$	$C_{\parallel}$	$C_{\perp}$
NF_3 [c]	-13.3	----	----	53.6	c	150			
CH_3F [d]	+ .22	$C_{\perp}$=4.0 $C_{\parallel}$=-51	----	472	-157 - 66	5.34	30	-92.8 [e] -38.5 [e]	8.45 [e] 3.67 [e]
CHF_3 [f]	- 5.5	5.4 8.5 10.6	----	299	105 - 35	148	120	- 6.31 [3]	-5.1 [3]
CCl_3F [g]	- 3.35	----	-3.78	195.6	----	493	344	- 0.20 - 5.43	-5.77 -1.74
ClO_3F [h]	-17.4	----	22 ±2	-98	----	149	160	1.2 -36.4	-27 -8.2
SF_6 [i]	- 5.05	4.61	16.5	138.6	----	315	315	-1.78 2.69	1.58 -0.66
CF_4 [j]	- 6.79	6.31	21.0 6.60	260	----	148.7	148.7		
F_2 [k]	-158	157		-227	----	0	31.7		
POF_3 [ℓ]	- 4.9		5.75±.85	287.3	-33.8	175	183	- 5.61 [3]	-4.50 [e]
AsF_3 [ℓ]	- 6.9	-8.5±1.5				213	137		
PF_6^{-} [m]	2.77	3.56	3.56	289.3	----	315	315		
PO_3F^{-2} [m]	4.08	23.6	323.8	----					

[a]All spin-rotation constants are given in units of kHz and moments of inertia are in units of 10^{-40} g cm^2. Shielding values are in units of ppm. C_σ values calculated from Equation (160).

[b]Shielding values, unless indicated differently, are from "Compilation of Reported ^{19}F NMR Chemical Shifts", C. H. Dungan and J. R. VanWazer, Wiley, New York 1970.

[c]Structural parameters for NF_3 are from J. Sheridan and W. Gordy, Phys. Rev. 79, 513 (1950). The shielding tensor was found (Reference 302) to be asymmetric.

[d]For CH_3F, the components of the spin-rotation tensor were determined in Reference 292, and the two measurements of the shielding anisotropy are from Reference 304 (liquid crystal) and Reference 303 (clathrate), respectively.

[e]Components of the spin-rotation tensor were calculated from Equation (161).

[f]For CHF_3, the molecule beam data are from References 255, 306, and 296, respectively, and the shielding anisotropies are from References 305 and 302, respectively.

[g]Reference 131.

[h]Reference 130.

[i]Reference 51.

[j]For CF_4, the molecular beam determination of C is from Reference 307, and the values of C_{eff} are from J. H. Rugheimer and P. S. Hubbard, J. Chem. Phys. 39, 552 (1963) and Reference 125, respectively.

[k]Reference 120.

[ℓ]Reference 76.

[m]M. F. Froix and E. Price, J. Chem. Phys. 56, 6050 (1972).

uncertainty in any discussion of spin-rotation tensors in that reliable data are as yet difficult to obtain. If we consider $C_{||}$ and $C_{\perp}$ in molecules for which seemingly complete and reliable information is available (ClO_3F[130], CCl_3F[131], and CH_3F[208]), it is at least possible to consider that, while small moments of inertia I_i produce correspondingly large values of C_i, the product $C_i I_i$ is not isotropic as has been suggested for ^{13}C spin-rotation tensors[226].

In Table 37 we calculate C_{eff} from the spin-lattice relaxation rate at the critical point using Equation(105) with the assumption $\tau_J^* = 1.0$. Since the relaxation rate at the critical temperature was extrapolated from the rate at lower temperatures for some of these compounds, the result is only approximate, however, for both these compounds and those for which the spin-lattice relaxation rate was measured at or very near the critical point (CF_3CCl_3, CF_3CF_3, CF_3Br and CF_2Br_2), the agreement of C_{eff} with C_σ is generally good. The molecules for which the discrepancy between C_{eff} and C_σ is the largest, CF_3Br and CF_3I, are also the only ones listed in Table 37 for which the effects of anisotropic motion should be important (compare Figures 46 and 47, the temperature dependent relaxation rates in CF_3Br and CF_2Br_2). Although no further calculations were performed for these two compounds, due to the discrepancy in the size of $R_{1,trans}$ in liquid CF_3Br and to a lack of data for CF_3I, if the relation $\tau_{J||}/\tau_{J\perp} = I_\perp/I_{||}$ is valid[131], then τ_J^* in Table 37, which was calculated using an average moment of inertia, will be larger than $\tau_{J\perp}^*$ and smaller than $\tau_{J||}^*$. In the case of CF_3CCl_3, the very good agreement of C_{eff} with C_σ leads one to question the tentative conclusion reached earlier concerning

Table 37. Effective ^{19}F spin-rotation constants obtained from the spin-lattice relaxation rate at the critical point with the assumption $\tau_J^* = 1.0$.

Molecule	I_{av} [a]	C [a]	$A(10^{10})$ [b]	R_1 (sec^{-1})	T_c(°K)	τ_J^* [c]	C_{eff} [a,d]
CF_3Br	317	-3.83	2.195	1.63	340.2	1.28	3.39
CF_3I	416	-3.10	2.553	2±.4	∿400	1.47	2.56
CF_2Cl_2	320	-4.00	1.994	1.52	385	0.96	3.97
CF_2Br_2	480	-2.81	2.69	∿1.2	471	0.80	3.14
$CFCl_3$	394	-3.30	2.37	1.43	454.5	0.940	3.40
ClO_3F	156	-17.4	2.161	10.0	368	1.06	16.9
CF_3CCl_3	517	-1.79	6.162	∿0.7	482.2	1.0	1.8
CF_3CF_3	297	-3.00	3.819	0.730	292.2	1.11	2.85
CF_2ClCCl_3				∿0.7			
$CFCl_2CFCl_2$				∿0.7			
CF_2ClCF_2Cl				∿0.8			

[a] Spin-rotation constants are given in units of kHz and moments of inertia are given in units of 10^{40} g cm^2.

[b] $A = \frac{\mu^2}{8\pi^2 kTIC^2} = 1.0207 \cdot 10^{-40} \cdot \frac{1}{IC^2}$.

[c] $\tau_J^* = A \cdot \frac{R_1}{T_c} \left(\frac{kT}{I}\right)^{1/2}$

[d] $C_{eff} = \frac{C_\sigma}{\tau_J^*}$

the validity of Equation (105) in describing spin-rotational relaxation for this $-CF_3$ containing molecule. Although thereare no data to support any adjustment of τ_θ' values, it is evident from the results of Table 37 that the data of Figure 45 will better fit the J-diffusion model if τ_θ values are adjusted rather than τ_J values. In order to resolve this point it would be helpful to have either temperature-dependent Raman results or temperature-dependent chlorine NMR relaxation times.

SUMMARY

An interface between an NMR pulse spectrometer and a Nicolet 1083 computer was constructed, and programs were written to allow computer-controlled data collection and analysis for most simple pulse sequences. A 5 mm, variable temperature, single-coil NMR probe was constructed which operated at 56 MHz and contained a pair of coils wound in an anti-Helmholtz configuration for use in the pulsed field-gradient, spin-echo experiment. Three approaches were tried in order to measure diffusion coefficients in liquids, the steady gradient technique employing the magnet's shim coils, the pulsed gradient technique employing the magnet's shim coils, and the pulsed gradient technique employing a hand wound set of gradient coils within the probe. The steady gradient technique proved satisfactory when sufficient calibrations of the size of the gradient were performed.

An external field/frequency lock was constructed using the Varian DP-60 console as the spectrometer monitoring the lock signal, and building a new probe, containing a doped water sample, which could be inserted in the back of the pulse probe and also easily transferred from one pulse probe to another.

A simpler interface was constructed which allowed Raman spectra to be digitized and punched onto IBM cards for analysis on the CDC 6500 computer. A FORTRAN computer program was written which calculated the reorientational broadening of Raman A_1 lines, from which the rotational correlation time was calculated.

Deuterium quadrupole coupling constants have been obtained for two symmetric-top molecules in the liquid phase by combining NMR

relaxation data with Raman line-shape analysis of bands of A_1 symmetry. The Raman lines have been corrected for vibrational and instrumental broadening by comparing the polarized and depolarized components of a single line. More than one A_1 line has been studied for each molecule. The previously uncertain deuterium quadrupole coupling constant for $CDBr_3$ has been determined in this work to be 177±5 kHz and deuterium coupling constants in CDX_3 molecules are discussed. The procedure described here provides a different method for obtaining nuclear quadrupole coupling constants in the liquid phase. The temperature dependence of the ^2D spin-lattice relaxation rate was used to analyze published ^{13}C relaxation data for $CHBr_3$, and limits were placed on the anisotropy of rotational motion, which at 20° C were $1.5<D_{||}/D_{\perp}>1.0$. Motion in liquid $CDBr_3$ was compared to motion in the much more intensively studied liquid $CDCl_3$ system.

Spin-lattice and spin-spin relaxation rates at 56 MHz were measured in CF_3CCl_3 from 141° K to 432° K. More limited measurements were made of T_1 at 15.87 MHz and of the self-diffusion coefficient in the liquid phase. A phase transition was observed in the solid at 147° K from a discontinuity in the T_1 data.

By means of linewidth, T_2, and variable-field T_1 measurements, spin-lattice relaxation in plastic crystalline CF_3CCl_3 was found to have contributions from intramolecular dipole-dipole interactions, translational diffusion, and spin-rotation. The activation energies for these processes were determined to be 1.8 kcal/mole, 12.9 kcal/mole, and ∿1.8 kcal/mole, respectively. At 56 MHz, spin-rotation was found to be more important in the solid than translational diffusion. The value of the translational diffusion coefficient

at the melting point was determined to be 2.1×10^{-8} or 1.3×10^{-8} $cm^2\ sec^{-1}$, depending on whether the crystal structure is fcc or bcc.

The separation of the terms contributing to the liquid phase ^{19}F relaxation in CF_3CCl_3 was made on the basis of self-diffusion measurements and a single room temperature Raman measurement coupled with the temperature dependence of the rotational correlation time determined from the solid phase data. The rotational motion was discussed in terms of Gordon's extended diffusion model and it was found that the Hubbard relation for isotropic reorientation predicted angular momentum correlation times which were in approximate agreement with the diffusion models, indicating that off-diagonal elements of the spin-rotation tensor are small in CF_3CCl_3.

Spin-lattice relaxation rates were measured from the melting point to the critical point for CF_3Br and CF_2Br_2; also the self-diffusion coefficient was measured in liquid CF_3Br from room temperature to the melting point. The separation of $R_{1,total}$ into the contributions from various mechanisms was discussed but was not quantitatively successful due to difficulties in obtaining satisfactory values for the intermolecular dipole-dipole relaxation rate.

Spin-lattice and spin-spin relaxation rates were measured over a limited temperature range for CF_2ClCCl_3, $CFCl_2CFCl_2$, CF_3CF_3, and CF_3I. The use of the difference R_2-R_1 to obtain the scalar coupling constant J_{FX}, where X is the other halogen, was discussed, but it was not, in general, possible to obtain reliable values. These substituted ethanes were found to behave very similarly to CF_3CCl_3 in that spin rotation dominated the liquid range, with translational

diffusion making only a minor contribution to the total spin-lattice relaxation rate (R_1) both in the liquid and solid, at 56 MHz. Also the presence of a minimum in R_1 in the solid indicated the probable presence of a spin rotational relaxation mechanism.

"Effective" spin-rotation interaction constants were calculated for a number of compounds where experimental data were available from the relaxation rates at the critical point, and were compared with chemical shielding-derived values. The agreement was found generally to be good, indicating that off-diagonal elements of the spin-rotation tensor were small for these compounds and that the motion was roughly isotropic.

REFERENCES

REFERENCES

1. R. Zwanzig, Ann. Rev. Phys. Chem. 16, 67 (1965).
2. R. G. Gordon, Advan. Magn. Resonance 3, 1 (1969).
3. B. J. Berne,"Physical Chemistry, An Advanced Treatise", Vol. 8, Academic Press, New York (1971).
4. B. J. Berne and G. D. Harpe, Advan. Chem. Phys. 17, 63 (1970).
5. W. A. Steele, "Transport Phenomena in Fluids", M. Dekker, New York (1969).
6. N. Wax, "Selected Papers on Noise and Stochastic Processes", Dover, New York (1954).
7. J. L. Doob, Ann. Math. 43, 351 (1942).
8. H. B. Callen and T. A. Welton, Phys. Rev. 83, 34 (1951).
9. R. G. Gordon, J. Chem. Phys. 43, 1307 (1965).
10. D. K. Green and J. G. Powles, Proc. Phys. Soc. 85, 87 (1965).
11. M. Bloom, F. Bridges, and W. N. Hardy, Can. J. Phys. 45, 3533 (1967).
12. For a discussion of correlation functions for dilute gases see J. M. Deutch and I. Oppenheim, Advan. Magn. Resonance 2, 225 (1966).
13. P. Debye, "Polar Molecules", Dover, New York (1945).
14. C-M. Hu and R. Zwanzig, J. Chem. Phys. 60, 4354 (1974).
15. R. I. Cukier and K. Lakatos-Lindenberg, J. Chem. Phys. 57, 3427 (1972)
16. E. N. Ivanov, Zh. Eksp. Teor. Fiz. 45, 1509 (1963)[Sov. Phys-JETP 18, 1041 (1964)].
17. Egelstaff, "An Introduction to the Liquid State", Ch. 10, Academic Press, New York (1967).
18. F. Perrin, J. Phys. Radium 5, 497 (1934); 7, 1(1936).
19. L. D. Favro, Phys. Rev. 119, 53 (1960).
20. D. E. Woessner, J. Chem. Phys. 37, 647 (1962).

21. W. T. Huntress, Advan. Magn. Resonance 4, 1 (1970).

22. M. E. Rose "Elementary Theory of Angular Momentum", Wiley, New York (1957).

23. R. K. Wangsness and F. Bloch, Phys. Rev. 89, 728 (1953).

24. F. Bloch, Phys. Rev. 105, 1206 (1957).

25. A. G. Redfield, Advan. Magn. Resonance 1, 1 (1965).

26. R. Kubo and K. Tomita, J. Phys. Soc. Japan 9, 888 (1954).

27. J. M. Deutch and I. Oppenheim, Advan. Magn. Resonance 3, 43 (1968).

28. A. Abragam, "The Principles of Nuclear Magnetism", Oxford UP, London (1961).

29. R. A. Valiev, Opt. Spectry (USSR)(English Transl.) 13, 282 (1961).

30. F. J. Bartoli and T. A. Litovitz, J. Chem. Phys. 56, 404 (1972).

31. S. Bratos and E. Marechal, Phys. Rev. A4, 1078 (1971).

32. S. Sykora, U.S. Clearinghouse Fed. Sci. Tech. Inf. No. 724330 (1971).

33. R. Loudon, Advan. Phys. 13, 423 (1964).

34. N. Bloembergen, E. M. Purcell, and R. V. Pound, Phys. Rev. 73, 679 (1948).

35. N. Bloembergen, J. Chem. Phys. 27, 572 (1957).

36. J. Winter, Compt. Rend. 249, 1346 (1959).

37. R. R. Sharp, J. Chem. Phys. 57, 5321(1972).

38. M. Bloom, Physica 23, 237 (1957).

39. C. S. Johnson and J. S. Waugh, J. Chem. Phys. 35, 2020 (1961).

40. M. Lipsicas and M. Bloom, Can. J. Phys. 39, 881 (1961).

41. M. Bloom, Can. J. Phys. 40, 289 (1962).

42. C. S. Johnson and J. S. Waugh, J. Chem. Phys. 36, 2266 (1962).

43. W. P. Haas, G. Seidal, and N. J. Poulis, Physica 26, 834 (1960).

44. H. S. Gutowsky and D. E. Woessner, Phys. Rev. 104, 843 (1956).

45. H. S. Gutowsky, I. J. Lawrenson, and K. Shimomura, Phys. Rev. Lett. 6, 349 (1961).

46. R. J. C. Brown, H. S. Gutowsky, and K. Shimomura, J. Chem. Phys. 38, 76 (1963).

47. I. Solomon and N. Bloembergen, J. Chem. Phys. 25, 261 (1956).

48. H. M. McConnell and C. H. Holm, J. Chem. Phys. 25, 1289 (1956).

49. P. S. Hubbard, Phys. Rev. 131, 1155 (1963).

50. R. Blinc and G. Lahajnar, Phys. Rev. Lett. 19, 685 (1967).

51. W. R. Hackleman and P. S. Hubbard, J. Chem. Phys. 39, 2688 (1963).

52. P. Rigney and J. Virlet, J. Chem. Phys. 51, 3807 (1969).

53. M. M. Pintar, A. R. Sharp, and S. Vrscaj, Phys. Lett. 27A 169 (1968).

54. A. R. Sharp and M. M. Pintar, J. Chem. Phys. 53 2428 (1970).

55. N. Boden and R. Folland, Chem. Phys. Lett. 10, 167 (1971).

56. N. Boden and R. Folland, Mol. Phys. 21, 1123 (1971).

57. R. Ikeda and C. A. McDowell, Chem. Phys. Lett. 14, 389 (1972).

58. D. W. Sawyer and J. G. Powles, Mol. Phys. 21,83 (1971).

59. C. Brot and I. Darmon, Mol. Phys. 21, 725 (1971).

60. A. Gierer and K. Wirtz, Z. Naturforsch. A8, 532 (1953).

61. N. E. Hill, Proc. Roy. Soc. (London) B67, 149 (1954).

62. E. N. daC. Andrade, Phil. Mag. 17, 497, 698 (1934).

63. R. C. Miller and C. P. Smyth, J. Chem. Phys. 24, 814 (1956).

64. K. A. Valiev and M. M. Zaripov, Zh. Eksp. Teor. Fiz. 42, 503 (1962) [Sov. Phys. - JETP 15,353 (1962)].

65. H. Shimizu, J. Chem. Phys. 37, 765 (1962).

66. H. Shimizu, J. Chem. Phys. 48, 754 (1964).

67. C. Brot, Chem. Phys. Lett. 3, 319 (1969).

68. D. Wallach and W. T. Huntress, Jr., J. Chem. Phys. 50, 1219 (1969).

69. A. Allerhand, J. Chem. Phys. 52, 3596 (1970).

70. H. J. Bender and M. D. Zeidler, Ber. Bunsenges. Physik. Chem. 75, 236 (1971).

71. T. T. Bopp, J. Chem. Phys. 47, 3621 (1967).

72. W. T. Huntress, J. Phys. Chem. 73, 103 (1969).

73. K. T. Gillen and J. H. Noggle, J. Chem. Phys. 53, 801 (1970).

74. D. E. Woessner, B. B. Snowden, Jr., and E. T. Strom, Mol. Phys. 14, 265 (1968).

75. J. Jonas and T. M. DiGennaro, J. Chem. Phys. 50, 2392 (1969).

76. K. T. Gillen, J. Chem. Phys. 56, 1573 (1972).

77. K. T. Gillen and J. E. Griffiths, Chem. Phys. Lett. 17, 359 (1972).

78. J. P. Kintzinger and J. M. Lehn, Mol. Phys. 22, 273 (1971).

79. J. P. Kintzinger and J. M. Lehn, Mol. Phys. 27, 491 (1974).

80. K. T. Gillen, M. Schwartz and J. H. Noggle, Mol. Phys. 20, 899 (1971).

81. J. E. Griffiths, Chem. Phys. Lett. 21, 354 (1973).

82. W. A. Steele, J. Chem. Phys. 38, 2404 (1963).

83. W. A. Steele, J. Chem. Phys. 38, 2411 (1963).

84. W. B. Moniz, W. A. Steele and J. A. Dixon, J. Chem. Phys. 38, 2418 (1963).

85. P. W. Atkins, Mol. Phys. 17, 321 (1969).

86. P. W. Atkins, A. Loewenstein, and Y. Margalit, Mol. Phys. 17, 329 (1969).

87. B. D. Nageswara Rao and P. K. Mishra, Chem. Phys. Lett. 27, 592 (1974).

88. G. Birnbaum and W. Ho, Chem. Phys. Lett. 5, 334 (1970).

89. P. V. Huong, M. Corizi, and M. Perrot, Chem. Phys. Lett. 7, 189 (1970).

90. J. P. Perchard, W. F. Murphy, and H. J. Bernstein, Chem. Phys. Lett. 8, 559 (1971).

91. G. Birnbaum, Mol. Phys. 25, 241 (1973).

92. S. H. Glarum, Mol. Phys. 27, 1139 (1974).

93. R. G. Gordon, J. Chem. Phys. 44, 1830 (1965).

94. R. I. Cukier, J. Chem. Phys. 60, 734 (1974).

95. R. E. D. McClung, J. Chem. Phys. 51, 3842 (1969); 54, 3248 (1971).

96. R. E. D. McClung and H. Versmold, J. Chem. Phys. 57, 2596 (1972).

97. M. Fixman and K. Rider, J. Chem. Phys. 51, 2425 (1969).

98. R. D. Mountain, J. Chem. Phys. 54, 3243 (1971).

99. R. E. D. McClung, J. Chem. Phys. 57, 5478 (1972).

100. T. E. Eagles and R. E. D. McClung, Chem. Phys. Lett. 22, 414 (1973).

101. D. Frenkel, G. H. Wegdam, and J. van der Elsken, J. Chem. Phys. 57, 2691 (1972).

102. A. G. St. Pierre and W. A. Steele, Phys. Rev. 184, 172 (1969).

103. A. G. St. Pierre and W. A. Steele, J. Chem. Phys. 57, 4638 (1972).

104. D. Chandler, J. Chem. Phys. 60, 3500; 3508 (1974).

105. K. E. Larsson, J. Chem. Phys. 59, 4612 (1973).

106. H. Mori, Progr. Theoret. Phys. (Kyoto) 33, 423 (1965).

107. H. Mori, Progr. Theoret. Phys. (Kyoto) 34, 399 (1965).

108. D. Kivelson, M. G. Kivelson, and I. Oppenheim, J. Chem. Phys. 52, 1810 (1970).

109. T. Keyes and D. Kivelson, J. Chem. Phys. 56, 1057 (1972).

110. D. Kivelson and T. Keyes, J. Chem. Phys. 57, 4599 (1972).

111. D. Kivelson, Mol. Phys. 28, 321 (1974).

112. H. W. Spiess, D. Schweitzer, U. Haberlen, and K. H. Hauser, J. Magn. Resonance 5, 101 (1971).

113. K. Krynicki and J. G. Powles, Proc. Phys. Soc. (London) 86, 549 (1965).

114. J. G. Powles and M. Rhodes, Phys. Lett. A24, 523 (1967).

115. K. Krynicki and J. G. Powles, J. Magn. Resonance 6, 539 (1972).

116. R. E. Morgan and J. H. Strange, Mol. Phys. 17, 397 (1969).

117. J. H. Strange and R. E. Morgan, J. Phys. C Solid State Physics 3, 1999 (1970).

118. H. Boehme and M. Eisner, J. Chem. Phys. 46, 4242 (1967).

119. D. E. O'Reilly and E. M. Peterson, J. Chem. Phys. 49, 2872 (1968).

120. D. E. O'Reilly, E. M. Peterson, D. C. Hogenbloom, and C. E. Scheie, J. Chem. Phys. 54, 4194 (1971).

121. C. J. Gerritsma and N. J. Trappeniers, Physica 51, 365 (1971).

122. C. J. Gerritsma, P. H. Oosting, and N. J. Trappeniers, Physica 51, 381 (1971).

123. P. H. Oosting and N. J. Trappeniers, Physica 51, 395 (1971).

124. P. H. Oosting and N. J. Trappeniers, Physica 51, 418 (1971).

125. J. H. Campbell, S. J. Seymour, and J. Jonas, J. Chem. Phys. 59, 4151 (1973).

126. K. T. Gillen, J. H. Noggle, and T. K. Leipert, Chem. Phys. Lett. 17, 505 (1972).

127. R. M. Hawk and R. R. Sharp, J. Chem. Phys. 60, 1009 (1974).

128. R. R. Sharp, J. Chem. Phys. 60, 1149 (1974).

129. Discussed by T. C. Farrar, A. A. Maryott, and M. S. Malmberg, Ann. Rev. Phys. Chem. 23, 193 (1972).

130. A. A. Maryott, T. C. Farrar, and M. S. Malmberg, J. Chem. Phys. 54, 64 (1971).

131. K. T. Gillen, D. C. Douglass, M. S. Malmberg, and A. A. Maryott, J. Chem. Phys. 57, 5170 (1972).

132. R. A. Assink and J. Jonas, J. Chem. Phys. 57, 3329 (1972).

133. J. DeZwaan, R. J. Finney, and J. Jonas, J. Chem. Phys. 60, 3223 (1974).

134. J. E. Anderson and R. Ullman, J. Chem. Phys. 55, 4406 (1971).

135. J. Kushick and B. J. Berne, J. Chem. Phys. 59, 4486 (1973).

136. H. Shimizu, J. Chem. Phys. 43, 2453 (1965).

137. S. Bratos and J. Rios, Compt. Rend. 269, 90 (1969).

138. Y. Guissani, S. Bratos, and J. C. Leicknam, Compt. Rend. 269, 137 (1969).

139. S. Bratos, J. Rios, and Y. Guissani, J. Chem. Phys. 52, 439 (1970).

140. R. G. Gordon, J. Chem. Phys. 42, 3658 (1965).

141. F. J. Bartoli and T. A. Litovitz, J. Chem. Phys. 56, 413 (1972).

142. H. S. Goldberg and P. S. Pershan, J. Chem. Phys. 58, 3816 (1973).

143. I. Laulicht and S. Meirman, J. Chem. Phys. 59, 2521 (1973).

144. M. Constant and R. Fanquemberque, J. Chem. Phys. 58, 4031 (1973).

145. C. H. Wang and P. A. Fleury, J. Chem. Phys. 53, 2243 (1970).

146. R. B. Wright, M. Schwartz, and C. H. Wang, J. Chem. Phys. 58, 5125 (1973).

147. Y. LeDuff, J. Chem. Phys. 59, 1984 (1973).

148. M. Schwartz and C. H. Wang, J. Chem. Phys. 59, 5258 (1973).

149. J. P. Perchard, W. F. Murphy, and H. J. Bernstein, Mol. Phys. 23, 499 (1972).

150. J. P. Perchard, W. F. Murphy, and H. J. Bernstein, Mol. Phys. 23, 519 (1972).

151. J. P. Perchard, W. F. Murphy, and H. J. Bernstein, Mol. Phys. 23, 535 (1972).

152. R. C. Livingston, W. G. Rothschild, and J. J. Rush, J. Chem. Phys. 59, 2498 (1973).

153. W. G. Rothschild, J. Chem. Phys. 57, 991 (1972).

154. M. Schwartz and C. H. Wang, Chem. Phys. Lett. 25, 26 (1974).

155. J. H. Campbell and J. Jonas, Chem. Phys. Lett. 18, 441 (1973).

156. C. H. Wang and R. B. Wright, J. Chem. Phys. 59, 1706 (1973).

157. T. T. Wall, J. Chem. Phys. 52, 2792 (1970).

158. W. G. Rothschild, J. Chem. Phys. 55, 1402 (1971).

159. W. G. Rothschild, Macromol. 1, 43 (1968).

160. G. Levi, M. Chalaye, and A. Dayan, Chem. Phys. Lett. 12, 462 (1972).

161. R. E. D. McClung, J. Chem. Phys. 55, 3459 (1971).

162. C. Dreyfus and J. Vincent-Geisse, Chem. Phys. Lett. 21, 170 (1973).

163. J. Yarwood, Advan. Mol. Relax. Proc. 5, 375 (1973).

164. J. P. Marsault, F. Marsault-Herail, and G. Lévi, Mol. Phys. 26, 997 (1973).

165. T. E. Eagles and R. E. D. McClung, J. Chem. Phys. 59, 435 (1973).

166. G. Lévi and M. Chalaye, Chem. Phys. Lett. 19, 263 (1973).

167. P. vanKonynenburg and W. A. Steele, J. Chem. Phys. 56, 4776 (1972).

168. D. A. Jackson and B. Simic-Glavaski, Mol. Phys. 18, 393 (1970).

169. H. D. Hardy, V. Volterra, and T. A. Litovitz, J. Chem. Phys. 59, 4491 (1973).

170. M. J. Bird, D. A. Jackson, and J. G. Powles, Mol. Phys. 25, 1051 (1973).

171. G. B. Alms, D. R. Bauer, J. I. Brauman, and R. Pecora, J. Chem. Phys. 59, 5321 (1973).

172. W. G. Rothschild, J. Chem. Phys. 53, 3265 (1970).

173. J. H. Campbell, S. J. Seymour, and J. Jonas, J. Chem. Phys. 61, 346 (1974).

174. G. R. Alms, D. R. Bauer, J. I. Brauman, and R. Pecora, J. Chem. Phys. 59, 5310 (1973).

175. D. R. Bauer, G. R. Alms, J. I. Brauman, and R. Pecora, J. Chem. Phys. 61, 2255 (1974).

176. J. P. McCullough, J. Pure and Appl. Chem. 2, 221 (1961).

177. L. Pauling, Phys. Rev. 36, 430 (1930).

178. J. Frenkel, Acta Physicochim. USSR, 3, 23 (1935).

179. G. B. Guthrie and J. P. McCullough, J. Phys. Chem. Solids 18, 53 (1961).

180. For a discussion of the history of plastic solids see J. Tinmermans, J. Phys. Chem. Solids 18, 1 (1961).

181. I. Darmon and C. Brot, Mol. Crys. 2, 301 (1967).

182. C. P. Smyth, J. Phys. Chem. Solids 18, 40 (1961).

183. C. Clemett and M. Davies, Trans. Faraday Soc. 58, 1705, (1962).

184. C. Clemett and M. Davies, Trans. Faraday Soc. 58, 1718 (1962).

185. C. P. Slichter, "Principles of Magnetic Resonance", p. 59, Harper and Row, New York (1963).

186. H. C. Torrey, Phys. Rev. 92, 962 (1953).

187. H. C. Torrey, Phys. Rev. 96, 690 (1954).

188. H. A. Resing and H. C. Torrey, Phys. Rev. 131, 1102 (1963).

189. N. Boden, J. Cohen, and P. P. Davis, Mol. Phys. 23, 819 (1972).

190. P. Bladon, N. C. Lockhart, and J. N. Sherwood, Mol. Cryst. Liquid Cryst. 19, 315 (1973).

191. G. W. Smith, J. Chem. Phys. 50, 3595 (1969).

192. H. A. Resing, Mol. Cryst. Liquid Cryst. 9, 101 (1969).

193. E. O. Stejskal, D. E. Woessner, T. C. Farrar, and H. S. Gutowsky, J. Chem. Phys. 31, 55 (1959).

194. J. E. Anderson and W. P. Slichter, J. Chem. Phys. 41, 1922 (1964).

195. R. L. Jackson and J. H. Strange, Mol. Phys. 22, 313 (1971).

196. S. Albert and J. A. Ripmeester, J. Chem. Phys. 59, 1069 (1973).

197. J. M. Chezeau, J. Dufoureq, and J. H. Strange, Mol. Phys. 20, 305 (1971).

198. S. Albert, H. S. Gutowsky, and J. A. Ripmeester, J. Chem. Phys. 56, 1332 (1972).

199. R. Folland, S. M. Ross, and J. H. Strange, Mol. Phys. 26, 27 (1973).

200. H. A. Resing, J. Chem. Phys. 37, 2575 (1962).

201. J. E. Anderson and W. P. Slichter, J. Chem. Phys. 44, 3647 (1966).

202. G. W. Smith, J. Chem. Phys. 42, 4229 (1965).

203. G. A. Matzkanin, T. A. Scott, and P. J. Haigh, J. Chem. Phys. 42, 1646 (1965).

204. G. W. Smith, J. Chem. Phys. 45, 3483 (1966).

205. D. C. Look, I. J. Lowe, and J. A. Northby, J. Chem. Phys. 44, 3441 (1966).

206. D. J. Genin, D. E. O'Reilly, E. M. Peterson, and T. Tsang, J. Chem. Phys. 48, 4525 (1968); 50 2786 (1969).

207. J. A. Pople and F. E. Karasz, J. Phys. Chem. Solids 18, 28 (1961).

208. F. E. Karasz and J. A. Pople, J. Phys. Chem. Solids 20, 294 (1961).

209. L. M. Amzel and L. N Becka, J. Phys. Chem. Solids 30, 521 (1969).

210. R. L. Streever and H. Y. Carr, Phys. Rev. 121, 20 (1960).

211. A. Csaki and G. Bené, Compt. Rend. 251, 228 (1960).

212. Dinesh and M. T. Rogers, Rev. Sci. Instrum. 43, 555 (1972).

213. D. C. Look and D. R. Locker, Rev. Sci. Instrum. 41, 250 (1970).

214. R. Freeman, H. D. W. Hill and R. Kaptin, J. Magn. Resonance 7, 82 (1972).

215. Varian Associates, Palo Alto, California.

216. Nicolet Instrument Corporation, Madison, Wisconsin.

217. C. P. Slichter and D. Ailion, Phys. Rev. 135, A1099 (1964).

218. C. Deverell, R. E. Morgan, and J. H. Strange, Mol. Phys. 18, 553 (1970).

219. E. J. Wells and K. J. Abramson, J. Magn. Resonance 1, 378 (1969).

220. I. Solomon, Compt. Rend. 249, 1613 (1959).

221. H. Y. Carr and E. M. Purcell, Phys. Rev. 94, 630 (1954).

222. S. Meiboom and D. Gill, Rev. Sci. Instr. 29, 688 (1958).

223. A. Kumar and C. S. Johnson, Jr., J. Magn. Resonance, 7, 13 (1972).

224. U.Haberlen, Ph.D. Thesis, Technishe Hochschule, Stuttgart (1967).

225. I. J. Lowe and C. E. Tarr, J. Sci. Instr. 1, 320 (1968).

226. In general, any computer command which generates an output pulse can be used; however, the Nicolet 1082 has commands and output jacks specifically for this purpose.

227. J. S. Waugh, J. Chem. Phys. 48, 662 (1968).

228. D. D. Traficante, private communication.

229. E. D. Becker and T. C. Farrar, "Pulse and Fourier Transform NMR", Academic Press, New York (1971).

230. J. E. Tanner, Rev. Sci. Instr. 36, 1086 (1965).

231. J. E. Tanner, J. Chem. Phys. 52, 2523 (1970).

232. J. E. Tanner and E. O. Stejskal, J. Chem. Phys. 49, 1768 (1968).

233. K. J. Packer, C. Rees, and D. J. Tomlinson, Mol. Phys. 18, 421 (1970).

234. G. G. McDonald and J. S. Leigh, Jr., J. Magn. Resonance 9, 358 (1973).

235. Handbook of Chemistry and Physics, Chemical Rubber Company.

236. D. L. VanderHart, J. Chem. Phys. 60, 1858 (1974).

237. W. F. Murphy, M. V. Evans, and P. Bender, J. Chem. Phys. 47, 1836 (1967).

238. A. Savitzky, and M. J. E. Golay, Anal. Chem. 36, 1627 (1964).

239. T. C. Farrar, S. J. Druck, R. R. Shoup, and E. D. Becker, J. Am. Chem. Soc. 94, 699 (1972).

240. E. A. C. Lucken,"Nuclear Quadrupole Coupling Constants"(Academic Press, New York, 1969).

241. K. T. Gillen and J. H. Noggle, J. Chem. Phys. 52, 4905 (1970).

242. J. W. Reed and P. M. Harris, J. Chem. Phys. 35, 1730 (1961).

243. J. L. Ragle and K. L. Sherk, J. Chem. Phys. 50, 3553 (1969).

244. J. L. Ragle, G. Minott, and M. Mokarram, J. Chem. Phys. 60, 3184 (1974).

245. M. Rinne and J. Depireaux,"Advances in Nuclear Quadrupole Resonance" J. A. S. Smith, editor, Vol. I (Heyden and Son, London, 1974).

246. F. S. Millett and B. P. Dailey, J. Chem. Phys. 56, 3249 (1972).

247. W. J. Caspary, F. S. Millett, M. Reichbach, and B. P. Dailey, J. Chem. Phys. 51, 623 (1969).

248. N. Zumbulyadis and B. P. Dailey, J. Chem. Phys. 60, 4223 (1974).

249. Dinesh and M. T. Rogers, J. Magn. Resonance, 7, 30 (1972).

250. W. B. Moniz and H. S. Gutowsky, J. Chem. Phys. 38, 1155 (1963).

251. G. J. Jenks, J. Chem. Phys. 54, 658 (1971).

252. G. Bonera and A. Rigamonti. J. Chem. Phys. 42, 175 (1965).

253. J. G. Powles, M. Rhodes, and J. H. Strange, Mol. Phys. 11, 575 (1966).

254. R. A. Assink and J. Jonas, J. Magn. Resonance 4, 347 (1971).

255. S. G. Kukolich, A. C. Nelson, and D. J. Ruben, J. Mol. Spectry. 40, 33 (1971).

256. S. G. Kukolich, D. J. Ruben, J. H. S. Wang, and J. R. Williams J. Chem. Phys. 58, 3155 (1973).

257. K. H. Caselton and S. G. Kukolich, Chem. Phys. Lett. 22, 331 (1973).

258. P. B. Davies, R. M. Neumann, S. C. Wolfsy, and W. Klemperer, J. Chem. Phys. 55, 3564 (1971).

259. D. Schwartz and J. L. Ragle, J. Chem. Phys. 61, 429 (1974).

260. A. M. Pritchard and R. E. Richards, Trans. Faraday Soc. 62, 2014 (1966).

261. T. L. Pendred, A. M. Pritchard, and R. E. Richards, J. Chem. Soc. A 1009 (1966).

262. C. W. Kern and M. Karplus, J. Chem. Phys. 42, 1062 (1965).

263. L. Salem, J. Chem. Phys 38, 1227 (1963).

264. J. F. Harrison, J.Chem. Phys. 48, 2379 (1968).

265. A. B. Anderson, N. C. Hardy, and R. G. Parr, J. Chem. Phys. 50, 3634 (1969).

266. J. P. Zietlow, F. F. Cleveland, and A. B. Meister, J. Chem. Phys. 18, 1076 (1950).

267. A. Ruoff and H. Burger, Spectrochim. Acta, 26A, 989 (1970).

268. H. Burger and J. Cichon, Spectrochim. Acta. 27A, 2191 (1971).

269. R. Bersohn, J. Chem. Phys. 32, 85 (1960).

270. Q. Williams. J. T. Cox, and W. Gordy, J. Chem. Phys. 20, 1524 (1952).

271. S. N. Ghosh, R. Trambarulo, and W. Gordy, J. Chem. Phys. 20, 605 (1952).

272. M. Jen and D. R. Lide, Jr., J. Chem. Phys. 36, 2525 (1962).

273. M. Z. Pajak, Comp. Rend. 249, 1211 (1959).

274. K. F. Kuhlmann, D. M. Grant, and R. K. Harris, J. Chem. Phys. 52, 3439 (1970).

275. R. R. Shoup and T. C. Farrar, J. Magn. Resonance, 7, 48 (1972).

276. H. Hiraoka and J. H. Hildebrand, J. Phys. Chem. 67, 916 (1963).

277. G. W. Smith, J. Chem. Phys. 36, 3081 (1962).

278. J. E. Jones and A. E. Ingham, Proc. Roy. Soc. (London) A107, 636 (1925).

279. W. J. Dunning, J. Phys. Chem. Solids 18, 21 (1961).

280. H. Suga, M. Sugasaki, and S. Seki, Mol. Cryst. 1, 377 (1966).

281. P. S. Hubbard, Phys. Rev. 131, 275 (1963).

282. W. T. Toth, Ph.D. Thesis, Michigan State University (1974).

283. T. E. Burke and S. I. Chan, J. Magn. Resonance 3, 55 (1970).

284. C. R. Ward and C. H. Ward, J. Mol. Spectry. 12, 289 (1964).

285. C. S. Yannoni, B. P. Dailey, and G. P. Ceasar, J. Chem. Phys. 54, 4020 (1971).

286. C. H. Wang, J. Magn. Resonance 9, 75 (1973).

287. R. E. J. Sears, J. Chem. Phys. 56, 983 (1972).

288. R. W. Gallant, Hydrocarbon Process. Petrol. Refiner. 47, 128 (1968).

289. R. K. Nikul'shin, Khelodil'n Tekhn. 43, 30 (1966).

290. Z. I. Geller, R. K. Nikul'shin, and Yu. G. Zatvornitskii, Zh. Prilk. Khim. (Leningrad) 42, 1121 (1969).

291. C. H. Townes and A. L. Schawlow, "Microwave Spectroscopy", McGraw-Hill, New York (1955).

292. S. C. Wofsy, J. S. Muenter and W. Klemperer, J. Chem. Phys. 55, 2014 (1971).

293. S. G. Kukolich, Chem. Phys. Lett. 10, 52 (1971).

294. S. G. Kukolich, Phys. Rev. 156, 83 (1967).

295. S. G. Kukolich, J. H. S. Wang, and D. J. Reuben, J. Chem. Phys. 58, 5474 (1973).

296. J. M. H. Reynders, A. W. Ellenbroek and A. Dymanns, Chem. Phys. Lett. 17, 351 (1972).

297. N. F. Ramsey, Phys. Rev. 78, 699 (1950).

298. W. H. Flygare, J. Chem. Phys. 41, 793 (1964).

299. C. Deverell, Mol. Phys. 18, 319 (1970).

300. S. I. Chan and A. S. Dubin, J. Chem. Phys. 46, 1745 (1967).

301. R. Y. Dong and M. Bloom, Can. J. Phys. 48, 793 (1970).

302. A. B. Harris, E. Hunt, and H. Meyer, J. Chem. Phys. 42, 2851 (1965).

303. E. Hunt and H. Meyer, J. Chem. Phys. 41, 353 (1964).

304. R. A. Bernheim and T. R. Krugh, J. Am. Chem. Soc. 89, 6784 (1967).

308. B. J. Laver, Thesis, Pennsylvania State University, 1967.

306. R. L. Armstrong and J. A. Courtney, Can. J. Phys. 50, 1262 (1974).

307. L. M. Crapo and G. W. Flynn, J. Chem. Phys. 43, 1443 (1965).

308. J. R. Lyerla, Jr., D. M. Grant, and C. H. Wang, J. Chem. Phys. 55, 4676 (1971).

APPENDIX A

APPENDIX A

RELAX2 - Measurement of Relaxation Times

This program provides computer-controlled timing and data acquisition for two-pulse experiments. In addition it provides operator directed data analysis of the exponential curves whether generated by these experiments or by externally timed multiple-pulse (e.g. spin-echo, triplet T_1) trains.

If the data are collected automatically (two-pulse experiment) they are immediately ready for analysis as described in Section 4. If, however, the collection is manual (externally timed pulse trains), then further steps must be taken before the analysis may be performed. These steps are performed using the DISPLAY routines as described in Section 3.

1. Commands and Constants

Operator control of the program is via the subroutine SERVO, which accepts two character alphaneumeric commands and checks them against internal lists of legal commands. As described in the SERVO listing, there are three types of legal commands and consequently three possible responses. These are:

C. Execute the operation requested

R. Accept a real constant*

I. Accept an integer constant*

*Using the Floating Point Package FLIP routine.

Legal commands are listed on page 256. Also noted is whether they are of type C, R, or I.

2. Acquiring Data

a. Multiple-Pulse Experiments

In this mode of operation the computer functions merely as a signal averager during data acquisition. The trigger is set on external and the autostop limit is put to 1. The number of sweeps desired is set with the NS command. The dwell time selected on the main frame thumbwheel switches must be entered with the dwell (DW) command. After each sweep the displayed memory is baseline corrected; if this is not desired change address 1517;2000135/JMS STATWD to 1544/JMP 1544.

b. Two-Pulse Experiments

In this mode the program calculates the discrete data directly from the input parameters and the signal from the spectrometer. The main frame controls are usually set as follows:

Trigger - auto recur

Block size - 1K

Autostop - 1

Dwell time - 20 μsec

Delay - off

The input parameters are T1, T2 (necessary only for spin-echo experiments), NP, NS and IL. Data are collected with N (=NPxNS) sequences.

[8T - pulse 1 - nτ - pulse 2 - (nτ) - measure signal]

where $n\tau$ is varied by the computer from ≈0 to 4T1 (or 2T2) and the second $n\tau$ may or may not be present depending on whether G1 or G2 was typed. The integration limit, IL, is the number of points of the digitized FID which are summed to obtain y_i, the intensity at time x_i. For maximum S/N it should be set roughly equal to T_2^* the rate of the FID†. However any value of IL less than the displayed memory size will work. The time span over which the decay is determined may be varied from 4T by changing the value of the multiplicative constant CON1 address 1154. The current value of 172044_8 (=1,000,000/16_{10}) gives the time span of 4T. The wait between successive two-pulse sequences may be reduced from $8T_1$ to $4T_1$ by changing address 1040; 5023/RASH3 to 5024/RASH4.

3. Display Routines

After an experiment has been performed and the receiver output digitized and stored in memory it is usually necessary to separate the useful data from the rest of the receiver output. For example, for spin 1/2 nuclei in liquids the Carr-Purcell pulse spacing is usually large enough that the echoes are well resolved. In this case the amplitude of each echo is the useful data while the rest is superfluous. The display routines allow this separation to be easily made.

These routines select points from the displayed (DS) section of memory using one of six methods (see Data Transfer). The points must

---

†Remember that IL gives the number of points in the digitized FID, not the decay time.

occur at regular intervals to be transferred in one operation. The data thus selected* may then be fitted to an exponential decay as described in Section 4.

a. Data Selection - Choosing the Right Interval

Intensified points will always appear in the displayed (DS) memory unless they have been suppressed by setting DL=0. The interval between intensified points is IN-IN/FR, where IN and FR are integer constants which may be given any positive value. Let the displayed memory size be B. There are four cases of interest:

1. FR<B. All intensified points have the separation IN.
2. IN<FR<B. All intensified points have separation IN except every (FR/IN)th point which has separation IN-1 from the preceding intensified point.
3. FR<IN. All intensified points have separation IN-IN/FR.
4. FR=nIN. Only n points are intensified, all with separation IN.

Cases 1 and 2 are generally useful, since either the desired points are spaced evenly with an integral spacing (case 1) or they are spaced evenly with a non-integral spacing (case 2). Cases 2 and 3 are redundant. Case 4 is occasionally a nuisance but is useful when points after a certain time are not desired.

The point at which the train of intensified points begins is determined by the delay (DL) constant.

---

*Hereafter referred to as the discrete data set or discrete set.

b. Data Transfer

Points in the displayed memory which are intensified by means of the commands IN, FR and DL are transferred to another section of memory (2000-3777 currently) for further processing by the Data Transfer (DT) or Add Data (AD) commands. There are three options for preconditioning the points to be transferred and two options for storage of these points. The preconditioning options are:

1. Appending an M to the command (DTM or ADM) initiates a search over a predetermined range (RA) and the transfer of that point which has the maximum (algebraic) value.
2. Appending an A to the command (DTA or ADA) averages the 2^n+1 points centered about the intensified point (n=RA) and transfers this average multiplied by $\frac{n+1}{n}$.
3. Setting RA=1 and appending either A or M transfers the intensified points exactly.

The storage options are:

1. The DT command writes the new data over the old, and only those points which were transferred with the last command are available for further manipulation.
2. The AD command adds data to the existing discrete set. If there is no discrete data set as yet the DT and AD commands are equivalent.

The M transfers are useful when the echoes are clearly defined and signal-to-noise is good. M transfers are also convenient when the interval between intensified points does not exactly equal the

interval between echoes. An A transfer will be preferable when the pulse repetition rate is such that clear echoes do not form, or when the decay is noisy. AD transfers are a remnant from manual data collection for 2-pulse T_1 measurements but may be of some use in combining two data sets.

4. The Discrete Data Set

The discrete data set consists of precisely those points* which are to be fitted to an exponential decay, and can be displayed on the scope by the D2 command. Before performing the least-square analysis points which are obviously in error may be removed by the Delete Point (DP) command.

If the baseline is not already at zero the Baseline Correction (BC) command will subtract the average value of the last BL points from the rest of the discrete set.

a. Fitting to an Exponential Decay

The LS command will take the logarithm of each point† in the discrete set and fit the resulting data to a straight line. A weighted least-squares method is used with each point weighted by its magnitude in the exponential. This is done because we really want to give each point equal weight so that an uncertainty for any point contributed equally to the uncertainty in the slope. But $\ln x_i = \frac{\delta x_i}{x_i}$ and small values

---

*Stored in memory as $x_1, y_1; x_2, y_2; \ldots x_n, y_n$ DTA1=x_1, DTAN=y_n+1.

†Multiplied by a scaling factor, FACTR, equal to 1024.

of x are unduly important after the curve has been linearized. So multiplying each point by a weight of y_i removes the erroneous importance the linearization process gives to small values. The weights are stored sequentially following y_{NP}. After the fitting process the scope displays the deviations from theoretical (straight) line. If there is systematic deviation or if some points are obviously erroneous the exponential data may be regained with the EX command. Then the baseline may be adjusted (AC) or the offensive points removed (DP) and the slope recalculated (LS). Baseline adjustment is most useful in T_1 measurements, when the points taken as baseline (BC) may not be equilibrium values.

If the fitting procedure encounters points which are negative whether through excessive noise or operator error, an error message is typed but the calculation proceeds. This usually results in a reasonably accurate slope but large standard deviation. The offending point may be easily identified in the display. No matter what the display looks like at this point the data can be recalled with the EX command and the appropriate corrections made. The equation used to determine the time constant is

$$\frac{1}{T_1} = \frac{\Sigma w_i^2 x_i^2 \; \Sigma w_i^2 y_i - \Sigma w_i^2 \Sigma w_i^2 x_i y_i}{(\Sigma w_i^2 x_i)^2 - \Sigma w_i^2 \Sigma w_i^2 x_i^2} \qquad \text{(A1)}$$

where $w_i = \frac{S_i}{\Sigma S_i}$ $\quad S_i$ = signal amplitude at point i

The standard deviation is calculated as

$$\sigma = \frac{2}{x_{max} - x_{min}} \left[\frac{\sum_i^n \left(\frac{x_i}{T_1} + b - y_i\right)^2}{N - 1} \right]^{1/2} \qquad \text{(A2)}$$

$$\text{when } b = \frac{\Sigma w_i^2 x_i \Sigma w_i^2 x_i y_i - \Sigma w_i^2 x_i^2 \Sigma w_i^2 y_i}{(\Sigma w_i^2 x_i)^2 - \Sigma w_i^2 \Sigma w_i^2 x_i^2} . \qquad \text{(A3)}$$

If the data points are distributed about their true values in a Gaussian distribution then the true decay rate will have a 95% probability of lying in the interval $\frac{1}{T_1} \pm 2\sigma$. The teletype output will consist of $\frac{1}{T_1}$ and σ, then T_1 and σ', where $\sigma' = T_1{}^2\sigma$.

5. Other Features

PRINT (PR) The points which are contained in the discrete data set may be printed out in the sequence x_i, y_i, where x_i is the time in seconds from the 180° pulse and y_i is the magnitude of the ith point.

UP, DOWN and D1 (UP, DN,D1) Since the memory reserved for the discrete data is larger than the typical data set more than one set may be stored. This is done by using the UP command. To avoid needing a directory to these data sets it is assumed that they are all the same size (NP points). By means of the UP and DN commands one may shift from displaying the nth discrete set to the (n+1)th and the (n-1)th set, respectively. The D1 command allows the first data set to be viewed. Only the data viewed can be manipulated as described in Section 3 but note that a least squares analysis of set n will destroy set n+1.

PAGE 1 (P1) For convenience in permanently storing teletype output a division and sequential page number is typed every 11" (100_8 lines). The P1 command initializes this line count.

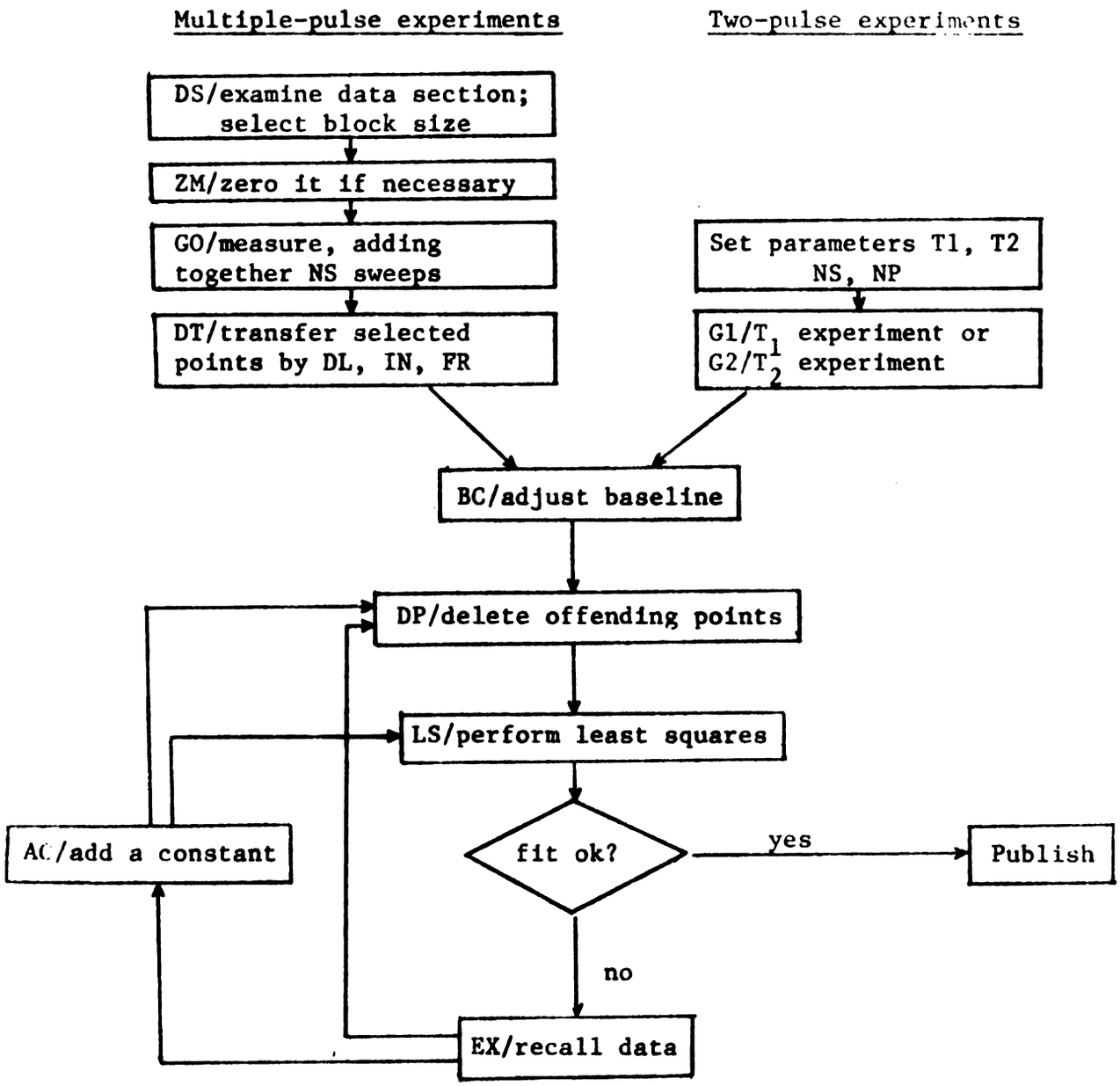

Figure A1. A flow chart for the operation of RELAX2.

Table A1. Legal Commands for RELAX2

Commands are listed grouped according to that part of the program to which they are relevant.

Displayed Memory

ZM - zero memory (c)
DS - display data section selected by pushbuttons (C)
IN - interval between points (I)
FR - fraction of interval (I)
DL - delay to 1st intensified point (I)
DT(A,M) - data transfer intensified points (C)
AD(A,M) - data transfer intensified points (C)
RA - range over which to search for maximum (M) or average (A)(I)

Discrete Set

D2 - display current discrete set (C)
UP - display next higher discrete set (C)
DN - display next lower discrete set (C)
D1 - display 1st discrete set (C)

Data Manipulation

DW - dwell time in seconds (R)
BC - subtract average of last BL points from rest of data (C)
BL - number of points to be taken as baseline (I)
LS - perform weighted least squares (C)
EX - recall data prior to LS calculation (C)
AC - add a constant (BA) to data (C)
BA - constant to be added to data (I)
DP - delete point (I)

Data Acquisition

G0 - jump to measure mode and take NS·Autostop sweeps. (C)
G1 - perform T_1 180°-τ-90° experiment (C)
G2 - perform T_2 90°-τ-180°-τ experiment (C)
NS - number of sweeps to take with G0, G1 or G2 (I)
NP - number of points to take with G1 and G2 (I)
T1 - the estimate of T_1 (R)
T2 - the estimate of T_2 (R)
IL - integration limit for T_1(I)
SE - set up mode produces a long series of pulses at a convenient repetition rate

Miscellaneous

P1 - reset page counter (C)
PR - print out data in discrete set (C)
MO - call monitor (C)

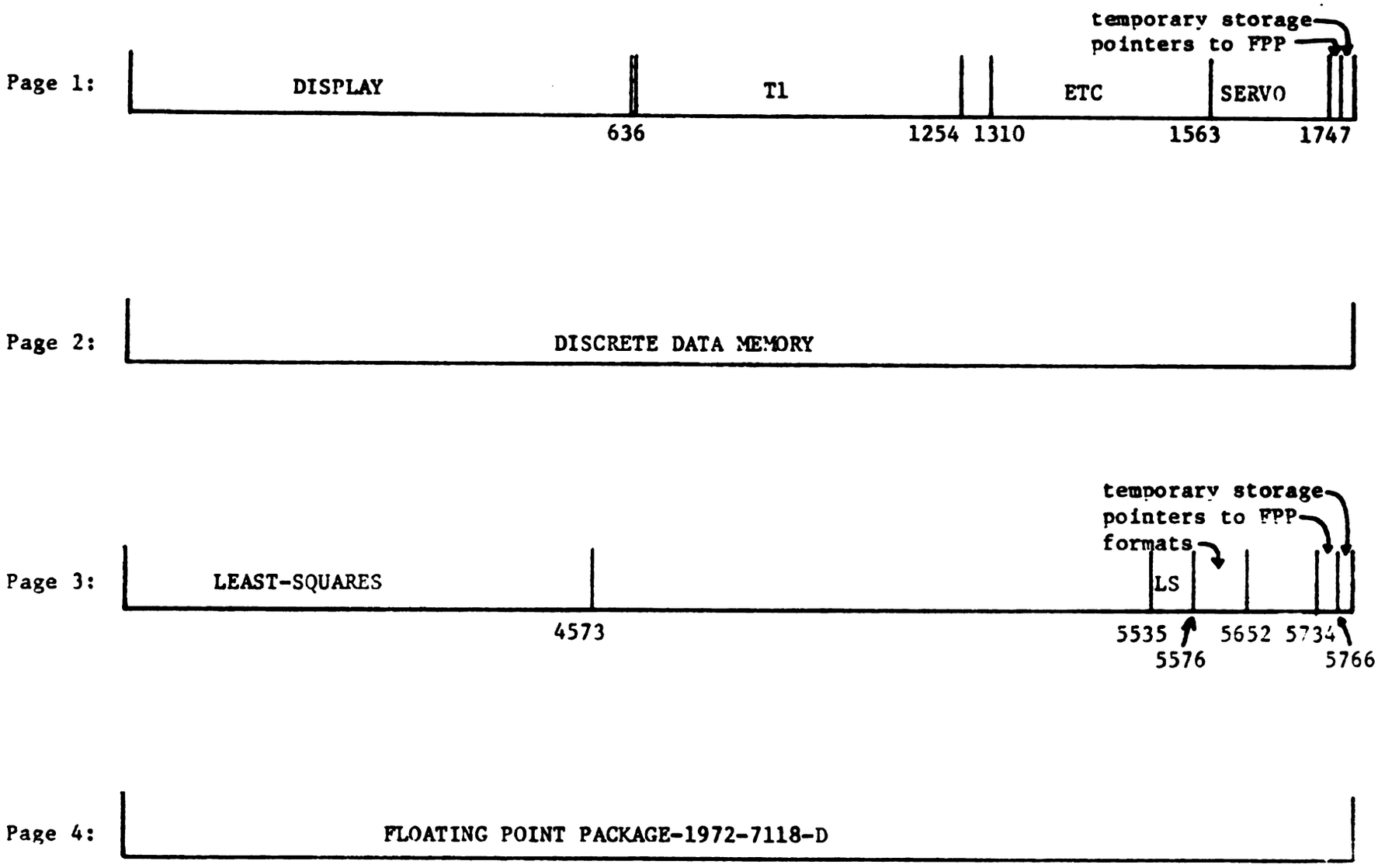

Figure A2. Core map for RELAX2.

Table A2. Useful addresses

Address	Contents	
577	2000	/LLIMIT; absolute lower limit discrete data set
600		/DTA1; current lower limit
601		/DTAN; current upper limit
602	3776	/ULIMIT; absolute upper limit
5646	20000	/FACTR; multiplicative factor for least squares.

Table A3. Error messages

NO MORE ROOM - Discrete data memory full

RA TOO LARGE - obvious

BL TOO LARGE - obvious

A OR M MUST FOLLOW DT - obvious

SET RA = 2**N - obvious

#X's.NE.#Y's - should never occur

NEG POINT - Discrete point set should contain only positive numbers during LS

FPP ERROR FLAG - should never occur.

```
*0/      DATA HANDLING AND DISPLAY ROUTINES

       0   44453  RDTTY
       1 2001573  START,JMS SERVO
       2    5431  REALS
       3    5435  COMMANDS
       4    5462  INTEGERS
       5    5474  CDEST

/MATH ROUTINE ENTRIES
       6 3001765  CALC1,JMS @MASTER
       7     577  DTA1
      10     600  DTAN
      11     155  JMP DSPLY2


/DISPLAY #1
      12 2000135  D1,JMS STATWD
      13 2165771  ZERM BLOCK
      14 2110153  MEMA STAT2
      15 2405770  ACCM DECR
      16 2110624  MEMA INTV
      17 2405772  ACCM INTDEC
      20 2110627  MEMA DELAY
      21 2405773  ACCM DELDEC
      22 2110602  MEMA DATA1
      23 2405776  ACCM DATAP
      24 2110623  MEMA INTADJ
      25 2405775  ACCM ADJDEC
      26  170000  ZERA
      27  214001  TACXD

      30 3111776  D2,MEMA @DATAP
      31  105000  VDSH
      32    4012  TACYD
      33 2103771  MEMZ BLOCK
      34      41  JMP D11
      35 2707773  MMOMZ DELDEC
      36      51  JMP D5
      37 2025771  ONEM BLOCK
      40      50  JMP D6
      41 2707775  D11,MMOMZ ADJDEC
      42      46  JMP D4
      43 2705772  MMOM INTDEC
      44 2110623  MEMA INTADJ
      45 2405775  ACCM ADJDEC
      46 2707772  D4,MMOMZ INTDEC
      47      51  JMP D5
      50 2000060  D6,JMS INTZ
      51    4014  D5,INCXD
      52 2125776  MPOM DATAP
      53 2707770  MMOMZ DECR
```

```
 54        30  JMP D2
 55      6454  TTYRF

 56        12  D7,JMP D1
 57         1  JMP START

 60         0  INTZ,0
 61    110300  MEMA (300
 62   2404614  ACCM TEMP1     /# OF TIMES BRI HT NED POINT
 63   3111776  D3,MEMA @DATAP
 64    105000  VDSH
 65      4012  TACYD
 66   2706614  MMOMZ TEMP1
 67        63  JMP D3
 70   2110624  MEMA INTV
 71   2405772  ACCM INTDEC      /RESTORES INTERVAL COUNTER
 72   1000060  JMP @INTZ


/DATA TRANSFER
 73   2110577  DT1,MEMA DTA1     /DATA TRANS FOR INTZ PTS
 74   2404600  ACCM DTAN
 75   2110050  MEMA D6
 76   2404612  ACCM D6STOR
 77    110107  MEMA (DTRANS     /GETS ADDRESS OF SUBROUTINE
100   2510575  A+MA CNST1
101   2404050  ACCM D6
102    110186  MEMA (DT2        /PROVIDES FOR EXIT7W6T6
103   2404056  ACCM D7          /OF INSTRUCTIONS AFTER
104   2001613  JMS ECHO
105   2404621  ACCM WORD1      /STORE  A OR M COMMAND
106        12  JMP D1

107         0  DTRANS,0
110   2000445  JMS DPREP
111   2110611  MEMA MAXP       / X
112   2470574  A-MA ONEHT
113   3404600  ACCM @DTAN
114   2124600  MPOM DTAN
115   2110607  MEMA YMAX      / Y
116   3404600  ACCM @DTAN
117   2134600  MPOMA DTAN
120   2330601  M-AA ULIMIT     /PREVENTS DATA OVERFLOW
121      5144  EXCT AC19
122       554  JMP ERRX3
123   2110624  MEMA INTV
124   2405772  ACCM INTDEC       /RESTORES INTERVAL COUNTER
125   1000107  JMP @DTRANS

126   2102610  DT2,MEMZ ADDENT
127   2000861  JMS ADDATA
130   2110612  MEMA D6STOR
131   2404050  ACCM D6           /RESTORES OLD INSTRUCTION
```

```
    132  110012  MEMA (D1
    133 2404056  ACCM D7            /DITTO
    134     155  JMP DSPLY2

/STATUS WORD
    135       0  STATWD,0      /GETS STATUS WORD & STORED
      136   44034  STATUS       /ADDRESS IN STAT1 AND READ
      137   10017  ANDA (17      /IN STAT2
    140    5012  LASH 12
    141 2510154  A+MA STAT3
    142 2404602  ACCM DATA1
    143   44034  STATUS
    144  210000  ACPA
    145   12360  ANDAZ (360
    146  162000  ZERZ
    147  110400  MEMA (400
    150    5006  LASH 6
    151 2404153  ACCM STAT2
    152 1000135  JMP @STATWD

    153       0  STAT2,0
    154  100000  STAT3,100000

/DISPLAY #2
    155 2110577  DSPLY2,MEMA DTA1
    156 2332600  M-AZA DTAN
    157    5144  EXCT AC19
    160       1  JMP START
    161 2404615  ACCM TEMP2
    162 2110577  MEMA DTA1
    163 2405776  ACCM DATAP

    164 3111776  D23,MEMA @DATAP
    165    5002  LASH 2      /X AXIS SCALE
    166  214001  TACXD
    167 2125776  MPOM DATAP
    170  110300  MEMA (300
    171 2404614  ACCM TEMP1
    172 3111776  D24,MEMA @DATAP
    173  105000  VDSH
    174    4012  TACYD
    175 2706614  MMOMZ TEMP1
    176     172  JMP D24
    177 2125776  MPOM DATAP
    200 2704615  MMOM TEMP2
    201 2706615  MMOMZ TEMP2
    202     164  JMP D23
    203    6454  TTYRF
    204     155  JMP DSPLY2
    205       1  JMP START

/TYPE 3
    206       0  TYPE3,0
```

```
207 3110206  MEMA @TYPE3      /GETS ADDRESS OF WORDS
210 2404266  ACCM T3PTR
211 2124206  MPOM TYPE3
212 3112266  T31,MEMAZ @T3PTR
213  162000  ZERZ
214     252  JMP T33
215 2024605  ONEM TO
216  110003  MEMA (3            / 3 CHARS PER WOR
217 2404604  ACCM FROM
220 3110266  MEMA @T3PTR
221    5104  SKIP AC19
222 2164605  ZERM TO
223   10077  T32,ANDA (77
224  470040  A-MA (40
225    5144  EXCT AC19       / NO. LESS THAN 40
226  510100  A+MA (100
227  510240  A+MA (240       /NO
230  462312  A-MZ (312       /  CR/J ?
231  162000  ZERZ
232     235  JMP T34
233  462315  A-MZ (315       /  LF/M ?
234     237  JMP T35         /NOT CR OR LF
235 2102605  T34,MEMZ TO
236  470100  A-MA (100       /ITS A CR OR LF
237 2001624  T35,JMS TYPE
240 3110266  MEMA @T3PTR
241    5066  RLSH 6
242 3404266  ACCM @T3PTR
243 2706604  MMOMZ FROM
244     223  JMP T32
245 3110266  MEMA @T3PTR
246    5062  RLSH 2         /RESTORES WORD TO ORIGINAL
247 3404266  ACCM @T3PTR
250 2124266  MPOM T3PTR
251     212  JMP T31
252 1000206  T33,JMP @TYPE3


/ADD DATA ROUTINE
253 2110577  ADD1,MEMA DTA1
254 2404613  ACCM OLDD1
255 2110600  MEMA DTAN
256 2404577  ACCM DTA1
257 2024610  ONEM ADDENT
260      73  JMP DT1

261       0  ADDATA,0
262 2110613  MEMA OLDD1
263 2404577  ACCM DTA1
264 2164610  ZERM ADDENT
265 1000261  JMP @ADDATA
```

```
/PACKS WORDS FOR TYPE3
    266        0  T3PTR,0
    267        0  PACK,0
    270  3110267  MEMA @PACK
    271  2405770  ACCM NUMBER      /ADDRESS
    272  3111770  MEMA @NUMBER
    273  2405770  ACCM NUMBER      /VALUE
    274  2124267  MPOM PACK
    275  3110267  MEMA @PACK
    276  2405771  ACCM ADDRESS      /ADDRESS
    277  2124267  MPOM PACK
    300   110007  MEMA (7
    301  2404614  ACCM TEMP1
    302  2111770  MEMA NUMBER
    303     5063  RLSH 3
    304     5043  W3,LLSH 3
    305  2404621  ACCM WORD1
    306  2704614  MMOM TEMP1
    307  2012573  ANDAZ MASK3
    310      313  JMP W4
    311  2110621  MEMA WORD1
    312      304  JMP W3

    313  2714614  W4,MMOMA TEMP1
    314  2404615  ACCM TEMP2
    315  2110346  MEMA BLNKWD
    316  2102615  W2,MEMZ TEMP2
    317   162000  ZERZ
    320      324  JMP W5
    321     5066  RLSH 6
    322  2704615  MMOM TEMP2
    323      316  JMP W2

    324  2405772  W5,ACCM PAKDWD
    325  2111770  MEMA NUMBER
    326  2404621  W1,ACCM WORD1
    327    10007  ANDA (7
    330   510020  A+MA (20
    331  2515772  A+MMA PAKDWD
    332  2102614  MEMZ TEMP1
    333   162000  ZERZ
    334      343  JMP W6
    335     5046  LLSH 6
    336  2405772  ACCM PAKDWD
    337  2110621  MEMA WORD1
    340     5063  RLSH 3
    341  2704614  MMOM TEMP1
    342      326  JMP W1
    343  2111772  W6,MEMA PAKDWD
    344  3405771  ACCM @ADDRESS
    345  1000267  JMP @PACK

    346  2404040  BLNKWD,2404040
```

```
/BASELINE CORRECTION
    347 2110622  BSLN,MEMA BASEL
    350    5144  EXCT AC19
    351 2234622  ANGMA BASEL     /BASEL MUST BE POSITIVE
    352 2404614  ACCM TEMP1
    353 2110600  MEMA DTAN
    354 2470577  A-MA DTA1
    355    5021  RASH 1
    356 2472622  A-MAZ BASEL      /BASEL TOO LARGE?
    357    5144  EXCT AC19
    360     562  JMP ERRX5       /YES
    361  170000  ZERA            /ZEROES FAC
    362 3001766  JMS @IFLOC
    363 2704600  MMOM DTAN
    364 3110600  BS1,MEMA @DTAN
    365 3001767  JMS @IFLOR
    366 3001750  JMS @FADD
    367 2704600  MMOM DTAN
    370 2704600  MMOM DTAN
    371 2706614  MMOMZ TEMP1
    372     364  JMP BS1
    373 2124600  MPOM DTAN
    374 2110622  MEMA BASEL
    375 3001767  JMS @IFLOR
    376 3001752  JMS @FDIV
    377 3001761  JMS @FIX
    400     401  JMP BSLN2

    401 2130577  BSLN2,MPOA DTA1
    402 2405773  ACCM PNTR2
    403 3111763  BS2,MEMA @FACM
    404 3325773  M-AM @PNTR2
    405 2135773  MPOMA PNTR2
    406 2322600  M-AZ DTAN
    407  162000  ZERZ
    410     155  JMP DSPLY2
    411 2125773  MPOM PNTR2
    412     403  JMP BS2

/SHIFTS DISPL 2 UP ONE BLOCK OF DATA
    413 2110600  UP,MEMA DTAN
    414 2404577  ACCM DTA1
    415 2110630  UP1,MEMA NPOINTS
    416    5001  LASH 1
    417 2510600  A+MA DTAN
    420 2330601  M-AA ULIMIT    /OUTSIDE ALLOWED REGION?
    421    5144  EXCT AC19
    422     426  JMP DOWN       /YES
    423 2330601  M-AA ULIMIT
    424 2404600  ACCM DTAN
    425     155  JMP DSPLY2
/SHIFTS DOWN ONE
```

```
426 2110577  DOWN,MEMA DTA1
427 2404600  ACCM DTAN
430 2110630  MEMA NPOINTS
431     5001  LASH 1
432 2330577  M-AA DTA1
433 2470576  A-MA LLIMIT   /OUTSIDE ALLOWED REGION?
 434     5144  EXCT AC19
435      413  JMP UP        /YES
436 2510576  A+MA LLIMIT
437 2404577  ACCM DTA1
440      155  JMP DSPLY2
/GOES BACK TO THE FIRST DISPLAY
441 2110576  FIRST,MEMA LLIMIT
442 2404577  ACCM DTA1
443 2404600  ACCM DTAN
444      415  JMP UP1


445        0  DPREP,0
446 2110626  MEMA RANGE      /RANGE IS T  # OF POINTS
  447  405021  RISH 1          /OR SEARCHED
450 2404616  ACCM RANGE1
451 2511776  A+MA DATAP
452 2404605  ACCM TO
453 2110616  MEMA RANGE1
454 2331776  M-AA DATAP
455 2404604  ACCM FROM

456 2110621  MEMA WORD1      /STORAGE FOR A OR M COMMAND
  457  462301  A-MZ (301       / A?
460  162000  ZERZ
461      466  JMP SIGAVE
462  462315  A-MZ (315      / M?
463      565  JMP ERRX6     /NEITHER
464 2000530  JMS MAX
465 1000445  JMP @DPREP

466 2164607  SIGAVE,ZERM YMAX
467     5210  CLL
470 3110604  SIG1,MEMA @FROM      /SUMS N POINTS
471 2504607  A+MM YMAX
472 2134604  MPOMA FROM
473 2330605  M-AA TO
474  422000  APOZ          /DONE?
475      470  JMP SIG1

476     5141  EXCT L     /TESTS FOR OVERFLOW
477      557  JMP ERRX4
500  110010  MEMA (10
501 2404620  ACCM OOPS       /PREVENTS ENDLESS LOOPING
502 2164617  ZERM COUNT
503 2110626  MEMA RANGE
504 2002527  SIG2,ANDZ MASK5   /3777776
```

```
505      513  JMP SIG4
506  2110526  MEMA SHIFT          /STORES CODE FOR "RASH"
507  2510617  A+MA COUNT
510  2404521  ACCM SIG3
511  2110607  MEMA YMAX
512      521  JMP SIG3
513  2124617  SIG4,MPOM COUNT
514  2706620  MMOMZ OOPS
515   162000  ZERZ
516      570  JMP ERRX7
517     5061  RLSH 1
520      504  JMP SIG2
521     5021  SIG3,RASH 1
522  2404607  ACCM YMAX
523  2111776  MEMA DATAP
524  2404611  ACCM MAXP
525  1000445  JMP @DPREP

526     5020  SHIFT,5020
527  3777776  MASK5,3777776
530        0  MAX,0
531  2110604  MEMA FROM
532  2404606  ACCM XMAX
533  2404611  ACCM MAXP
534  3110606  MEMA @XMAX
535  2404607  ACCM YMAX
536  2134606  M1,MPOMA XMAX
537  2330605  M-AA TO
540   422000  APOZ
541   162000  ZERZ
542  1000530  JMP @MAX
543  3110606  MEMA @XMAX          /NO
544  2330607  M-AA YMAX      /NEW Y LARGER THAN OLD?
545     5104  SKIP AC19
546      536  JMP M1               /NO
547  2110606  MEMA XMAX
550  2404611  ACCM MAXP
551  3110611  MEMA @MAXP
552  2404607  ACCM YMAX            /YES
553      536  JMP M1

554  2000206  ERRX3,JMS TYPE3
555     5366  ERROR3
556      126  JMP DT2
557  2000206  ERRX4,JMS TYPE3
560     5375  ERROR4
561      126  JMP DT2
562  2000206  ERRX5,JMS TYPE3
563     5403  ERROR5
564        1  JMP START
565  2000206  ERRX6,JMS TYPE3
566     5411  ERROR6
567      126  JMP DT2
```

```
570 2000206  ERRX7, JMS TYPE3
571     5422  ERROR7
572      126  JMP DT2

573  700000  MASK3,700000
574  100000  ONEHT,100000
575 2000000  CNST1,2000000
576     2000  LLIMIT,2000     /ABSOLUTE LOWER LIMIT
 577     2000  DTA1,2000
600        0  DTAN,0
601     3776  ULIMIT,3776     /ABSOLUTE UPPER LIMIT
 602  100000  DATA1,100000
603  107777  DATAN,107777
604        0  FROM,0
605        0  TO,0
606        0  XMAX,0
607        0  YMAX,0
610        0  ADDENT,0        /ENTRY MARKER MUST BE SAVED
  611        0  MAXP,0
612        0  D6STOR,0
613        0  OLDD1,0
614        0  TEMP1,0
615        0  TEMP2,0
616        0  RANGE1,0
617        0  COUNT,0
620        0  OOPS,0
621        0  WORD1,0
/THE FOLLOWING LOCATIONS MUST BE SAVED
/AS THEY ARE THE CONSTANTS SET VIA SERVO
622        1  BASEL,1         /BL-# OF PTS TAKEN AS BAS
  623     5000  INTADJ,5000     /FR-FRACTIONAL PART OF
  624      500  INTV,500        /IN-INTERVAL BETWEENED
  625      400  ILIMIT,400      /IL-INTEGRATION LIMIT
  626        0  RANGE,0         /RA-SEARCHING INTRVL FOR
  627        0  DELAY,0         /DL-DELAY TO 1ST INTENSI
  630        0  NPOINTS,0       /NP
631        0  NSWEEPS,0       /NS
632        0  BLSHIFT,0       /BA-AMT BASELINE IS SHIFTED
  633        0  T1EST,0

634        0  0
635        0  T2EST,0
636        0  0
*1770
/THE FOLLOWING LOCATIONS ARE USED ONLY BY PACK
 1770        0  NUMBER,0
1771        0  ADDRESS,0
1772        0  PAKDWD,0
/AND TH S IS USED BY BSLN
1773        0  PNTR2,0
*1770
/THE FOL  WING ARE USED BY DISPLAY #1
1770        0  DECR,0
```

```
   1771        0  BLOCK,0
   1772        0  INTDEC,0
   1773        0  DELDEC,0
   1774        0  DLPDEC,0
   1775        0  ADJDEC,0
   1776        0  DATAP,0
*7600
DEMON,
/THE FOLLOWING ARE ADDRESSES IN T1 PROGRAM
*1230
GO-T1,
*1236
GO-T2,
*1075
ZRMEM,
*1162
EXPNT,
*1203
SETUP,
*1212
ADCNST,
/THE FOLLOWING ARE ADDRESSES IN SERVO
*1573
   1573        0  SERVO,0
*1613
   1613        0  ECHO,0
*1624
   1624        0  TYPE,0
/THE FOLLOWING ARE ADDRESSES IN ETC
*1310
PRINT,
*1447
PAGE1,
*1452
DLPNT,
*1515
MEASURE,
/THIS IS ALL FROM LEAST-SQUARES
*4017
   4017     2000  DWELL,2000
   4020  1000000  1000000
*1750
   1750     7245  FADD,7245
   1751     7416  FMULT,7416
   1752     7461  FDIV,7461
   1753     6736  FLIP,6736
   1754     7062  GETAC,7062
   1755     7050  GETAR,7050
   1756     7026  FACFAR,7026
   1757     7074  PUTAC,7074
   1760     7534  FLOAT,7534
   1761     7541  FIX,7541
   1762     7572  FACE,7572
```

```
   1763     7573  FACM,7573
   1764     7574  FACML,7574
   1765     4000  MASTER,4000
   1766     4021  IFLOC,4021
   1767     4026  IFLOR,4026

*5366
   5366 3171640  ERROR3,3171640       /NO MORE ROOM
     5367  171540  0171540
   5370 2400522  2400522
   5371 3171722  3171722
   5372  404015  0404015
   5373 2121215  2121215
   5374        0  0
   5375 3012240  ERROR4,3012240       /RA TOO LARGE
     5376 3172440  3172440
   5377 3144017  3144017
   5400 3072201  3072201
   5401 2121505  2121505
   5402        0  0
   5403 3140240  ERROR5,3140240      / BL TOO LARGE
     5404 3172440  3172440
   5405 3144017  3144017
   5406 3072201  3072201
   5407 2121505  2121505
   5410        0  0
   5411 2400140  ERROR6,2400140      /A OR M MUST FOLLOW DT
     5412 2402217  2402217
   5413  154015  0154015
   5414 3242325  3242325
   5415 3170640  3170640
   5416 3171414  3171414
   5417 3044027  3044027
   5420 2121524  2121524
   5421        0  0
   5422 3052340  ERROR7,3052340    /SET RA = 2**N
     5423 3224024  3224024
   5424 2754001  2754001
   5425 2526240  2526240
   5426 2401652  2401652
/TABLE OF LEGAL INSTRUCTIONS
   5427 2121540  2121540
   5430        0  0
   5431  304327  REALS,304327     /DW
   5432  324261  324261           /T1
   5433  324262  324262           /T2
   5434        0  0
   5435  304323  COMMANDS,304323  /DS
   5436  315317  315317           /MO
   5437  301304  301304           /AD
   5440  304320  304320           /DP
   5441  314323  314323           /LS
   5442  302303  302303           /BC
```

```
   5443  304324  304324              /DT
   5444  332315  332315              /ZM
   5445  325320  325320              /UP
   5446  304316  304316              /DN
   5447  323305  323305              /SE
   5450  304261  304261              /D1
   5451  304262  304262              /D2
   5452  320261  320261              /P1
   5453  307317  307317              /GO
   5454  307261  307261              /G1
   5455  307262  307262              /G2
   5456  305330  305330              /EX
   5457  301303  301303              /AC
   5460  320322  320322              /PR
   5461       0  0
   5462  322301  INTEGERS,322301     /RA
   5463  304314  304314              /DL
   5464  311316  311316              /IN
   5465  306322  306322              /FR
   5466  302314  302314              /BL
   5467  316323  316323              /NS
   5470  316320  316320              /NP
   5471  311314  311314              /IL
   5472  302301  302301              /BA
   5473       0  0
/TABLE OF DESTINATIONS
   5474    4017  CDEST,DWELL
   5475     633  T1EST
   5476     635  T2EST
   5477      12  D1
   5500    7600  DEMON
   5501     253  ADD1
   5502    1452  DLPNT
   5503       6  CALC1
   5504     347  BSLN
   5505      73  DT1
   5506    1075  ZRMEM
   5507     413  UP
   5510     426  DOWN
   5511    1203  SETUP
   5512     441  FIRST
   5513     155  DSPLY2
   5514    1447  PAGE1
   5515    1515  MEASURE
   5516    1230  GO-T1
   5517    1236  GO-T2
   5520    1162  EXPNT
   5521    1212  ADCNST
   5522    1310  PRINT
   5523     626  RANGE
   5524     627  DELAY
   5525     624  INTV
   5526     623  INTADJ
```

5527	622	BASEL
5530	631	NSWEEPS
5531	630	NPOINTS
5532	625	ILIMIT
5533	632	BLSHIFT

```
*640/   COMPUTER CONTROL FOR TWO PULSE EXPERIMENTS

SETM=4306
PULSE1=4102
PULSE2=4104
SENSE1=6112

    640 2110577  BEGIN,MEMA LLIMIT /LOWER LIMIT DATA STORE
    641 2404600  ACCM PNTR2
    642 2110630  MEMA NPOINTS      /NUMBER OF POINTS DESIRE
    643 2405770  ACCM NMPTS1
    644 2110631  MEMA NSWEEPS      /NUMBER OF SWEEPS PER PO
    645 2404615  ACCM SWDEC
    646 2164616  ZERM TIME            /DELAY TIME BETWEEN

    647 3001754  JMS @GETAC
    650     633  T1EST              /THE ESTIMATE OF T1
    651 2111154  MEMA CON1       /10**6/16
    652 3001767  JMS @IFLOR
    653 3001751  JMS @FMULT
    654  110100  MEMA (100      /16 TIMES 4 (OCTAL)
    655 3001767  JMS @IFLOR
    656 3001751  JMS @FMULT
    657 2000135  JMS STATWD
    660 2110153  MEMA STAT2      /READOUT BLOCK SIZE
    661 3001767  JMS @IFLOR
    662 3001752  JMS @FDIV

    663 3001253  JMS @FACTEM
    664 3001761  JMS @FIX
    665 3111763  MEMA @FACM
    666 2405775  ACCM IDWELL      /SOLEY FOR 8T1 WAIT
    667 3001254  JMS @TEMFAC
    670 2103250  MEMZ T1FLAG
    671 2001215  JMS SCALE        /REPLACE T1 WITH T2
    672 3001757  JMS @PUTAC
    673    1251  DWELL
    674 2111154  MEMA CON1        /NOW DIVIDE BY 10**6
    675 3001767  JMS @IFLOR
    676 3001752  JMS @FDIV
    677  110020  MEMA (20
    700 3001767  JMS @IFLOR
    701 3001752  JMS @FDIV
    702 3001757  JMS @PUTAC
    703    4017  DWELL2          /DWELL IN SECONDS

    704 2110630  MEMA NPOINTS
    705 3001767  JMS @IFLOR
    706 3001754  JMS @GETAC
    707     633  T1EST
    710 3001752  JMS @FDIV
    711 2103250  MEMZ T1FLAG
```

```
712 2001215  JMS SCALE
713 2111154  MEMA CON1
714 3001767  JMS @IFLOR
715 3001751  JMS @FMULT
716 3001761  JMS @FIX
717 3111763  MEMA @FACM
720 2405116  ACCM MULT1
721  110004  MEMA (4
722 2103250  MEMZ T1FLAG
723    5021  RASH 1        /SINCE T2 GOES THRU TIMER T
724 2001113  JMS MULTIPLY
725 2404617  ACCM INTRVL       / T1.(10**6)/4N =CYCLES
726 3111764  MEMA @FACML
727 2011156  ANDA MASK1       /3000000
730    5042  LLSH 2

731 2514617  A+MMA INTRVL       /T1(10**6)/4N
732 2404616  ACCM TIME       /IN UNITS OF 16 MICROSECS
733 2001100  JMS ZERMEM
734 2110620  MEMA P1HI
735 2405774  ACCM HITIME
736    1035  JMP AGAIN
737 2111774  PULSE,MEMA HITIME
740 2404612  ACCM WAIT2
741 2164614  ZERM COUNT2
742 2110616  MEMA TIME
743    4102  PULSE1
744 2001051  JMS TIMER
745    4104  PULSE2
746 2103250  MEMZ T1FLAG
747    1285  JMP ECHO      /T2-WAIT FOR THE ECHO
750  410000  ACCA           /THE SENSE LOOP GOES HERE
751  410000  ACCA
752    4306  P2,SETM
753    5220  STOP
754    6454  TTYRF
755  162000  ZERZ
756       1  JMP START
757 2706615  MMOMZ SWDEC
760    1035  JMP AGAIN         A/ANOTHER SWEEP WITH THI
761 2110612  MEMA WAIT2     /NO
762 3001766  JMS @IFLOC
763 2110621  MEMA COUNT
764 3001767  JMS @IFLOR
765 3001751  JMS @FMULT
766 3001755  JMS @GETAR
767    1152  CORRECTION   /MINIMUM PULSE SEP POSSIBLE
770 3001750  JMS @FADD
771 3001755  JMS @GETAR
772    1251  DWELL
773 3001752  JMS @FDIV
774 2111155  MEMA CON2     /10000
775 3505762  A+MM @FACE    / MULTIPLY BY 16
```

```
 776 3001761   JMS @FIX
 777 3111763   MEMA @FACM     / (WAIT2).(COUNT).16/DWELL=X
1000 2001066   JMS DTRANS
1001 2000135   JMS STATWD
1002 2110602   MEMA DATA1
1003 2405771   ACCM PNTR
1004 2510625   A+MA ILIMIT
1005 2405161   ACCM LAST
1006 3111771   S1,MEMA @PNTR
1007 2504613   A+MM SUM
1010 2135771   MPOMA PNTR
1011 2323161   M-AZ LAST        /100033
1012    1006   JMP S1
1013 2110613   MEMA SUM
1014 2001066   JMS DTRANS       / Y
1015 2164613   ZERM SUM
1016 2110617   MEMA INTRVL
1017 2514616   A+MMA TIME
1020    5104   SKIP AC19
1021    1027   JMP T11
1022  405021   RISH 1
1023 2404616   ACCM TIME       /HALVES LOW WORD
1024 2111774   MEMA HITIME
1025    5001   LASH 1
1026 2405774   ACCM HITIME     /DOUBLES HIGH WORD
1027 2707770   T11,MMOMZ NMPTS1       /DONE?
1030  162000   ZERZ
1031     155   JMP DSPLY8    /YES
1032 2110631   MEMA NSWEEPS
1033 2404615   ACCM SWDEC

1034 2001100   JMS ZERMEM

1035 2131775   AGAIN,MPOA IDWELL    /IDWELL CAN BE .LT. 1
1036 2405116   ACCM MULT1
1037 2110153   MEMA STAT2
1040    5023   RASH 3
1041 2001113   JMS MULTIPLY      / 2 DWELL(STAT2)/16= 8
1042 2404611   ACCM WAIT
1043 2110620   MEMA P1HI
1044 2404612   ACCM WAIT2
1045 2110611   MEMA WAIT
1046 2164614   ZERM COUNT2
1047 2001051   JMS TIMER
1050     737   JMP PULSE


1051       0   TIMER,0
1052 2404611   ACCM WAIT
1053 2164621   TI2,ZERM COUNT
1054 2134681   TI1,MPOMA COUNT
1055 2332611   M-AZA WAIT
1056    5144   EXCT AC19
```

```
1057     1061  JMP TIMER2
1060     1054  JMP TI1

1061 2134614  TIMER2,MPOMA COUNT2
1062 2332612  M-AZA WAIT2
1063     5144  EXCT AC19
1064 1001051  JMP @TIMER
1065     1053  JMP TI2

1066        0  DTRANS,0
1067 3404600  ACCM @PNTR2
1070 2134600  MPOMA PNTR2
1071 2332601  M-AZA ULIMIT
1072     5144  EXCT AC19
1073      554  JMP ERRX3
1074 1001066  JMP @DTRANS

1075  110012  ZRMEM,MEMA (DSPLY1 /FAKES JMS SO THAT
1076 2405100  ACCM ZERMEM        /ZERMEM CAN BE ENTERED
 1077  162000  ZERZ               /WITH A JMP COMMAND
 1100       0  ZERMEM,0
1101 2000135  JMS STATWD
1102 2110602  MEMA DATA1
1103 2405776  ACCM DATAP
1104 2510153  A+MA STAT2
1105 2404603  ACCM DATAN
1106 3165776  ZM1,ZERM @DATAP
1107 2135776  MPOMA DATAP
1110 2322603  M-AZ DATAN
1111     1106  JMP ZM1
1112 1001100  JMP @ZERMEM

1113        0  MULTIPLY,0
1114     4354  TACMQ
1115   505320  MULT
1116        0  MULT1,0
1117 2404620  ACCM P1HI
1120     4343  TMQAC
1121 2404611  ACCM WAIT
1122 2025116  ONEM MULT1
1123 2102620  M1,MEMZ P1HI
1124     1133  JMP LONGTIME     /PRODUCT .GT.2**20
  1125     5144  EXCT AC19
1126     1133  JMP LONGTIME     /WAIT IS TOO LARGE
1127 2111116  MEMA MULT1        /LONGTIME MAKES THIS LARG.
1130 2404620  ACCM P1HI         /NOW 1 IF ORIGIONALLY 0
1131 2110611  MEMA WAIT
1132 1001113  JMP @MULTIPLY

/LONGTIME HALVES LOW WORD, DOUBLES HIGH WORD
1133   405021  LONGTIME,RISH 1
1134 2404611  ACCM WAIT         /WAIT/2
1135 2110620  MEMA P1HI
```

```
1136     5110  SKIP AC0          /BIT 0 = 1?
1137     1142  JMP L1
1140 2111157  MEMA CON3
1141 2504611  A+MM WAIT         /YES, ADD IT TO WAIT
1142 2110620  L1,MEMA P1HI
1143   405021  RISH 1
1144 2404620  ACCM P1HI
1145 2111116  MEMA MULT1
1146     5001  LASH 1
1147 2405116  ACCM MULT1        /MULT1 * 2
1150 2110611  MEMA WAIT
1151     1123  JMP M1

1152     4000  CORRECTION,4000
1153 1100000  CORRM,1100000
1154   172044  CON1,172044
1155    10000  CON2,10000
1156 3000000  MASK1,3000000
1157 2000000  CON3,2000000      /TRANSFER BIT FOR LONGT
1160     7640  CON4,7640
1161   100033  LAST,100033

1162 2110577  EXPNT,MEMA LLIMIT
1163 2332600  M-AZA PNTR2            /DATA STOP
1164     5144  EXCT AC19
1165        1  JMP START
1166 2130577  MPOA LLIMIT            / Y1
1167 2405772  ACCM PNTR1
1170 2110600  MEMA PNTR2            / W1
1171 2405773  ACCM PNTR3
1172 3111773  EX1,MEMA @PNTR3
1173 3405772  ACCM @PNTR1
1174 2125772  MPOM PNTR1
1175 2125773  MPOM PNTR3
1176 2135772  MPOMA PNTR1
1177 2332600  M-AZA PNTR2
1200     5144  EXCT AC19
1201      155  JMP DSPLY2
1202     1172  JMP EX1

1203 2165774  SETUP,ZERM HITIME
1204 2111160  MEMA CON4
1205 2404616  ACCM TIME
1206 2224615  ANGM SWDEC          /JUST SOME LARGE NUMBER
1207   110764  MEMA (764
1210 2405775  ACCM IDWELL
1211      737  JMP PULSE

1212 2110632  ADCNST,MEMA LVLADJ
1213 3225763  ANGM @FACM
1214      401  JMP BSLN2
```

```
   1215        0  SCALE,0
   1216  3001755  JMS @GETAR
   1217      635  T2EST
   1220  3001751  JMS @FMULT
   1221  3001755  JMS @GETAR
   1222      633  T1EST
   1223  3001752  JMS @FDIV
   1224  1001215  JMP @SCALE

   1225  2110616  ECHO,MEMA TIME
   1226  2001051  JMS TIMER
   1227      752  JMP P2

/DETERMINES WHETIER OR NOT TO WAIT FOR THE ECHO
   1230  2165250  T1,ZERM T1FLAG
   1231  2111244  MEMA T1CONST
   1232  2405155  ACCM CON2
   1233  2111246  MEMA T1CORR
   1234  2405153  ACCM CORRM
   1235      640  JMP BEGIN
   1236  2025250  T2,ONEM T1FLAG
   1237  2111245  MEMA T2CONST
   1240  2405155  ACCM CON2
   1241  2111247  MEMA T2CORR
   1242  2405153  ACCM CORRM
   1243      640  JMP BEGIN
   1244    10000  T1CONST,10000
   1245    12000  T2CONST,12000
   1246  1120000  T1CORR,1120000
   1247  1100000  T2CORR,1100000
   1250        0  T1FLAG,0
   1251        0  DWELL,0
   1252        0  0
   1253     7034  FACTEM,7034
   1254     7042  TEMFAC,7042
*611
    611        0  WAIT,0
    612        0  WAIT2,0
    613        0  SUM,0
    614        0  COUNT2,0
    615        0  SWDEC,0
    616        0  TIME,0
    617        0  INTRVL,0
    620        0  P1HI,0
    621        0  COUNT,0
*1770
   1770        0  NMPTS1,0
   1771        0  PNTR,0
   1772        0  PNTR1,0
   1773        0  PNTR3,0
   1774        0  HITIME,0
   1775        0  IDWELL,0
   1776        0  DATAP,0
```

```
*401
BSLN2,
*135
    135        0  STATWD,0
*153
    153        0  STAT2,0
*1
START,
*155
DSPLY2,
*12
DSPLY1,
*625
    625      400  ILIMIT,400
*630
    630        0  NPOINTS,0
    631        0  NSWEEPS,0
    632        0  LVLADJ,0
    633        0  T1EST,0
    634        0  0
    635        0  T2EST,0
    636        0  0
*577
    577     2000  LLIMIT,2000
    600        0  PNTR2,0
    601     3774  ULIMIT,3774
    602   100000  DATA1,100000
    603   107777  DATAN,107777
*4017
   4017     2000  DWELL2,2000
   4020  1000000  1000000
*554
ERRX3,
*1750
   1750     7245  FADD,7245
   1751     7416  FMULT,7416
   1752     7461  FDIV,7461
   1753     6736  FLIP,6736
   1754     7062  GETAC,7062
   1755     7050  GETAR,7050
   1756     7026  FACFAR,7026
   1757     7074  PUTAC,7074
   1760     7534  FLOAT,7534
   1761     7541  FIX,7541
   1762     7572  FACE,7572
   1763     7573  FACM,7573
   1764     7574  FACML,7574
   1765     4000  MASTER,4000
   1766     4021  IFLOC,4021
   1767     4026  IFLOR,4026
```

```
*1350/  ETC (ADDITIONS TO DISPLAY ROUTINES)

SETM=4306
   1350        0  LCOUNT,0      / # OF LINE FEEDS THIS PAGE
     1351        0  NEWPG,0
   1352 2165350  NP1,ZERM LCOUNT
   1353 2001404  JMS LINEF
   1354 2001413  JMS DASH
   1355 2125560  MPOM PAGENUM
   1356 2000267  JMS PACK
   1357    1560  PAGENUM
   1360    1556  PAGE
   1361 2110206  MEMA TYPE3  /SAVES TYPE3 CONSTANTS
   1362 2405770  ACCM NP101
   1363 2110266  MEMA T3PNTR
   1364 2405771  ACCM NP102
   1365 2110604  MEMA TEMP1
   1366 2405772  ACCM NP103
   1367 2110605  MEMA TEMP2
   1370 2405773  ACCM NP104
   1371 2001422  JMS HEADING
   1372 2111770  MEMA NP101  /RECALLS TYPE3 CONSTANTS
   1373 2404206  ACCM TYPE3
   1374 2111771  MEMA NP102
   1375 2404266  ACCM T3PNTR
   1376 2111772  MEMA NP103
   1377 2404604  ACCM TEMP1
   1400 2111773  MEMA NP104
   1401 2404605  ACCM TEMP2
   1402 2001404  JMS LINEF
   1403 1001351  JMP @NEWPG

/GENERATES 2 LINE FEEDS
   1404        0  LINEF,0
   1405   110212  MEMA (212
   1406 2405774  ACCM CHAR
   1407   110002  MEMA (2
   1410 2405775  ACCM REP
   1411 2001437  JMS TYPE'M
   1412 1001404  JMP @LINEF

/GENERATES THE DASHES BETWEEN PAGES
   1413        0  DASH,0
   1414   110255  MEMA (255
   1415 2405774  ACCM CHAR
   1416   110010  MEMA (10
   1417 2405775  ACCM REP
   1420 2001437  JMS TYPE'M
   1421 1001413  JMP @DASH

   1422        0  HEADING,0
   1423   110240  MEMA (240
```

```
1424 2405774  ACCM CHAR
1425  110022  MEMA (22
1426 2405775  ACCM REP
1427 2001437  JMS TYPE'M
1430  110212  MEMA (212
1431 2001624  JMS TYPE
1432 2000206  JMS TYPE3
1433    1554  PAGEHEAD
1434  110215  MEMA (215
1435 2001624  JMS TYPE
1436 1001422  JMP @HEADING

/TYPES "CHAR" REP NUMBER OF TIMES
1437       0  TYPE'M,0
1440 2111775  MEMA REP
1441 2405776  ACCM REPDEC
1442 2111774  TP1,MEMA CHAR
1443 2001624  JMS TYPE
1444 2707776  MMOMZ REPDEC
1445    1442  JMP TP1
1446 1001437  JMP @TYPE'M

1447 2165560  PAGE1,ZERM PAGENUM
1450 2025351  ONEM NEWPG
1451    1352  JMP NP1

/POINT DELETE
1452 2111562  DLPNT,MEMA EQUALS
1453 2001564  JMS TYPE2
1454 3001753  JMS @FLIP
1455 3001761  JMS @FIX
1456 2110600  MEMA DTAN
1457 2470577  A-MA DTA1
1460    5021  RASH 1
1461 3473763  A-MAZ @FACM
1462  162000  ZERZ
1463    1512  JMP DP3
1464    5104  SKIP AC19       /POINT # MUST BE POS
1465    1471  JMP DP1
1466  110277  MEMA (277
1467 2001624  JMS TYPE
1470       1  JMP START
1471 3111763  DP1,MEMA @FACM
1472    5001  LASH 1
1473 2510577  A+MA DTA1
1474 2405771  ACCM OLDP
1475  750000  MTOA
1476 2511771  A+MA OLDP
1477 2405770  ACCM NEWP

1500 3111771  DP2,MEMA @OLDP
1501 3405770  ACCM @NEWP
1502 2125771  MPOM OLDP
```

```
   1503 2125770  MPOM NEWP
   1504 3111771  MEMA @OLDP
   1505 3405770  ACCM @NEWP          /SHIFTS Y DOWN TOO
   1506 2125770  MPOM NEWP
   1507 2135771  MPOMA OLDP
   1510 2322600  M-AZ DTAN
   1511    1500  JMP DP2

   1512 2704600  DP3,MMOM DTAN
   1513 2714600  MMOMA DTAN
   1514     155  JMP DISP2
/MEASURE
   1515 2130631  MPOA NSWEEPS
   1516 2405770  ACCM SWPDEC
   1517 2000135  ME1,JMS STATWD
   1520 2111561  MEMA AVENUM       /# OF POINTS TO BE AVERAG
   1521 2405771  ACCM AVEDEC
   1522 2165772  ZERM LVLADJ       /CORRECTION TO BE ADDED
   1523 2110602  MEMA DATA1
   1524 2510153  A+MA STAT2
   1525 2405773  ACCM DATAP
   1526 2705773  ME2,MMOM DATAP
   1527 3111773  MEMA @DATAP
   1530 2515772  A+MMA LVLADJ
   1531 2707771  MMOMZ AVEDEC
   1532    1526  JMP ME2
   1533    5023  RASH 3             /DIVIDE BY 10
   1534 2405772  ACCM LVLADJ        /THIS IS THE CORRECTION
   1535 2110602  MEMA DATA1
   1536 2405773  ACCM DATAP
   1537 2111772  ME3,MEMA LVLADJ    /START CORRECTING EACH PT
   1540 3325773  M-AM @DATAP
   1541 2135773  MPOMA DATAP
   1542 2706153  MMOMZ STAT2
   1543    1537  JMP ME3
   1544 2707770  MMOMZ SWPDEC
   1545  162000  ZERZ
   1546      12  JMP DSPL1
   1547    4306  SETM
   1550    5220  STOP
   1551    6454  TTYRF
   1552    1517  JMP ME1
   1553       1  JMP START

   1554 3012040  PAGEHEAD,3012040    /PAGE N
     1555 2400507  2400507
   1556       0  PAGE,0
   1557       0  0
   1560       1  PAGENUM,1
   1561      10  AVENUM,10
   1562  275240  EQUALS,275240
   1563    5535  PFLOP,5535    /FOR PRINT
*1310
```

```
   1310 2001607  PRINT,JMS CRLF
   1311 2001607  JMS CRLF
   1312 2110577  MEMA DTA1
   1313 2404606  ACCM TEMP3
   1314 2332600  PR1,M-AZA DTAN     /ANY POINTS?
     1315    5144  EXCT AC19
   1316       1  JMP START         /NO
   1317 3110606  MEMA @TEMP3
   1320 3001766  JMS @IFLOC
   1321 3001755  JMS @GETAR
   1322    4017  DWELL2
   1323 3001751  JMS @FMULT
   1324 2000206  JMS TYPE3
   1325    1346  FRMAT1
   1326 3001563  JMS @PFLOP
   1327 2124606  MPOM TEMP3
   1330 3110606  MEMA @TEMP3        /Y
   1331 3001766  JMS @IFLOC
   1332 3001755  JMS @GETAR
   1333    4017  DWELL2
   1334 3001751  JMS @FMULT
   1335 2000206  JMS TYPE3
   1336    1346  FRMAT1
   1337 3001563  JMS @PFLOP
   1340 2001607  JMS CRLF
   1341 2134606  MPOMA TEMP3
   1342    6454  TTYRF
   1343  162000  ZERZ
   1344     155  JMP DISP2
   1345    1314  JMP PR1
   1346 2404040  FRMAT1,2404040
   1347       0  0
*1564
   1564       0  TYPE2,0
*1753
   1753    6736  FLIP,6736
*1761
   1761    7541  FIX,7541
*1763
   1763    7573  FACM,7573
*12
DSPL1,
*153
    153       0  STAT2,0
*135
    135       0  STATWD,0
*1
START,
*155
DISP2,
*266
    266       0  T3PNTR,0
*604
```

```
   604        0  TEMP1,0
   605        0  TEMP2,0
   606        0  TEMP3,0     /FOR PRINT
*631
   631        1  NSWEEPS,1
*577
   577     2000  DTA1,2000
   600        0  DTAN,0
   601     3776  ULIMIT,3776
   602   100000  DATA1,100000
   603   107777  DATAN,107777
*1751
  1751     7416  FMULT,7416
*1755
  1755     7050  GETAR,7050
/FROM LEAST-SQUARES
*1766
  1766     4021  IFLOC,4021
*4017
  4017     2000  DWELL2,0002000
/FROM SERVO
*1607
  1607        0  CRLF,0
/USED ONLY AROUND HEADING
*1770
  1770        0  NP101,0
  1771        0  NP102,0
  1772        0  NP103,0
  1773        0  NP104,0
*1770
  1770        0  NEWP,0
  1771        0  OLDP,0
  1772        0  NPTS,0
*1624
  1624        0  TYPE,0
*1770
  1770        0  SWPDEC,0
  1771        0  AVEDEC,0
  1772        0  LVLADJ,0
  1773        0  DATAP,0
  1774        0  CHAR,0
  1775        0  REP,0
  1776        0  REPDEC,0
*206
   206        0  TYPE3,0
*267
   267        0  PACK,0
```

```
*1573/  A GENERAL SUBROUTINE FOR REAL-TIME PROGRAM CON

/THIS SURROUTINE PERFORMS THREE FUNCTIONS:
/ (1)  IT WILL ACCEPT ANY NUMBER OF FLOATING POINT DECI
 /        CONSTANTS AND PLACE THEM IN USER SELECTED ADDR
 / AND
/ (2)  IT WILL ACCEPT TYPED COMMANDS TO JUMP TO USER
 /        SELCETED ADDRESSES IN THE MAIN PROGRAM
/AND
/ (3)  IT WILL ALSO ACCEPT AND TRANSFER DECIMAL INTEGEF

/TWO CHARACTER ALPHANUMERIC ABBREVIATIONS ARE USED FOR
 / VARIOUS CONSTANTS AND COMMANDS.  THESE MUST BE LISTED
 /THEIR ASCII CODES STARTING AT LOCATION REALS.  THE TWO
 / ACTER CODES TO BE IDENTIFIED WITH CONSTANTS MUST BE 1
 / A ZERO (0) SEPARATES THEM FROM THE ABBREVIATIONS FOR
 / (DESIGNATED COMMANDS).  SEPARATED BY ANOTHER ZREOARE
 /THE ABBREVIATIS FOR INTEGERS (DESIGNATED INTEGERS).
 / TABLE MUST END WITH A ZERO

/THE TABLE OF DESTINATIONS MAY, LIKE THE TABLE OF LEGAL
 / ACTERS, BE LOCATED AT ANY POINT IN THE PROGRAM.  THIS
 / IS MERELY A LISTING OF THE LABELS, IN THE PROPER ORDE
 / WHICH THE ALPHANUMERIC COMMANDS REFER.

/THE FOLLOWING SEQUENCE IS USED TO CALL SERVO

/       ADDRESS--------CONTENTS

/          4          3000047   JMS @ SERVO
/          5                50   REALS
/          6                53   COMMANDS
/          7                55   INTEGERS
/         10                56   CDEST

/                .
/                .
/                .

/TABLE OF LEGAL CHARACTERS (ASCII CODES)
/         50          301302   REALS,30130((0188
/         51          302301   302301          /BA
/         52                0   0
/         53          307317   COMMANDS,307317 /GO
/          54               0   0
/         55                0   INTEGERS,0
/TABLE OF DESTINATIONS
/         56              406   CDEST,CONST1     /AB
/         60              187   CONST2           /BA
/         60               61   START            /GO
```

```
/THE ACTUAL PROGRAM STARTS HERE
/            61            44453  START,RDTTY
/
/                  .
/                  .
/           127                0  CONST2,0
/
/                  .
/                  .
/                  .
/
/           406                0  CONST1,0
```

```
/IN THIS EXAMPLE, TWO CONSTANTS ARE INPUTTED BY TYPING
 / "BA" ON THEPTELETYPE, FOLLOWED BYTYPING THE DECIMAL
  / CONSTANT.  THESE CONSTANTS ARE PLACED IN LOCATIONS
  / RESP.  ASSUMING THAT ADDERSS 61 IS THE START OF THE
  / CONTROL CAN BE TRANSFERED TO THIS LOCATION AT ANY T
   /  THERE ARE NO INTEGERS TO BE INPUTTED.
```

```
   1573        0  SERVO,0
   1574  2001607  S1,JMS CRLF
   1575  2001613  JMS ECHO
   1576     5011  LASH 11
   1577  2405770  ACCM CHAR      /STORES TYPED CHAR
   1600  2001613  JMS ECHO
   1601  2001651  JMS TBSRCH
   1602   110277  MEMA (277
   1603  2001624  JMS TYPE       /TYPES ?
   1604   110003  S2,MEMA (3 /RESETS POINTER TO TABLES
   1605  2325573  M-AM SERVO /COMMAND HAS BEEN TYPED
   1606     1574  JMP S1

   1607        0  CRLF,0
   1610  2111746  MEMA CONST
   1611  2001564  JMS PRINT
   1612  1001607  JMP @CRLF

   1613        0  ECHO,0
   1614  2001617  JMS READ
   1615  2001624  JMS TYPE
   1616  1001613  JMP @ECHO

   1617        0  READ,0
   1620     6454  R1,TTYRF
   1621     1620  JMP R1
   1622    44453  RDTTY
   1623  1001617  JMP @READ
```

```
1624        0  TYPE,0
1625 2405571  ACCM TEMP1      /SAVE ACC
1626  462212  A-MZ (212      /A LINE FEED?
1627  162000  ZERZ
1630 2125350  MPOM LCOUNT
1631     6444  T1,TTYPF
1632     1631  JMP T1
1633     4443  PRTTY
1634 2111350  MEMA LCOUNT
1635  332100  M-AZA (100      / 100 LINES PER PAGE
 1636     5144  EXCT AC19
1637 2001642  JMS TY2
1640 2111571  MEMA TEMP1
1641 1001624  JMP @TYPE

1642        0  TY2,0
1643 2111624  MEMA TYPE
1644 2405572  ACCM TEMP2     /SAVES RETURN ADDRESS
1645 2001351  JMS NEWPG
1646 2111572  MEMA TEMP2
1647 2405624  ACCM TYPE
1650 1001642  JMP @TY2


1651        0  TBSRCH,0  /TABLE SEARCHING ROUTINE
1652 2505770  A+MM CHAR
1653 3111573  MEMA @SERVO     /GETS ADDESS OF CHAR TABL
1654 2405771  ACCM TABL1
1655 2125573  MPOM SERVO
1656 3111573  MEMA @SERVO      /GETS ADDRESS ON COM TAB
1657 2405772  ACCM TABL2
1660 2125573  MPOM SERVO
1661 3111573  MEMA @SERVO      /GETS ADDRESS OF INTEGER
1662 2405773  ACCM TABL3
1663 2125573  MPOM SERVO
1664 3111573  MEMA @SERVO      /GETS ADDRESS OF DESTINA
1665 2405733  ACCM DESTN


1666 3113771  TB1,MEMAZ @TABL1    /SEARVH TABLE OF REAL
  1667  162000  ZERZ
1670     1677  JMP TB2
1671 2323770  M-AZ CHAR     /COMPERE WITH CHAR JUST TYP
  1672  162000  ZERZ
1673     1724  JMP DSET
1674 2125771  MPOM TABL1
1675 2125733  MPOM DESTN
1676     1666  JMP TB1


1677 3113772  TB2,MEMAZ @TABL2    / SEARCH TABLE OF COM
```

```
1700  162000  ZERZ
1701    1710  JMP TB3
1702 2323770  M-AZ CHAR
1703  162000  ZERZ
1704    1721  JMP DGO
1705 2125772  MPOM TABL2
1706 2125733  MPOM DESTN
1707    1677  JMP TB2

1710 3113773  TB3,MEMAZ @TABL3   /SEARCH TALBE OF INTE
  1711  162000  ZERZ
1712 1001651  JMP @TBSRCH     /ERROR EXIT
1713 2323770  M-AZ CHAR
1714  162000  ZERZ
1715    1735  JMP DINT
1716 2125773  MPOM TABL3
1717 2125733  MPOM DESTN
1720    1710  JMP TB3

1721 3111733  DGO,MEMA @DESTN
1722 2405733  ACCM DESTN
1723 1001733  JMP @DESTN

1724 2111747  DSET,MEMA CONST2
1725 2001564  JMS PRINT    /PRINTS =
1726 3111733  MEMA @DESTN   /CONVERTS POINTER TO DEST
1727 2405733  ACCM DESTN     /TO ACTUAL DESTINATION
1730 3001753  JMS @FLIP
1731 3111733  MEMA @DESTN
1732 3001757  JMS @PUTAC
1733       0  DESTN,0
1734    1604  JMP S2

1735 2111747  DINT,MEMA CONST2
1736 2001564  JMS PRINT     / PRINTS  =
1737 3111733  MEMA @DESTN   / CONVERTS POINTER TO DEST
1740 2405733  ACCM DESTN       /TO ACTUAL DESTINATION
1741 3001753  JMS @FLIP
1742 3001761  JMS @FIX
1743 3111763  MEMA @FACM       /LOCATION OF FIXED  #
1744 3405733  ACCM @DESTN
1745    1604  JMP S2

1746  212215  CONST,212815
1747  275240  CONST2,275240
*1564
1564       0  PRINT,0    /PRINTS 18-BIT WORD IN ACC AS
1565 2001624  JMS TYPE   /TWO ASCII CHARACTERS
1566    5031  RASH 11
```

```
   1567 2001624  JMS TYPE
   1570 1001564  JMP @PRINT
   1571        0  TEMP1,0     /ACC DURING TYPE
   1572        0  TEMP2,0     /RETURN ADDRESS DURING TYPE

*1770
   1770        0  CHAR,0
   1771        0  TABL1,0
   1772        0  TABL2,0
   1773        0  TABL3,0
*1350
   1350        0  LCOUNT,0
   1351        0  NEWPG,0
*1757
   1757     7074  PUTAC,7074
*1763
   1763     7573  FACM,7573
*1761
   1761     7541  FIX,7541
*1753
   1753     6736  FLIP,6736
```

```
*4000/    LEAST-SQUARES FOR EXPONENTIAL DECAY

   4000        0  MASTER,0      /DOES ALL CALCS, PRINTS OUTPUT
   4001 3110000  MEMA @MASTER
   4002 2405770  ACCM DATA1
   4003 3111770  MEMA @DATA1
   4004 2405770  ACCM DATA1
   4005 2124000  MPOM MASTER
   4006 3110000  MEMA @MASTER
   4007 2405771  ACCM DATAN
   4010 3111771  MEMA @DATAN
   4011 2405771  ACCM DATAN
   4012 2000204  JMS LOG
   4013 2000036  JMS LSQAR
   4014 2000514  JMS OUTPUT
   4015 2124000  MPOM MASTER
   4016 1000000  JMP @MASTER

   4017    2000  DWELL,0002000
   4020     500  0000500

   4021        0  IFLOC,0    /A ROUTINE TO FLOAT AN INTEGE
   4022 3405766  ACCM @FACM  / AC TO FAC
   4023 3165744  ZERM @FACML
   4024 3001755  JMS @FLOAT
   4025 1000021  JMP @IFLOC

   4026        0  IFLOR,0     /FLOATS AN INTEGER FROM AC TO
   4027 2405776  ACCM DATAP   /STORES NUMBER TOBE FLOATED
   4030 3001742  JMS @FACTEM   /PRESERVES FAC
   4031 2111776  MEMA DATAP
   4032 2000021  JMS IFLOC
   4033 3001753  JMS @FACFAR
   4034 3001743  JMS @TEMFAC
   4035 1000026  JMP @IFLOR

/LEAST SQUARES
   4036        0  LSQAR,0      /CALCULATES A LEAST SQUARES
   4037 2111771  MEMA DATAN   /OCCUPYING DATAI TO DATAN,
   4040 2405650  ACCM CNTR3   /X2,Y2;... XN,YN
   4041 2111770  MEMA DATA1
   4042 2405772  ACCM CNTR2
   4043 2323771  M-AZ DATAN
   4044  162000  ZERZ
   4045 1000036  JMP @LSQAR
   4046 3165764  ZERM @ERRF
   4047 3111772  L1,MEMA @CNTR2
   4050 2000021  JMS IFLOC
   4051 2103547  MEMZ ALT     /BRANCH FOR X OR Y
   4052     100  JMP BR1
   4053 3001742  JMS @FACTEM   /BRANCH FOR X
   4054 2000460  JMS WCALC     /ENDS WITH TEMFAC
```

```
4055 2000453  JMS WEIGHT
4056 3001752  JMS @GETAR
4057    4355  SUMX
4060 3001740  JMS @FADD
4061 3001754  JMS @PUTAC
4062    4355  SUMX
4063 3001743  JMS @TEMFAC
4064 3001761  JMS @FSQAR
4065 2000453  JMS WEIGHT
4066 3001752  JMS @GETAR
4067    4363  SUMXSQ
4070 3001740  JMS @FADD
4071 3001754  JMS @PUTAC
4072    4363  SUMXSQ
4073 2125547  MPOM ALT      /FLIPS FLIPFLOP
4074 2135772  L2,MPOMA CNTR2
4075 2323771  M-AZ DATAN       /DONE ?
4076      47  JMP L1
4077     125  JMP COLL
4100 3001754  BR1,JMS @PUTAC       /BRANCH FOR Y
4101    1772  PROD1
4102 2125777  MPOM NUM
4103 2000453  JMS WEIGHT
4104 3001752  JMS @GETAR      / SUMY
4105    4357  SUMY
4106 3001740  JMS @FADD
4107 3001754  JMS @PUTAC
4110    4357  SUMY
4111 3001752  JMS @GETAR
4112    1772  PROD1
4113 3001743  JMS @TEMFAC       / X
4114 3001745  JMS @FMULT
4115 2000453  JMS WEIGHT
4116 3001752  JMS @GETAR
4117    4361  SUMXY
4120 3001740  JMS @FADD
4121 3001754  JMS @PUTAC
4122    4361  SUMXY
4123 2705547  MMOM ALT    /FLOPS FLIPFLOP
4124      74  JMP L2
4125 2103547  COLL,MEMZ ALT
4126    1557  JMP ERRX2     /ERROR IF #X'S .NE. #Y'S
4127 3001751  JMS @GETAC
4130    4367  SUMWSQ
4131 3001752  JMS @GETAR
4132    4361  SUMXY
4133 3001745  JMS @FMULT
4134 3001754  JMS @PUTAC
4135    1772  PROD1
4136 3001752  JMS @GETAR
4137    4363  SUMXSQ
4140 3001751  JMS @GETAC
4141    4367  SUMWSQ
```

```
4142 3001745  JMS @FMULT
4143 3001754  JMS @PUTAC
4144    1774  PROD2
4145 3001751  JMS @GETAC
4146    4355  SUMX
4147 3001742  JMS @FACTEM
4150 3001752  JMS @GETAR
4151    4357  SUMY
4152 3001745  JMS @FMULT
4153 3001752  JMS @GETAR
4154    1772  PROD1        / N(SUMXY)
4155 3001741  JMS @FSUB
4156 3001754  JMS @PUTAC
4157    1772  PROD1
4160 3001743  JMS @TEMFAC
4161 3001761  JMS @FSQAR
4162 3001752  JMS @GETAR
4163    1774  PROD2          / N(SUMXSQ)
4164 3001741  JMS @FSUB
4165 3001754  JMS @PUTAC
4166    1774  PROD2           /DENOMINATOR
4167 3001753  JMS @FACFAR
4170 3001751  JMS @GETAC
4171    1772  PROD1        /NUMERATOR
4172 3001746  JMS @FDIV
4173 3001752  JMS @GETAR
4174    4017  DWELL
4175 3001746  JMS @FDIV       /CONVERTS SLOPE TO DECONDS
4176 3001754  JMS @PUTAC
4177    5550  SLOPE
4200 2000241  JMS DEV
4201 3113764  MEMAZ @ERRF
4202    1573  JMP ERRX4
4203 1000036  JMP @LSQAR

/LOG ROUTINE
4204       0  LOG,0
4205 2111770  MEMA DATA1
4206 2425772  APOM CNTR2
4207 2111771  MEMA DATAN
4210 2405650  ACCM CNTR3
4211     353  JMP ZERO
4212 3111772  LN1,MEMA @CNTR2
4213 2000502  JMS NORM
4214 3111772  MEMA @CNTR2
4215 2000021  JMS IFLOC
4216 3111766  MEMA @FACM
4217    5144  EXCT AC19
4220    1562  JMP ERRX3
4221 3001757  LN2,JMS @FLN
4222 2111652  MEMA FACTR
4223 3505765  A+MM @FACE
4224 3001756  JMS @FIX
```

```
4225 3111766  MEMA @FACM
4226 3405772  ACCM @CNTR2
4227 2135772  MPOMA CNTR2
4230 2323771  M-AZ DATAN
4231  162000  ZERZ
4232 1000204  JMP @LOG
4233 2125772  MPOM CNTR2
4234 2135650  MPOMA CNTR3
4235 3331734  M-AA @ULIMIT
4236    5144  EXCT AC19
4237 1001735  JMP @ERRX5       /PREVENTS PROGRAM OVERWR
4240     212  JMP LN1


/STANDARD DEVIATION
4241       0  DEV,0
4242 3001751  JMS @GETAC
4243    4355  SUMX
4244 3001752  JMS @GETAR
4245    4361  SUMXY
4246 3001745  JMS @FMULT
4247 3001742  JMS @FACTEM     /SUMX . SUM Y
4250 3001751  JMS @GETAC
4251    4363  SUMXSQ
4252 3001752  JMS @GETAR
4253    4357  SUMY
4254 3001745  JMS @FMULT
4255 3001753  JMS @FACFAR
4256 3001743  JMS @TEMFAC
4257 3001741  JMS @FSUB      /SUNXSUNXY - SUMXAQ SUMY
4260 3001752  JMS @GETAR
4261    1774  PROD2
4262 3001746  JMS @FDIV
4263 3001754  JMS @PUTAC
4264    5552  B
4265 2111770  MEMA DATA1
4266 2405651  ACCM PNTR2
4267 2111771  MEMA DATAN
4270 2405650  ACCM CNTR3
4271 2000460  DEV1,JMS WCALC
4272 3001752  JMS @GETAR
4273    5550  SLOPE
4274 3001751  JMS @GETAC
4275    4017  DWELL
4276 3001745  JMS @FMULT
4277 3001753  JMS @FACFAR       /CORRECTS FOR DWELL
4300 3111651  MEMA @PNTR2
4301 2000021  JMS IFLOC
4302 3001745  JMS @FMULT      /MX
4303 3001752  JMS @GETAR
4304    5552  B
4305 3001740  JMS @FADD     /MX + B
4306 2125651  MPOM PNTR2
```

```
4307 3111651  MEMA @PNTR2
4310 2000026  JMS IFLOR
4311 3001741  JMS @FSUB
4312 3001742  JMS @FACTEM
4313 3001756  JMS @FIX
4314 3111766  MEMA @FACM
4315 3405651  ACCM @PNTR2
4316 3001743  JMS @TEMFAC
4317 3001761  JMS @FSQAR
4320 3001752  JMS @GETAR
4321    4371  PROD3
4322 3001740  JMS @FADD
4323 3001754  JMS @PUTAC
4324    4371  PROD3      /SUM(Y - (MX+B)) SQUARED
4325 2135651  MPOMA PNTR2
4326 2323771  M-AZ DATAN
4327     271  JMP DEV1
4330 3001751  JMS @GETAC
4331    4371  PROD3
4332 2711777  MMOA NUM
4333 2000026  JMS IFLOR       /N-1
4334 3001746  JMS @FDIV
4335 3001760  JMS @FSQRT
4336 2000406  JMS MINMAX
4337 2111774  MEMA MIN
4340 2331775  M-AA MAX
4341 2000026  JMS IFLOR      /X SUB N - X SUB 1)
4342 3001746  JMS @FDIV
4343 3001752  JMS @GETAR
4344    4017  DWELL
4345 3001746  JMS @FDIV      /CONVERTS TO SECONDS
4346  131777  MPOA (1777     /MULTIPLY BY 2
4347 3505765  A+MM @FACE
4350 3001754  JMS @PUTAC
4351    5554  SIGMA
4352 1000241  JMP @DEV

4353 2165777  ZERO,ZERM NUM
4354 2000373  JMS Z1
4355       0  SUMX,0
4356       0  0
4357       0  SUMY,0
4360       0  0
4361       0  SUMXY,0
4362       0  0
4363       0  SUMXSQ,0
4364       0  0
4365       0  SUMSSQ,0
4366       0  0
4367       0  SUMWSQ,0
4370       0  0
4371       0  PROD3,0
4372       0  0
```

```
4373        0  Z1,0
4374  2110373  MEMA Z1
4375  2405651  ACCM PNTR2
4376   110373  MEMA (Z1
4377  2404373  ACCM Z1
4400  3165651  Z2,ZERM @PNTR2
4401  2135651  MPOMA PNTR2
4402  2322405  M-AZ Z3     /ZERO UP TO THE ADDRESS OF Z1
4403      400  JMP Z2
4404      212  JMP LN1
4405     4373  Z3,Z1

/FINDS MINIMUM AND MAXIMUM
4406        0  MINMAX,0
4407  2111770  MEMA DATA1
4410  2405776  ACCM DATAP
4411  3111776  MEMA @DATAP
4412  2405773  ACCM TEST
4413  2405775  ACCM MAX
4414  2125776  MM1,MPOM DATAP
4415  2135776  MPOMA DATAP
4416  2323771  M-AZ DATAN
4417   162000  ZERZ
4420      431  JMP MM2      /LOOK FOR MIN
4421  3111776  MEMA @DATAP
4422  2331773  M-AA TEST
4423     5104  SKIP AC19
4424      414  JMP MM1
4425  3111776  MEMA @DATAP
4426  2405773  ACCM TEST
4427  2405775  ACCM MAX
4430      414  JMP MM1

4431  2111770  MM2,MEMA DATA1
4432  2405776  ACCM DATAP
4433  3111776  MEMA @DATAP
4434  2405773  ACCM TEST
4435  2405774  ACCM MIN
4436  2125776  MM3,MPOM DATAP
4437  2135776  MPOMA DATAP
4440  2323771  M-AZ DATAN
4441   162000  ZERZ
4442  1000406  JMP @MINMAX
4443  3111776  MEMA @DATAP
4444  2331773  M-AA TEST
4445     5144  EXCT AC19
4446      436  JMP MM3
4447  3111776  MEMA @DATAP
4450  2405774  ACCM MIN
4451  2405773  ACCM TEST
4452      436  JMP MM3
```

```
/WEIGHT MULTIPLYS EACH TERM BY W SQUARED
   4453        0  WEIGHT,0
   4454 3001752  JMS @GETAR
   4455    1770  WSQ
   4456 3001745  JMS @FMULT
   4457 1000453  JMP @WEIGHT

/CALCULATES NORM. WEIGHT AND SUM WEIGHT SQUARED
   4460        0  WCALC,0
   4461 3111650  MEMA @CNTR3
   4462 2000021  JMS IFLOC
   4463  410000  ACCA     /COULD PUT HERE JMS @FSQAR
   4464 3001752  JMS @GETAR
   4465    4365  SUMSSQ
   4466 3001746  JMS @FDIV
   4467 3001761  JMS @FSQAR
   4470 3001754  JMS @PUTAC
   4471    1770  WSQ
   4472 3001752  JMS @GETAR
   4473    4367  SUMWSQ
   4474 3001740  JMS @FADD
   4475 3001754  JMS @PUTAC
   4476    4367  SUMWSQ
   4477 2125650  MPOM CNTR3
   4500 3001743  JMS @TEMFAC
   4501 1000460  JMP @WCALC

/CALCULATES NORMALIZING FACTOR
   4502        0  NORM,0
   4503 3405650  ACCM @CNTR3
   4504 2000021  JMS IFLOC
   4505  410000  ACCA     /COULD PUT HERE JMS @FSQAR
   4506 3001752  JMS @GETAR
   4507    4365  SUMSSQ
   4510 3001740  JMS @FADD
   4511 3001754  JMS @PUTAC
   4512    4365  SUMSSQ
   4513 1000502  JMP @NORM
/OUTPUT
   4514        0  OUTPUT,0
   4515 3001736  JMS @TYPE3
   4516    5577  FRMAT1
   4517 3001751  JMS @GETAC
   4520    5550  SLOPE
   4521 2111652  MEMA FACTR
   4522 3325765  M-AM @FACE
   4523 3001754  JMS @PUTAC
   4524    5550  SLOPE
   4525 2001535  JMS PFLOP
   4526 3001736  JMS @TYPE3
   4527    5605  FRMAT2
   4530 3001751  JMS @GETAC
   4531    5554  SIGMA
```

```
4532 2111652  MEMA FACTR
4533 3325765  M-AM @FACE
4534 3001754  JMS @PUTAC
4535    5554  SIGMA
4536 2001535  JMS PFLOP
4537 3001736  JMS @TYPE3
4540    5611  FRMAT3
4541 2000556  JMS INVT
4542 2001535  JMS PFLOP
4543 3001736  JMS @TYPE3
4544    5605  FRMAT2
4545 3001751  JMS @GETAC
4546    5554  SIGMA          /NOW SIGMA/SLOPE SQUARED
4547 2001535  JMS PFLOP
4550 3001737  JMS @PACK
4551    5777  NUM
4552    5622  NPTWD
4553 3001736  JMS @TYPE3
4554    5617  FRMAT4
4555 1000514  JMP @OUTPUT


4556       0  INVT,0           /CONVERTS SLOPE TO 1/SL
4557 3001751  JMS @GETAC       /TO SIGMA/SLOPE SQUARED
4560    5550  SLOPE
4561 3001761  JMS @FSQAR
4562 3001753  JMS @FACFAR
4563 3001751  JMS @GETAC
4564    5554  SIGMA
4565 3001746  JMS @FDIV
4566 3001754  JMS @PUTAC
4567    5554  SIGMA
4570 3001752  JMS @GETAR
4571    5550  SLOPE
4572   30000  ONEA
4573 2000021  JMS IFLOC
4574 3001746  JMS @FDIV
4575 1000556  JMP @INVT

*5535
5535       0  PFLOP,0
5536  110015  MEMA (15
5537 3225763  ANGM @CARCNT
5540 3001747  JMS @FLOP
5541 3103763  PF1,MEMZ @CARCNT
5542  162000  ZERZ
5543 1001535  JMP @PFLOP
5544  110240  MEMA (240
5545 3001762  JMS @PCHAR
5546    1541  JMP PF1        /LOOP TIL 14 CHARS TYPED
5547       0  ALT,0
5550       0  SLOPE,0
5551       0  0
```

```
5552        0  B,0
5553        0  0
5554        0  SIGMA,0
5555        0  0
5556        0  0

/ERROR EXITS
5557 3001736  ERRX2,JMS @TYPE3
5560    5630  ERROR2
5561 1000036  JMP @LSQAR
5562 3111736  ERRX3,MEMA @TYPE3   /WHAT WAS JUST TYPED
5563 2463576  A-MZ EX31AD         /WAS IT ERROR3?
  5564  162000  ZERZ
5565    1570  JMP ERRX31
5566 3001736  JMS @TYPE3          /NO, GO AHEAD
5567    5636  ERROR3
5570  170000  ERRX31,ZERA         /A NEGATIVE ACC WILL
5571 2000021  JMS IFLOC           /GIVE AN ERROR IN LOG
5572     221  JMP LN2
5573 3001736  ERRX4,JMS @TYPE3
5574    5642  ERROR4
5575 1000036  JMP @LSQAR
5576    5570  EX31AD,ERRX31

5577 2121215  FRMAT1,2121215
5600 2404040  2404040
5601 3240122  3240122
5602 3404005  3404005
5603 2404075  2404075
5604        0  0
5605 3248340  FRMAT2,3248340
5606 3044004  3044004
5607 3402605  3402605
5610        0  0
5611 2121215  FRMAT3,2121215
5612 2576140  2576140
5613 3240122  3240122
5614 3404005  3404005
5615 2404075  2404075
5616        0  0
5617 2404040  FRMAT4,2404040   /
5620 3030523  3030523         /SEC
5621 2121215  2121215         /CRLFLF
5622 2404040  NPTWD,2404040    /
5623 3172040  3172040          / PO
5624 3241611  3241611          /INT
5625 3404023  3404023          /S
5626 2121215  2121215          /CRLFLF
5627        0  0

/ERROR MESSAGES
5630  473043  ERROR2,473043     /#X'S .NE. #Y'S
5631  564023  564023
```

```
   5632  560516  560516
   5633  314340  314340
   5634  402347  402347
   5635       0  0
   5636   70516  ERROR3,070516      /NEG POINT
   5637  172040  172040
   5640  241611  241611
   5641       0  0
   5642  202006  ERROR4,202006      /FPP ERROR FLAG
   5643  220540  220540
   5644  221722  221722
   5645  140640  140640
   5646  400701  400701
   5647       0  0
   5650       0  CNTR3,0
   5651       0  PNTR2,0
   5652   20000  FACTR,20000
*1770
   1770       0  WSQ,0
   1771       0  0
   1772       0  PROD1,0
   1773       0  0
   1774       0  PROD2,0
   1775       0  0
*5770
   5770       0  DATA1,0
   5771       0  DATAN,0
   5772       0  CNTR2,0
   5773       0  TEST,0
   5774       0  MIN,0
   5775       0  MAX,0
   5776       0  DATAP,0
   5777       0  NUM,0
*5734
   5734     601  ULIMIT,601
   5735     550  ERRX5,550
   5736     206  TYPE3,206
   5737     267  PACK,267
   5740    7245  FADD,7245
   5741    7314  FSUB,7314
   5742    7034  FACTEM,7034
   5743    7042  TEMFAC,7042
   5744    7574  FACML,7574
   5745    7416  FMULT,7416
   5746    7461  FDIV,7461
   5747    6510  FLOP,6510
   5750    6736  FLIP,6736
   5751    7062  GETAC,7062
   5752    7050  GETAR,7050
   5753    7026  FACFAR,7026
   5754    7074  PUTAC,7074
   5755    7534  FLOAT,7534
   5756    7541  FIX,7541
```

```
5757    6330  FLN,6330
5760    6176  FSQRT,6176
5761    6352  FSQAR,6352
5762    7013  PCHAR,7013
5763    7021  CARCNT,7021
5764    7555  ERRF,7555
5765    7572  FACE,7572
5766    7573  FACM,7573
```

APPENDIX B

APPENDIX B

Other Nicolet Programs

1. Pulsed Field Gradient Timing and Data Collection

The basic structure of the program for computer control of the pulsed field gradient experiment, PFGRAD, is essentially identical to RELAX2. The differences arise, naturally, in the timing section, which is as follows:

```
PULSE,MEMA HITIME
ACCM WAIT2
ZERM COUNT2
MEMA TIME
PULSE1
JMS TIMER
FGPULSE
JMS TAU2
PULSE2
MEMZ T1FLAG
JMS TAU2
FGPULSE
JMS ECHO

TAU2,Ø
MEMA INTRVL
JMS TIMER
JMP@TAU2
```

This section of code replaces locations 737-747 in RELAX2; since the length is different the program must be reassembled. The subroutine TAU2, of course, is placed at some other point in the program. All labels have the same meaning as in RELAX2; FGPULSE generates the C output pulse as shown in Table 5 . The timing produced by PFGRAD was shown in Figure 20, with reference to that Figure, τ_2 is fixed as $\frac{2T_2}{NP}$ while τ_1 varies in the normal fashion from 0 to $2T_2$. This sequence produces the usual e^{-t^3} time dependence of the echo train.

```
*640/    COMPUTER CONTROL FOR TRIPLET T1 SEQUENCE

RDGRED=44375
SETM=4306
PULSE1=4102
PULSE2=4104
LOR=4341

    640 2110765  BEGIN,MEMA ADC2    /CODE FOR PULSE1
    641 2404740  ACCM NUTATE        /SETUP CHANGES THIS LO
    642 2110631  MEMA NSWEEPS       /NUMBER OF SWEEPS PER
    643 2405216  ACCM SWDEC
    644 2165217  BEG1,ZERM TIME      /SUB SEQUENCE SEP

    645 3001754  JMS @GETAC
    646    1237  GUESS             /THE ESTIMATE OF T1 OR T2
    647 2111136  MEMA CON1        /10**6/16
    650 3001767  JMS @IFLOR
    651 3001751  JMS @FMULT
    652  110100  MEMA (100      /16 TIMES 4 (OCTAL)
    653 3001767  JMS @IFLOR
    654 3001751  JMS @FMULT
    655 2000135  JMS STATWD         /
    656 2110153  MEMA STAT2         /READ OUT BLOCK SIZE
    657 3001767  JMS @IFLOR
    660 3001752  JMS @FDIV
    661 3001757  JMS @PUTAC
    662    1241  DWELL
    663 3001761  JMS @FIX
    664 3111763  MEMA @FACM
    665 2405243  ACCM IDWELL

    666 2111136  MEMA CON1
    667 3001767  JMS @IFLOR
    670  110020  MEMA (20
    671 3001766  JMS @IFLOC
    672 3001751  JMS @FMULT      /ONE MILLION DECIMAL
    673 3001756  JMS @FACFAR
    674 3001754  JMS @GETAC
    675    1241  DWELL
    676 3001752  JMS @FDIV
    677 3001757  JMS @PUTAC
    700    4017  DWELL2          /DWELL IN SECONDS

    701 3001754  JMS @GETAC
    702    1235  PULSEP         /PULSE SEPARATION
    703  110024  MEMA (24
    704 3001767  JMS @IFLOR
    705 3001752  JMS @FDIV      /PULSEP IN UNITS OF 20 MS
    706 3001761  JMS @FIX
    707 3113763  MEMAZ @FACM
    710  550000  AMOA           /ADDS A ONE IF
```

```
711 2425225  APOM TAU2      /FACM IS ZERO
712 2110630  MEMA NPOINTS
713 3001767  JMS @IFLOR
714 3001754  JMS @GETAC
715    1237  GUESS
716 3001752  JMS @FDIV
717 2111136  MEMA CON1
720 3001767  JMS @IFLOR
721 3001751  JMS @FMULT
722 3001761  JMS @FIX
723 3111763  MEMA @FACM
724 2405117  ACCM MULT1
725  110004  MEMA (4
726 2001114  JMS MULTIPLY
727 2405220  ACCM INTRVL       / T1.(10**6)/4N =CYCL
730 3111764  MEMA @FACML
731 2011140  ANDA MASK1       /3000000
732    5042  LLSH 2

733 2515220  A+MMA INTRVL       /T1(10**6)/4N
734 2405217  ACCM TIME       /IN UNITS OF 16 MICROSEC
735 2111222  MEMA P1HI
736 2405234  ACCM HITIME
737 2001100  JMS ZERMEM
740    4102  NUTATE,PULSE1      /NUTATION PULSE
741 2110577  MEMA LLIMIT
742 2404600  ACCM PNTR2       /RESET POINTER TO X1
743 2110630  MEMA NPOINTS   /NEW SWEEP REQUIRES
744 2405231  ACCM NMPTS1    /RESETTING POINT COUNTER
745 2111234  TRIPLET,MEMA HITIME
746 2405214  ACCM WAIT2
747 2111225  MEMA TAU2
750 2405226  ACCM WTAU21
751 2405227  ACCM WTAU22
752 2165215  ZERM COUNT2
753 2165230  ZERM YSUM
754 2111217  MEMA TIME
755 2001010  JMS TIMER
756    4104  PULSE2             / 90 DEGREE PULSE


757    4372  ADC1,STDG
760 2001110  JMS BLOB
761   44375  RDGRED       /RDG REDS
762 2325230  M-AM YSUM       /SIGNALS ARE OF OPP. PHASE
763 2707226  MMOMZ WTAU21
764     757  JMP ADC1

765    4102  ADC2,PULSE1         / 180 DEGREE PULSE
766    4372  ADC7,STDG
767 2001110  JMS BLOB
770   44375  RDGRED       /RDG REDS
771 2515230  A+MMA YSUM
```

```
 772 2707227  MMOMZ WTAU22
 773     766  JMP ADC7

 774    4104  PULSE2                  / 90 DEGREE PULSE

 775    6454  TTYRF
 776  162000  ZERZ
 777       1  JMP START
1000 2124600  MPOM PNTR2       /SKIPPING X(K)
1001 2001025  JMS DTRANS
1002 2707231  MMOMZ NMPTS1
1003     745  JMP TRIPLET        /MORE POINTS
1004 2707216  MMOMZ SWDEC
1005     740  JMP NUTATE         /MORE SWEEPS
1006 2001034  JMS XCALC

1007     155  JMP DSPLY2
1010       0  TIMER,0
1011 2405213  ACCM WAIT
1012 2165224  T2,ZERM COUNT
1013 2135224  T1,MPOMA COUNT
1014 2333213  M-AZA WAIT
1015    5144  EXCT AC19
1016    1020  JMP TIMER2
1017    1013  JMP T1

1020 2135215  TIMER2,MPOMA COUNT2
1021 2333214  M-AZA WAIT2
1022    5144  EXCT AC19
1023 1001010  JMP @TIMER
1024    1012  JMP T2

1025       0  DTRANS,0
1026 3504600  A+MM @PNTR2      /NOTE THAT PNTR2 MUST BE
1027 2134600  MPOMA PNTR2
1030 2332601  M-AZA ULIMIT
1031    5144  EXCT AC19
1032 1000544  JMP @ERRX3
1033 1001025  JMP @DTRANS


1034       0  XCALC,0         /CALCULATES VALUES OF X
1035 2025221  ONEM PTNUM
1036 2110577  MEMA LLIMIT     /RESETS POINTER FOR SECO
1037 2404600  ACCM PNTR2      /PASS THROUGH DISPLAY SE
1040 2111214  XC1,MEMA WAIT2
1041 3001766  JMS @IFLOC
1042 2111224  MEMA COUNT
1043 3001767  JMS @IFLOR
1044 3001751  JMS @FMULT       / TAU1
1045 2111221  MEMA PTNUM
1046 3001767  JMS @IFLOR
1047 3001751  JMS @FMULT      / TAU1 . N
```

```
1050 3001755  JMS @GETAR
1051    1134  CORRECTION
1052 3001750  JMS @FADD       / TAU1 .N + B
1053 2111225  MEMA TAU2
1054    5003  LASH 3
1055 3001767  JMS @IFLOR
1056 3001750  JMS @FADD       / TAU1 . N + B + 8TAU2
1057 3001755  JMS @GETAR
1060    1241  DWELL
1061 3001752  JMS @FDIV
1062 2111137  MEMA CON2       / 10000
1063 3505762  A+MM @FACE      / MULT BY 16
1064 3001761  JMS @FIX
1065 3111763  MEMA @FACM
1066 2001025  JMS DTRANS
1067 2134600  MPOMA PNTR2     /SKIPS Y(I)
1070 2135221  MPOMA PTNUM     /FOR X(I+1)
1071 2330630  M-AA NPOINTS     /DONE?
1072    5104  SKIP AC19
1073    1040  JMP XC1         /NO
1074 1001034  JMP @XCALC

1075  110012  ZRMEM,MEMA (DSPLY1 /FAKES JMS SO THAT
1076 2405100  ACCM ZERMEM        /ZERMEM CAN BE ENTER
1077  162000  ZERZ               /WITH A JMP COMMAND
1100       0  ZERMEM,0        /ZEROES DISPLY2 SECTION
1101 2110577  MEMA LLIMIT
1102 2405244  ACCM DATAP
1103 3165244  ZM1,ZERM @DATAP
1104 2135244  MPOMA DATAP
1105 2322601  M-AZ ULIMIT
1106    1103  JMP ZM1
1107 1001100  JMP @ZERMEM

1110       0  BLOB,0       /FIDDLES AROUND FOR 20 MS
1111    1112  JMP BB1
1112    1113  BB1,JMP BB2
1113 1001110  BB2,JMP @BLOB

1114       0  MULTIPLY,0
1115    4354  TACMQ
1116  505320  MULT
1117       0  MULT1,0
1120 2405222  ACCM P1HI
1121    4343  TMQAC
1122 2405213  ACCM WAIT
1123 2025117  ONEM MULT1
1124 2103222  M1,MEMZ P1HI
1125    1143  JMP LONGTIME     /PRODUCT .GT. 2**20
1126    5144  EXCT AC19
1127    1143  JMP LONGTIME     /WAIT IS TOO LARGE
1130 2111117  MEMA MULT1       /LONGTIME MAKES THIS LA
1131 2405222  ACCM P1HI        /NOW 1 IF ORIGIONALLY 0
```

```
1132 2111213  MEMA WAIT
1133 1001114  JMP @MULTIPLY


1134    2000  CORRECTION,2000
1135 1740000  1740000
1136  172044  CON1,172044
1137   10000  CON2,10000
1140 3000000  MASK1,3000000
1141 2000000  CON3,2000000      /TRANSFER BIT FOR LONGT
1142  100033  LAST,100033

/LONGTIME HALVES LOW WORD, DOUBLES HIGH WORD
1143  405021  LONGTIME,RISH 1
1144 2405213  ACCM WAIT        /WAIT/2
1145 2111222  MEMA P1HI
1146    5110  SKIP AC0         /BIT 0 =1?
1147    1152  JMP L1           / NO
1150 2111141  MEMA CON3
1151 2505213  A+MM WAIT        /YES, ADD IT TO WAIT
1152 2111222  L1,MEMA P1HI
1153  405021  RISH 1
1154 2405222  ACCM P1HI        /P1HI/2
1155 2111117  MEMA MULT1
1156    5001  LASH 1
1157 2405117  ACCM MULT1       /MULT1 . 2
1160 2111213  MEMA WAIT
1161    1124  JMP M1


1162 2110577  EXPNT,MEMA LLIMIT
1163 2332600  M-AZA PNTR2
1164    5144  EXCT AC19
1165       1  JMP START
1166 2130577  MPOA LLIMIT        / Y1
1167 2405232  ACCM PNTR1
1170 2110600  MEMA PNTR2         / W1
1171 2405233  ACCM PNTR3
1172 3111233  EX1,MEMA @PNTR3
1173 3405232  ACCM @PNTR1
1174 2125232  MPOM PNTR1
1175 2125233  MPOM PNTR3
1176 2135232  MPOMA PNTR1
1177 2332600  M-AZA PNTR2
1200    5144  EXCT AC19
1201     155  JMP DSPLY2
1202    1172  JMP EX1

1203  110740  SETUP,MEMA CNUTATE /THE ADDRESS
1204   11777  ANDA C1777          /PAGE RELATIV3
1205 2424740  APOM NUTATE         /JMP TO NEXT LOC
1206     644  JMP BEG1
1207 2110632  ADCNST,MEMA LVLADJ
```

```
   1210 3225763  ANGM @FACM
   1211 1001212  JMP @BSLN2
   1212      443  BSLN2,443

   1213        0  WAIT,0
   1214        0  WAIT2,0
   1215        0  COUNT2,0
   1216        0  SWDEC,0
   1217        0  TIME,0
   1220        0  INTRVL,0
   1221        0  PTNUM,0
   1222        0  P1HI,0
   1223        0  PNTR,0
   1224        0  COUNT,0

   1225        0  TAU2,0
   1226        0  WTAU21,0
   1227        0  WTAU22,0
   1230        0  YSUM,0
   1231        0  NMPTS1,0
   1232        0  PNTR1,0
   1233        0  PNTR3,0
   1234        0  HITIME,0
   1235        0  PULSEP,0
   1236        0  0
   1237        0  GUESS,0
   1240        0  0
   1241        0  DWELL,0
   1242        0  0
   1243        0  IDWELL,0
   1244        0  DATAP,0
*401
BSLN,
*135
    135        0  STATWD,0
*153
    153        0  STAT2,0
*1
START,
*155
DSPLY2,
*12
DSPLY1,
*625
    625      400  ILIMIT,400
*630
    630        0  NPOINTS,0
    631        0  NSWEEPS,0
    632        0  LVLADJ,0
    633        0  T1EST,0
    634        0  0
    635        0  T2EST,0
    636        0  0
```

```
*577
    577     2000  LLIMIT,2000
    600        0  PNTR2,0
    601     3774  ULIMIT,3774
    602   100000  DATA1,100000
    603   107777  DATAN,107777
*4017
   4017     2000  DWELL2,2000
   4020  1000000  1000000
*544
ERRX3,
*1750
   1750     7245  FADD,7245
   1751     7416  FMULT,7416
   1752     7461  FDIV,7461
   1753     6736  FLIP,6736
   1754     7062  GETAC,7062
   1755     7050  GETAR,7050
   1756     7026  FACFAR,7026
   1757     7074  PUTAC,7074
   1760     7534  FLOAT,7534
   1761     7541  FIX,7541
   1762     7572  FACE,7572
   1763     7573  FACM,7573
   1764     7574  FACML,7574
   1765     4000  MASTER,4000
   1766     4021  IFLOC,4021
   1767     4026  IFLOR,4026
```

```
*4036/  SECOND MOMENT CALCULATION FROM CW LINESHAPE

/THIS PROGRAM IS TO BE READ OVER RELAX2.  IT MODIFIES NI
/AND DESTROYS THE LEAST-SAUARES SUBROUTINE.  THE LS COMM
/IS REPLACED WITH AN M2 COMMAND.

/COMMANDS:
/
/    G - STARTS CALCULATION OF UNNORMALIZED SECOND MOMENT
/
/    I - STARTS CALCULATION OF NORMALIZATION CONSTANT
/        (WHICH IS THE AREA UNDER THE LINE)
/
/    C - CONTINUES EITHER THE SECOND MOMENT OR NORMALIZ
/        CALCULATION.
/
/    Q - STOPS CALCULATION AND JUMPS TO DISPLAY MODE,
/        BRIGHTENED POINT WILL SHOW THE INTEGRATION LIM
/        G WAS THE PRIOR COMMAND
/
/ALL COMMANDS MUST BE PRECEDED BY AN OCTAL NUMBER WHICH
/THE NUMBER OF POINTS OVER WHICH THE CALCULATION IS TO B
/PERFORMED.  FOR EXAMPLE, 10G MEANS CALCULATE THE SECOND
/ FOR THE FIRST 10 POINTS, AND 100C MEANS CONTINUE THIS
/CALCULATION FOR 100 MORE POINTS.
   4036   44453  RDTTY
   4037 2001043  START,JMS CRLF
   4040 2000770  JMS OCTIN
   4041  462303  LIST,A-MZ (303 /C
   4042  162000  ZERZ
   4043     123  JMP CONTINUE
   4044 2405773  ACCM COMWD     /STORE END CHAR
   4045  462307  A-MZ (307      /G
   4046  162000  ZERZ
   4047      66  JMP GO
   4050  462311  A-MZ (311      /I
   4051  162000  ZERZ
   4052      66  JMP GO         /BUT JUST INTEGRATE
   4053  462321  A-MZ (321      /Q
   4054  162000  ZERZ
   4055      61  JMP DISPLY
   4056  110277  ERROR,MEMA (277
   4057 2001035  JMS TYPE       /?
   4060      37  JMP START

   4061 2111774  DISPLY,MEMA COUNT
   4062 3404125  ACCM @INTADJ  /SETUP FOR DISPLAY WITH
   4063 3404126  ACCM @INTV    /CURSOR SHOWING INTEGRAT
   4064 3404127  ACCM @DELAY   /LIMIT
   4065 1000133  JMP @DISP
```

```
4066 2165771  GO,ZERM M2SUM
4067 2165772  ZERM M2SUMA
4070 3000130  JMS @STATWD
4071 3110131  MEMA @STAT2
4072 2405770  ACCM Y          /STARTING ADDRESS
4073 2035774  ONEMA COUNT     /FREQ FROM CENTER
4074 2000021  IN1,JMS IFLOC
4075 3001761  JMS @FSQAR
4076 3111770  MEMA @Y
4077 2000026  JMS IFLOR
4100 3001745  JMS @FMULT
4101 3001752  JMS @GETAR
4102    5771  M2SUM
4103 3001740  JMS @FADD
4104 3001754  JMS @PUTAC
4105    5771  M2SUM
4106 2135770  MPOMA Y
4107 2322132  M-AZ BLOCK     /.GT. DISPLAYED SIZE?
4110  162000  ZERZ
4111 1000133  JMP @DISP      /YES
4112 2111773  MEMA COMWD
4113  462307  A-MZ (307       /G?
4114 2165774  ZERM COUNT      /NO,MUST BE I
4115 2135774  MPOMA COUNT
4116 2707027  MMOMZ WORD     /ANY MORE THIS INCREMENT?
4117      74  JMP IN1        /YES
4120 2001043  JMS CRLF
4121 3001747  JMS @FLOP      /M2SUM STILL IN FAC
4122      37  JMP START      /BACK FOR MORE

4123 2111774  CONTINUE,MEMA COUNT
4124      74  JMP IN1

4125     623  INTADJ,623
4126     624  INTV,624
4127     627  DELAY,627
4130     135   STATWD,135
4131     154  STAT2,154
4132     153  BLOCK,153
4133      12  DISP,12
*5770
5770       0  Y,0
5771       0  M2SUM,0
5772       0  M2SUMA,0
5773       0  COMWD,0        /THE COMMAND CHAR(BUT NOT
5774       0  COUNT,0

*5043
5043       0  CRLF,0
*4770
4770       0  OCTIN,0
*5035
5035       0  TYPE,0
```

```
*4021
   4021        0  IFLOC,0
*5021
   5021       41  JMP LIST
*5761
   5761     6352  FSQAR,6352
*5745
   5745     7416  FMULT,7416
*5751
   5751     7062  GETAC,7062
   5752     7050  GETAR,7050
   5753     7026  FACFAR,7026
   5754     7074  PUTAC,7074
*5740 .
   5740     7245  FADD,7245
*5747
   5747     6510  FLOP,6510
*5503
   5503     4036  4036          /DESTINATION FOR M2 COM
 *5441
   5441   315262  315262        /M2 COMMAND FOR SERVO
*4026
   4026        0  IFLOR,0
*5027
   5027        0  WORD,0
```

```
*5653/   RAMAN CORRELATION FUNCTION DIVISION

/THIS PROGRAM DIVIDES THE DEPOLARIZED FOURIER INVERTED S
/WITH THE POLARIZED, POINT BY POINT.  IT IS TO BE READ IN
/RELAX2, WHICH IS NOT MODIFIED BY THIS PATCH.  ISO IN THE
/STARTING ADDRESS OF THE POL CORRELATION FUNCTION, ANIS
/STARTING POINT OF THE DEPOLARIZED CORRELATION FUNCTION,
/AND THE RESULT STARTS AT RESULT.

/THE PROGRAM IS STARTED THROUTH NICOBUG (S.A. 4700) AS:
/AFTER EXECUTION IT RETURNS TO NICOBUG.  RELAX2 MAY THEN
/STARTED (G) TO CALCULATE THE LOGARITHM OF THE RESULTING
/ROTATIONAL CORRELATION FUNCTION.

   5653 2111704  MEMA ISO
   5654 2405702  ACCM P2
   5655 2111705  MEMA ANIS
   5656 2405701  ACCM P1
   5657 2111706  MEMA RESULT
   5660 2405703  ACCM P3
   5661 3111701  D1,MEMA @P1      /C(ANIS)
   5662 2000021  JMS IFLOC
   5663 3111702  MEMA @P2         /C(ISO)
   5664 2000026  JMS IFLOR
   5665 3001711  JMS @FDIV
   5666 2111710  MEMA CON1        /SCALING FACTOR
   5667 3505712  A+MM @FACE
   5670 3001714  JMS @FIX
   5671 3111713  MEMA @FACM
   5672 3405703  ACCM @P3         /C(ROT)
   5673 2125701  MPOM P1
   5674 2125703  MPOM P3
   5675 2135702  MPOMA P2
   5676 2323707  M-AZ END         /DONE?
   5677    1661  JMP D1
   5700     700  JMP NBUG        /YES

   5701       0  P1,0
   5702       0  P2,0
   5703       0  P3,0
   5704  100000  ISO,100000
   5705  110000  ANIS,110000
   5706  112000  RESULT,112000
   5707  111777  END,111777
   5710   30000  CON1,30000
   5711    7461  FDIV,7461
   5712    7572  FACE,7572
   5713    7573  FACM,7573
   5714    7541  FIX,7541
*4021
   4021       0  IFLOC,0
*4026
```

```
   4026          0   IFLOR,0
*4700
NBUG,
```

APPENDIX C

APPENDIX C

RMANFIT - Raman Lineshape Fitting Program

RMANFIT is a program for determining the orientational broadening of Raman vibrational bands which uses the procedure suggested by Bartoli and Litowitz[30] (their method A) of convolving the polarized component of the line with a Lorentzian and fitting the result to the depolarized component. The program as written converges strongly to a solution even though the minimization routine is very primitive. A number of improvements could be made especially for the purpose of reducing the program size (125K) and running time (∿5 W-H of CM time per spectrum). Some features of the program operation will be discussed and then possible improvements will be suggested.

1. Operation

All of the adjustments which one might wish to make to the data are done through subroutines SELECT and FUDGE. Therefore one may avoid reading in a long deck by placing the main program on a permanent file. The procedure for running the program is then to read in SELECT and FUDGE (and the one data card, to be discussed) with the following control cards:

```
FTN(B=X)
ATTACH(TAPE2,"the raman data PF name")
ATTACH(RMANFIT,  FITPARA,PLOT11,CALNDER,INVR1)
LOAD(RMANFIT,X,FITPARA,PLOT11,CALNDER,INVR1)
EXECUTE(RMANFIT)
```

This presumes that the data have previously been placed on permanent

file. The only data whichare read in with SELECT and FUDGE are on a single card giving the experimental polarization leakage (RHO) and the relative efficiency of the detector for different polarizations (POLEFF). These parameters should be determined from the relative intensities of the various lines of CCl_4 as discussed in the Experimental section.

If the linewidths are greatly different from $\sim 5\ cm^{-1}$ then the initial guess of the orientational width (XHDWTH) of $2.0\ cm^{-1}$, and the step size for the minimization routine (XMSTEP) of $0.5\ cm^{-1}$ may be changed in SELECT by inserting a COMMON/SEARCH/XHWDTH,XMSTEP card and then redefining these parameters in the subroutine. Also, currently all 1023 point spectra are reduced to 511 points by subroutine TRIM, with the parameter ICHOP entering as

$$I_{new}(\omega) = I_{old}(\omega + ICHOP).$$

Consequently ICHOP determines which 511 points of the old spectrum are saved. If a full 1023 point spectrum is to be retained, the call card for TRIM must be deleted.

Subroutine FITPARA is used twice; both to fit the baseline and to fit the center of the data to find the center frequency. The coefficients for both these least-squares fits are printed (the equation used is F(X) = C(1)*X + C(2) + C(3)*X*X) but the plot is suppressed by setting IPLOT = 0 before calling FITPARA). Little is gained by viewing these plots, and as long as both remain suppressed the subroutine PLOT13 need not be attached. The baseline is fit to a parabola rather than a straight line in order to handle the case where the line of interest is on the shoulder of another peak. The "goodness of fit"

for lines which do not require this feature is, however, slightly worse.

The messages "UNSAT EXTERNAL PLOT13" and "UNSAT EXTERNAL HEADING" normally appear in the dayfile.

The correction $I_{pol}(\omega) = I_{pol}(\omega) - 4I_{depol}(\omega)/3$ is only made when the depolarization ratio $\rho < 0.1$. It may be desired to make this correction regardless of the size of ρ, in which case the appropriate statement must be removed from subroutine INTNCOR.

2. Suggested Improvements

The greatest problem with this program is the cost per spectrum. The only lengthy calculation is the convolution, which is recalculated for each iterative step and requires $(6n)^2$ operations for a spectrum of n points. Currently every fifth point in the spectrum is calculated (ISKIP = 5 in MINN - but note that PLOT11 also has an ISKIP). Clearly a larger value of ISKIP would greatly decrease the running time, however, no other values were tried (except 1). Note that the procedure for making the baseline correction in CONVOLV will only work for values of ISKIP which are integer divisors of 510.

Three other improvements were considered but not deemed necessary for the present. The first was improving (or replacing) the minimization routine since the present version will converge very slowly if the initial guess is off by more than a few wavenumbers. The second improvement considered was to weight the points in determining the residual in order that the points on the baseline not be so important. Finally, depolarization ratios are presently calculated from band

center intensities, which is not strictly correct. They are properly calculated from areas, and when the widths are greatly different the two methods of calculation will clearly disagree. The correct calculation could quite readily be added to subroutine INTNCOR.

```
      PROGRAM RMANFIT(INPUT,TAPE2,OUTPUT,TAPE3)
C REQUIRES SUBROUTINES INVR1, PLOT11, AND FITCRV2 WITH THE FITTING
C EQUATION WRITTEN AS F(X) = C(1) + C(2)*X + C(3)*X*X(WRITTEN BY W.G.
C WALLER, CHEM DEPT.,MSU).  THE LOCAL FILE NAMES SHOULD BE INVR1,PLOT11,
C AND FITPARA.  THIS PROGRAM DETERMINES THE ORIENTATIONAL COMPONENT OF
C RAMAN LINES USING THE CONVOLUTION TECHNIQUE SUGGESTED BY BARTOLI AND
C LITOVITZ(J.CHEM. PHYS.56,404(1972)).  IT ASSUMES THAT THE SPECTRA HAVE
C BEEN PUNCHED IN VARIAN CAT FORMAT(SIX OCTAL BITS/WORD, TWELVE WORDS/
C CARD, STARTING COLUMN 9), AND CAN BE ATTACHED FROM PERMANENT FILE WITH
C THE LOCAL FILE NAME TAPE2.    THE INPUT DATA SHOULD CONSIST OF THE
C POLARIZED  AND THEN THE DEPOLARIZED COMPONENTS OF A SINGLE LINE, WITH
C THE CENTER FREQUENCY OF THE LINE ROUGHLY CENTERED IN EACH SPECTRUM.
C THE STRUCTURE OF THE DATA DECK SHOULD BE AS FOLLOWS
C
C     NUMBER OF GROUPS TO BE ANALYZED
C     NUMBER OF SPECTRA/GROUP, NUMBER OF POINTS/SPECTRUM
C     TITLE CARD TO SPECTRUM 1
C     TITLE CARD TO SPECTRUM 2
C     PMT COUNTS/SEC FOR SPECTRA 1 AND 2
C     NUMBER OF SWEEPS FOR SPECTRA 1 AND 2
C     A DECK OF 86 CARDS OF DATA
C     A SECOND DECK OF 86 CARDS OF DATA(ONLY IF 1023 POINTS/SPECTRUM)
C
C REPEAT THIS SEQUENCE STARTING WITH CARD 2 AS MANY TIMES AS NECESSARY.
C THE PROGRAM DETERMINES THE CENTER FREQUENCY AND THEN VARIES THE WIDTH
C OF THE LORENTZIAN ORIENTATIONAL SPECTRUM TO OBTAIN THE BEST FIT
C BETWEEN THE POLARIZED AND DEPOLARIZED SPECTRA.  THE POINTS ARE NOT
C WEIGHTED.  THE RESULT(MINIMUM HALF-WIDTH) IS IN THE SAME UNITS AS THE
C ORIGINAL SPECTRUM.  MOST NOISE SPIKES WILL BE AUTOMATICALLY DELETED.
C A 17-POINT SMOOTH IS DONE TO THE DEPOLARIZED SPECTRUM WITH THE METHOD
C OF SAVITZKY AND GOLAY(ANAL. CHEM. 36,1627(1964)).  AN OUTPUT FILE
C CONSISTING OF THE POL., DEPOL., AND CONVOLUTION IS WRITTEN ON TAPE3
C FOR PLOTTING WITH THE TEKTRONIX GRAPHICS TERMINAL.  THE CURRENT FORMAT
C IS COMPATIBLE WITH THE SUBROUTINE LPLOTIT(L.A.PACHLA,CHEM.DEPT.,MSU).
      DIMENSION X1(1023),Y(1023),C(3),WT(1023),IHEAD2(8),D(3),CF(10)
      COMMON/CONV/D(6,1023),ERROR(4),SCALC(8)
      COMMON/SPECT/S(6,1023)
      COMMON/V/V(3,1024)
      COMMON/SCRAP/IGONE(1023)
      COMMON/AMP/SCALF(8),ICF(8),RHO,POLEFF,GAIN(8)
      COMMON/DATA/IDATA(1023)
      COMMON/SEARCH/XHWDTH,XMSTEP
      COMMON/TITLE/ITITLE(8),NDATE(3)
      COMMON/PLOT/LENGTH,IBORDER,IPAGE,ISKIP,IOVER,IHEAD,FORM,ENUM,AUGM
      COMMON/FIT/NTHP,XBEG,XEND
      COMMON/SYMBOL/ISYMBOL(3)
      DATA ISYMBOL/1R0,1RX,1RC/,LENGTH/5/,IBORDER/2/,IPAGE/1/,ISKIP/0/,I
     DOVER/0/,IHEAD/0/,FORM/5.1/
      DATA WT/1023*1.0/
  100 FORMAT (8X,12O6)
  101 FORMAT (/(10X,14(O6,2X)))
  102 FORMAT(//,* AFTER NORMALIZATION AT*,T44,*CENTER FREQUENCY= *,I4,8X
     1,*THE SCALING FACTOR= *,G13.7)
  103 FORMAT (8A10)
  104 FORMAT(I3)
  105 FORMAT(I3,6X,I4)
  106 FORMAT(E6.0,3X,E6.0)
  108 FORMAT(/,10X,*PROGRAM RMANFIT READING *,I2,* DECKS WITH *,I4,* POI
     1NTS PER SPECTRUM*)
  109 FORMAT(/,2X,*THE TITLE CARD FOR SPECTRUM NUMBER *,I2,* READS : *,8
     1A10)
  110 FORMAT(I3,6X,I3)
  111 FORMAT(//,* THE FOLLOWING POINTS WERE DELETED AS NOISE SPIKES*,/,(
     110X,30(1X,I3)))
  112 FORMAT(///,2X,*INPUT PARAMETERS FOR THE NEXT PAIR OF SPECTRA ARE*,
     1/10X,*SPECTRUM 1*,5X,G11.5,*  PMT COUNTS/SEC*,I3,*  SCANS*,/,10X,*
     2SPECTRUM 2*,5X,G11.5,*  PMT COUNTS/SEC*,I3,*  SCANS*)
      CALL CALNDER(NDATE)
      XHWDTH=20.   *   XMSTEP=5.
      READ(2,104) NGRPS
C GO THROUGH THIS LOOP UNTIL ALL DATA READ
      DO 20 KGRP=1,NGRPS
      READ (2,105) NSPGRP,NPOINTS
      NDECKS=NSPGRP
      IF(NPOINTS.EQ.511) NDECKS=(NSPGRP+1)/2
      PRINT 108, NDECKS,NPOINTS
```

```
C GO THROUGH THIS LOOPONCE FOR EACH DECK OF 86 CARDS.  EACH DECK WILL
C CONTAIN EITHER 1 OR 2 SPECTRA DEPENDING ON  WHETHER THE SPECTRA
C CONTAIN 511 OR 1023 POINTS.
      DO 20 KK=1,NDECKS
      IF(KK.A.1) 13,14
   14 IF(NPOINTS.EQ.1023) GO TO 15
   13 READ(2,103)ITITLE
      READ (2,103) IHEAD2
      READ(2,106) GAIN1,GAIN2
      READ(2,110) NSWEEP1,NSWEEP2
      PRINT 112, GAIN1,NSWEEP1,GAIN2,NSWEEP2
      GAIN1=GAIN1/SQRT(FLOAT(NSWEEP1))$GAIN2=GAIN2/SQRT(FLOAT(NSWEEP2))
   15 READ(2,100) (IDATA(K),K=1,1023)
C THIS LOOP READS 511 POINTS AT A TIME.  EACH SPECTRUM IN A GROUP HAS A
C UNIQUE VALUE OF J.
      DO 11 JJ=1,2
      J=JJ+2*KK-2
      NPPS =NPOINTS
      IF(NPPS.EQ.1023) J=KK
      IF(NPPS.EQ.1023.A.JJ.EQ.2) GO TO 11
      ISKIP=0  $  ICHOP=254  $  CALL SELECT(J,KGRP,ISKIP,ICHOP)
      IF(ISKIP.EQ.1) GO TO 8
      GAIN(J)=GAIN1
      PRINT 109, J,ITITLE
C ************  REMOVE NOISE PEAKS  *****************
      OLDPNT=IDATA(1)  $  OLDSLP=.05  $  IDELETE=0
      DO 2 K=1,NPPS
      XNEWPNT=FLOAT(IDATA(K))  $  XNEWSLP=ABS(XNEWPNT-OLDPNT)
      IF(XNEWSLP.EQ.0) XNEWSLP=OLDSLP
      EPS=OLDSLP*500.
      IF(XNEWSLP.GT.EPS) GO TO 1
      OLDSLP=XNEWSLP  $  OLDPNT=XNEWPNT  $  GO TO 2
    1 XNEWSLP=OLDSLP  $  XNEWPNT=OLDPNT  $  IDATA(K)=IFIX(OLDPNT)
      IDELETE=IDELETE+1  $  IGONE(IDELETE)=K
    2 CONTINUE
      IF(IDELETE.NE.0) PRINT 111, (IGONE(K),K=1,IDELETE)
      IF(IDELETE.GT.05) GO TO 11
      IF(J.NE.1) CALL SMOOTH(NPPS)
      IF(NPPS.EQ.1023) CALL TRIM(J,NPPS,ICHOP)
C ********  TAKE MAX VALUE AS INITIAL GUESS FOR MDPNT   ************
      MAX=IDATA(1)   $   MDPNT=1
      DO 12 K=2,NPPS
      IF(IDATA(K).LE.MAX) GO TO 12
      MAX=IDATA(K)  $  MDPNT=K
   12 CONTINUE
C ****(************CALCULATE BASELINE************
      L=0      $  IUP=NPPS-50
      DO 3 K=1,50
      L=L+1
      X1(L)=K-MDPNT
    3 Y(L)=FLOAT(IDATA(K))
      DO 4 K=IUP,NPPS
      L=L+1
      X1(L)=K-MDPNT
    4 Y(L)=FLOAT(IDATA(K))
      NTHP=100  $  XBEG=-25.6  $  XEND=25.6  $  NP=100
      NF=3  $  IPLOT=0  $  IPRINT=0
      CALL FITPARA(IPLOT,NF,NP,X1,WT,Y,C,IPRINT)
C ********(********DETERMINE CENTER FREQUENCY**************
      IWDTH=20
      M=0      $  MLO=MDPNT-IWDTH$ MHI=MDPNT+IWDTH
      DO 5 K=MLO,MHI
      M=M+1
      Y(M)=FLOAT(IDATA(K))
    5 X1(M)=K
      IPLOT=1  $  NF=3  $  NP=2*IWDTH+1
      NTHP=2*NP  $  XBEG=FLOAT(MLO)  $  XEND=FLOAT(MHI)
      IPLOT=0
      CALL FITPARA(IPLOT,NF,NP,X1,WT,Y,D,IPRINT)
C ****************MAKE BASELINE CORRECTION*************
      CF(J)=-D(1)/(2*D(3))  $  ICF(J)=IFIX(CF(J))
      FNUM=D(1)/(20.*D(3))  $  AUGM=.1
      CALL FUDGE(C,J,KGRP)
      DO 6 K=1,NPPS
      K2=K-ICF(J)-1 $XK=FLOAT(K2)
    6 S(J,K)=FLOAT(IDATA(K))-C(1)*XK-C(2)-C(3)*XK*XK
```

```
C ******************NORMALIZE********************
      CALL NORM(S,J,NPPS,ICF(J),SCALE(J))
      PRINT 102, ICF(J),SCALE(J)
      SCALE(J)=SCALE(J)*GAIN(J)
C GET 2 SPECTRA BEFORE ENTERING INTNCOR AND MINN.
      IF(J.EQ.1) GO TO 8
      CALL INTNCOR(J,NPPS)
      L=1  $  M=2
C LOAD 2/3 OF V MATRIX FOR PLOT13.
      DO 7 K=1,NPPS
      V(L,K)=S(L,K)
    7 V(M,K)=S(J,K)
      CALL MINN(J,NPPS)
    8 IF(NPOINTS.EQ.1023) GO TO 16
C READ SECOND SPECTRUM INTO FIRST 511 POINTS OF DATA.
      DO 9 K=1,511
    9 IDATA(K)=IDATA(K+512)
   16 DO 10 K=1,8
   10 ITITLE(K)=THEAD2(K)
      GAIN1=GAIN2
   11 CONTINUE
   20 CONTINUE
      END
```

SUBROUTINE TRIM

```
      SUBROUTINE TRIM(J,NPPS,ICHOP)
C CONVERTS A 1023 POINT SPECTRUM TO A 511 POINT SPECTRUM.  THIS IS DONE
C NE UNLESS ICHOP IS SET TO 0 IN SUBROUTINE SELECT.
      COMMON/AMP/SCALE(8),ICF(8)
      COMMON/DATA/IDATA(1023)
      DO 1 K=1,511
    1 IDATA(K)=IDATA(K+ICHOP)
      NPPS=511
      RETURN
      END
```

SUBROUTINE SAVEPLT

```
      SUBROUTINE SAVEPLT(JL,NPPS,M)
C SAVES THE DATA FOR THE TEKTRONIX PLOTTER
      DIMENSION LABEL(2)
      DIMENSION X(1024)
      COMMON/V/V(3,1024)
      COMMON/TITLE/ITITLE(8),NDATE(3)
      COMMON/AMP/SCALE(8),ICF(8),RHO,POLEFF,GAIN(8)
      DATA LABEL/4HFREQ,6HINTENS/
      DATA VAR/3HRHO/
  100 FORMAT (I5,(F11.4))
  101 FORMAT (3A10,I5)
  102 FORMAT ((A5))
  103 FORMAT ((E11.4))
  104 FORMAT (2I5,(E11.4))
      TITLE=ITITLE(1)   $   K=1
      DO 20 KK=1,NPPS
   20 X(KK)=FLOAT(KK)
      DO 10 KK=1,JL
      WRITE(3,100) NPPS,(X(J),J=1,NPPS),(V(KK,J),J=1,NPPS)
      WRITE(3,101) LABEL(1),LABEL(2),TITLE,K
      REALDPR=SCALE(M)/SCALE(1)
      WRITE(3,102) VAR
   10 WRITE(3,103) REALDPR
      RETURN
      END
```

SUBROUTINE NORM

```
      SUBROUTINE NORM(F,M,NPPS,ICF,SCALE)
      DIMENSION F(6,1023)
      MLO=ICF-2  $  MHI=ICF+2
      SCALE=0.
      DO 1 K=MLO,MHI
    1 SCALE=SCALE+F(M,K)
      SCALE =SCALE/5.
      DO 2 K=1,NPPS
    2 F(M,K)=F(M,K)/SCALE
      RETURN
      END
```

SUBROUTINE MINN

```
      SUBROUTINE MINN(M,NPPS)
C THIS SUBROUTINE TAKES A STEP IN BOTH DIRECTIONS AROUND THE CURRENT
C VALUE OF CPOINT AND CALCULATES THE NEW CPOINT, WHICH IS THAT VALUE
C WHICH GIVESS THE LEAST ERROR BETWEEN THE CONVOLUTION AND THE DEPOLART
C ZED SPECTRUM.  THIS VALUE IS DETERMENED FROM THE PARABOLA OBTAINED
C FROM SUBROUTINE PARABOL.
C     THE STEP SIZE IS REDUCED BY ONE-HALF FOR EACH SUBSEQUENT CYCLE AND
C THE ITERATION STOPS WHEN THE ERROR CHANGES BY LESS THAN .01.
C     THE INITIAL ESTIMETE OF THE HALF-WIDTH AND THE STEP SIZE ARE IN THE
C LABELLED COMMON SEARCH, ACCESIBLE IN SUBROUTINE SELECT, AS XHWDTH
C AND XMSTEP, RESPECTIVELY.  DEFAULT VALUES ARE 20 (2.0 CM-1) AND 5 (.5)
      COMMON/V/V(3,1024)
      COMMON/CONV/C(6,1023),ERROR(4),SCALC(8)
      COMMON/AMP/SCALE(8),ICF(8),RHO,POLEFF
      COMMON/SEARCH/XHWDTH,XMSTEP
      DIMENSION F(3),X1(4),WT(3)
      CPOINT=XHWDTH  $  STEP=XMSTEP  $  NTIMES=1  $  ISKIP=5  $  MORE=0
    5 DO 1 K=1,3
      XSTEP=(K-2)*STEP
      CALL CONVOLV(K,NPPS,CPOINT,XSTEP,ICF(M),M,ISKIP)
      WT(K)=1.
    1 X1(K)=CPOINT+XSTEP
      CALL PARABOL(X1,ERROR,P1,P2,P3)
      X1(4)=-P2/(2*P1)
      IFOUR=4  $  XDIFF=X1(4)-CPOINT
      CALL CONVOLV(IFOUR,NPPS,CPOINT,XDIFF,ICF(M),M,ISKIP)
      KFLAG=0. $  ERRMIN=ERROR(4)
      DO 2 K=1,3
      IF(ERROR(K)-ERRMIN.LE.0) KFLAG=K
      IF(ERROR(K)-ERRMIN.LE.0) ERRMIN=ERROR(K)
      STEPDIF=ABS(XDIFF)-.01
      IF (STEPDIF.LT.0) KFLAG=4
    2 CONTINUE
      PRINT 100, NTIMES,X1(4),ERROR(4)
      IF(KFLAG.NE.0) GO TO 3
    4 CPOINT=X1(4) $  STEP=STEP/2.  $  NTIMES=NTIMES+1  $  GO TO 5
    3 IF(MORE.EQ.1.0.KFLAG.EQ.4) GO TO 7
      MORE=1 $ CPOINT=X1(KFLAG) $ STEP=STEP/2 $ NTIMES=NTIMES+1 $GO TO 5
    7 KALL=1  $  XDIFF=X1(KFLAG)-CPOINT  $  JL=3
      CALL CONVOLV(KFLAG,NPPS,CPOINT,XDIFF,ICF(M),M,KALL)
      DO 6 K=1,NPPS
    6 V(JL,K)=C(KFLAG,K)
      PRINT 101, NTIMES,X1(KFLAG),ERROR(KFLAG)
  100 FORMAT(/(40X,*CYCLE*,I3,* OF SUBROUTINE MINN*,//,60X,*THE MINIMUM
     1HALF-WIDTH= *,G13.7,/,60X,*THE CHI-SQUARED ERROR=  *,G13.7))
  101 FORMAT(//(40X,*AFTER *,I3,* CYCLES THE VALUES ARE*,//,40X,*BEST HA
     1LF-WIDTH=*,G13.7,/,40X,*THE CHI SQUARED ERROR= *,G13.7))
      CALL PLOT11(JL,NPPS)
      CALL SAVEPLT(JL,NPPS,M)
      RETURN
      END
```

SUBROUTINE INTNCOR

```
      SUBROUTINE INTNCOR(M,NPPS)
C CORRECTS SPECTRA ACCORDING TO FORMULA
C
C     I(DEPOL,ACTUAL)=I(DEPOL,EXP)/POLEFF-I(POL,EXP)*RHO
C
C ALSO CORRECTS THE POLARIZED SPECTRUM IF THE DEPOLARIZATION RATIO IS
C GREATER THAN .1 ACCORDING TO
C     I(POL) = I(POL)-4/3*I(DEPOL)
C
      COMMON/SCRAP/REP(1023)
      COMMON/SPECT/S(6,1023)
      COMMON/AMP/SCALE(8),ICF(8),RHO,POLEFF,GAIN(8)
      RAWDPR=SCALE(M)/SCALE(1)
      SCALE(M)=SCALE(M)*POLEFF
      IOFFSET=ICF(1)-ICF(M)
      ISHIFT=NPPS-IABS(IOFFSET)
      IF(IOFFSET.EQ.0) GO TO 4
      IF(IOFFSET.LT.0)GO TO 2
      DO 1 K=1,ISHIFT
    1 REP(K+IOFFSET)=S(M,K)-RHO*S(1,K+IOFFSET)*(SCALE(1)/SCALE(M))
      DO 7 K=1,IOFFSET
    7 S(M,K)=REP(K+IOFFSET)
      DO 8 K=1,ISHIFT
    8 S(M,K+IOFFSET)=REP(K+IOFFSET)
      GO TO 6
    2 DO 3 K=1,ISHIFT
    3 S(M,K)=S(M,K-IOFFSET)-RHO*S(1,K)*(SCALE(1)/SCALE(M))
      IUP=ISHIFT+IOFFSET+1  $  DO 9 K=IUP,ISHIFT
    9 S(M,K-IOFFSET)=S(M,K)
      GO TO 6
    4 DO 5 K=1,NPPS
    5 S(M,K)=S(M,K)-RHO*S(1,K)*(SCALE(1)/SCALE(M))
    6 ICF(M)=ICF(1)
      CALL NORM(S,M,NPPS,ICF(M),SCOR)
      SCALE(M)=SCALE(M)*SCOR
      REALDPR=SCALE(M)/SCALE(1)
      PRINT 1001, RHO,POLEFF,GAIN(M),IOFFSET,RAWDPR,SCALE(M),REALDPR
      SLOSS=(1.-SCOR)*100.  $  LOSS=IFIX(SLOSS)
      IF(REALDPR.LT..1) GO TO 11
      DO 10 K=1,NPPS
   10 S(1,K)=S(1,K)-S(M,K)*1.3333*REALDPR
      CALL NORM(S,1,NPPS,ICF(1),AA)
      PRINT 1003
 1003 FORMAT(///,*  THE POLARIZED LINE WAS CORRECTED BY I(POL)=I(POL)-4/
     13I(DEPOL)*)
   11 PRINT 1002, LOSS
 1001 FORMAT(/,* AFTER INTENSITY CORRECTION WITH*,T40,*POLARIZATION LEAK
     1AGE= *,F6.4,/,T41,*DETECTOR EFFICIENCY= *,F5.3,/,T42,*PM TUBE COUN
     2TS/SEC= *,G11.5,/,T46,* CENTER OFFSET= *,I3,/,T34,*CRUDE DEPOLARIZ
     3ATION RATIO= *,F7.5,10X,*THE SCALING FACTOR= *,G13.7,/,T74,*THE DE
     4POLARIZATION RATIO= *,F7.5)
 1002 FORMAT(///,* THIS CORRECTION ACCOUNTED FOR*,I3,* PER CENT OF THE T
     1OTAL LINE INTENSITY*)
      RETURN
      END
```

SUBROUTINE CONVOLV

```
      SUBROUTINE CONVOLV(M,NPPS,XHWDTH,XCHNGE,ICF,L,ISKIP)
      DIMENSION WOR(2400)
      COMMON/SPECT/S(6,1023)
      COMMON/CONV/C(6,1023),ERROR(4),SCALC(8)
      NPTT=ICF*4+100
      JJ=1
      DO 2 K=1,NPTT
      J=K-ICF*2$  XJ=FLOAT(J)-50.
    2 WOR(K)=1./(1.+(XJ*XJ)/(XHWDTH+XCHNGE)**2)
      DO 10 K=1,NPPS
   10 C(M,K)=0.
      DO 1 K=1,NPPS,ISKIP
      DO 1 N=1,NPPS,ISKIP
      KKK=K+2*ICF-N+50
    1 C(M,K)=C(M,K)+WOR(KKK)*S(JJ,N)
      NHSLINE=5*ISKIP  $  IUP=NPPS-4*ISKIP  $  HLCORR=0.
```

```
      DO 3 K=1,NBSLINE,ISKIP
    3 BLCORR=BLCORR+C(M,K)
      DO 4 K=IUP,NPPS,ISKIP
    4 BLCORR=BLCORR+C(M,K)
      BLCORR=BLCORR/10.
      DO 5 K=1,NPPS,ISKIP
    5 C(M,K)=C(M,K)-BLCORR
      DO 7 K=1,ISKIP
      ICENT=ICF+K-1 $   J=ICENT-(ICENT/ISKIP)*ISKIP
      IF(J.EQ.1) IRCENT=ICENT
    7 CONTINUE
      IF(ISKIP.EQ.1) GO TO 9
      ICENTL=IRCENT-2  $  ICENTH=IRCENT+2
      DO 8 K=ICENTL,ICENTH
    8 C(M,K)=C(M,IRCENT)
      GO TO 13
    9 IRCENT=ICF  $  IFOUR=4  $  JKL=1
   13 CALL NORM(C,M,NPPS,IRCENT,SCALC(M))
      ERROR(M)=0.
      DO 6 K=1,NPPS,ISKIP
    6 ERROR(M)=ERROR(M)+(S(L,K)-C(M,K))*(S(L,K)-C(M,K))
      RETURN
      END
```

SUBROUTINE SMOOTH

```
      SUBROUTINE SMOOTH(NPPS)
      COMMON/DATA/IDATA(1023)
      DIMENSION NP(17)
      NPPS=NPPS-16
      DO 1 K=1,16
    1 NP(K+1)=IDATA(K)
      DO 2 J=1,NPPS  $  DO 3 K=1,16
    3 NP(K)=NP(K+1)
      NP(17)=IDATA(J+16)
      NSUM=43*NP(9)+42*(NP(8)+NP(10))+39*(NP(7)+NP(11))+34*(NP(6)+NP(12)
     1)+27*(NP(5)+NP(13))+18*(NP(4)+NP(14))+7*(NP(3)+NP(15))-6*(NP(2)+NP
     2(16))-21*(NP(1)+NP(17))
      IDATA(J)=NSUM/323
    2 CONTINUE
      L=NPPS  $  DO 4 K=1,NPPS
      IDATA(L+8)=IDATA(L)
    4 L=L-1
      DO 5 K=1,8
      J=NPPS+8+K-1  $  L=NPPS+K-1
    5 IDATA(J)=IDATA(L)
      NPPS=NPPS+16
      RETURN
      END
```

SUBROUTINE PARABOL

```
      SUBROUTINE PARABOL(X,V,A,B,C)
      DIMENSION X(3),V(3),Y(3),ERROR(3),ERRSQ(3)
      PRINT 100
      X1=X(1)  $  X2=X(2)  $  X3=X(3)
      V1=V(1)  $  V2=V(2)  $  V3=V(3)
      TM1 = (X1-X2)*(V2-V3) $ TM2 = (X2-X3)*(V1-V2)
      ALPHA = -TM1+TM2
      BETA = TM1*(X1+X2)-TM2*(X2+X3)
      D = -(X1-X2)*(X2-X3)*(X3-X1)
      IF(ALPHA.EQ.0.0) ALPHA = 1.0E-20
      IF(D.EQ.0.0) D = 1.0E-20
      A = ALPHA/D
      B = BETA/D
      C = V1-A*X1*X1-B*X1
      PRINT 101, A,B,C
      CHISQ=0.
      PRINT 102
      DO 1 K=1,3
      Y(K)=A*X(K)*X(K)+B*X(K)+C
      ERROR(K)=Y(K)-V(K)
      ERRSQ(K)=ERROR(K)*ERROR(K)
    1 PRINT 103, X(K),V(K),Y(K),ERROR(K),ERRSQ(K)
```

```
100 FORMAT(1H0,T24,*OPTIMIZING THE ORIENTATIONAL HALF-WIDTH BY THE PAR
   1ABOLIC METHOD*)
101 FORMAT(///,20X,*COEFFICIENTS*,//20X,*A = *,G13.7,/,20X,*B = *,G13.
   17,/,20X,*C = *,G13.7)
102 FORMAT(///,10X,*RESULTS*,//,15X,*VARIABLE*,T30,*EXPERIM. VALUE*,T4
   15,*THEOR. VALUE*,T60,*DIFFERENCE*,T75,*DIFF. SQUARED*)
103 FORMAT(14X,G13.7,T32,G13.7,T46,G13.7,T59,G13.7,T75,G13.7)
    RETURN
    END
```